Error estimates for numerical solutions of one- and two-dimensional integral equations

Michelle Claire Tenwick

The University of Leeds

Department of Applied Mathematics

A thesis submitted for the degree of

Doctor of Philosophy

September, 2012

The candidate confirms that the work submitted is her own, except where work which has formed part of jointly-authored publications has been included. The contribution of the candidate and the other authors to this work has been explicitly indicated below. The candidate confirms that appropriate credit has been given within the thesis where reference has been made to the work of others.

To my wonderful parents

"When you have eliminated all which is impossible, then whatever remains, however improbable, must be the truth."

– A. Conan Doyle

Jointly-Authored Publications

The work in chapter 2 is based on work from jointly-authored publications. The details of the publications are:

M. A. Kelmanson and M. C. Tenwick. A modified orthogonal-polynomial Nyström method for Fredholm integral equations of the second kind. In *Proceedings of the 7th UK conference on Boundary Integral Methods*, pp. 181–192, 2009.

M. A. Kelmanson and M. C. Tenwick. Error reduction in Gauss-Jacobi-Nyström quadrature for Fredholm integral equations of the second kind. *CMES*, 1392(1):1–20, 2010.

Acknowledgements

First and foremost I wish express my sincere gratitude to my supervisor Professor Mark Kelmanson for his patience, support and enthusiasm. It has been a real privilege to work with such an inspirational mathematician whose guidance over the last four years has been invaluable; this thesis would not have been possible without him.

I would also like to thank all of the postgraduates and lecturers in the applied mathematics department, including my advisor Dr Evy Kersalé and my examiners Dr Jitse Niesen and Professor Henry Power for their helpful advice. In particular, I would like to give a special thanks to the inhabitants of the computer room on level 9 and the satellite area, especially Dr. Tina Davies who on top of providing me with essential coffee breaks has been a supportive, entertaining and fabulous friend.

Finally, I would like to thank my family and friends for their understanding and endless love: my parents John and Sandie, for always supporting and encouraging me without fail; my grandma Ethel for all of her kindness and generosity; my brother Andrew for knowing how to make me laugh; my friend Vorn for always being there when needed, and last but not least my partner Adam for providing endless support and encouragement regardless of how much I complained.

This research has been funded by the EPSRC and has been carried out by myself and Professor Mark Kelmanson. My contribution to the work has been the programming of the numerical methods discussed in this thesis, as well as acquiring the analytical results presented throughout, unless otherwise stated. Professor Mark Kelmanson has provided guidance in accordance with standard supervisory roles.

Abstract

This thesis is concerned with the improvement of numerical methods, specifically boundary-element methods (BEMs), for solving Fredholm integral equations in both one- and two-dimensions. The improvements are based on novel (computer-algebra-based) error analyses that yield explicit forms of correction terms for *a priori* incorporation into BEM methods employing piecewise-polynomial interpolation in the numerical approximation. The work is motivated by the aim of reducing errors of BEM methods *for low-degree interpolating polynomials*, without significantly increasing the computational cost associated with higher-degree interpolation. The present thesis develops, implements and assesses improved BEMs on two fronts.

First, a modified Nyström method is developed for the solution of one-dimensional Fredholm integral equations of the second kind (FIE2s). The method is based upon optimal approximation and inclusion of an explicit form of orthogonal-polynomial integration error, and it can be extended to systems of integral equations. It is validated, in both the single and system cases, on challenging FIE2s that contain a finite number of (integrable) singularities, or points of limited differentiability, within the integral kernels.

Second, BEMs are developed for solving two-dimensional FIE2s in the widely applicable context of harmonic boundary value problems in which the boundary conditions may be either continuous or discontinuous. In the latter case, modifying the BEM to conquer the adverse effect (on convergence with decreasing mesh size) caused by *boundary singularities* requires considerable additional theory and implementation; the motivation for doing so is that such singularities arise naturally in the modelling of, e.g., stress fractures in solid mechanics and dielectrics in electrostatics. For both non-singular and singular BVPs, standard BEMs are improved herein by optimal approximation and inclusion of explicit forms of Lagrange-interpolation integration errors. The modified BEMs are validated against pseudo-analytic results obtained by a conformal-transformation method, for which a novel implementation of the inverse transformation (needed to recover the physical solution) is included explicitly by use of an algebraic manipulator.

Through a set of test problems with known (or otherwise computable) solutions, both the one- and two-dimensional modified methods, for both regular and singular BVPs, are demonstrated to show marked improvements in performance over their unmodified counterparts.

Contents

List of Abbreviations

FIE	Fredholm integral equation
FIE2	Fredholm integral equation of the second kind
BVP	Boundary value problem
SBVP	Singular boundary value problem
FDM	Finite difference method
FEM	Finite element method
BEM	Boundary element method
CBEM	Constant boundary element method
SIM	Singularity incorporation method
SSM	Singularity subtraction method
SICBEM	Singularity incorporated constant boundary element method
SSCBEM	Singularity subtracted constant boundary element method
MCBEM	Modified constant boundary element method
MSICBEM	Modified singularity incorporated constant boundary element method
MSSCBEM	Modified singularity subtraction constant boundary element method
FDMCBEM	Finite-difference modified constant boundary element method
CTM	Conformal transformation method
RMSE	Root-mean-square error

List of Figures

List of Tables

Chapter 1

Introduction

1.1 Background and motivation

Many problems in applied sciences can be modelled and formulated in two distinct ways, namely as differential equations or integral equations. In the latter, the boundary and/or initial conditions are incorporated *a priori* which, in practice, can often make integral-equation formulations advantageous over their differential-equation counterparts.

Integral equations, categorised by the unknown function occurring under an integral sign, arise in the modelling of a wide range of physical problems, e.g. in the mechanics of solids, acoustics, viscous flow and electromagnetism. Hence there exists an abundance of research in the study of integral equations, including both theoretical and numerical solution techniques, e.g. Muskhelishvili [1953], Bernkopf [1966], Green [1969], Baker [1977], Tricomi [1985], Kress [1990], Porter and Stirling [1990], Power and Wrobel [1995], Hackbusch [1995], and Atkinson [1997]. Generally, there are two classifications: Volterra (VIEs) and Fredholm integral equations (FIEs), with respectively variable and constant limits of integration. In this thesis we focus on Fredholm integral equations due to their frequent occurrence in the representation of boundary-value problems (BVPs).

A BVP, like an initial-value problem, is a partial differential equation coupled with additional restraints whose solution, in general, lies beyond the reach of purely-analytical approaches. Consequently there are numerous methods, such as finite elements and finite difference, which

can be classified as *domain* methods, that provide approximate solutions to BVPs. Finite element and finite difference methods are the most widely used spacial discretisation techniques, whereby the governing partial differential equation is approximated locally by a discretised equation whose solution is defined at a set of prespecified points in the domain. An alternative (global) approach, upon which the present work concentrates, considers the reformulated integral-equation form of the partial differential equation resulting from the divergence theorem, known as a boundary-integral equation.

The philosophy behind various boundary-integral equation formulations is that the divergence-theorem reformulation of the partial differential equation, in terms of an integral equation and an accompanying fundamental solution (a Green's function), reduces the spatial order of the problem by one. For example, with reference to Laplace's equation $\nabla^2\phi = 0$ in two-dimensions, by Green's integral formula (Green [1969]), the harmonic function ϕ defined within a domain Ω enclosed by a boundary $\partial\Omega$ satisfies

$$\phi(p) = \frac{1}{2\pi}\int_{\partial\Omega}\left[\phi(q)\log'|p-q| - \phi'(q)\log|p-q|\right]dq, \tag{1.1.1}$$

where $p \in \Omega\cup\partial\Omega$, $q \in \partial\Omega$, the prime represents differentiation with respect to the outward normal to $\partial\Omega$ at q and dq denotes the differential increment of $\partial\Omega$ at q. Eqn. (1.1.1) relates the harmonic function ϕ at any point in the domain to the boundary distributions of both ϕ and ϕ', in which if both of the distributions are known, then ϕ may be obtained at any interior point. Alternatively, when given one of the boundary distributions, (1.1.1) becomes closed-form equation whose solution completes the boundary distribution data. Note, when only the boundary distribution ϕ' is known, (1.1.1) is an integral equation of the *second kind* (Atkinson [1997]).

The work presented in this thesis can be divided into two broad categories of integral equations[1]: one-dimensional Fredholm integral equations of the second kind (FIE2) and two-dimensional boundary-integral equation reformulations of Laplace's equation, the latter of which motivated the original work of Ivar Fredholm [1903] on the solvability of integral equations of the second kind.

An explicit closed-form solution of a boundary-integral equation is generally not obtainable,

[1] Muskhelishvili [1953], Elliott [1979, 1989], Jen and Srivastav [1981], Monegato and Scuderi [1998], Smith [2000], Jin et al. [2008]

necessitating the development of numerical methods (Blue [1977], Fairweather et al. [1979], Fairweather and Karageorghis [1998], Atkinson and Chandler [1990], Cheng [1994], Elliotis et al. [2002, 2006]). Most uses of boundary-integral equations in engineering applications have involved approximating the solution using piecewise-polynomial functions over a decomposition of the boundary; such approximations are known as boundary element methods[2] (BEM).

BEMs readily incorporate the boundary conditions; contrast this with the finite-element and finite-difference methods, in which special relations are necessary at the mesh points along and/or near the boundary. Furthermore, BEMs have proved to be a successful tool in solving numerous engineering problems, e.g., elasticity, including crack problems, (Blue [1977], Jaswon and Symm [1977]), fluid flow (Bush et al. [1984], Brebbia and Trevelyan [1986], Grilli and Svendsen [1990], Hansen and Kelmanson [1994]) and heat conduction (Mera et al. [2001, 2002]).

As noted by Mason and Smith [1982], rigorous convergence and error analyses for BEMs are particularly hard to achieve: Wendland [1982] and Hsiao and Wendland [2004] presented error analyses for the asymptotic convergence of the BEM based on Galerkin methods, Rencis et al. [1990] and Liang et al. [1999] considered a posteriori error of the BEM and Lu et al. [2004] presented error analyses on the collocation Trefftz method for a harmonic problem. However, these concentrate on error bounds rather than implementable formulae. The existence of literature investigating the error in BEMs on a practical basis is sparse, e.g., Kelmanson [1985] presented a technique for assessing the nature of the error incurred in the constant BEM for both harmonic and biharmonic problems, providing an insight into the behaviour of the error in the numerical scheme.

In practical problems the boundary conditions often exhibit singular behaviour. Most commonly, the singular behaviour arises from sudden changes in boundary geometry or conditions, e.g., sharp corners (Kelmanson [1983a]) and changes in dielectric properties (Daly [1973]). The presence of these boundary singularities have an adverse affect on the convergence rate of the solution computed by the standard numerical techniques, such as BEMs (Motz [1946], Woods [1953]). Consequently, the possibility of modifying the BEMs to improve the treatment of the boundary singularities has received considerable attention (Symm [1973], Jaswon and Symm [1977], Xanthis

[2]Jaswon and Symm [1977], Brebbia [1978], Brebbia and Trevelyan [1986], Brebbia and Dominguez [1989], Fenner [1983], Bush et al. [1984], Ingham and Kelmanson [1984], Kelmanson [1984], Manzoor [1984], Kelmanson [1985], Aitchison and Karageorghis [1988], Brebbia and Dominguez [1989], Hsiao [2006], Ang [2007]

et al. [1981], Ingham et al. [1981a], Manzoor [1984]). It was shown by Symm [1973] that, by a suitable modification of the BEM, harmonic problems containing boundary singularities could be accurately solved in an efficient manner. The improved accuracy, however, was often obtained at the expense of a large increase in analysis. Alternatively, Xanthis et al. [1981] offered a modification technique for harmonic problem which, compared with Symm [1973], required minimal extra analysis. Both types of modified methods have been subsequently applied to physical problems, e.g., in transmission-line singularities, (Ingham et al. [1981c]), heat transfer (Manzoor [1984], Mohammadi et al. [2010]) and viscous flows (Wrobel [1981], Kelmanson [1983a,b]).
The discussion above motivates the investigation into improving the accuracy of numerical methods, for both singular and nonsingular integral equations.

1.2 Aims and objectives

The present work aims to provide both accurate and reliable numerical methods for approximating the solutions of integral equations. To achieve this, the present work is based on three main aims:

- To compute numerical solutions for one- or two-dimensional integral equations;
- To provide rigorous analyses of the numerical methods in order to yield an explicit understanding of the numerical errors, and;
- To modify the existing numerical methods by incorporating this error information in an explicit way, so that the accuracy of the approximate solution is improved for a minimal increase in cost and effort.

The new modified methods, which are based on incorporating *a priori*, as accurately as possible, an explicit form of the error in the standard method, are always validated by test problems to ensure that improvements over existing methods are obtained in an economic and efficient fashion. As part of the validation process for our new methods, the present work also focusses on deriving pseudo-analytic solutions of singular BVPs.
Two specific objectives in the latter part of this thesis are: first, to modify the constant BEM so

that it emulates higher-order Lagrangian interpolation (which would demand both more complex algorithms and the solution of larger systems of equations) without increasing the size of the system, and; second, to use the modified BEM to improve the numerical solution of a BVP in the presence of a boundary singularity.

1.3 Outline of thesis

Throughout this thesis, three persistent themes are followed: to outline a numerical method and its error formulae for solving an integral equation; to derive an explicit error formulae of the numerical method, and; to build the explicit error formulae into the numerical method *a priori* thus defining a, new, modified method. With these themes in mind, the structure is as follows.

In chapters 2 and 4 we present the modification techniques used to improve the numerical solutions of one- and two-dimensional integral equations respectively. In chapters 3 and 6 we extend the range of applications of the modification techniques to more complex integral equations.

In chapter 2 a FIE of the second kind (Fredholm [1903]) is presented in which the integrand is singular at one or both extrema of the integration domain. Although there exist a plethora of numerical solutions of FIEs (Kantorovich et al. [1964], Bernkopf [1966], Baker [1977], Anselone [1981], Graham et al. [1985], Elliott [1979, 1989], Kress [1990], Hackbusch [1995]), the present work considers the Nyström approach (Nyström [1930], Atkinson [1974, 1989, 1997], Benko et al. [2008]). The Nyström method, which is based upon employing Gaussian quadrature, determines the solution of the FIE at a set of predefined quadrature nodes, which is then extended to all points in the domain (Patterson [1968], Porter and Stirling [1990], Crow [1993], Laurie [2001], Ralston and Rabinowitz [2001], Smith [2000]). The cost of Nyström 's method is minimised by using a high-degree orthogonal-based quadrature rule (Karpenko [1966], Gerasoulis and Srivastav [1982], Kelmanson and Tenwick [2010]) that requires only low numbers of quadrature nodes. A modified Nyström method is then presented, the essence of which is to include the best possible error estimate into the standard Nyström method *a priori*. Comparisons of solutions of test FIEs are conducted to reveal the improved accuracy of the modified Nyström method compared with the standard Nyström method.

Chapter 2 illustrates the basic concept of the modified Nyström method, in particular its restriction upon the type of integrand and the size of the integration domain. The restrictions of chapter 2 are investigated in chapter 3, where a FIE with an integrand that is singular at multiple points within the domain is considered: this integral equation is expressible as a *system* of FIEs. Numerical techniques for solving of systems of FIEs have seen a sudden growth in popularity over the past decade, to the extent that they now include: Adomian decompositions (Babolian et al. [2004]), Chebyshev-collocation (Akyüz-Daşcıolu [2004]), block-pulse function methods (Maleknejad et al. [2005]), Taylor-series methods (Maleknejad et al. [2006]), homotopy perturbation methods (Javidi and Golbabai [2007]), Sinc-collocation (Rashidinia and Zarebnia [2007]) and Legendre wavelets (Jafari et al. [2010]). However, we are primarily concerned with the approach of De Bonis and Laurita [2008], as it is based on the aforementioned Nyström–type method which we also adopt. As in chapter 2, a modification of the Nyström method for the system of FIEs is presented in chapter 3, which is restricted to low numbers of quadrature nodes.

The standard and modified Nyström method for systems of FIEs, illustrated for only one internal singularity, are applied to several different test problems with known exact solution to reveal the superior accuracy of the modified Nyström method. The position of the singularity in the integration domain, however, transpires to be essential for determining the extent of improvement in the degree of accuracy in the modified Nyström method compared to the standard Nyström method.

In chapter 4 we consider Laplace's equation in two-dimensions, the boundary-integral equation reformulation of which is conducted following the work of Jaswon [1963] and Symm [1963]. The present work considers solving the boundary-integral equation using the constant BEM algorithm (Brebbia [1978]). To gain a complete understanding of the behaviour of the constant BEM, we present rigorous error analyses in terms of explicit error formulae. We remark that, to our knowledge, the existence of error analyses that provide explicit error formulae for the BEM is sparse (Mason and Smith [1982], Kelmanson [1985]).

Brebbia [1978] improved upon the constant BEM by taking higher-order piecewise-polynomial functions over each element. However, this requires the solution of larger systems of equations than in the constant BEM. Instead, in chapter 4 we present a novel modification technique to improve the accuracy of the constant BEM, one that emulates the higher-order piecewise-polynomial

functions without increasing the size of the discrete system. The new modified method, which incorporates the leading behaviour of error into the standard method *a priori*, is illustrated for a nonsingular test BVP revealing an improved accuracy over the unmodified method. Furthermore, the illustration shows that the rate of convergence of the modified constant BEM is predictable *a priori*, depending upon the degree of the leading order in the incorporated terms. That is, the modification technique, which requires only a minor modification of the constant BEM, provides an efficient, straightforward and computationally superior method to the higher-order piecewise-polynomial BEMs.

Another contribution of the present work is to extend the modified BEM of chapter 4 to solve a BVP in which there is a boundary singularity. Motz [1946] defined a BVP with mixture of Dirichlet and Neumann boundary conditions, known as the "Motz problem", in which the presence of a boundary singularity was due to a sudden change in boundary conditions. The Motz problem is a fundamental singular BVP, inspiring many subsequent studies to obtain pseudo-analytic or numerical solutions[3].

In chapter 5, a new singular harmonic BVP known as the "stripline problem" is presented, where a flat strip of conducting metal is sandwiched in a grounded non-insulating material, as illustrated in Fig. 1.3.1. The importance of the stripline problem is three-fold: first, its application in electromagnetism; second, the presence of a singularity at the ends of the conducting strip, and; third, its near-identical geometrical resemblance to the Motz problem. The similarity between the Motz and the stripline is important because it indicates that the pseudo-analytic and numerical methods for the Motz problem are applicable to the stripline problem (subject to minor adaptations) and vice versa.

In a remarkable paper by Whiteman and Papamichael [1971], a conformal mapping technique is presented to derive a near-exact (subject to machine precision) pseudo-analytic solution for the Motz problem. Adapting the algorithms of Whiteman and Papamichael [1971] and Rosser and Papamichael [1975], chapter 5 presents the derivation of a pseudo-analytic solution for the stripline

[3]Motz [1946], Kelman [1970], Whiteman and Papamichael [1971], Papamichael and Whiteman [1973], Papamichael and Symm [1975], Blue [1977], Crank and Furzeland [1978], Kermode and McKerrell [1985], Li et al. [1987], Steinberg [1987], Wigley [1988], Olson et al. [1991], Karageorghis et al. [1996], Poullikkas et al. [1998], Li and Lu [2000], Hu [2003], Lu et al. [2004], Li et al. [2005], Dosiyev [2005], Bernal and Kindelan [2010], Pashos et al. [2010]

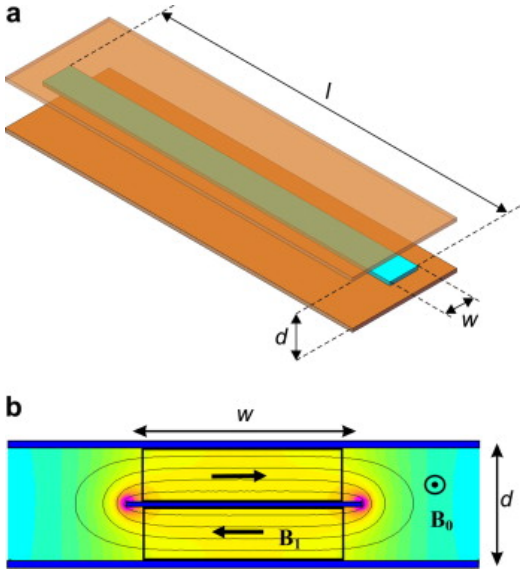

Figure 1.3.1: *As shown by Bart et al. [2009]:(a) 3D representation of a stripline configuration; the blue central strip is the conducting metal. Here the dimensional parameters are: l (length of the strip), w (width of the strip) and d (distance between the ground planes). (b) Cross-sectional field pattern of a stripline. The field pattern is homogeneous, except for the field around the extreme edges of the strip, due to the presence of singularities.*

problem by the means of a conformal mapping technique: this constitutes the first direct attempt at deriving the analytic solution of the stripline problem by the use of conformal mappings.

In chapter 6, a numerical approach is first presented for the solution of the stripline problem using the constant BEM algorithm of Brebbia [1978]. As outlined in Motz [1946] and Woods [1953], the existence of a singularity adversely affects the convergence rate of any standard numerical method. Symm [1973] and Xanthis et al. [1981] presented two approaches in which the asymptotic nature of the singularity may be incorporated into the constant BEM. The work of Symm [1973], Ingham et al. [1981a], Manzoor [1984], Xanthis et al. [1981] and Kelmanson [1983a] cover a wide range of BEM approximations for the solution of harmonic BVPs with boundary singularities. Ingham et al. [1981c] in particular, considered a BEM solution of the stripline problem, although no numerical results were presented for comparison making the pseudo-analytic solution ever more essential.

Based on the modification technique of chapter 4, in chapter 6 we improve the rate of convergence in the methods of Symm [1973] and Xanthis et al. [1981]. The modified BEMs are again based on

incorporating the leading behaviour of the error into the original BEM *a priori*. The application of the modified BEMs is illustrated for the stripline problem where, by using the analytic solution in chapter 5, its ability to improve the accuracy and the rate of convergence in the standard BEM is shown. However, as only the leading behaviour of the singularity is accounted for in Symm [1973] and Xanthis et al. [1981], it is hardly surprising that the accuracy of the modified BEM results are restricted by the residual behaviour of the singularity.

In summary, chapters 4, 5 and 6 present distinct contributions to the solution of harmonic BVPs including the modification and refinement of the constant BEM. Finally, a general summary is given in chapter 7, concluding the key observations and achievements in the thesis plus any possible future work extending from the work presented.

Chapter 2

Numerical Solutions of One-Dimensional Fredholm Integral Equations of the Second Kind

In the early 20^{th} century, Erik Ivar Fredholm [1903] made significant contributions to the field of mathematics now known as Fredholm theory, which concerns classifying and solving related types of *integral equations*. The basic form of a linear Fredholm integral equation for an unknown function $U(S)$ defined on $S \in [a, b]$ is that of the *first kind* (FIE1),

$$F(T) = \int_a^b \widetilde{K}(T, S)U(S)\, dS, \quad T \in [a, b], \tag{2.0.1}$$

in which the interval limits a and b are real constants, $\widetilde{K}$ is the *kernel* and F is the *source function*. When U occurs both inside and outside the integral, a linear Fredholm integral equation of the *second kind* (FIE2) is then defined by

$$U(T) = F(T) + \Lambda \int_a^b \widetilde{K}(T, S)U(S)\, dS, \quad T \in [a, b] \tag{2.0.2}$$

which, provided $F(T) \neq 0$, is *inhomogeneous*. Here the *associated constant* Λ plays the role of an eigenvalue i.e. the existence and/or uniqueness of solutions of (2.0.2) may be affected by Λ; when Λ is known *a priori*, it is often absorbed into the kernel. An analysis and implementation of new numerical solution techniques for approximating the solution of (2.0.2) will form the substantial

part of this chapter.

To demonstrate the efficacy of the new methods, we shall consider the challenging case of non-infinitely differentiable kernel functions (and hence integrands of FIE2 (2.0.2)) with respect to $S \in (a, b)$, in which the kernel function is factorised into the form

$$\widetilde{K}(T, S) = W(S)K(T, S), \tag{2.0.3}$$

where $K(T, S)$ is infinitely differentiable but $W(S)$, the "badly-behaved" part of the kernel, is not. To admit the possibility that $\widetilde{K}(T, S)$ in (2.0.3) is either singular at the interval limits or limited-continuously differentiable at the interval limits in the sense that one or more of its derivatives is not finite at the interval limits (i.e. has end-point singularities), the singular behaviour is more specifically given in the form

$$W(S) = (b - S)^{\mu}(S - a)^{\nu}, \tag{2.0.4}$$

in which $\mu, \nu > -1$, so that the FIE2 may be singular but not hypersingular. We also admit the possibility that the weight function $W(S)$ can simply be equal to unity.

For our subsequent analysis, we proceed by mapping $T, S \in [a, b]$ in (2.0.2) onto $t, s \in [-1, 1]$ by

$$(T, S) = \frac{1}{2}\left[(b - a)(t, s) + (b + a)\right]. \tag{2.0.5}$$

Accordingly, rescaling Λ using

$$\lambda = \Lambda \left(\frac{(b - a)}{2}\right)^{\mu+\nu+1}, \tag{2.0.6}$$

the canonical form of FIE2 (2.0.2) becomes

$$u(t) = f(t) + \lambda \int_{-1}^{1} w(s)k(t, s)u(s)\, ds, \quad t \in [-1, 1], \tag{2.0.7}$$

where the lower-case functions correspond to their upper-case counterparts in (2.0.2), and the transformed weight function, which now has potential discontinuous derivatives at $s = \pm 1$, is

$$w(s) = (1 - s)^{\mu}(1 + s)^{\nu}. \tag{2.0.8}$$

Defining the integral operator $\mathcal{K}$ by

$$(\mathcal{K}u)(t) \equiv \int_{-1}^{1} w(s)k(t, s)u(s)\, ds, \tag{2.0.9}$$

the symbolic form of (2.0.7) is

$$u - \lambda \mathcal{K} u = f, \tag{2.0.10}$$

with corresponding unique solution (Atkinson [1997])

$$u = (\mathcal{I} - \lambda \mathcal{K})^{-1} f, \tag{2.0.11}$$

where $\mathcal{I}$ denotes the identity operator and $\|(\mathcal{I} - \lambda \mathcal{K})^{-1}\|$ is bounded for any suitable norm $\|\cdot\|$. An explicit closed-form solution $u(t)$ of FIE2 (2.0.7) is generally not obtainable, necessitating the implementation of numerical approximation techniques. We shall focus on applying the Nyström method and describing novel modifications thereof that improve the accuracy of the approximate solution.

The remainder of this chapter is structured as follows. First, the theory of approximating FIE2 (2.0.7) via the Nyström method using Gaussian quadrature is outlined in §2.1. In §2.2 a theoretical error is included in the Nyström method, which forms the basis for a new, modified, Nyström method. An explicit definition of the theoretical error is given in §2.3. Finally, the modified Nyström method is validated by a series of test problems in §2.4. The validation highlights the accuracy, reliability and robustness of the method, hence justifying its application to integral equations in higher dimensions.

2.1 The Nyström method

The Nyström method is one of numerous techniques employed to approximate the solution $u(t)$ of (2.0.7), e.g. Kaneko and Xu [1994], Benko et al. [2008], Dick et al. [2007], Kang et al. [2003] and Mastroianni and Monegato [2003]. The basis of the Nyström method is the optimally accurate approximation of the integrand in (2.0.7) using an n-point quadrature of the form

$$\int_{\Omega} g(s)\, ds \approx \sum_{j=1}^{n} c_{j,n} g(\sigma_{j,n}), \tag{2.1.1}$$

where $c_{j,n}$ are the *weights* and $\sigma_{j,n}$ the *abscissae* defined by the particular choice of the integration scheme. In (2.1.1) we use well-known integration schemes based upon orthogonal-polynomial approximation of $g(s)$: see, e.g., Delves and Mohamed [1988], Atkinson [1989], Ralston and

Rabinowitz [2001] and Gautschi [2004]. Nyström [1930] originally adopted a high-order Gaussian quadrature in (2.1.1).

Taking into account the factorisation of $\widetilde{K}(T,S)$ in (2.0.3), the n^{th}-order Gaussian quadrature (2.1.1) can be used to integrate only the continuous part $K(T,S)$ of the integrand in (2.0.2). Hence, by (2.0.3), the Nyström method is referred to as the *product Nyström method* (Atkinson [1997]).

In view of the explicit form of the weight function in (2.0.8), we shall employ Gauss-Jacobi quadrature. Gauss-Jacobi quadrature is based on the Jacobi polynomials $P_n(s;\mu,\nu)$ because these are orthogonal on $s \in [-1,1]$ with respect to the weight function (2.0.8), i.e.

$$\langle P_i, P_j \rangle = \int_{-1}^{1} (1-s)^{\mu}(1+s)^{\nu} P_i(s;\mu,\nu) P_j(s;\mu,\nu)\, ds = \delta_{ij}, \quad \forall i,j \in \mathbb{N}, \tag{2.1.2}$$

where δ_{ij} is the Kronecker delta function. The explicit form of the Gaussian quadrature approximation $\mathcal{K}_n u$ of $\mathcal{K}u$ in (2.0.9) is then

$$(\mathcal{K}_n u)(t) \equiv \sum_{j=1}^{n} c_{j,n} k(t,\sigma_j) u(\sigma_j), \quad t \in [-1,1], \tag{2.1.3}$$

for which $(\mathcal{K}u)(t) \equiv (\mathcal{K}_n u)(t)$ when $k(t,s)u(s)$ is a polynomial of degree $\leq 2n-1$ (Atkinson [1989]). In (2.1.3) the weights, $c_{j,n}$, are defined by

$$c_{j,n} = -\frac{A_{n+1}\gamma_n}{A_n P_{n+1}(\sigma_j;\mu,\nu)\partial_1 P_n(\sigma_j;\mu,\nu)}, \tag{2.1.4}$$

where

$$A_n = \frac{(2n+\mu+\nu)!}{2^n n!(n+\mu+\nu)!} \tag{2.1.5}$$

is the leading coefficient in $P_n(s;\mu,\nu)$, σ_j are the n distinct roots of $P_n(s;\mu,\nu)$ for $j = 1,\ldots,n$ and ∂_1 denotes the partial differential of $P_n(s;\mu,\nu)$ with respect to s. In (2.1.4) γ_n is given by

$$\gamma_n = \int_{-1}^{1} (1-s)^{\mu}(1+s)^{\nu} \left[P_n(s;\mu,\nu)\right]^2\, ds, \tag{2.1.6}$$

that can be evaluated exactly (Abramowitz and Stegun [1972]). Using (2.1.5) and (2.1.6), the weights $c_{j,n}$ in (2.1.4) can be evaluated explicitly (Kelmanson and Tenwick [2010]) as

$$c_{j,n} = \frac{2^{\mu+\nu}(2n+\mu+\nu+2)\Gamma(n+\mu+1)\Gamma(n+\nu+1)}{\Gamma(n+2)\Gamma(n+\mu+\nu+2)P_{n+1}(\sigma_j;\mu,\nu)\partial_1 P_n(\sigma_j;\mu,\nu)} \tag{2.1.7}$$

for $j = 1,\ldots,n$.

The quadrature error is defined to be

$$(\mathcal{E}_n u)(t) \equiv ((\mathcal{K} - \mathcal{K}_n)u)(t) \tag{2.1.8}$$

which, although is pointwise convergent to zero for a sufficiently differentiable function $u(t)$,

$$(\mathcal{E}_n u)(t) \to 0, \quad n \to \infty, \tag{2.1.9}$$

is not norm convergent (Hackbusch [1995]), i.e.

$$\|\mathcal{E}_n\| \geq \|\mathcal{K}\| \tag{2.1.10}$$

for all $n \in \mathbb{N}$. But note that, by (2.0.9), (2.1.3) and (2.1.8),

$$\|\mathcal{E}_n u\| \to 0, \quad n \to \infty \tag{2.1.11}$$

and, based upon a convergence analysis of the quadrature rule (2.1.3) for continuous integrands, Atkinson [1997] proves the results, needed for our subsequent analysis,

$$\|\mathcal{E}_n \mathcal{K}\|, \|\mathcal{E}_n \mathcal{K}_n\| \to 0, \quad n \to \infty. \tag{2.1.12}$$

The Nyström application of FIE2 (2.0.7) is, in symbolic form,

$$u_n - \lambda \mathcal{K}_n u_n = f, \tag{2.1.13}$$

in which u_n is the finite-dimensional approximation to u and $\mathcal{K}_n$ is defined by (2.1.3). By (2.0.10) and (2.1.13), the *Nyström error* $u - u_n$ satisfies

$$(\mathcal{I} - \lambda \mathcal{K}_n)(u - u_n) = \lambda(\mathcal{K} - \mathcal{K}_n)u, \tag{2.1.14}$$

which admits the observation that the error $u - u_n$ is explicitly dependent upon the existence of $(\mathcal{I} - \lambda \mathcal{K}_n)^{-1}$. Both (2.1.13) and (2.1.14) require the invertibility of $(\mathcal{I} - \lambda \mathcal{K}_n)$, which cannot be assumed but can be shown as follows.

Since, by hypothesis, FIE2 (2.0.10) has the explicit solution (2.0.11), $(\mathcal{I} - \lambda \mathcal{K})$ must be invertible and so

$$\|(\mathcal{I} - \lambda \mathcal{K})^{-1}\| < \infty. \tag{2.1.15}$$

By (2.1.12) and (2.1.15), there exists an $m \in \mathbb{N}$ such that

$$\|\mathcal{E}_n \mathcal{K}_n\| \leq \frac{1}{\lambda^2 \|(\mathcal{I} - \lambda \mathcal{K})^{-1}\|}, \tag{2.1.16}$$

for $n > m$. That is,

$$\lambda^2 \|(\mathcal{K} - \mathcal{K}_n)\mathcal{K}_n\| < \frac{1}{\|(\mathcal{I} - \lambda\mathcal{K})^{-1}\|}, \quad n > m. \tag{2.1.17}$$

Now

$$\begin{aligned}\mathcal{I} = \mathcal{I} - \lambda\mathcal{K}_n + \lambda\mathcal{K}_n &= \mathcal{I} - \lambda\mathcal{K}_n + \lambda(\mathcal{I} - \lambda\mathcal{K}_n)(\mathcal{I} - \lambda\mathcal{K}_n)^{-1}\mathcal{K}_n \\ &= (\mathcal{I} - \lambda\mathcal{K}_n)\left[\mathcal{I} + \lambda(\mathcal{I} - \lambda\mathcal{K}_n)^{-1}\mathcal{K}_n\right],\end{aligned} \tag{2.1.18}$$

and hence

$$(\mathcal{I} - \lambda\mathcal{K}_n)^{-1} = \left[\mathcal{I} + \lambda(\mathcal{I} - \lambda\mathcal{K}_n)^{-1}\mathcal{K}_n\right]. \tag{2.1.19}$$

Without any justification at this stage, we make the assumption that (2.1.19) can be approximated by (Atkinson [1997])

$$(\mathcal{I} - \lambda\mathcal{K}_n)^{-1} \approx \left[\mathcal{I} + \lambda(\mathcal{I} - \lambda\mathcal{K})^{-1}\mathcal{K}_n\right], \tag{2.1.20}$$

since $\mathcal{K}_n \approx \mathcal{K}$. In order to check such an approximation, consider

$$\begin{aligned}&\left[\mathcal{I} + \lambda(\mathcal{I} - \lambda\mathcal{K})^{-1}\mathcal{K}_n\right](\mathcal{I} - \lambda\mathcal{K}_n) \\ &= (\mathcal{I} - \lambda\mathcal{K}_n) + \lambda(\mathcal{I} - \lambda\mathcal{K})^{-1}\mathcal{K}_n(\mathcal{I} - \lambda\mathcal{K}_n) \\ &= (\mathcal{I} - \lambda\mathcal{K}_n) + \lambda(\mathcal{I} - \lambda\mathcal{K})^{-1}\mathcal{K}_n - \lambda^2(\mathcal{I} - \lambda\mathcal{K})^{-1}\mathcal{K}_n\mathcal{K}_n \\ &= \mathcal{I} + (\mathcal{I} - \lambda\mathcal{K})^{-1}\left[I - (\mathcal{I} - \lambda\mathcal{K})\right]\lambda\mathcal{K}_n - \lambda^2(\mathcal{I} - \lambda\mathcal{K})^{-1}\mathcal{K}_n\mathcal{K}_n \\ &= \mathcal{I} + (\mathcal{I} - \lambda\mathcal{K})^{-1}\lambda^2(\mathcal{K} - \mathcal{K}_n)\mathcal{K}_n,\end{aligned} \tag{2.1.21}$$

the right-hand side of which is invertible by geometric series theorem (Appendix A) because, by condition (2.1.17), $\|(\mathcal{I} - \lambda\mathcal{K})^{-1}\lambda^2(\mathcal{K} - \mathcal{K}_n)\mathcal{K}_n\| < 1$. Then the geometric series theorem also implies

$$\left\|\left[\mathcal{I} + (\mathcal{I} - \lambda\mathcal{K})^{-1}\lambda^2(\mathcal{K} - \mathcal{K}_n)\mathcal{K}_n\right]^{-1}\right\| \leq \frac{1}{1 - \lambda^2\|(\mathcal{I} - \lambda\mathcal{K})^{-1}\|\|(\mathcal{K} - \mathcal{K}_n)\mathcal{K}_n\|}. \tag{2.1.22}$$

Since the right-hand side of (2.1.21) is invertible, the same must be true for the left-hand side, thus $(\mathcal{I} - \lambda\mathcal{K}_n)$ is invertible and satisfies

$$(\mathcal{I} - \lambda\mathcal{K}_n)^{-1} = \left[\mathcal{I} + (\mathcal{I} - \lambda\mathcal{K})^{-1}\lambda^2(\mathcal{K} - \mathcal{K}_n)\mathcal{K}_n\right]^{-1}\left[\mathcal{I} + (\mathcal{I} - \lambda\mathcal{K})^{-1}\lambda\mathcal{K}_n\right]. \tag{2.1.23}$$

By (2.1.22), the norm of $(\mathcal{I} - \lambda\mathcal{K}_n)^{-1}$ is uniformly bounded for sufficiently large n as

$$\|(\mathcal{I} - \lambda\mathcal{K}_n)^{-1}\| \leq \frac{1 + |\lambda|\|(\mathcal{I} - \lambda\mathcal{K})^{-1}\|\|\mathcal{K}_n\|}{1 - \lambda^2\|(\mathcal{I} - \lambda\mathcal{K})^{-1}\|(\mathcal{K} - \mathcal{K}_n)\mathcal{K}_n\|} \leq \xi_n, \tag{2.1.24}$$

in which

$$\|\mathcal{K}_n\| = \max_{t\in[-1,1]} \sum_{j=1}^{n} |c_{j,n} k(t,\sigma_j)| \leq \sup_{n\geq 1} \sum_{j=1}^{n} |c_{j,n}| \max_{t,s\in[-1,1]} |k(t,s)| < \infty \tag{2.1.25}$$

and ξ_n is a constant. Collecting the results, in particular (2.1.14) and (2.1.24), we have shown that

$$\|(u-u_n)\|_\infty \leq \xi_n |\lambda| \|(\mathcal{K}-\mathcal{K}_n)u\|_\infty, \tag{2.1.26}$$

for sufficiently large n; hence the Nyström error converges to zero with n at the same rate as that of the error of the quadrature scheme.

For the specific case of Gauss-Jacobi quadrature, the Nyström error bound in (2.1.26) can be asymptotically estimated for large-n (Kelmanson and Tenwick [2009]) as

$$\|u-u_n\|_\infty \leq \frac{\pi}{2^{2n+\mu+\nu}} \|\partial_{2n}[k(t,s)u(s)]\|_\infty, \quad n\to\infty, \tag{2.1.27}$$

in which ∂_m denotes the m^{th} derivative with respect to s. Taking logarithms of (2.1.27)

$$\begin{aligned} \log\|u-u_n\|_\infty &\leq \log\pi + \log\|\partial_{2n}[k(t,s)u(s)]\|_\infty - (2n+\mu+\nu)\log 2 \\ &= \log\pi + \log\|\partial_{2n}[k(t,s)u(s)]\|_\infty - (\mu+\nu)\log 2 - 2n\log 2, \end{aligned} \tag{2.1.28}$$

in which the first three terms on the right-hand side are constant. Letting $c = \log\pi + \log\|\partial_{2n}[k(t,s)u(s)]\|_\infty - (\mu+\nu)\log 2$ then, by (2.1.28),

$$\log\|u-u_n\|_\infty \leq c - 2n\log 2. \tag{2.1.29}$$

Given the kernel function $k(t,s)$ is, by construction, infinitely differentiable with respect to s, (2.1.27) and (2.1.29) reveal that $\|u-u_n\|_\infty$ converges to zero exponentially with n when $\partial_{2n}u(s)$ is bounded.

In Fig. 2.1.1 the logarithm of the actual error $\|u-u_n\|_\infty$ and error bound (2.1.27) in the Nyström solution of a test FIE2 (with known solution) is depicted as a function of n. The exponential convergence of $\|u-u_n\|_\infty$ is reflected in Fig. 2.1.1 in both the maximum norm of the actual error and the error bound (2.1.27), e.g. in the latter the linear line of best fit has gradient $\log 1/4$, as predicted by (2.1.29).

Our aim is to modify the standard Nyström method in such a way that, if $\overline{u}_n$ is the numerical solution of the new modified Nyström method, we require

$$\|u-\overline{u}_n\| \ll \|u-u_n\|, \tag{2.1.30}$$

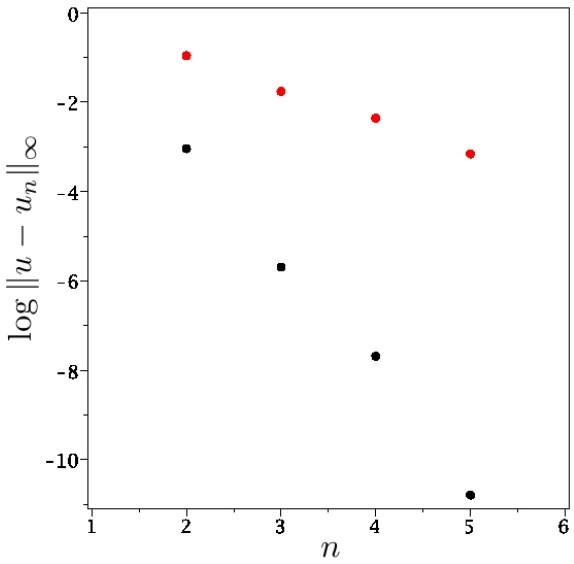

Figure 2.1.1: *Log plot of the maximum norm of the actual Nyström error* $\|u - u_n\|_\infty$ *(black) and the error bound* (2.1.27) *(red) for the test FIE2 with kernel* $K(T,S) = \exp(-T^2 S)$*,* $\Lambda = 1/2$*,* $[a,b] = [-\frac{2}{3}, \frac{1}{3}]$*,* $\mu = 1/2$*,* $\nu = 1/3$ *and exact solution* $U(S) = \exp(S)\cos(S)$ *for different values of* n*. The exponential convergence of the actual error of the Nyström method is evident here for increasing* n*. As is the exponential convergence of error bound* (2.1.27)*, whose line of best fit through the logarithmic data is linear with a gradient of* $\log 1/4$*, as predicted by* (2.1.29)*.*

particularly for low values of n in order to maximise the potential for practical applications.

2.2 The modified Nyström method

In order to modify the standard Nyström method of §2.1, we shall first establish the nomenclature following that in Kelmanson and Tenwick [2009, 2010]. Recalling $\mathcal{E}_n \equiv \mathcal{K} - \mathcal{K}_n$ in (2.1.8), the basis of the modified Nyström method lies in finding an error $\widetilde{\mathcal{E}}_n u$ where

$$\widetilde{\mathcal{E}}_n \approx \mathcal{K} - \mathcal{K}_n, \tag{2.2.1}$$

whose effect is incorporated *a priori* into the standard Nyström method to achieve condition (2.1.30). That is, we augment the standard Nyström method such that

$$\overline{u}_n - \lambda(\mathcal{K}_n \overline{u}_n + \widetilde{\mathcal{E}}_n \overline{u}_n) = f, \tag{2.2.2}$$

where $\overline{u}_n$ denotes the solution of the modified Nyström method and, consistent with (2.1.12), we hypothesise

$$\|\widetilde{\mathcal{E}}_n\mathcal{K}\|, \|\widetilde{\mathcal{E}}_n\mathcal{K}_n\| \to 0, \quad n \to \infty. \tag{2.2.3}$$

The difference between the real error $\mathcal{E}_n u$ and its approximate counterpart $\widetilde{\mathcal{E}}_n u$ is denoted as the *error discrepancy*

$$(\Delta\widetilde{\mathcal{E}}_n u)(t) \equiv ((\widetilde{\mathcal{E}}_n - \mathcal{E}_n)u)(t), \tag{2.2.4}$$

whose norm converges in a pointwise sense

$$\|\Delta\widetilde{\mathcal{E}}_n u\| \to 0, \quad n \to \infty, \tag{2.2.5}$$

for suitably continuous functions $u(t)$ and must, by construction, satisfy

$$\|\Delta\widetilde{\mathcal{E}}_n\| \to 0, \quad n \to \infty. \tag{2.2.6}$$

Equations (2.0.10), (2.2.2) and (2.2.4) define the *modified Nyström error* as the solution of the perturbed FIE2

$$(\mathcal{I} - \lambda\mathcal{K}_n - \lambda\widetilde{\mathcal{E}}_n)(u - \overline{u}_n) = \lambda\Delta\widetilde{\mathcal{E}}_n u, \tag{2.2.7}$$

which should be compared with the "standard" error (2.1.14). Furthermore, (2.2.7) demonstrates the dependence of the modified Nyström error upon the existence of the inverse of $(\mathcal{I}-\lambda\mathcal{K}_n-\lambda\widetilde{\mathcal{E}}_n)$ which, by (2.1.8) and (2.2.4), is equivalent to

$$(\mathcal{I} - \lambda\mathcal{K} - \lambda\Delta\widetilde{\mathcal{E}}_n). \tag{2.2.8}$$

Hence the modified Nyström method (2.2.2) can be alternatively stated as

$$(\mathcal{I} - \lambda\mathcal{K} - \lambda\Delta\widetilde{\mathcal{E}}_n)\overline{u}_n = f. \tag{2.2.9}$$

Thus, the evaluation of the modified Nyström error (2.2.7) depends upon the invertibility of the operator $(\mathcal{I} - \lambda\mathcal{K} - \lambda\Delta\widetilde{\mathcal{E}}_n)$. To prove this, we consider the identity (Kelmanson and Tenwick [2010])

$$(\mathcal{I} - \lambda\mathcal{K} - \lambda\Delta\widetilde{\mathcal{E}}_n)^{-1} = (\mathcal{I} - \lambda(\mathcal{I} - \lambda\mathcal{K})^{-1}\Delta\widetilde{\mathcal{E}}_n)^{-1}(\mathcal{I} - \lambda\mathcal{K})^{-1}, \tag{2.2.10}$$

in which $(\mathcal{I} - \lambda\mathcal{K})^{-1}$ exists by (2.0.11). Defining

$$\mathcal{A}_n = \lambda(\mathcal{I} - \lambda\mathcal{K})^{-1}\Delta\widetilde{\mathcal{E}}_n, \tag{2.2.11}$$

the limit in (2.2.6) implies there exists a sufficiently large $N \in \mathbb{N}$ such that (Groh and Kelmanson [2008])

$$\|\mathcal{A}_n\| \leq |\lambda|\|(\mathcal{I}-\lambda\mathcal{K})^{-1}\|\|\Delta\widetilde{\mathcal{E}}_n\| < 1, \quad n \geq N. \tag{2.2.12}$$

Thus $(\mathcal{I}-\mathcal{A}_n)^{-1}$ may be expanded by the geometric series theorem as the Neumann series

$$(\mathcal{I}-\mathcal{A}_n)^{-1} = \sum_{j=0}^{\infty} A_n^j, \tag{2.2.13}$$

from which

$$\|(\mathcal{I}-\mathcal{A}_n)^{-1}\| \leq \frac{1}{1-\|\mathcal{A}_n\|},$$

i.e.

$$\|(\mathcal{I}-\lambda(\mathcal{I}-\lambda\mathcal{K})^{-1}\Delta\widetilde{\mathcal{E}}_n)^{-1}\| \leq \frac{1}{1-|\lambda|\|(\mathcal{I}-\lambda\mathcal{K})^{-1}\|\|\Delta\widetilde{\mathcal{E}}_n\|}. \tag{2.2.14}$$

Hence provided the standard FIE2 (2.0.11) has a unique solution the limit in (2.2.6) exists, and we have

$$\|(\mathcal{I}-\lambda\mathcal{K}_n-\lambda\widetilde{\mathcal{E}}_n)^{-1}\| \leq \zeta_n, \tag{2.2.15}$$

for some finite constant, ζ_n say. Thus the modified Nyström error (2.2.7) is bounded such that

$$\|u-\overline{u}_n\|_\infty \leq \zeta_n|\lambda|\|\Delta\widetilde{\mathcal{E}}_n u\|_\infty, \tag{2.2.16}$$

i.e. the modified Nyström error is proportional to an *error discrepancy*. By contrast, (2.1.26) may be written as

$$\|u-u_n\|_\infty \leq \xi_n|\lambda|\|\mathcal{E}_n u\| \tag{2.2.17}$$

in which, by construction,

$$\|\Delta\widetilde{\mathcal{E}}_n u\| \ll \|\mathcal{E}_n u\|. \tag{2.2.18}$$

Therefore, by (2.2.16)-(2.2.18) we have

$$\|u-\overline{u}_n\|_\infty \ll \|u-u_n\|_\infty, \tag{2.2.19}$$

thereby achieving condition (2.1.30).

2.2.1 Implementation of the modified Nyström method

As shown in §2.3, the standard and approximate Nyström error operands, $\mathcal{E}_n$ and $\widetilde{\mathcal{E}}_n$, are differential operators whose direct action upon the unknown function $\overline{u}_n$ in (2.2.9) is prevented by expressing (2.2.9) in the implicit form

$$\overline{u}_n = f + \lambda(\mathcal{K}_n + \widetilde{\mathcal{E}}_n)\overline{u}_n, \tag{2.2.20}$$

and then recursively replacing $\overline{u}_n$ that is directly acted upon by $\widetilde{\mathcal{E}}_n$. That is, by applying M Neumann iterations to $\overline{u}_n$ whenever it occurs at the operand of $\widetilde{\mathcal{E}}_n$ yields

$$\overline{u}_n = \sum_{m=0}^{M} (\lambda\widetilde{\mathcal{E}}_n)^m f + \lambda \sum_{m=0}^{M} (\lambda\widetilde{\mathcal{E}}_n)^m \mathcal{K}_n \overline{u}_n + (\lambda\widetilde{\mathcal{E}}_n)^{M+1}\overline{u}_n, \quad M > 0. \tag{2.2.21}$$

By introducing the linear operator

$$\widetilde{\mathcal{E}}_n^{(\lambda,M)} \equiv \sum_{m=1}^{M} (\lambda\widetilde{\mathcal{E}}_n)^m, \tag{2.2.22}$$

(2.2.21) can be represented in the more compact form

$$(\mathcal{I} - \lambda\mathcal{K}_n - \lambda\widetilde{\mathcal{E}}_n^{(\lambda,M)}\mathcal{K}_n - (\lambda\widetilde{\mathcal{E}}_n)^{M+1})\overline{u}_n^{(M)} = f + \widetilde{\mathcal{E}}_n^{(\lambda,M)} f, \tag{2.2.23}$$

where the M^{th} iteration of $\overline{u}_n$ using (2.2.20) is denoted by $\overline{u}_n^{(M)}$. Here we take $\widetilde{\mathcal{E}}_n^{(\lambda,0)} \equiv 0$ and $\overline{u}_n^{(0)} \equiv 0$ so that the standard Nyström method (2.1.13) is recovered when $M = 0$. The standard Nyström error $\mathcal{E}_n u$ is a high-order differential whose order is dependent upon n: by construction, so is $\widetilde{\mathcal{E}}_n u$. However, as $\overline{u}_n^{(M)}$ is yet to be determined, the error term $\widetilde{\mathcal{E}}_n^{M+1}\overline{u}_n^{(M)}$ in (2.2.23) cannot be found explicitly, and so has to be neglected. This is justified if and only if

$$\|\lambda^{M+1}\widetilde{\mathcal{E}}_n^{M+1}\| \ll \|\mathcal{I} - \lambda\mathcal{K}_n - \lambda\widetilde{\mathcal{E}}_n^{(\lambda,M)}\mathcal{K}_n\| \leq \|\mathcal{I} - \lambda\mathcal{K}_n\| + |\lambda|\|\widetilde{\mathcal{E}}_n^{(\lambda,M)}\mathcal{K}_n\|, \tag{2.2.24}$$

which, due Eqn. (2.2.22) and the pointwise convergence of $\widetilde{\mathcal{E}}_n\mathcal{K}_n$ in (2.2.3), leads to

$$\|\widetilde{\mathcal{E}}_n^{M+1}\| \leq \frac{\|\mathcal{I} - \lambda\mathcal{K}_n\|}{|\lambda^{M+1}|}, \quad n \to \infty. \tag{2.2.25}$$

This bound, referred to as the *truncation condition*, becomes increasingly stringent when $|\lambda| > 1$. Provided condition (2.2.25) holds, (2.2.23) may then be approximated as

$$\left(\mathcal{I} - \lambda\mathcal{K}_n - \lambda\widetilde{\mathcal{E}}_n^{(\lambda,M)}\mathcal{K}_n\right)\overline{u}_n^{(M)} = f + \widetilde{\mathcal{E}}_n^{(\lambda,M)} f, \tag{2.2.26}$$

in which $\widetilde{\mathcal{E}}_n^{(\lambda,M)}$ now acts upon the known $\mathcal{K}_n$ and f only, both of which are computable. The modified Nyström method (2.2.26) yields an approximate solution of FIE2 (2.0.2) whose error is characterised by Eqn. (2.2.19). The method is entirely novel, and shall be implemented on several test problems.

2.2.2 Collocation equations

Before implementing the modified Nyström method (2.2.26), we first look at the standard Nyström method and the conditions thereupon. Taking a finite-dimensional space of candidate solutions evaluated at a series of collocation points $t = \sigma_i$, $i = 1, \ldots, n$, that are the roots of the Jacobi polynomial $P_n(t; \mu, \nu)$, a system of n linear equations are generated for the n nodal Nyström values $u_n(\sigma_i)$. Consequently, the collocated matrix-vector counterpart of the discrete approximation of the FIE2 (2.1.13)

$$(\mathbf{I} - \lambda\mathbf{K})\mathbf{u_n} = \mathbf{f}, \tag{2.2.27}$$

is satisfied by the n-dimensional vector $(\mathbf{u_n})_i = u_n(\sigma_i)$, where $\mathbf{I}$ is the $n \times n$ identity matrix and the components of $\mathbf{K}$ and $\mathbf{f}$ are respectively $K_{i,j} = c_{j,n}k(\sigma_i, \sigma_j)$ and $f_i = f(\sigma_i)$ for $i, j = 1, \ldots, n$. The nodal $u_n(\sigma_i)$ from system (2.2.27) are then used in (2.1.13) to interpolate a spectrally accurate solution for other source points in the interval. Furthermore, by Atkinson [1997, Eqn. 4.1.54],

$$\|(\mathbf{I} - \lambda\mathbf{K})^{-1}\|_\infty \leq \|(\mathcal{I} - \lambda\mathcal{K}_n)^{-1}\|, \tag{2.2.28}$$

the right-hand side of which is, by (2.1.24), bounded. Thus $(\mathbf{I} - \lambda\mathbf{K})$ is indeed invertible in (2.2.28) and $\mathbf{u_n}$ in (2.2.27) can be found.

In practice the systems in (2.2.27) and (2.2.29) are usually solved by LU-factorisation, in which an n-point quadrature yields a system that is inverted in $2n^3/3$ floating point operations. The $\mathcal{O}(n^3)$ cost of the Nyström-system inversion motivates, to some extent, the new modified-Nyström approach, in which improved accuracy is sought using low-order quadrature rules.

The application of a collocation method to the modified Nyström method (2.2.26) at the points $t = \sigma_i$ similarly results in a n-dimensional vector $\overline{\mathbf{u}}_\mathbf{n}^{(\mathbf{M})}$ consisting of nodal values $\overline{u}_n^{(M)}(\sigma_i)$. This new vector satisfies

$$(\mathbf{I} - \lambda\mathbf{K} - \lambda\widetilde{\mathcal{E}}_n^{(\lambda,M)}\mathbf{K})\overline{\mathbf{u}}_\mathbf{n}^{(\mathbf{M})} = \mathbf{f} + \widetilde{\mathcal{E}}_n^{(\lambda,M)}\mathbf{f}, \tag{2.2.29}$$

where the components of $\mathbf{K}$ and $\mathbf{f}$ are identical to those in the standard Nyström method; in addition, those of $\widetilde{\mathcal{E}}_n^{(\lambda,M)}\mathbf{K}$ and $\widetilde{\mathcal{E}}_n^{(\lambda,M)}\mathbf{f}$ require the explicit definition of $\widetilde{\mathcal{E}}_n^{(\lambda,M)}$.

Provided the operator $\widetilde{\mathcal{E}}_n$ closely approximates the existing quadrature operator $\mathcal{E}_n$, both should possess the same quantitative properties. For example, following (2.1.9), $\widetilde{\mathcal{E}}_n u$ also converges to zero in the pointwise sense,

$$(\widetilde{\mathcal{E}}_n u)(t) \to 0, \quad n \to \infty. \tag{2.2.30}$$

This implies that the linear operator $\widetilde{\mathcal{E}}_n^{(\lambda,M)}$ consisting of higher powers of $\widetilde{\mathcal{E}}_n$ acting upon a given matrix $\mathbf{A} = A_{i,j}$,

$$\widetilde{\mathcal{E}}_n^{(\lambda,M)}\mathbf{A} = \sum_{m=1}^{M} \lambda^m \widetilde{\mathcal{E}}_n^m A_{i,j}, \tag{2.2.31}$$

converges in a pointwise sense with increasing n. That is, for all $\mathbf{A}$,

$$\|\widetilde{\mathcal{E}}_n^{(\lambda,M)}\mathbf{A}\|_\infty \to 0, \quad n \to \infty. \tag{2.2.32}$$

Therefore, given the proven invertibility of $(\mathbf{I} - \lambda\mathbf{K})$ in the standard Nyström system, $(\mathbf{I} - \lambda\mathbf{K} - \lambda\widetilde{\mathcal{E}}_n^{(\lambda,M)}\mathbf{K})$ in (2.2.29) is invertible if (Golub and Van Loan [1996], Groh and Kelmanson [2008])

$$\|\lambda(\mathbf{I} - \lambda\mathbf{K})^{-1}\widetilde{\mathcal{E}}_n^{(\lambda,M)}\mathbf{K}\|_\infty < 1, \tag{2.2.33}$$

i.e.

$$|\lambda|\|(\mathbf{I} - \lambda\mathbf{K})^{-1}\|_\infty \|\widetilde{\mathcal{E}}_n^{(\lambda,M)}\mathbf{K}\|_\infty < 1, \tag{2.2.34}$$

and this is indeed guaranteed for sufficiently large n because of (2.2.32).

2.3 Error analysis

We now consider the explicit form of the error $\mathcal{E}_n u$ and its approximation $\widetilde{\mathcal{E}}_n u$ required for the implementation of the modified Nyström method. For *any* given orthogonal-polynomial quadrature rule, the explicit form of the error $(\mathcal{E}_n u)(t)$ is (Ralston and Rabinowitz [2001], Gautschi [2004])

$$(\mathcal{E}_n^* u)(t, s^*) \equiv \beta_n \delta_n^*(u; t, s^*), \tag{2.3.1}$$

where, by the mean-value theorem,

$$\beta_n = \frac{\gamma_n}{A_n^2(2n)!} \quad \text{and} \quad \delta_n^*(u;t,s^*) = \left[\frac{\partial^{2n}}{\partial s^{2n}}(k(t,s)u(s))\right]_{s=s^*} \tag{2.3.2}$$

for some undefined $s^* \in [-1,1]$. Using A_n and γ_n in (2.1.5) and (2.1.6) respectively, for the Gauss-Jacobi polynomials $P_n(s;\mu,\nu)$,

$$\beta_n = \frac{2^{\mu+\nu+1}\sqrt{\pi}\,\Gamma(n+\nu+1)\,\Gamma(n+\mu+1)\,\Gamma(n+\mu+\nu+1)}{\Gamma(n+\frac{1}{2})\,\Gamma(2n+\mu+\nu+1)\,\Gamma(2n+\mu+\nu+2)}, \tag{2.3.3}$$

whose asymptotic behaviour (Kelmanson and Tenwick [2010]) yields

$$\frac{\beta_{n+1}}{\beta_n} \sim \frac{1}{16n^2} - \frac{3}{32n^3} + \frac{4-\mu^2-\nu^2}{32n^4} + \mathcal{O}(n^{-5}), \quad n \to \infty. \tag{2.3.4}$$

This demonstrates the exponential convergence of β_n to zero with increasing n *independent* of the choice of μ and ν. A rather more complicated manipulation (Kelmanson and Tenwick [2010]) of (2.3.3) yields the asymptotic formula

$$\beta_n \sim \frac{\pi}{2^{2n+\mu+\nu}(2n)!}\left(1 + \frac{2\mu^2+2\nu^2-1}{4n} + O(n^{-2})\right), \quad n \to \infty, \tag{2.3.5}$$

which is highly accurate, even for low values of n. For example, when $\mu = \nu = \frac{1}{4}$, the two-term asymptotic series for β_n in (2.3.5) is in error from the true value in (2.3.3) by 3.01%, 1.45% and 0.86% for $n = 2, 3$ and 4 respectively. Alternatively, for $\mu = \nu = -\frac{1}{2}$, $P_n(s;\mu,\nu) = T_n(s)$, the Chebyshev polynomial of the first kind, and for $\mu = \nu = \frac{1}{2}$, $P_n(s;\mu,\nu) = U_n(s)$, the Chebyshev polynomial of the second kind, the coefficient of every inverse power of n in series (2.3.5) vanishes so that, without error,

$$\beta_n = \frac{\pi}{2^{2n\pm1}(2n)!}, \quad \mu = \nu = \pm\frac{1}{2}, \forall n. \tag{2.3.6}$$

When $\mu = \nu = 0$ the weight function $W(S)$ in (2.0.4) is simply equal to unity hence $\widetilde{K}(T,S)$, by (2.0.3), is a nonsingular kernel such that it is infinitely-continuously differentiable and exists for all $T, S \in [a,b]$. In this case, Gauss-Jacobi quadrature is equivalent to Gauss-Legendre quadrature, i.e. $P_n(s;\mu,\nu) = P_n(s)$, the Legendre polynomial of the first kind, and the constant β_n in (2.3.2) takes the form

$$\beta_n = \frac{2^{2n+1}(n!)^4}{(2n+1)\,[(2n)!]^3}, \tag{2.3.7}$$

with asymptotic behaviour (Kelmanson and Tenwick [2009])

$$\beta_n \to \frac{\pi}{4^n(2n)!}, \quad n \to \infty. \tag{2.3.8}$$

The error $\mathcal{E}_n u$ in (2.3.1) cannot be explicitly implemented in the modified Nyström method as δ_n^* contains the undetermined parameter s^*. To overcome this, we apply the integral mean-value theorem to $\delta_n^*(u;t)$ to obtain

$$\delta_n^* = \overline{\delta}_n + \epsilon_n^*, \tag{2.3.9}$$

where

$$\overline{\delta}_n(u;t) = \frac{1}{2}\left[\frac{\partial^{2n-1}}{\partial s^{2n-1}}\left[k(t,s)u(s)\right]\right]_{s=-1}^{s=1}, \tag{2.3.10}$$

in which $u(s)$ must be $(2n-1)$-times continuously differentiable for all s because $k(t,s)$ satisfies this property by construction. By the hypothesis $\|\epsilon_n^*\| \ll \|\overline{\delta}_n\|$ for all n, (2.3.1) and (2.3.9) yield the *computable* predicted error as

$$(\overline{\mathcal{E}}_n u)(t) \equiv \beta_n \overline{\delta}_n(u;t), \tag{2.3.11}$$

which approximates the true error $(\mathcal{E}_n^* u)(t, s^*)$ with a sub-error of order $O(\beta_n \epsilon_n^*)$. We now define the true and computable *error discrepancies* respectively as

$$\Delta\mathcal{E}_n^* u \equiv (\mathcal{E}_n - \mathcal{E}_n^*)u \tag{2.3.12}$$

and

$$\Delta\overline{\mathcal{E}}_n u \equiv (\mathcal{E}_n - \overline{\mathcal{E}}_n)u. \tag{2.3.13}$$

Computation of the predicted quadrature error (2.3.11) requires, by (2.3.10), a knowledge of the solution $u(s)$. Although one could use finite-difference schemes, this is impractical for high-order derivatives. An advantage of the new modified Nyström method is the circumvention of the need to estimate the derivatives in (2.3.10) explicitly. This is so because $\overline{\mathcal{E}}_n$ in (2.3.11) acts directly upon $\mathcal{K}_n$ and f only by the argument immediately following (2.2.26).

2.3.1 Validation of the predicted error

To validate the predicted quadrature error (2.3.11), we quantify the error discrepancies (2.3.12) and (2.3.13) using series of prespecified test problems. The test problems in both this section and the remainder of the chapter are based on the FIE2

$$U(T) = F(T) + \Lambda \int_{-\frac{5}{3}}^{\frac{2}{3}} \left(\frac{2}{3} - S\right)^{\mu} \left(S + \frac{5}{3}\right)^{\nu} \exp(-T^2 S) U(S)\, dS, \tag{2.3.14}$$

where given a known exact solution $U(S) = \exp(S)\cos(S)$, the forcing function is defined by

$$F(T) = \exp(T)\cos(T) - \Lambda \int_{-\frac{5}{3}}^{\frac{2}{3}} \left(\frac{2}{3} - S\right)^{\mu} \left(S + \frac{5}{3}\right)^{\nu} \exp(-T^2 S)\exp(S)\cos(S)\ dS. \tag{2.3.15}$$

For example, taking $n = 2, 4, 6, 8$ the theory is tested for FIE2 (2.3.14) with parameters $\mu = \frac{1}{2}$ and $\nu = \frac{1}{3}$. Results are presented in Fig. 2.3.1, which demonstrates two facts: first, $\Delta\overline{\mathcal{E}}_n u(t)$ is both smaller in modulus and more uniform than the true error discrepancy $\Delta\mathcal{E}_n^* u(t, s^*)$; second, the convergence of the true and predicted error discrepancies indeed satisfies

$$\|\Delta\mathcal{E}_n^* u\|_\infty, \|\Delta\overline{\mathcal{E}}_n u\|_\infty \to 0 \quad n \to \infty, \tag{2.3.16}$$

as required by (2.2.5).

For a given function $F(p)$, its root-mean-square, denoted by $\sigma(F)$, is defined as

$$\sigma(F) \equiv \sqrt{\frac{1}{M}\sum_{i=1}^{M} [F(t_{i,M})]^2}, \tag{2.3.17}$$

where M is the number of mesh points $t_{i,M}$ over the internal grid. Using (2.3.17), the root-mean-square values of $\Delta\mathcal{E}_n^* u$ and $\Delta\overline{\mathcal{E}}_n u$ in Fig. 2.3.1 are given in Table 2.3.1. The data shows the mean of the predicted error discrepancy is smaller than the mean of the true discrepancy and closer to the exact global discrepancy $(\Delta\mathcal{E}_n u) = 0$. Thus the predicted error $\overline{\mathcal{E}}_n$, which is closer to the exact global error, is potentially suited for FIE2s with oscillatory kernels $\widetilde{K}(T, S)$ as it takes the mean-value of the oscillating data.

Further comparisons of the exact error $\mathcal{E}_n u(t)$ in (2.1.9) against its predicted $\overline{\mathcal{E}}_n u(t)$ counterpart can be seen in Fig. 2.3.2. In keeping with the discrepancy comparisons demonstrated in Fig. 2.3.1, the error comparisons of Fig. 2.3.2 indicate good prediction of the true error by the predicted error, where the slight discrepancy between lines and circles quantifies the sub-error ϵ_n^* in (2.3.9). In summary, we have demonstrated the ability to predict, with quantifiable accuracy, the action of the error operator $\overline{\mathcal{E}}_n$ that is key to the application of the new modified Nyström method.

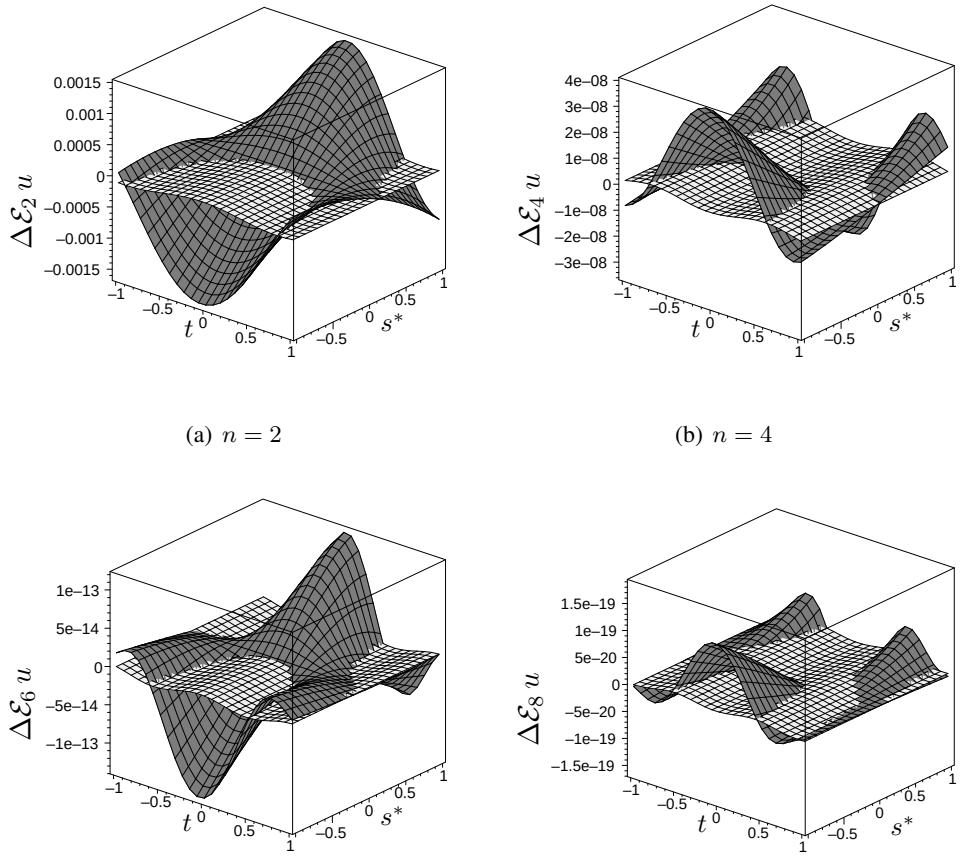

(a) $n = 2$ (b) $n = 4$

(c) $n = 6$ (d) $n = 8$

Figure 2.3.1: *True error discrepancy* $\Delta\mathcal{E}_n^* u(t, s^*)$ *(dark) and predicted error discrepancy* $\Delta\overline{\mathcal{E}}_n u(t)$ *(light), for* $n = 2, 4, 6, 8$ *in* (2.3.12) *and* (2.3.13) *for a singular kernel function using Gauss-Jacobi quadrature with* $\mu = \frac{1}{2}$ *and* $\nu = \frac{1}{3}$ *in the test FIE2* (2.3.14)*.*

2.4 Comparison of numerical schemes

The theory of §2.1- §2.3 is now used to test the standard Nyström method against the modified Nyström method for both nonsingular and singular kernel functions. Based upon the findings of §2.3, we take $\overline{\mathcal{E}}_n u$ to approximate $\widetilde{\mathcal{E}}_n u$ in the implementation of the modified Nyström method, in which the required terms are therefore $(\overline{\mathcal{E}}_n^{(\lambda,M)}\mathbf{K})_{ij}$ and $(\overline{\mathcal{E}}_n^{(\lambda,M)}\mathbf{f})_i$, previously seen in the vector-

n	$\sigma(\Delta\mathcal{E}_n^* u)$	$\sigma(\Delta\overline{\mathcal{E}}_n u)$
2	6.1984×10^{-4}	7.8009×10^{-5}
4	1.3465×10^{-8}	1.9759×10^{-9}
6	4.1956×10^{-14}	6.4700×10^{-15}
8	1.5386×10^{-19}	1.5008×10^{-19}

Table 2.3.1: *The true root-mean-square error of $\Delta\mathcal{E}_n^* u$ and the predicted root-mean-square error of $\Delta\overline{\mathcal{E}}_n u$. Here we have a quantification of the errors in Fig. 2.3.1. The mean value of the predicted error discrepancy is both smaller than the mean value of the true discrepancy and closer to the exact global discrepancy $(\Delta\mathcal{E}_n u) = 0$.*

matrix system (2.2.29). Defining

$$\mathcal{D}_{n,r}\left[F(s_r)\right] \equiv \frac{\lambda\beta_n}{2}\,\frac{\partial^{2n-1}}{\partial s_r^{2n-1}}\left[F(s_r)\right]\Big|_{s_r=-1}^{s_r=1}, \tag{2.4.1}$$

then, by the definition of the error operator $\overline{\mathcal{E}}_n$ in (2.3.10) and (2.3.11),

$$\begin{aligned}(\overline{\mathcal{E}}_n^{(\lambda,M)}\mathbf{K})_{ij} = c_{j,n}\,(&\mathcal{D}_{n,1}[k(\sigma_i,s_1)k(s_1,\sigma_j)]\\ &+\mathcal{D}_{n,1}\left[k(\sigma_i,s_1)\mathcal{D}_{n,2}\left[k(s_1,s_2)k(s_2,\sigma_j)\right]\right]+\ldots),\end{aligned} \tag{2.4.2}$$

and

$$(\overline{\mathcal{E}}_n^{(\lambda,M)}\mathbf{f})_i = \mathcal{D}_{n,1}[k(\sigma_i,s_1)f(s_1)] + \mathcal{D}_{n,1}\left[k(\sigma_i,s_1)\mathcal{D}_{n,2}\left[k(s_1,s_2)f(s_2)\right]\right]+\ldots, \tag{2.4.3}$$

each terminating with $\mathcal{D}_{n,M}$. Here the components of (2.4.2) and (2.4.3) comprise increasing powers of β_n that, by (2.3.4), converge exponentially to zero with increasing n. By (2.3.1), (2.3.9) and (2.3.11), along with $\|\widetilde{\mathcal{E}}_n - \overline{\mathcal{E}}_n\| = O(\beta_n\epsilon_n^*)$, it is clear that $\|\widetilde{\mathcal{E}}_n - \overline{\mathcal{E}}_n\| \to 0$ exponentially with n. Hence the M-term truncation (2.2.22) should approximate the action of $\overline{\mathcal{E}}_n$ for relatively low values of M; a maximum of $M = 3$ will be imposed in the subsequent numerical implementations. The modified Nyström method of §2.2 was implemented and validated for the test FIE2 (2.3.14) with known exact solution $U(S)$ and varying parameters Λ, μ and ν: the corresponding forcing function $F(T)$ and quadrature rule $\mathcal{K}_n$ were generated using (2.3.15) and (2.1.3) respectively. For notational convenience, we introduce the *modified Nyström error*,

$$e_n^{(M)}u(t) \equiv \|u - \overline{u}_n^{(M)}\|_\infty, \quad M \geq 0. \tag{2.4.4}$$

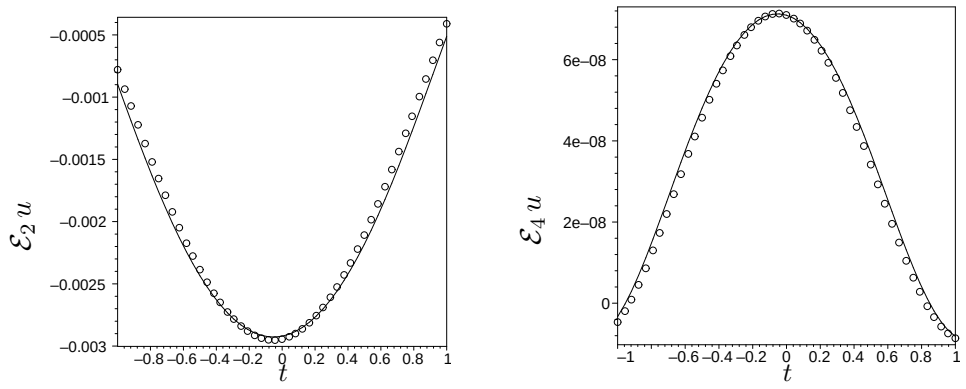

(a) $n = 2$ (b) $n = 4$

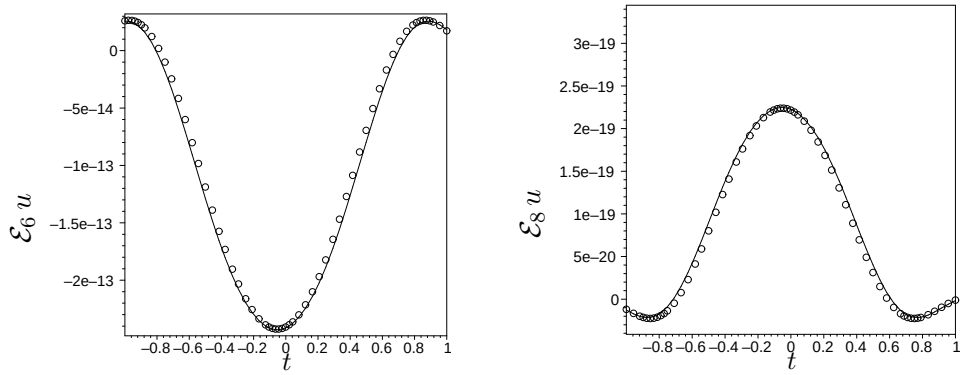

(c) $n = 6$ (d) $n = 8$

Figure 2.3.2: *Actual error $\mathcal{E}_n u(t)$ (line) and predicted error $\overline{\mathcal{E}}_n u(t)$ (circles) for $n = 2, 4, 6, 8$ in* (2.1.9) *and* (2.3.11)*, computed using the Gauss-Jacobi quadrature of* (2.1.3)*. The test problem is the same as that used in Fig. 2.3.1. It is evident that discrepancy between both the curves scales with β_n and reflects the truncation ϵ_n^* in* (2.3.10)*.*

Recalling that the original aim was to obtain improved accuracy in the modified Nyström approach for low values of n over the standard Nyström approach, Figs. 2.4.1-2.4.5 show the modified Nyström error (2.4.4) for low orders of quadrature for test FIE2 (2.3.14). For the results in Fig. 2.4.1 we take $\mu = \nu = 0$ to which we recover identical results to those generated independently by Gauss-Legendre quadrature (Kelmanson and Tenwick [2009]). Fig. 2.4.1 shows the modified Nyström error for the lowest possible order of quadrature n, where each separate sub-figure is for

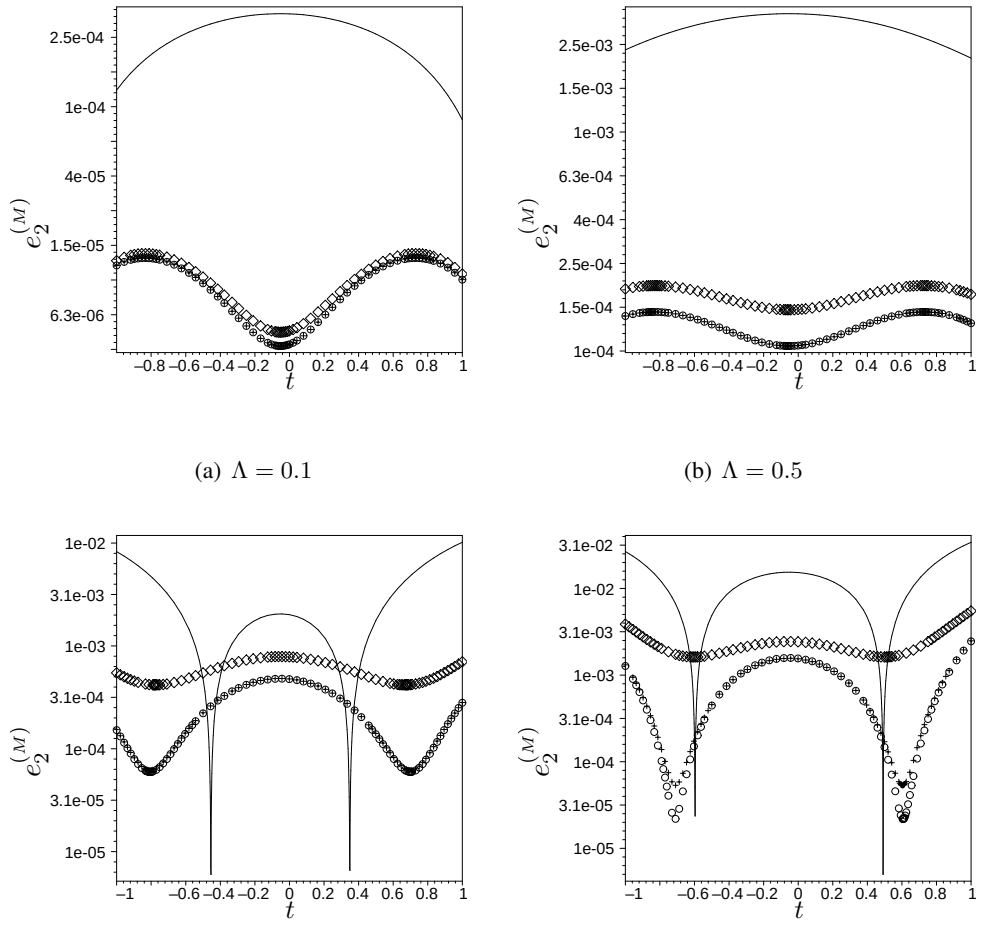

(a) $\Lambda = 0.1$ (b) $\Lambda = 0.5$

(c) $\Lambda = 5$ (d) $\Lambda = 25$

Figure 2.4.1: *The modified Nyström errors* $e_n^{(M)}u(t)$ *of* (2.4.4) *for fixed* $n = 2$ *and different values of* Λ*, computed using Gauss-Jacobi quadrature* (2.1.3)*. The above numerical experiment uses* $\mu = \nu = 0$ *in the test FIE2* (2.3.14)*. Successive modifications of the standard Nyström error,* $M = 0$ $(-)$*, are shown by* $M = 1$ $(\diamond)$*,* $M = 2$ $(\circ)$ *and* $M = 3$ $(+)$*. Validating computations using Gauss-Legendre quadrature yield results indistinguishable from those presented. These results are also comparable with those in Kelmanson and Tenwick [2009].*

a fixed value of Λ and separate curves on each sub-figure are for different values of M.

In Fig. 2.4.1 we note an impressive error reduction due to simply taking first-order error terms (i.e. $M = 1$) in the modified Nyström method, for a crude quadrature based on only $n = 2$ nodes. Fig. 2.4.1 also demonstrates two features: first, the convergence to zero of $e_n^{(M)}$ with M is most

pronounced for $|\Lambda| \ll 1$ and least so for $|\Lambda| \gg 1$. This follows since (2.4.2) and (2.4.3) are power series in $\lambda\beta_n$, equivalently $\Lambda\beta_n$ via (2.0.6), so that the convergence of the error $\|\widetilde{\mathcal{E}}_n - \overline{\mathcal{E}}_n\|$ is eroded as $|\Lambda|$ increases. Second, the results for $M = 2$ and $M = 3$ are indistinguishable for any Λ, which indicates that the exponential decay of β_n with n leads to negligible changes in computed data for M as low as 3.

An identical trend in the behaviour of the modified Nyström error of Fig. 2.4.1 reoccurs in Figs. 2.4.2 and 2.4.3, in which $\mu = \nu = -\frac{1}{2}$ and $\mu = \nu = \frac{1}{2}$ matching Gauss-Chebyshev (of the first and second kind) quadrature.

In Figs. 2.4.4 and 2.4.5 the number of nodes in the quadrature are varied as $n = 2$ and $n = 3$ respectively for a highly singular test FIE2 in which $\mu = -\frac{4}{5}$ and $\nu = -\frac{9}{10}$. In Fig. 2.4.4(d) the modified Nyström error when $M = 3$ is uniformly larger than that when $M = 2$, which indicates a violation of condition (2.2.25) for $|\Lambda| \gg 1$. However, as Fig. 2.4.5(d) reveals, condition (2.2.25) can be recovered by increasing n. Fig. 2.4.5 also demonstrates no gained accuracy in the modified Nyström method by taking $M > 1$ when $n = 3$; the exponential convergence of β_n in (2.3.4) means that the omitted error ϵ_n^* in operator $\overline{\mathcal{E}}_n$ determines the accuracy threshold that can be achieved.

When $|b-a| > 2$, the domain must be broken into subintervals: if not, then the power series (2.4.2) and (2.4.3) will diverge when $\lambda\beta_n > 1$ via the scaling (2.0.6). The domain division ensures that $\lambda\beta_n < 1$ in all subintervals. An in-depth analysis of such an amendment is considered in detail in the following chapter.

Finally, note that the inclusion of M error terms in the modified Nyström method requires a greater number of operations to be undertaken than the standard Nyström method in order to obtain the approximate solution $\overline{u}_n^{(M)}$, as evidenced by the increase in CPU system times of 626%, 2813% and 8220% respectively for $M = 1, 2$ and 3 from the CPU system time for $M = 0$.

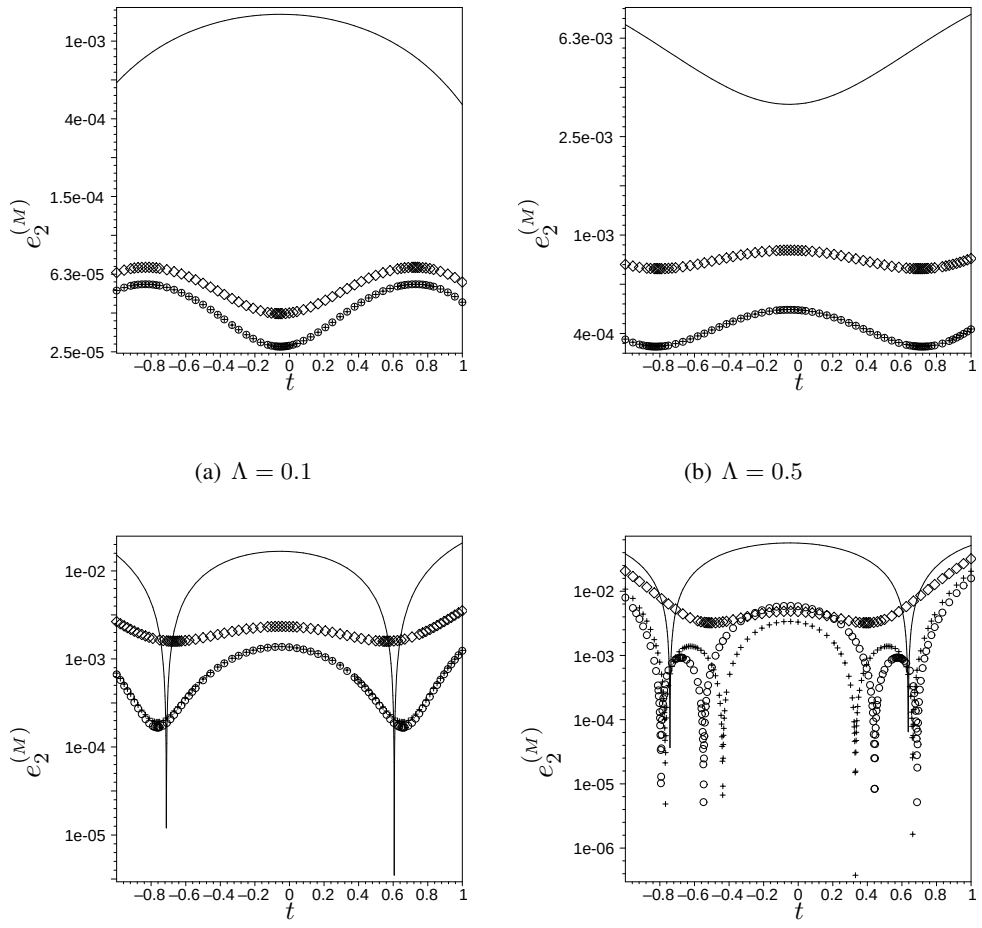

(a) $\Lambda = 0.1$

(b) $\Lambda = 0.5$

(c) $\Lambda = 5$

(d) $\Lambda = 25$

Figure 2.4.2: *The modified Nyström errors* $e_n^{(M)}u(t)$ *of* (2.4.4) *for fixed* $n = 2$ *and different values of* Λ*, computed using Gauss-Jacobi quadrature* (2.1.3)*. The above numerical experiment uses* $\mu = \nu = -\frac{1}{2}$ *in the test FIE2* (2.3.14)*. Successive modifications of the standard Nyström error,* $M = 0$ $(-)$*, are shown by* $M = 1$ $(\diamond)$*,* $M = 2$ $(\circ)$ *and* $M = 3$ $(+)$*. Validating computations using Gauss-(first-kind-)-Chebyshev quadrature yield results indistinguishable from those presented.*

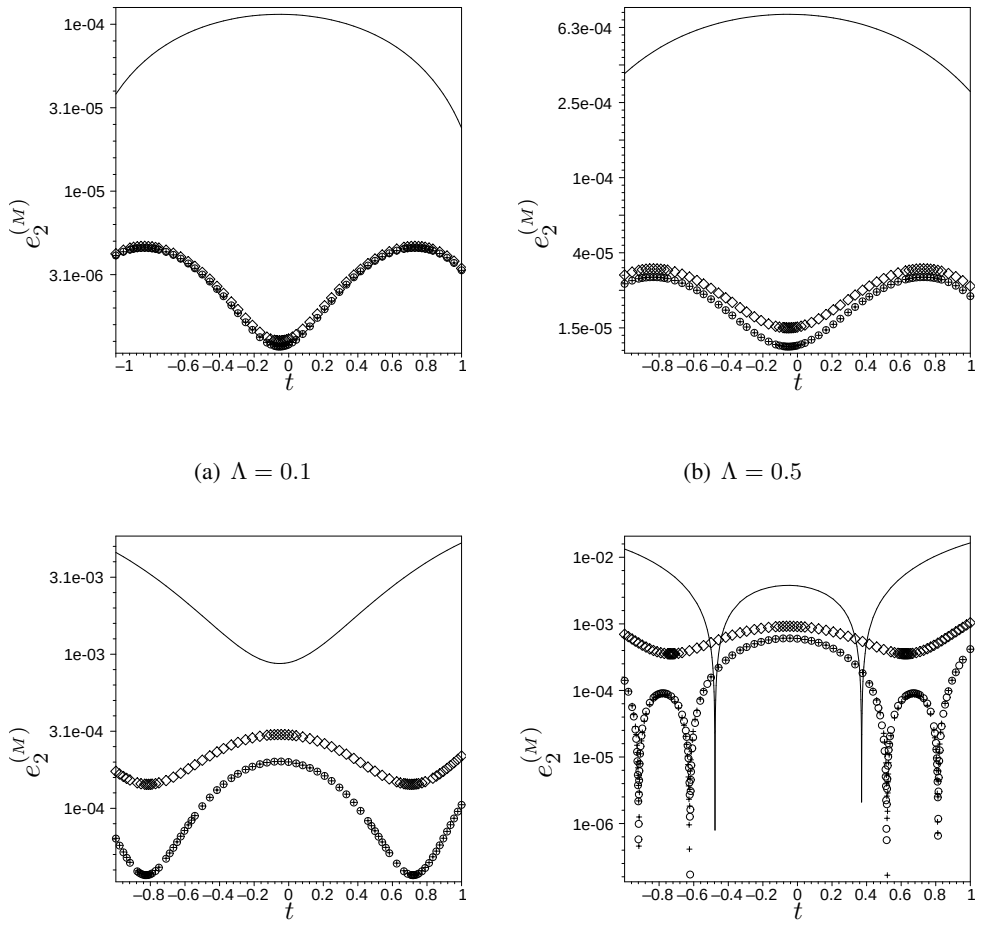

(a) $\Lambda = 0.1$

(b) $\Lambda = 0.5$

(c) $\Lambda = 5$

(d) $\Lambda = 25$

Figure 2.4.3: *The modified Nyström errors* $e_n^{(M)}u(t)$ *of* (2.4.4) *for fixed* $n = 2$ *and different values of* Λ*, computed using Gauss-Jacobi quadrature* (2.1.3)*. The above numerical experiment uses* $\mu = \nu = \frac{1}{2}$ *in the test FIE2* (2.3.14)*. Successive modifications of the standard Nyström error,* $M = 0\ (-)$*, are shown by* $M = 1\ (\diamond)$*,* $M = 2\ (\circ)$ *and* $M = 3\ (+)$*. Validating computations using Gauss-(second-kind-)-Chebyshev quadrature yield results indistinguishable from those presented.*

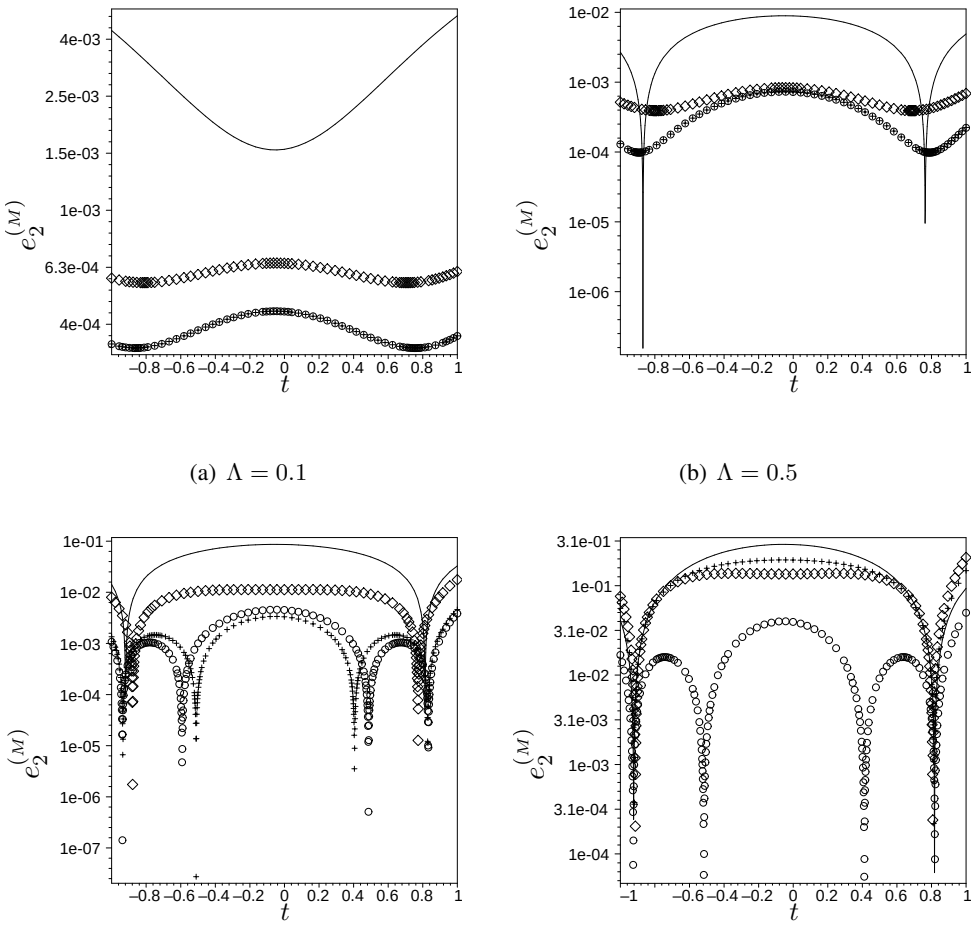

(a) $\Lambda = 0.1$

(b) $\Lambda = 0.5$

(c) $\Lambda = 5$

(d) $\Lambda = 25$

Figure 2.4.4: *The modified Nyström errors* $e_n^{(M)}u(t)$ *of* (2.4.4) *for fixed* $n = 2$*, different values of* Λ *and a highly-singular kernel function with* $\mu = -\frac{4}{5}$ *and* $\nu = -\frac{9}{10}$ *in the test FIE2* (2.3.14)*, computed using Gauss-Jacobi quadrature* (2.1.3)*. Successive modifications of the standard Nyström error,* $M = 0$ $(-)$*, are shown by* $M = 1$ $(\diamond)$*,* $M = 2$ $(\circ)$ *and* $M = 3$ $(+)$*.*

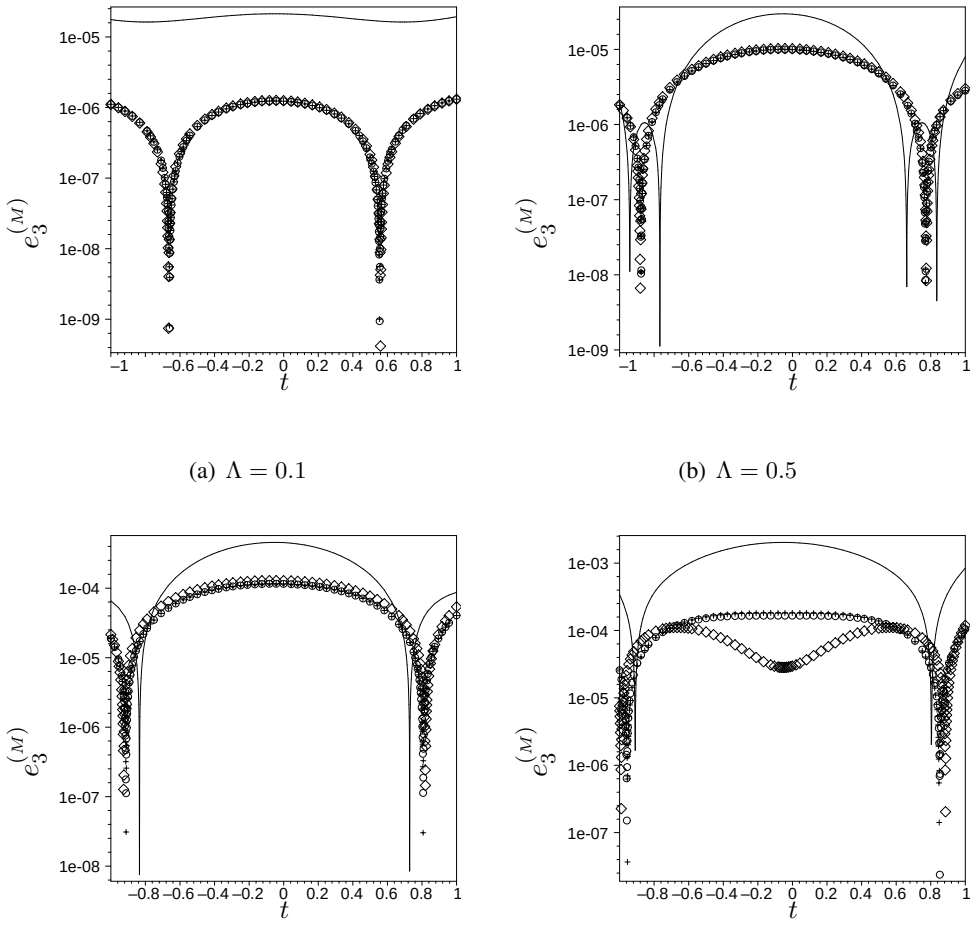

(a) $\Lambda = 0.1$

(b) $\Lambda = 0.5$

(c) $\Lambda = 5$

(d) $\Lambda = 25$

Figure 2.4.5: *The modified Nyström errors* $e_n^{(M)}u(t)$ *of* (2.4.4) *for fixed* $n = 3$*, different values of* Λ *and a highly-singular kernel function with* $\mu = -\frac{4}{5}$ *and* $\nu = -\frac{9}{10}$ *in the test FIE2* (2.3.14) *computed using Gauss-Jacobi quadrature of Eqn.* (2.1.3)*. Successive modifications of the standard Nyström error,* $M = 0$ $(-)$*, are shown by* $M = 1$ $(\diamond)$*,* $M = 2$ $(\circ)$ *and* $M = 3$ $(+)$*.*

2.5 Summary and discussion

The aim of this chapter was to modify the classical Nyström method so that it could accommodate problems in which the kernels in FIE2s have challenging end-point singularities.

The presented new modified Nyström method enables the accurate treatment of singular FIE2 in a computationally efficient and economical manner. The crudest modified Nyström method solutions required an 626% increase in CPU system time compared against the CPU system time for the classical Nyström method. The modified Nyström results were, however, more accurate than those obtained from the classical approach: a substantial improvement throughout the entire solution domain of approximately one hundredfold for only $n = 2$ quadrature nodes.

Numerous test FIE2s have been considered to demonstrate the applicability of the modified (and classical) Nyström method with singular kernels, for which Gauss-Jacobi quadrature is appropriate.

The theory on which the modified Nyström method is founded has been conducted in the context of general orthogonal polynomials, although is applicable to any such FIE2 with a kernel function factorisable as a product of "well-behaved" and "poorly-behaved" functions, i.e. a product of infinitely-differentiable and finitely-differentiable functions.

Further investigations in this area include: finding improved estimates of the true Nyström method error $\mathcal{E}_n u$ in order to reduce the inherent error ϵ_n^* developed by the removal of second and higher-order error terms in $\overline{\mathcal{E}}_n u$; implementing Clenshaw-Curtis quadrature (Trefethen [2008]), based on unevenly spaced abscissae, as an alternative to Gauss-Jacobi quadrature, and; extending the Nyström method to a Chebyshev-spectral method (Boyd [2001]) that leads to nested quadrature rules.

Given that in this chapter the outlined theory is for nonsingular or end-point singular kernel functions only, in the subsequent chapter, we aim to extend the modified Nyström method to solving FIE2s with more complicated singular kernel functions. In particular, we shall consider kernel functions with singularities at *any* location in a bounded interval.

Chapter 3

Numerical Solutions of One-Dimensional Fredholm Integral Equations of the Second Kind with Internal Singularities

We progress from the end-point singular kernel functions in chapter 2 by considering the FIE2

$$U(T) = F(T) + \Lambda \int_a^b \widetilde{K}(T,S)U(S)\,dS, \quad T \in [a,b], \tag{3.0.1}$$

with more complicated kernel functions; that is, $\widetilde{K}(T,S)$ is now singular (or finitely-continuously differentiable) at $m > 1$ points say, $\{\xi_i\}_{i=1}^m \in (a,b)$. The aim of this chapter is to therefore develop and apply the numerical solution techniques of chapter 2 to solve (3.0.1) in the presence of multiple singularities.

Following chapter 2, the kernel function in (3.0.1) is factorised as

$$\widetilde{K}(T,S) = W(S)K(T,S), \tag{3.0.2}$$

where $K(T,S)$ is again an infinitely-differentiable function. To admit the possibility that $\widetilde{K}(T,S)$ in (3.0.2) has limited differentiability at multiple points $\{\xi_i\}_{i=1}^m \in (a,b)$, (2.0.4) is now amended

to

$$W(S) = \prod_{i=1}^{m} |S - \xi_i|^{\alpha_i}, \tag{3.0.3}$$

in which the parameters $\alpha_i > -1$ for $i = 1, \ldots, m$, so that FIE2 (3.0.1) is singular but not hypersingular.

The interval $[a, b]$ in (3.0.1) is divided into $m + 1$ subintervals

$$\bigcup_{i=0}^{m} [\xi_i, \xi_{i+1}], \tag{3.0.4}$$

where

$$\xi_0 = a < \xi_1 \leq \xi_2 \leq \ldots \leq \xi_{m-1} \leq \xi_m < \xi_{m+1} = b, \tag{3.0.5}$$

in which $\{\xi_i\}_{i=1}^{m}$ are located at the subinterval limits. Considering (3.0.2), the kernel function is defined over each subinterval by

$$\widetilde{K}(T, S) = W_p(S) K_p(T, S), \quad S \in [\xi_{p-1}, \xi_p], \quad p = 1, \ldots, m + 1, \tag{3.0.6}$$

where $W_p(S)$ contains the "badly-behaved" (i.e. finitely-differentiable) part of the kernel and $K_p(T, S)$ is infinitely-differentiable. By (3.0.2) and (3.0.3),

$$W_1(S) = W_2(S) = |S - \xi_1|^{\alpha_1}, \tag{3.0.7}$$

and

$$K_1(T, S) = K_2(T, S) = K(T, S), \tag{3.0.8}$$

if $m = 1$. Otherwise, for all $m > 1$

$$W_p(S) = \begin{cases} |S - \xi_1|^{\alpha_1} & p = 1 \\ |S - \xi_{p-1}|^{\alpha_{p-1}} |S - \xi_p|^{\alpha_p} & p = 2, \ldots, m \\ |S - \xi_m|^{\alpha_m} & p = m + 1 \end{cases} \tag{3.0.9}$$

and

$$K_p(T, S) = \begin{cases} \displaystyle\prod_{j=2}^{m} |S - \xi_j|^{\alpha_j} K(T, S) & p = 1 \\ \displaystyle\prod_{\substack{j=1 \\ j \neq p, p-1}}^{m} |S - \xi_j|^{\alpha_j} K(T, S) & p = 2, \ldots, m \\ \displaystyle\prod_{j=1}^{m-1} |S - \xi_j|^{\alpha_j} K(T, S) & p = m + 1. \end{cases} \tag{3.0.10}$$

Without loss of generality, for the remainder of the chapter we presume only *one* singular interior point, e.g. $\xi_1 = c$ say, exists within the interval $[a, b]$. This is sufficient enough to illustrate the different principle of internal singularities without complicating the issue with over-complex algebra. Weight function (3.0.7) is equivalent, on the first interval, to

$$W_1(S_1) = (c - S_1)^\alpha, \quad S_1 \in [a, c], \tag{3.0.11}$$

and, on the second interval, to

$$W_2(S_2) = (S_2 - c)^\alpha, \quad S_2 \in [c, b], \tag{3.0.12}$$

with $\alpha_1 = \alpha$.

Given the existence of a unique singular point in (a, b), FIE2 (3.0.1) becomes

$$U(T) = F(T) + \Lambda \left[\int_a^c W_1(S_1) K_1(T, S_1) U(S_1)\, dS_1 + \int_c^b W_2(S_2) K_2(T, S_2) U(S_2)\, dS_2 \right], \tag{3.0.13}$$

where $T \in [a, b]$. Thus the domain of T does not match that of S_1 or S_2 in either integrand in (3.0.13), hence (3.0.13) is not a FIE2 in the formal sense. However, if the solution $U(T)$ of integral equation (3.0.13) exists when $T \in [a, b]$ then it must also exist when $T \in [a, c] \cup [c, b]$. In other words, (3.0.13) is equivalent to the *system of Fredholm integral equations of the second kind*

$$U(T) = F(T) + \Lambda \left[\int_a^c W_1(S_1) K_1(T, S_1) U(S_1)\, dS_1 + \int_c^b W_2(S_2) K_2(T, S_2) U(S_2)\, dS_2 \right], \tag{3.0.14}$$

for $T \in [a, c]$ and

$$U(T) = F(T) + \Lambda \left[\int_a^c W_1(S_1) K_1(T, S_1) U(S_1)\, dS_1 + \int_c^b W_2(S_2) K_2(T, S_2) U(S_2)\, dS_2 \right], \tag{3.0.15}$$

for $T \in [c, b]$, where $K_1(T, S), K_2(T, S), W_1(S), W_2(S)$ and $F(T)$ are given but $U(T)$ is yet to be determined.

For compatibility with (2.0.5), the mapping of $T, S_1 \in [a, c]$ and $T, S_2 \in [c, b]$ onto $t, s \in [-1, 1]$ is achieved by a combination of

$$\begin{aligned} (T, S_1) &= \tfrac{1}{2}[(c - a)(t, s_1) + (c + a)], \qquad (T, S_1) \in [a, c], \\ (T, S_2) &= \tfrac{1}{2}[(b - c)(t, s_2) + (b + c)], \qquad (T, S_2) \in [c, b]. \end{aligned} \tag{3.0.16}$$

Using (3.0.16), the FIE2s (3.0.14) and (3.0.15) have respective canonical forms

$$u_1(t) = f_1(t) + \lambda_1 \int_{-1}^{1} w_1(s)k^{(1,1)}(t,s)u_1(s)\ ds + \lambda_2 \int_{-1}^{1} w_2(s)k^{(1,2)}(t,s)u_2(s)\ ds \quad (3.0.17)$$

and

$$u_2(t) = f_2(t) + \lambda_1 \int_{-1}^{1} w_1(s)k^{(2,1)}(t,s)u_1(s)\ ds + \lambda_2 \int_{-1}^{1} w_2(s)k^{(2,2)}(t,s)u_2(s)\ ds, \quad (3.0.18)$$

for $t \in [-1,1]$, where

$$\lambda_1 = \Lambda \left(\frac{c-a}{2}\right)^{\alpha+1}, \quad (3.0.19)$$

$$\lambda_2 = \Lambda \left(\frac{b-c}{2}\right)^{\alpha+1}, \quad (3.0.20)$$

and the canonical form of the weight function, with potential discontinuous derivatives at $s = \pm 1$, is

$$w_i(s) = \begin{cases} (1-s)^{\alpha} & i = 1, \\ (1+s)^{\alpha} & i = 2, \end{cases} \quad (3.0.21)$$

corresponding to its transformed upper-case counterpart $W_i(S_i)$ in (3.0.11) and (3.0.12). Similarly, in (3.0.17) and (3.0.18), the functions $u_i(t)$, $f_i(t)$ and $k^{(i,j)}(t,s)$ with $t, s \in [-1,1]$ correspond to their upper-case counterparts $U(T)$, $F(T)$ and $K_j(T,S_j)$ in (3.0.14) and (3.0.15) in which $T = S_i$ and $i, j = 1, 2$.

We note that applying the linear transformations (2.0.5) and (3.0.16) to (3.0.13) *before* splitting the domain of T results in the canonical integral equation

$$u(t) = f(t) + \lambda_1 \int_{-1}^{1} w_1(s)k_1(t,s)u_1(s)ds + \lambda_2 \int_{-1}^{1} w_2(s)k_2(t,s)u_2(s)ds, \quad (3.0.22)$$

for $t \in [-1,1]$, where u and f are as defined in chapter 2. Essentially, (3.0.22) has *three* unknown functions $u(t)$, $u_1(s)$ and $u_2(s)$ and is therefore unsolvable.

Defining

$$\boldsymbol{k}(t,s) = \begin{pmatrix} k^{(1,1)}(t,s) & k^{(1,2)}(t,s) \\ k^{(2,1)}(t,s) & k^{(2,2)}(t,s) \end{pmatrix}, \quad \boldsymbol{u}(t) = \begin{pmatrix} u_1(t) \\ u_2(t) \end{pmatrix}, \quad \boldsymbol{f}(t) = \begin{pmatrix} f_1(t) \\ f_2(t) \end{pmatrix}, \quad (3.0.23)$$

and

$$\boldsymbol{w}(t) = \begin{pmatrix} w_1(t) & 0 \\ 0 & w_2(t) \end{pmatrix}, \quad (3.0.24)$$

the vector form of the system of equations (3.0.17) and (3.0.18) is

$$\boldsymbol{u}(t) = \boldsymbol{f}(t) + \int_{-1}^{1} \boldsymbol{k}(t,s)\boldsymbol{\lambda}\boldsymbol{w}(s)\boldsymbol{u}(s)\, ds, \tag{3.0.25}$$

where

$$\boldsymbol{\lambda} = \begin{pmatrix} \lambda_1 & 0 \\ 0 & \lambda_2 \end{pmatrix}, \tag{3.0.26}$$

hence the vector $\boldsymbol{\lambda}$ cannot be taken outside the integral in (3.0.25). Now we define the linear operator $\mathcal{K}_\lambda^{(i,j)}$ by

$$(\mathcal{K}_\lambda^{(i,j)} u_j)(t) \equiv \int_{-1}^{1} k^{(i,j)}(t,s)\lambda_j w_j(s) u_j(s)\, ds, \quad i,j = 1,2, \tag{3.0.27}$$

and matrix operators

$$\boldsymbol{\mathcal{K}_\lambda} = \begin{pmatrix} \mathcal{K}_\lambda^{(1,1)} & \mathcal{K}_\lambda^{(1,2)} \\ \mathcal{K}_\lambda^{(2,1)} & \mathcal{K}_\lambda^{(2,2)} \end{pmatrix} \quad \text{and} \quad \boldsymbol{\mathcal{I}} = \begin{pmatrix} \mathcal{I} & 0 \\ 0 & \mathcal{I} \end{pmatrix}, \tag{3.0.28}$$

in which $\mathcal{I}$ denotes the identity operator. By (3.0.23), (3.0.24) and (3.0.26), we have

$$(\boldsymbol{\mathcal{K}_\lambda}\boldsymbol{u})(t) \equiv \int_{-1}^{1} \boldsymbol{k}(t,s)\boldsymbol{\lambda}\boldsymbol{w}(s)\boldsymbol{u}(s)\, ds, \tag{3.0.29}$$

and the symbolic form of system (3.0.25) is

$$(\boldsymbol{\mathcal{I}} - \boldsymbol{\mathcal{K}_\lambda})\boldsymbol{u} = \boldsymbol{f} \tag{3.0.30}$$

which, provided $\boldsymbol{f} \equiv \boldsymbol{0}$ and $(\boldsymbol{\mathcal{I}} - \boldsymbol{\mathcal{K}_\lambda})\boldsymbol{u} = \boldsymbol{0}$ has only the trivial solution $\boldsymbol{u} = \boldsymbol{0}$, the unique vector solution is

$$\boldsymbol{u} = (\boldsymbol{\mathcal{I}} - \boldsymbol{\mathcal{K}_\lambda})^{-1}\boldsymbol{f}. \tag{3.0.31}$$

Using (3.0.23) and (3.0.28), the expanded form of (3.0.30) satisfies

$$u_1 - \mathcal{K}_\lambda^{(1,1)} u_1 - \mathcal{K}_\lambda^{(1,2)} u_2 = f_1 \tag{3.0.32}$$

and

$$u_2 - \mathcal{K}_\lambda^{(2,1)} u_1 - \mathcal{K}_\lambda^{(2,2)} u_2 = f_2, \tag{3.0.33}$$

with corresponding solutions

$$u_1 = (\mathcal{I} - \mathcal{K}_\lambda^{(1,1)} - \mathcal{K}_\lambda^{(1,2)}(\mathcal{I} - \mathcal{K}_\lambda^{(2,2)})^{-1}\mathcal{K}_\lambda^{(2,1)})^{-1}(f_1 + \mathcal{K}_\lambda^{(1,2)}(\mathcal{I} - \mathcal{K}_\lambda^{(2,2)})^{-1} f_2) \tag{3.0.34}$$

and

$$u_2 = (\mathcal{I} - \mathcal{K}_\lambda^{(2,2)} - \mathcal{K}_\lambda^{(2,1)}(\mathcal{I} - \mathcal{K}_\lambda^{(1,1)})^{-1}\mathcal{K}_\lambda^{(1,2)})^{-1}(f_2 + \mathcal{K}_\lambda^{(2,1)}(\mathcal{I} - \mathcal{K}_\lambda^{(1,1)})^{-1}f_1). \quad (3.0.35)$$

When $\lambda_2 = 0$, by (3.0.27), $\mathcal{K}_\lambda^{(i,2)} = 0$ for all i and (3.0.32) is reduced to

$$u_1 - \mathcal{K}_\lambda^{(1,1)}u_1 = f_1. \quad (3.0.36)$$

Similarly, when $\lambda_1 = 0$ (3.0.35) reduces to

$$u_2 - \mathcal{K}_\lambda^{(2,2)}u_2 = f_2. \quad (3.0.37)$$

Eqns. (3.0.36) and (3.0.37) are FIE2s (Atkinson [1997]), the numerical solution of which was discussed in chapter 2.

The remainder of this chapter is structured, parallel to that in chapter 2, as follows. In §3.1 we numerically approximate the solution of system (3.0.30) via the vector-Nyström method using Gaussian quadrature. In §3.2 the new, modified, vector-Nyström method for approximating the solution of *systems* of FIE2s is discussed. Then §3.3 provides an error analysis of the standard vector-Nyström method, whose approximation is essential in the implementation of the new modified method. Finally §3.4 presents a series of validations of the modified vector-Nyström method using prespecified test problems.

3.1 The vector-Nyström method

The past decade has seen systems of FIE2s (3.0.30) solved by various numerical methods (Maleknejad et al. [2006], Babolian et al. [2004], Javidi and Golbabai [2007], Jafari et al. [2010]). Rashidinia and Zarebnia [2007] applied a Sinc collocation method for solving system of linear Fredholm integral equations. On ther other hand, a vector-Nyström method based on orthogonal-Jacobi polynomials (discussed in §2.1) to approximate the solutions of a system of FIE2s, has been proposed by De Bonis and Laurita [2008]. In this chapter, we extend the theory of Rashidinia and Zarebnia [2007] and De Bonis and Laurita [2008] to solve the system of FIE2s in (3.0.25).

Owing to the composition of the weight function $w_j(s)$ in (3.0.21)

$$w_j(s) \equiv (1-s)^{\mu_j}(1+s)^{\nu_j}, \quad (3.1.1)$$

where

$$\mu_j = \begin{cases} \alpha & j = 1, \\ 0 & j = 2, \end{cases} \quad \text{and} \quad \nu_j = \begin{cases} 0 & j = 1, \\ \alpha & j = 2, \end{cases} \tag{3.1.2}$$

hence we employ Gauss-Jacobi quadrature to approximate the integrals in (3.0.25). Analogous with (3.0.28), the definition of the explicit orthogonal-polynomial quadratures approximating the linear operators (3.0.27) are now

$$(\mathcal{K}_{\lambda,n}^{(i,1)} u_1)(t) \equiv \sum_{k=1}^{n} k^{(i,1)}(t, \sigma_k)\, \lambda_1 c_{k,n}^{(1)} u_1(\sigma_k), \quad t \in [-1, 1] \tag{3.1.3}$$

and

$$(\mathcal{K}_{\lambda,n}^{(i,2)} u_2)(t) \equiv \sum_{k=1}^{n} k^{(i,2)}(t, \rho_k)\, \lambda_2 c_{k,n}^{(2)} u_2(\rho_k), \quad t \in [-1, 1], \tag{3.1.4}$$

where $i = 1, 2$ and $(\mathcal{K}_{\lambda,n}^{(i,j)} u_j) \equiv (\mathcal{K}_{\lambda}^{(i,j)} u_j)$ when $k^{(i,j)}(t, s) u_j(s)$ is a polynomial of degree $\leq 2n - 1$ (Atkinson [1989]). In (3.1.3) and (3.1.4), the weights $c_{k,n}^{(j)}$, defined in accordance with the weight function $w_j(s)$, are

$$c_{k,n}^{(j)} = \begin{cases} -\dfrac{A_{n+1}^{(1)} \gamma_n^{(1)}}{A_n^{(1)} P_{n+1}(\sigma_k; \mu_1, \nu_1) \partial_1 P_n(\sigma_k; \mu_1, \nu_1)}, & j = 1, \\ -\dfrac{A_{n+1}^{(2)} \gamma_n^{(2)}}{A_n^{(2)} P_{n+1}(\rho_k; \mu_2, \nu_2) \partial_1 P_n(\rho_k; \mu_2, \nu_2)}, & j = 2, \end{cases} \tag{3.1.5}$$

where

$$A_n^{(j)} = \frac{(2n + \mu_j + \nu_j)}{2^n n! (n + \mu_j + \nu_j)!} \tag{3.1.6}$$

is the leading coefficient in $P_n(s; \mu_j, \nu_j)$ invariant for any choice of j because of the symmetry of μ_j and ν_j in (3.1.2),

$$\gamma_n^{(j)} = \int_{-1}^{1} (1 - s)^{\mu_j} (1 + s)^{\nu_j} [P_n(s; \mu_j, \nu_j)]^2 ds, \tag{3.1.7}$$

and ∂_1 denotes the first-order partial derivative of $P_n(s; \mu_j, \nu_j)$ with respect to s. The abscissae σ_k and ρ_k, $k = 1, \ldots, n$, in (3.1.3), (3.1.4) and (3.1.5) are the n distinct roots of $P_n(s; \mu_1, \nu_1)$ and $P_n(s; \mu_2, \nu_2)$ respectively.

In what follows, all subsequent i, j, l and m take the values of $i, j, l, m = 1, 2$ unless otherwise stated. By comparing (3.1.3) and (3.1.4) with (3.0.27), the quadrature error is defined as

$$(\mathcal{E}_{\lambda,n}^{(i,j)} u_j)(t) \equiv ((\mathcal{K}_{\lambda}^{(i,j)} - \mathcal{K}_{\lambda,n}^{(i,j)}) u_j)(t). \tag{3.1.8}$$

Although the quadrature error (3.1.8) is pointwise convergent to zero for a sufficiently differentiable function $u_j(t)$,

$$(\mathcal{E}_{\lambda,n}^{(i,j)}u_j)(t) \to 0, \quad n \to \infty, \tag{3.1.9}$$

it is not norm convergent (Hackbusch [1995]):

$$\|\mathcal{E}_{\lambda,n}^{(i,j)}\| \geq \|\mathcal{K}_{\lambda}^{(i,j)}\| \tag{3.1.10}$$

for all $n \in \mathbb{N}$. However, by (3.1.9),

$$\|\mathcal{E}_{\lambda,n}^{(i,j)}u_j\| \to 0, \quad n \to \infty \tag{3.1.11}$$

and (Atkinson [1997])

$$\|\mathcal{E}_{\lambda,n}^{(i,j)}\mathcal{K}_{\lambda}^{(l,m)}\|, \|\mathcal{E}_{\lambda,n}^{(i,j)}\mathcal{K}_{\lambda,n}^{(l,m)}\| \to 0, \quad n \to \infty. \tag{3.1.12}$$

Letting $\boldsymbol{\mathcal{E}}_{\boldsymbol{\lambda}n}$ be the matrix operator combining the quadrature errors (3.1.8); acting upon vector solution $\boldsymbol{u}$, $\boldsymbol{\mathcal{E}}_{\boldsymbol{\lambda}n}$ is defined by

$$(\boldsymbol{\mathcal{E}}_{\boldsymbol{\lambda}n}\boldsymbol{u})(t) = \begin{pmatrix} \mathcal{E}_{\lambda,n}^{(1,1)} & \mathcal{E}_{\lambda,n}^{(1,2)} \\ \mathcal{E}_{\lambda,n}^{(2,1)} & \mathcal{E}_{\lambda,n}^{(2,2)} \end{pmatrix} \boldsymbol{u}(t). \tag{3.1.13}$$

Then, by (3.1.11) and (3.1.12), corresponding to (2.1.12) we now have

$$\|\boldsymbol{\mathcal{E}}_{\boldsymbol{\lambda}n}\boldsymbol{u}\|, \|\boldsymbol{\mathcal{E}}_{\boldsymbol{\lambda}n}\boldsymbol{\mathcal{K}}_{\boldsymbol{\lambda}}\|, \|\boldsymbol{\mathcal{E}}_{\boldsymbol{\lambda}n}\boldsymbol{\mathcal{K}}_{\boldsymbol{\lambda}n}\| \to 0, \quad n \to \infty. \tag{3.1.14}$$

The Nyström approximation $u_{n,i}$ to u_i is, in symbolic-matrix form,

$$(\boldsymbol{\mathcal{I}} - \boldsymbol{\mathcal{K}}_{\boldsymbol{\lambda}n})\boldsymbol{u}_n = \boldsymbol{f}, \tag{3.1.15}$$

where, from (3.1.3) and (3.1.4),

$$\boldsymbol{\mathcal{K}}_{\boldsymbol{\lambda}n} = \begin{pmatrix} \mathcal{K}_{\lambda,n}^{(1,1)} & \mathcal{K}_{\lambda,n}^{(1,2)} \\ \mathcal{K}_{\lambda,n}^{(2,1)} & \mathcal{K}_{\lambda,n}^{(2,2)} \end{pmatrix}. \tag{3.1.16}$$

The *vector-Nyström error* $\boldsymbol{u} - \boldsymbol{u}_n$, by (3.0.30) and (3.1.15), satisfies

$$(\boldsymbol{\mathcal{I}} - \boldsymbol{\mathcal{K}}_{\boldsymbol{\lambda}n})(\boldsymbol{u} - \boldsymbol{u}_n) = (\boldsymbol{\mathcal{K}}_{\boldsymbol{\lambda}} - \boldsymbol{\mathcal{K}}_{\boldsymbol{\lambda}n})\boldsymbol{u}, \tag{3.1.17}$$

and thus depends upon the existence of the matrix $(\boldsymbol{\mathcal{I}} - \boldsymbol{\mathcal{K}}_{\boldsymbol{\lambda}n})^{-1}$. The proof of the invertibility of the matrix $(\boldsymbol{\mathcal{I}} - \boldsymbol{\mathcal{K}}_{\boldsymbol{\lambda}n})$ is similar to that for a single FIE2, as in §2.1. Recalling the hypothesis that the system of FIE2 (3.0.30) has a unique solution, then $(\boldsymbol{\mathcal{I}} - \boldsymbol{\mathcal{K}}_{\boldsymbol{\lambda}})^{-1}$ must exist and its norm is bounded, i.e.

$$\|(\boldsymbol{\mathcal{I}} - \boldsymbol{\mathcal{K}}_{\boldsymbol{\lambda}})^{-1}\| < \infty. \tag{3.1.18}$$

Following Rashidinia and Zarebnia [2007], provided $\boldsymbol{k}(t,s)$ in (3.0.23) is continuous for $t, s \in [-1,1]$, by (3.1.14) and (3.1.18), there exists an $m \in \mathbb{N}$ so that for $n > m$

$$\|(\boldsymbol{\mathcal{K}}_{\boldsymbol{\lambda}} - \boldsymbol{\mathcal{K}}_{\boldsymbol{\lambda}n})\boldsymbol{\mathcal{K}}_{\boldsymbol{\lambda}n}\| \leq \frac{1}{\|(\boldsymbol{\mathcal{I}} - \boldsymbol{\mathcal{K}}_{\boldsymbol{\lambda}})^{-1}\|}. \tag{3.1.19}$$

Extending (2.1.20)- (2.1.24), as shown by Rashidinia and Zarebnia [2007, Proof of Thm. IV], $(\boldsymbol{\mathcal{I}} - \boldsymbol{\mathcal{K}}_{\boldsymbol{\lambda}n})^{-1}$ exists and is bounded for sufficiently large n as

$$\|(\boldsymbol{\mathcal{I}} - \boldsymbol{\mathcal{K}}_{\boldsymbol{\lambda}n})^{-1}\| \leq \frac{1 + \|(\boldsymbol{\mathcal{I}} - \boldsymbol{\mathcal{K}}_{\boldsymbol{\lambda}})^{-1}\|\|\boldsymbol{\mathcal{K}}_{\boldsymbol{\lambda}n}\|}{1 - \|(\boldsymbol{\mathcal{I}} - \boldsymbol{\mathcal{K}}_{\boldsymbol{\lambda}})^{-1}\|\|(\boldsymbol{\mathcal{K}}_{\boldsymbol{\lambda}} - \boldsymbol{\mathcal{K}}_{\boldsymbol{\lambda}n})\boldsymbol{\mathcal{K}}_{\boldsymbol{\lambda}n}\|} \leq \psi_n, \tag{3.1.20}$$

where ψ_n is a constant. Thus the vector-Nyström error (3.1.17) is bounded as

$$\|\boldsymbol{u} - \boldsymbol{u}_n\|_\infty \leq \psi_n \|(\boldsymbol{\mathcal{K}}_{\boldsymbol{\lambda}} - \boldsymbol{\mathcal{K}}_{\boldsymbol{\lambda}n})\boldsymbol{u}\|_\infty \tag{3.1.21}$$

for sufficiently large n. Eqn. (3.1.21), by the definition of $\mathcal{E}_{\lambda,n}^{(i,j)}$ in (3.1.8), is therefore equivalent to

$$\|\boldsymbol{u} - \boldsymbol{u}_n\|_\infty \leq \psi_n \|\boldsymbol{\mathcal{E}}_{\boldsymbol{\lambda}n}\boldsymbol{u}\|_\infty, \tag{3.1.22}$$

in which the right-hand side converges to zero with increasing n by (3.1.14).

Recall for Gauss-Jacobi quadrature, by linearity with (2.1.27), the i^{th} component of the Nyström error vector bound can be estimated for large-n as (Kelmanson and Tenwick [2009])

$$\|u_i - u_{n,i}\|_\infty \leq \sum_{j=1}^{2} \frac{\pi}{2^{2n+\mu_j+\nu_j}} \left\| \partial_{2n} \left[k^{(i,j)}(t,s) u_j(s) \right] \right\|_\infty, \quad n \to \infty, \tag{3.1.23}$$

where $k^{(i,j)}(t,s)$ is infinitely differentiable with respect to s. Eqn. (3.1.23) shows $\|u_i - u_{n,i}\|_\infty$ converges to zero exponentially with n when $\partial_{2n} u_j(s)$ is bounded for all j. Fig. 3.1.1 depicts the exponential convergence of the actual error $\|u_i - u_{n,i}\|_\infty$ for a test FIE2 as its logarithm decreases linearly with increasing n.

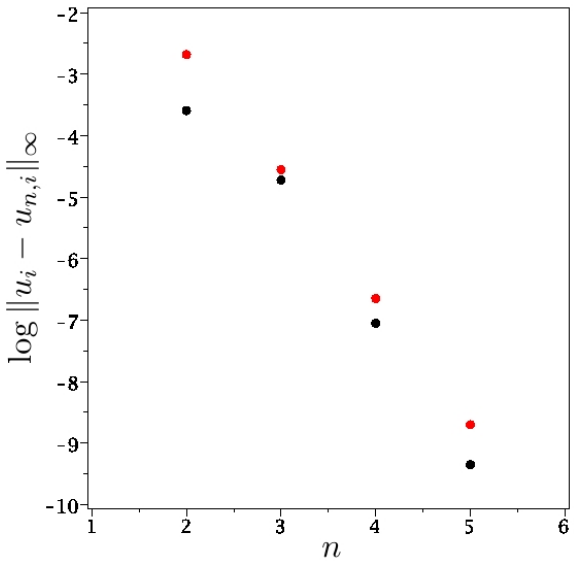

Figure 3.1.1: *Log plot of the maximum norm of the actual vector-Nyström error* $\|u_i - u_{n,i}\|_\infty$ *in* (3.1.23) *for the test FIE2* (3.0.1) *with kernel* $K(T,S) = \exp(-T^2 S)$, $\Lambda = 1/10$, $[a,b] = [-\frac{5}{4}, \frac{5}{3}]$, $\alpha = 1/2$ *and exact solution* $U(S) = \exp(S)\cos(S)$ *for different values of* n. *The two solutions of the system of FIE2s are shown as* $i = 1$ *(black) and* $i = 2$ *(red). The pure-exponential convergence of the actual error of the vector-Nyström method is evident here for increasing* n *by the linear relationship.*

We proceed by modifying the standard vector-Nyström method in such a way that, if $\overline{\boldsymbol{u}}_n$ is the solution of the new, modified, vector-Nyström method then

$$\|\boldsymbol{u} - \boldsymbol{u}_n\|_\infty \ll \|\boldsymbol{u} - \overline{\boldsymbol{u}}_n\|_\infty, \tag{3.1.24}$$

for low values of n, in precise accordance with (2.1.30).

3.2 The modified vector-Nyström method

The modified vector-Nyström method, with solution $\overline{\boldsymbol{u}}_n$, is based on incorporating the approximation $\widetilde{\boldsymbol{\mathcal{E}}}_{\boldsymbol{\lambda}n}\boldsymbol{u}$ to the real error $\boldsymbol{\mathcal{E}}_{\boldsymbol{\lambda}n}\boldsymbol{u}$ in the standard vector-Nyström method (3.1.15), so that (Kelmanson and Tenwick [2009, 2010])

$$\overline{\boldsymbol{u}}_n - (\boldsymbol{\mathcal{K}}_{\boldsymbol{\lambda}n} + \widetilde{\boldsymbol{\mathcal{E}}}_{\boldsymbol{\lambda}n})\overline{\boldsymbol{u}}_n = \boldsymbol{f}. \tag{3.2.1}$$

The matrix error operator $\widetilde{\boldsymbol{\mathcal{E}}}_{\boldsymbol{\lambda}n}$ acting upon vector $\boldsymbol{u}$ is defined by

$$(\widetilde{\boldsymbol{\mathcal{E}}}_{\boldsymbol{\lambda}n}\boldsymbol{u})(t) = \begin{pmatrix} \widetilde{\mathcal{E}}_{\lambda,n}^{(1,1)} & \widetilde{\mathcal{E}}_{\lambda,n}^{(1,2)} \\ \widetilde{\mathcal{E}}_{\lambda,n}^{(2,1)} & \widetilde{\mathcal{E}}_{\lambda,n}^{(2,2)} \end{pmatrix} \boldsymbol{u}(t), \tag{3.2.2}$$

with components $\widetilde{\mathcal{E}}_{\lambda,n}^{(i,j)} \approx \mathcal{E}_{\lambda,n}^{(i,j)} \equiv \mathcal{K}_{\lambda}^{(i,j)} - \mathcal{K}_{\lambda,n}^{(i,j)}$ which, consistent with (3.1.12), satisfy

$$\|\widetilde{\mathcal{E}}_{\lambda,n}^{(i,j)}\mathcal{K}_{\lambda}^{(l,m)}\|, \|\widetilde{\mathcal{E}}_{\lambda,n}^{(i,j)}\mathcal{K}_{\lambda,n}^{(l,m)}\| \to 0, \quad n \to \infty. \tag{3.2.3}$$

Comparing (3.2.2) with the real error matrix operator (3.1.13), the error discrepancy matrix

$$(\Delta\widetilde{\boldsymbol{\mathcal{E}}}_{\boldsymbol{\lambda}n}\boldsymbol{u})(t) \equiv ((\widetilde{\boldsymbol{\mathcal{E}}}_{\boldsymbol{\lambda}n} - \boldsymbol{\mathcal{E}}_{\boldsymbol{\lambda}n})\boldsymbol{u})(t), \tag{3.2.4}$$

and the norm of (3.2.4) converges in a pointwise sense

$$\|\Delta\widetilde{\boldsymbol{\mathcal{E}}}_{\boldsymbol{\lambda}n}\boldsymbol{u}\| \to 0, \quad n \to \infty \tag{3.2.5}$$

for some suitably continuous vector $\boldsymbol{u}(t)$ in which, as distinct from (2.2.6), we now have

$$\|\Delta\widetilde{\boldsymbol{\mathcal{E}}}_{\boldsymbol{\lambda}n}\| \to 0, \quad n \to \infty \tag{3.2.6}$$

because the modified method is based upon *error discrepancies* rather than the *errors*. That is, by definition of error discrepancy matrix (3.2.4), the modified method (3.2.1) is equivalent to

$$(\boldsymbol{\mathcal{I}} - \boldsymbol{\mathcal{K}}_{\boldsymbol{\lambda}} - \Delta\widetilde{\boldsymbol{\mathcal{E}}}_{\boldsymbol{\lambda}n})\overline{\boldsymbol{u}}_n = \boldsymbol{f}, \tag{3.2.7}$$

which combined with (3.1.15), yields the *modified vector-Nyström error* that satisfies

$$(\boldsymbol{\mathcal{I}} - \boldsymbol{\mathcal{K}}_{\boldsymbol{\lambda}} - \Delta\widetilde{\boldsymbol{\mathcal{E}}}_{\boldsymbol{\lambda}n})(\boldsymbol{u} - \overline{\boldsymbol{u}}_n) = \Delta\widetilde{\boldsymbol{\mathcal{E}}}_{\boldsymbol{\lambda}n}\boldsymbol{u}. \tag{3.2.8}$$

The existence of the modified vector-Nyström error clearly requires the existence of $(\boldsymbol{\mathcal{I}} - \boldsymbol{\mathcal{K}}_{\boldsymbol{\lambda}} - \Delta\widetilde{\boldsymbol{\mathcal{E}}}_{\boldsymbol{\lambda}n})^{-1}$. To prove the existence of this operator we follow (2.2.10)-(2.2.14) in §2.2, e.g. by considering the identity

$$(\boldsymbol{\mathcal{I}} - \boldsymbol{\mathcal{K}}_{\boldsymbol{\lambda}} - \Delta\widetilde{\boldsymbol{\mathcal{E}}}_{\boldsymbol{\lambda}n})^{-1} = (\boldsymbol{\mathcal{I}} - (\boldsymbol{\mathcal{I}} - \boldsymbol{\mathcal{K}}_{\boldsymbol{\lambda}})^{-1}\Delta\widetilde{\boldsymbol{\mathcal{E}}}_{\boldsymbol{\lambda}n})^{-1}(\boldsymbol{\mathcal{I}} - \boldsymbol{\mathcal{K}}_{\boldsymbol{\lambda}})^{-1}, \tag{3.2.9}$$

(3.1.18) and (3.2.6) imply there exists a significantly large $N \in \mathbb{N}$ such that (Groh and Kelmanson [2008])

$$\|(\boldsymbol{\mathcal{I}} - \boldsymbol{\mathcal{K}}_{\boldsymbol{\lambda}})^{-1}\|\|\Delta\widetilde{\boldsymbol{\mathcal{E}}}_{\boldsymbol{\lambda}n}\| < 1, \quad n \geq N. \tag{3.2.10}$$

Letting

$$\mathcal{A}_n \equiv (\boldsymbol{\mathcal{I}} - \boldsymbol{\mathcal{K}}_{\boldsymbol{\lambda}})^{-1}\Delta\widetilde{\boldsymbol{\mathcal{E}}}_{\boldsymbol{\lambda}n}, \tag{3.2.11}$$

then, by (3.2.10), $\|\mathcal{A}_n\| < 1$ when $n \geq N$ and the Neumann series (Appendix A) implies that $(\boldsymbol{\mathcal{I}} - \mathcal{A}_n)^{-1}$ exists and is bounded by

$$\|(\boldsymbol{\mathcal{I}} - \mathcal{A}_n)^{-1}\| \leq \frac{1}{1 - \|\mathcal{A}_n\|}; \tag{3.2.12}$$

that is,

$$\|(\boldsymbol{\mathcal{I}} - (\boldsymbol{\mathcal{I}} - \boldsymbol{\mathcal{K}}_{\boldsymbol{\lambda}})^{-1}\Delta\widetilde{\boldsymbol{\mathcal{E}}}_{\boldsymbol{\lambda}n})^{-1}\| \leq \frac{1}{1 - \|(\boldsymbol{\mathcal{I}} - \boldsymbol{\mathcal{K}}_{\boldsymbol{\lambda}})^{-1}\|\|\Delta\widetilde{\boldsymbol{\mathcal{E}}}_{\boldsymbol{\lambda}n}\|}. \tag{3.2.13}$$

Thus, provided the standard FIE2 system (3.0.31) has a unique solution and limit (3.2.6) exists then, by (3.2.9), $(\boldsymbol{\mathcal{I}} - \boldsymbol{\mathcal{K}}_{\boldsymbol{\lambda}} - \Delta\widetilde{\boldsymbol{\mathcal{E}}}_{\boldsymbol{\lambda}n})^{-1}$ exists and is bounded according to

$$\|(\boldsymbol{\mathcal{I}} - \boldsymbol{\mathcal{K}}_{\boldsymbol{\lambda}} - \Delta\widetilde{\boldsymbol{\mathcal{E}}}_{\boldsymbol{\lambda}n})^{-1}\| \leq \phi_n, \tag{3.2.14}$$

for some constant ϕ_n. Furthermore, by (3.2.8) and (3.2.14),

$$\|\boldsymbol{u} - \overline{\boldsymbol{u}}_n\|_\infty \leq \phi_n\|\Delta\widetilde{\boldsymbol{\mathcal{E}}}_{\boldsymbol{\lambda}n}\boldsymbol{u}\|_\infty, \tag{3.2.15}$$

for some constant ϕ_n and sufficiently large n.

Recalling the modified Nyström error bound (2.2.16) and standard Nyström error bound (2.2.17) in §2, then regardless of whether there is a system of FIE2s or an individual FIE2, the modified vector-Nyström error (3.2.15) is less than the standard vector-Nyström error (3.1.22) owing to the former being composed of the error discrepancy rather than the error itself, i.e.

$$\|\boldsymbol{u} - \overline{\boldsymbol{u}}_n\|_\infty \ll \|\boldsymbol{u} - \boldsymbol{u}_n\|_\infty, \tag{3.2.16}$$

as

$$\|\Delta\widetilde{\boldsymbol{\mathcal{E}}}_{\boldsymbol{\lambda}n}\boldsymbol{u}\|_\infty \ll \|\widetilde{\boldsymbol{\mathcal{E}}}_{\boldsymbol{\lambda}n}\boldsymbol{u}\|_\infty. \tag{3.2.17}$$

3.2.1 Implementation of the modified vector-Nyström method

As shown in §3.3, the standard and approximate vector-Nyström error-matrix operands, $\boldsymbol{\mathcal{E}}_{\boldsymbol{\lambda}n}$ and $\widetilde{\boldsymbol{\mathcal{E}}}_{\boldsymbol{\lambda}n}$, are differential operators whose direct action upon the unknown function $\overline{\boldsymbol{u}}_n$ in (3.2.1) are circumvented by expressing (3.2.1) as

$$\overline{\boldsymbol{u}}_n = \boldsymbol{f} + (\boldsymbol{\mathcal{K}}_{\boldsymbol{\lambda}n} + \widetilde{\boldsymbol{\mathcal{E}}}_{\boldsymbol{\lambda}n})\overline{\boldsymbol{u}}_n, \tag{3.2.18}$$

then recursively replacing $\overline{\boldsymbol{u}}_n$ whenever it is directly acted upon by $\widetilde{\boldsymbol{\mathcal{E}}}_{\boldsymbol{\lambda}n}$. That is, applying M successive Neumann iterations to $\overline{\boldsymbol{u}}_n$ whenever it occurs as the operand of the operator $\widetilde{\boldsymbol{\mathcal{E}}}_{\boldsymbol{\lambda}n}$ in (3.2.18) yields

$$\overline{\boldsymbol{u}}_n = \sum_{m=0}^{M} \widetilde{\boldsymbol{\mathcal{E}}}_{\boldsymbol{\lambda}n}{}^{m} \boldsymbol{f} + \sum_{m=0}^{M} \widetilde{\boldsymbol{\mathcal{E}}}_{\boldsymbol{\lambda}n}{}^{m} \boldsymbol{\mathcal{K}}_{\boldsymbol{\lambda}n} \overline{\boldsymbol{u}}_n + \widetilde{\boldsymbol{\mathcal{E}}}_{\boldsymbol{\lambda}n}{}^{M+1} \overline{\boldsymbol{u}}_n. \tag{3.2.19}$$

Introducing the matrix operator

$$\widetilde{\boldsymbol{\mathcal{E}}}_{\boldsymbol{\lambda}n}^{(M)} \equiv \sum_{m=1}^{M} \widetilde{\boldsymbol{\mathcal{E}}}_{\boldsymbol{\lambda}n}{}^{m}, \tag{3.2.20}$$

the compact form of (3.2.19) is

$$\overline{\boldsymbol{u}}_n^{(M)} = \boldsymbol{f} + \widetilde{\boldsymbol{\mathcal{E}}}_{\boldsymbol{\lambda}n}^{(M)} \boldsymbol{f} + \boldsymbol{\mathcal{K}}_{\boldsymbol{\lambda}n} \overline{\boldsymbol{u}}_n^{(M)} + \widetilde{\boldsymbol{\mathcal{E}}}_{\boldsymbol{\lambda}n}^{(M)} \boldsymbol{\mathcal{K}}_{\boldsymbol{\lambda}n} \overline{\boldsymbol{u}}_n^{(M)} + \widetilde{\boldsymbol{\mathcal{E}}}_{\boldsymbol{\lambda}n}{}^{M+1} \overline{\boldsymbol{u}}_n^{(M)}, \tag{3.2.21}$$

where the explicit dependence of $\overline{\boldsymbol{u}}_n$ on the M iterations is denoted by $\overline{\boldsymbol{u}}_n^{(M)}$. We take $\overline{\boldsymbol{u}}_n^{(0)} \equiv \overline{\boldsymbol{u}}_n$ and $\widetilde{\boldsymbol{\mathcal{E}}}_{\boldsymbol{\lambda}n}{}^{(0)} \equiv 0$ so that, when $M = 0$, (3.2.21) is equivalent to the standard vector-Nyström method (3.1.15).

The implicit scheme (3.2.21) can be applied only if the error operator $\widetilde{\boldsymbol{\mathcal{E}}}_{\boldsymbol{\lambda}n}{}^{M+1}$ acting upon $\overline{\boldsymbol{u}}_n^{(M)}$ is neglected, as $\overline{\boldsymbol{u}}_n^{(M)}$ is yet to be determined. This is justified if

$$\|\widetilde{\boldsymbol{\mathcal{E}}}_{\boldsymbol{\lambda}n}{}^{M+1}\| \ll \|\boldsymbol{\mathcal{I}} - \boldsymbol{\mathcal{K}}_{\boldsymbol{\lambda}n} - \widetilde{\boldsymbol{\mathcal{E}}}_{\boldsymbol{\lambda}n}^{(M)} \boldsymbol{\mathcal{K}}_{\boldsymbol{\lambda}n}\| \leq \|\boldsymbol{\mathcal{I}} - \boldsymbol{\mathcal{K}}_{\boldsymbol{\lambda}n}\| + \|\widetilde{\boldsymbol{\mathcal{E}}}_{\boldsymbol{\lambda}n}^{(M)} \boldsymbol{\mathcal{K}}_{\boldsymbol{\lambda}n}\|. \tag{3.2.22}$$

Eqn. (3.2.22) is referred to as the *vector-truncation condition* which, due to (3.2.3) and (3.2.20), i.e.

$$\|\widetilde{\boldsymbol{\mathcal{E}}}_{\boldsymbol{\lambda}n}^{(M)} \boldsymbol{\mathcal{K}}_{\boldsymbol{\lambda}n}\| \to 0, \quad n \to \infty \tag{3.2.23}$$

becomes

$$\|\widetilde{\boldsymbol{\mathcal{E}}}_{\boldsymbol{\lambda}n}{}^{M+1}\| \ll \|\boldsymbol{\mathcal{I}} - \boldsymbol{\mathcal{K}}_{\boldsymbol{\lambda}n}\|, \quad n \to \infty. \tag{3.2.24}$$

Vector condition (3.2.24) is more intricate than its scalar modified Nyström method counterpart (2.2.25); for the system of FIE2s (3.0.25) there are *four* truncation conditions that contain 2^M products of error operands. For example, when $M = 1$, the expanded form of (3.2.24) is

$$\begin{aligned}
&\|\widetilde{\mathcal{E}}_{\lambda,n}^{(1,1)} \widetilde{\mathcal{E}}_{\lambda,n}^{(1,1)} + \widetilde{\mathcal{E}}_{\lambda,n}^{(1,2)} \widetilde{\mathcal{E}}_{\lambda,n}^{(2,1)}\| \ll \|(\mathcal{I} - \mathcal{K}_{\lambda,n}^{(1,1)})\|, \\
&\|\widetilde{\mathcal{E}}_{\lambda,n}^{(1,2)} \widetilde{\mathcal{E}}_{\lambda,n}^{(2,2)} + \widetilde{\mathcal{E}}_{\lambda,n}^{(1,1)} \widetilde{\mathcal{E}}_{\lambda,n}^{(1,2)}\| \ll \|\mathcal{K}_{\lambda,n}^{(1,2)}\|, \\
&\|\widetilde{\mathcal{E}}_{\lambda,n}^{(2,1)} \widetilde{\mathcal{E}}_{\lambda,n}^{(1,1)} + \widetilde{\mathcal{E}}_{\lambda,n}^{(2,2)} \widetilde{\mathcal{E}}_{\lambda,n}^{(2,1)}\| \ll \|\mathcal{K}_{\lambda,n}^{(2,1)}\|, \\
&\|\widetilde{\mathcal{E}}_{\lambda,n}^{(2,1)} \widetilde{\mathcal{E}}_{\lambda,n}^{(1,2)} + \widetilde{\mathcal{E}}_{\lambda,n}^{(2,2)} \widetilde{\mathcal{E}}_{\lambda,n}^{(2,2)}\| \ll \|(\mathcal{I} - \mathcal{K}_{\lambda,n}^{(2,2)})\|,
\end{aligned} \tag{3.2.25}$$

which must be satisfied for all n. By standard norm inequalities, we have

$$\|\widetilde{\mathcal{E}}_{\lambda,n}^{(i_1,i_2)}\widetilde{\mathcal{E}}_{\lambda,n}^{(i_3,i_4)}+\widetilde{\mathcal{E}}_{\lambda,n}^{(i_5,i_6)}\widetilde{\mathcal{E}}_{\lambda,n}^{(i_7,i_8)}\| \leq \|\widetilde{\mathcal{E}}_{\lambda,n}^{(i_1,i_2)}\widetilde{\mathcal{E}}_{\lambda,n}^{(i_3,i_4)}\|+\|\widetilde{\mathcal{E}}_{\lambda,n}^{(i_5,i_6)}\widetilde{\mathcal{E}}_{\lambda,n}^{(i_7,i_8)}\|, \quad i_p = 1,2,\forall p, \tag{3.2.26}$$

in which each term on the right-hand side converges to zero for significantly large n by (3.2.3), i.e.

$$\|\widetilde{\mathcal{E}}_{\lambda,n}^{(i_1,i_2)}\widetilde{\mathcal{E}}_{\lambda,n}^{(i_3,i_4)}\| \approx \|\widetilde{\mathcal{E}}_{\lambda,n}^{(i_1,i_2)}(\mathcal{K}_{\lambda}^{(i_3,i_4)}-\mathcal{K}_{\lambda,n}^{(i_3,i_4)})\| \to 0, \quad n\to\infty, \quad i_p = 1,2,\forall p. \tag{3.2.27}$$

Due to the left-hand side of the conditions in (3.2.25) increasing in complexity with increasing M, the modified vector-Nyström method vector-truncation condition for systems of FIE2s is more stringent than that in the modified Nyström method in §2.2 (Eqn. (2.2.25)). In addition, the increasing complexity of (3.2.25) implies that, as per the modified Nyström method in §2.2, only a low value of M should be taken in the numerical implementations of the modified vector-Nyström method.

Provided condition (3.2.24) holds, the modified vector-Nyström method may be approximated as

$$\left(\boldsymbol{\mathcal{I}}+\boldsymbol{\mathcal{K}}_{\boldsymbol{\lambda}n}+\widetilde{\boldsymbol{\mathcal{E}}}_{\boldsymbol{\lambda}n}^{(M)}\boldsymbol{\mathcal{K}}_{\boldsymbol{\lambda}n}\right)\overline{\boldsymbol{u}}_n^{(M)} = \boldsymbol{f}+\widetilde{\boldsymbol{\mathcal{E}}}_{\boldsymbol{\lambda}n}^{(M)}\boldsymbol{f}, \tag{3.2.28}$$

with the error matrix operator $\widetilde{\boldsymbol{\mathcal{E}}}_{\boldsymbol{\lambda}n}$ acting only upon known matrix operator $\boldsymbol{\mathcal{K}}_{\boldsymbol{\lambda}n}$ and vector $\boldsymbol{f}$. The error of the modified vector-Nyström method in approximating the solutions of systems of FIE2s, as defined in (3.2.16) and (3.2.17), is therefore reduced by comparison with that in the standard vector-Nyström method.

3.2.2 Collocation equations

In the standard vector-Nyström method, each equation in the system (3.1.15) is evaluated at a series of collocation points thus generating a finite-dimensional space of candidate solutions. That is, the first equation in (3.1.15) is collocated at $t=\sigma_i$, $i=1,\ldots,n$, that are the roots of the Jacobi polynomial $P_n(t;\mu_1,\nu_1)$ and the second equation in (3.1.15) is collocated at $t=\rho_i$, $i=1,\ldots,n$, that are the roots of the Jacobi polynomial $P_n(t;\mu_2,\nu_2)$, i.e.,

$$\sum_{k=1}^{n}\left(\delta_{ik}-k^{(1,1)}(\sigma_i,\sigma_k)\lambda_1 c_{k,n}^{(1)}\right)u_{n,1}(\sigma_k)-\sum_{k=1}^{n}k^{(1,2)}(\sigma_i,\rho_k)\lambda_2 c_{k,n}^{(2)}u_{n,2}(\rho_k)=f_1(\sigma_i) \tag{3.2.29}$$

and

$$-\sum_{k=1}^{n} k^{(2,1)}(\rho_i,\sigma_k)\lambda_1 c_{k,n}^{(1)} u_{n,1}(\sigma_k) + \sum_{k=1}^{n}\left(\delta_{ik} - k^{(2,2)}(\rho_i,\rho_k)\lambda_2 c_{k,n}^{(2)}\right) u_{n,2}(\rho_k) = f_2(\rho_i), \tag{3.2.30}$$

where $i = 1,\ldots,n$ and δ_{ik} is the Kronecker delta. Eqns. (3.2.29) and (3.2.30) are a system of $2n$-linear equations for the nodal vector-Nyström values $u_{n,1}(\sigma_i)$ and $u_{n,2}(\rho_i)$, which via (3.1.15), are used to interpolate solution $\boldsymbol{u}_n$ for any point in the interval $[-1,1]$.

Specifically, let

$$\boldsymbol{A}_n = \begin{pmatrix} A_n^{(1,1)} & A_n^{(1,2)} \\ A_n^{(2,1)} & A_n^{(2,2)} \end{pmatrix} \tag{3.2.31}$$

be a particular *collocated-equation matrix* (CEM) with components

$$\begin{aligned} A_n^{(1,1)} &\equiv \left[\delta_{ik} - k^{(1,1)}(\sigma_i,\sigma_k)\lambda_1 c_{k,n}^{(1)}\right]_{i,k=1,\ldots,n} &&= \left[a_{i,k}^{(1,1)}\right]_{i,k=1,\ldots,n,} \\ A_n^{(1,2)} &\equiv \left[-k^{(1,2)}(\sigma_i,\rho_k)\lambda_2 c_{k,n}^{(2)}\right]_{i,k=1,\ldots,n} &&= \left[a_{i,k}^{(1,2)}\right]_{i,k=1,\ldots,n,} \\ A_n^{(2,1)} &\equiv \left[-k^{(2,1)}(\rho_i,\sigma_k)\lambda_1 c_{k,n}^{(1)}\right]_{i,k=1,\ldots,n} &&= \left[a_{i,k}^{(2,1)}\right]_{i,k=1,\ldots,n,} \\ A_n^{(2,2)} &\equiv \left[\delta_{ik} - k^{(2,2)}(\rho_i,\rho_k)\lambda_2 c_{k,n}^{(2)}\right]_{i,k=1,\ldots,n} &&= \left[a_{i,k}^{(2,2)}\right]_{i,k=1,\ldots,n.} \end{aligned} \tag{3.2.32}$$

Taking the $2n$-dimensional vectors $\boldsymbol{x}_n$ and $\boldsymbol{b}_n$ with components defined as

$$(\boldsymbol{x}_n)_i = \begin{cases} u_{n,1}(\sigma_i) & i = 1,\ldots,n, \\ u_{n,2}(\rho_{i-n}) & i = n+1,\ldots,2n \end{cases} \tag{3.2.33}$$

and

$$(\boldsymbol{b}_n)_i = \begin{cases} f_1(\sigma_i) & i = 1,\ldots,n, \\ f_2(\rho_{i-n}) & i = n+1,\ldots,2n, \end{cases} \tag{3.2.34}$$

then the collocated vector-Nyström system (3.2.29) and (3.2.30) are expressible as the $2n$-system

$$\boldsymbol{A}_n\boldsymbol{x}_n = \boldsymbol{b}_n, \tag{3.2.35}$$

with solution

$$\boldsymbol{x}_n = \boldsymbol{A}_n^{-1}\boldsymbol{b}_n. \tag{3.2.36}$$

By De Bonis and Laurita [2008, Proof of Thm. 3.1], the maximum norm of CEM $\boldsymbol{A}_n$ is

$$\|\boldsymbol{A}_n\|_\infty = \max\left\{\|(A_n^{(1,1)}A_n^{(1,2)})\|_\infty, \|(A_n^{(2,1)}A_n^{(2,2)})\|_\infty\right\}, \tag{3.2.37}$$

where

$$\|(A_n^{(1,1)}A_n^{(1,2)})\|_\infty = \max_{1\le i\le n}\left(\sum_{k=1}^{n}\left[|a_{i,k}^{(1,1)}| + |a_{i,k}^{(1,2)}|\right]\right) \tag{3.2.38}$$

and

$$\|(A_n^{(2,1)}A_n^{(2,2)})\|_\infty = \max_{1\le i\le n}\left(\sum_{k=1}^{n}\left[|a_{i,k}^{(2,1)}| + |a_{i,k}^{(2,2)}|\right]\right), \tag{3.2.39}$$

each being bounded for Gauss-Jacobi quadrature (De Bonis and Laurita [2008, Eqn. 45]). De Bonis and Laurita [2008] moreover show that

$$\|\boldsymbol{A}_n\|_\infty < \infty \tag{3.2.40}$$

and that, for some positive constant τ,

$$\|\boldsymbol{A}_n^{-1}\|_\infty \le \tau\|(\boldsymbol{\mathcal{I}} - \boldsymbol{\mathcal{K}}_{\boldsymbol{\lambda}n})^{-1}\|, \tag{3.2.41}$$

where the right-hand side is bounded by (3.1.20) and

$$cond(\boldsymbol{A}_n) \le \Psi\|(\boldsymbol{\mathcal{I}} - \boldsymbol{\mathcal{K}}_{\boldsymbol{\lambda}n})\|\|(\boldsymbol{\mathcal{I}} - \boldsymbol{\mathcal{K}}_{\boldsymbol{\lambda}n})^{-1}\| \equiv \Psi cond(\boldsymbol{\mathcal{I}} - \boldsymbol{\mathcal{K}}_{\boldsymbol{\lambda}n}), \tag{3.2.42}$$

in which Ψ is some positive constant and $cond(\boldsymbol{A}) = \|\boldsymbol{A}\|\|\boldsymbol{A}^{-1}\|$ is the condition number of the arbitrary matrix $\boldsymbol{A}$. Therefore, by (3.2.42), provided the vector-Nyström method is well-conditioned, so is its CEM (3.2.31) and hence $\boldsymbol{x}_n$ in (3.2.36) can be found.

The modified vector-Nyström method is similarly collocated at abscissae σ_i and ρ_i, $i = 1, \ldots, n$, that are roots of the respective Jacobi polynomials $P_n(t; \mu_1, \nu_1)$ and $P_n(t; \mu_2, \nu_2)$, providing a discrete approximation of the FIE2 system (3.0.25)

$$\widetilde{\boldsymbol{A}}_n\widetilde{\boldsymbol{x}}_n = \widetilde{\boldsymbol{b}}_n, \tag{3.2.43}$$

satisfied by the $2n$-dimensional vector

$$(\widetilde{\boldsymbol{x}}_n)_i = \begin{cases} \overline{u}_{n,1}^{(M)}(\sigma_i) & i = 1, \ldots, n, \\ \overline{u}_{n,2}^{(M)}(\rho_{i-n}) & i = n+1, \ldots, 2n, \end{cases} \tag{3.2.44}$$

where

$$\widetilde{\boldsymbol{A}}_n = \begin{pmatrix} \widetilde{A}_n^{(1,1)} & \widetilde{A}_n^{(1,2)} \\ \widetilde{A}_n^{(2,1)} & \widetilde{A}_n^{(2,2)} \end{pmatrix} \quad \text{and} \quad \widetilde{\boldsymbol{b}}_n = \begin{pmatrix} \widetilde{b}_{n,1} \\ \widetilde{b}_{n,2} \end{pmatrix}. \tag{3.2.45}$$

Defining the matrix operator (3.2.20) as

$$\widetilde{\boldsymbol{\mathcal{E}}}_{\boldsymbol{\lambda}n}^{(M)} = \begin{pmatrix} \left[\widetilde{\mathcal{E}}_{\lambda,n}^{(M)}\right]^{(1,1)} & \left[\widetilde{\mathcal{E}}_{\lambda,n}^{(M)}\right]^{(1,2)} \\ \left[\widetilde{\mathcal{E}}_{\lambda,n}^{(M)}\right]^{(2,1)} & \left[\widetilde{\mathcal{E}}_{\lambda,n}^{(M)}\right]^{(2,2)} \end{pmatrix}, \tag{3.2.46}$$

the components of the CEM $\widetilde{\boldsymbol{A}}_n$ in (3.2.45) are

$$\begin{aligned}
\widetilde{A}_n^{(1,1)} &\equiv \left[\delta_{i,k} - k^{(1,1)}(\sigma_i,\sigma_k)\lambda_1 c_{k,n}^{(1)} - \left(\left[\widetilde{\mathcal{E}}_{\lambda,n}^{(M)}\right]^{(1,1)} \mathcal{K}_{\lambda,n}^{(1,1)} + \left[\widetilde{\mathcal{E}}_{\lambda,n}^{(M)}\right]^{(1,2)} \mathcal{K}_{\lambda,n}^{(2,1)}\right)_{i,k}\right]_{i,k=1,\ldots,n} \\
&= \left[\widetilde{a}_{i,k}^{(1,1)}\right]_{i,k=1,\ldots,n}, \\
\widetilde{A}_n^{(1,2)} &\equiv \left[-k^{(1,2)}(\sigma_i,\rho_k)\lambda_2 c_{k,n}^{(2)} - \left(\left[\widetilde{\mathcal{E}}_{\lambda,n}^{(M)}\right]^{(1,1)} \mathcal{K}_{\lambda,n}^{(1,2)} + \left[\widetilde{\mathcal{E}}_{\lambda,n}^{(M)}\right]^{(1,2)} \mathcal{K}_{\lambda,n}^{(2,2)}\right)_{i,k}\right]_{i,k=1,\ldots,n} \\
&= \left[\widetilde{a}_{i,k}^{(1,2)}\right]_{i,k=1,\ldots,n}, \\
\widetilde{A}_n^{(2,1)} &\equiv \left[-k^{(2,1)}(\rho_i,\sigma_k)\lambda_1 c_{k,n}^{(1)} - \left(\left[\widetilde{\mathcal{E}}_{\lambda,n}^{(M)}\right]^{(2,1)} \mathcal{K}_{\lambda,n}^{(1,1)} + \left[\widetilde{\mathcal{E}}_{\lambda,n}^{(M)}\right]^{(2,2)} \mathcal{K}_{\lambda,n}^{(2,1)}\right)_{i,k}\right]_{i,k=1,\ldots,n} \\
&= \left[\widetilde{a}_{i,k}^{(2,1)}\right]_{i,k=1,\ldots,n}, \\
\widetilde{A}_n^{(2,2)} &\equiv \left[\delta_{i,k} - k^{(2,2)}(\rho_i,\rho_k)\lambda_2 c_{k,n}^{(2)} - \left(\left[\widetilde{\mathcal{E}}_{\lambda,n}^{(M)}\right]^{(2,1)} \mathcal{K}_{\lambda,n}^{(1,2)} + \left[\widetilde{\mathcal{E}}_{\lambda,n}^{(M)}\right]^{(2,2)} \mathcal{K}_{\lambda,n}^{(2,2)}\right)_{i,k}\right]_{i,k=1,\ldots,n} \\
&= \left[\widetilde{a}_{i,k}^{(2,2)}\right]_{i,k=1,\ldots,n}
\end{aligned} \tag{3.2.47}$$

and *collocated-equation vector* (CEV) $\widetilde{\boldsymbol{b}}_n$ are

$$\begin{aligned}
\widetilde{b}_{n,1} &= \left[f_1(\sigma_i) + \left(\left[\widetilde{\mathcal{E}}_{\lambda,n}^{(M)}\right]^{(1,1)} f_1(\sigma_i) + \left[\widetilde{\mathcal{E}}_{\lambda,n}^{(M)}\right]^{(1,2)} f_2(\sigma_i)\right)_i\right]_{i=1,\ldots,n,} \\
\widetilde{b}_{n,2} &= \left[f_2(\rho_i) + \left(\left[\widetilde{\mathcal{E}}_{\lambda,n}^{(M)}\right]^{(2,1)} f_1(\rho_i) + \left[\widetilde{\mathcal{E}}_{\lambda,n}^{(M)}\right]^{(2,2)} f_2(\rho_i)\right)_i\right]_{i=1,\ldots,n.}
\end{aligned} \tag{3.2.48}$$

The components of matrix operator (3.2.46) are summations of M products of the error operators $\widetilde{\mathcal{E}}_{\lambda,n}^{(i,j)}$: recall the left-hand side of truncation condition (3.2.25) when $M = 1$. Hence the explicit composition of the components

$$\left(\left[\widetilde{\mathcal{E}}_{\lambda,n}^{(M)}\right]^{(j_1,j_2)} \mathcal{K}_{\lambda,n}^{(i_1,i_2)}\right)_{i,k} \quad \text{and} \quad \left(\left[\widetilde{\mathcal{E}}_{\lambda,n}^{(M)}\right]^{(j_1,j_2)} f_{i_1}(\sigma_i)\right)_i, \quad i_p, j_p = 1,2, \forall p, \tag{3.2.49}$$

require the definition of $\widetilde{\mathcal{E}}_{\lambda,n}^{(i,j)}$.

Provided $\widetilde{\mathcal{E}}_{\lambda,n}^{(i,j)}$ closely approximates the exact quadrature operator $\mathcal{E}_{\lambda,n}^{(i,j)}$, both should possess the

same quantitative properties., e.g. following (3.1.9),

$$(\widetilde{\mathcal{E}}_{\lambda,n}^{(i,j)}u_j)(t) \to 0, \quad n \to \infty. \tag{3.2.50}$$

Eqn. (3.2.50) implies the matrix operator $\widetilde{\boldsymbol{\mathcal{E}}}_{\boldsymbol{\lambda}n}^{(M)}$, which consists of products of $\widetilde{\mathcal{E}}_{\lambda,n}^{(i,j)}$, acting upon an arbitrary matrix $\mathbf{A} = A_{i,j}$

$$\widetilde{\boldsymbol{\mathcal{E}}}_{\boldsymbol{\lambda}n}^{(M)}\mathbf{A} = \sum_{m=1}^{M} \widetilde{\boldsymbol{\mathcal{E}}}_{\boldsymbol{\lambda}n}{}^{m} A_{i,j}, \tag{3.2.51}$$

converges to zero in a pointwise sense with increasing n, i.e. (Kelmanson and Tenwick [2010])

$$\|\widetilde{\boldsymbol{\mathcal{E}}}_{\boldsymbol{\lambda}n}^{(M)}\boldsymbol{A}\|_\infty \to 0, \quad n \to \infty. \tag{3.2.52}$$

Letting $\boldsymbol{E}_n$ be the matrix (N.B. not operator) difference between the CEM $\boldsymbol{A}_n$ in the standard vector-Nyström method (3.2.31) and the CEM $\widetilde{\boldsymbol{A}}_n$ in the modified vector-Nyström method (3.2.45), namely

$$\boldsymbol{E}_n = \boldsymbol{A}_n - \widetilde{\boldsymbol{A}}_n, \tag{3.2.53}$$

then, by (3.1.15) and (3.2.28),

$$\boldsymbol{E}_n = \widetilde{\boldsymbol{\mathcal{E}}}_{\boldsymbol{\lambda}n}^{(M)}\boldsymbol{\mathcal{K}}_{\boldsymbol{\lambda}n} \tag{3.2.54}$$

and thus (3.2.52) yields

$$\|\boldsymbol{E}_n\|_\infty \to 0, \quad n \to \infty. \tag{3.2.55}$$

Therefore, provided $\boldsymbol{A}_n^{-1}$ exists, $\widetilde{\boldsymbol{A}}_n$ is also invertible if and only if (Golub and Van Loan [1996], Groh and Kelmanson [2008])

$$\|\boldsymbol{A}_n^{-1}\|_\infty\|\boldsymbol{E}_n\|_\infty < 1, \tag{3.2.56}$$

which is guaranteed for large n because of (3.2.41) and (3.2.55).

3.3 Error analysis

The explicit form of the error $\mathcal{E}_{\lambda,n}^{(i,j)}u_j$, denoted as $\widehat{\mathcal{E}}_{\lambda,n}^{(i,j)}u_j$, for any orthogonal-polynomial quadrature is

$$(\widehat{\mathcal{E}}_{\lambda,n}^{(i,j)}u_j)(t,s^*) \equiv \lambda_j\beta_n^{(j)}\widehat{\delta}_n^{(i,j)}(u_j;t,s^*), \tag{3.3.1}$$

where

$$\beta_n^{(j)} = \frac{\gamma_n^{(j)}}{\left[A_n^{(j)}\right]^2 (2n)!} \quad \text{and} \quad \widehat{\delta}_n^{(i,j)}(u_j;t,s^*) = \left[\frac{\partial^{2n}}{\partial s^{2n}}\left(k^{(i,j)}(t,s)u_j(s)\right)\right]_{s=s^*} \tag{3.3.2}$$

for some unknown $s^* \in [-1,1]$. The variables $\gamma_n^{(j)}$ and $A_n^{(j)}$ are respectively defined in (3.1.6) and (3.1.7) for Gauss-Jacobi polynomial $P_n(s;\mu_j,\nu_j)$.

Owing to the symmetry of μ_j and ν_j in (3.1.2) for $j = 1,2$, (3.3.2) implies $\beta_n^{(1)} = \beta_n^{(2)}$ and so $\beta_n^{(j)} = \beta_n$ for all j. Moreover,

$$\beta_n = \frac{2^{\mu_j+\nu_j+1}\sqrt{\pi}\Gamma(n+\nu_j+1)\Gamma(n+\mu_j+1)\Gamma(n+\mu_j+\nu_j+1)}{\Gamma(n+\frac{1}{2})\Gamma(2n+\mu_j+\nu_j+1)\Gamma(2n+\mu_j+\nu_j+2)} \tag{3.3.3}$$

is exponentially convergent to zero with n (Kelmanson and Tenwick [2010]) independently of μ_j and ν_j.

In parallel with §2.2, the implementation of error (3.3.1) is possible only if the unknown parameter s^* is removed. Therefore, we apply the integral mean-value theorem to $\widehat{\delta}_n^{(i,j)}$ in (3.3.2) so that

$$\widehat{\delta}_n^{(i,j)} = \overline{\delta}_n^{(i,j)} + \widehat{\epsilon}_n^{(j)}, \tag{3.3.4}$$

where

$$\overline{\delta}_n^{(i,j)}(u_j;t) = \frac{1}{2}\left[\frac{\partial^{2n-1}}{\partial s^{2n-1}}\left[k^{(i,j)}(t,s)u_j(s)\right]\right]_{s=-1}^{s=1} \tag{3.3.5}$$

and $k^{(i,j)}(t,s)$ is continuously differentiable for all s, by construction, but $u_j(s)$ must be $(2n-1)$-times continuously differentiable for all j. By the hypothesis $\|\widehat{\epsilon}_n^{(j)}\| \ll \|\overline{\delta}_n^{(i,j)}\|$ for all n, using (3.3.1) and (3.3.4) we approximate the true error $(\widehat{\mathcal{E}}_{\lambda,n}^{(i,j)}u_j)(t,s^*)$ as the mean value, over all s^*,

$$(\overline{\mathcal{E}}_{\lambda,n}^{(i,j)}u_j)(t) \equiv \lambda_j\beta_n\overline{\delta}_n^{(i,j)}(u_j;t), \tag{3.3.6}$$

referred to as the *computable* predictable error, with a sub-error of order $\mathcal{O}(\beta_n\widehat{\epsilon}_n^{(j)})$.

Finally, a comparison between (3.3.1), (3.3.6) and the actual error $(\mathcal{E}_{\lambda,n}^{(i,j)}u_j)$ in (3.1.8) yields the true and predicted error discrepancies respectively as

$$\Delta\widehat{\mathcal{E}}_{\lambda,n}^{(i,j)}u_j \equiv \left(\mathcal{E}_{\lambda,n}^{(i,j)} - \widehat{\mathcal{E}}_{\lambda,n}^{(i,j)}\right)u_j, \tag{3.3.7}$$

and

$$\Delta\overline{\mathcal{E}}_{\lambda,n}^{(i,j)}u_j \equiv \left(\mathcal{E}_{\lambda,n}^{(i,j)} - \overline{\mathcal{E}}_{\lambda,n}^{(i,j)}\right)u_j, \tag{3.3.8}$$

which lead to the matrix forms

$$\Delta\widehat{\boldsymbol{\mathcal{E}}}_{\boldsymbol{\lambda}n} = \begin{pmatrix} \Delta\widehat{\mathcal{E}}^{(1,1)}_{\lambda,n} & \Delta\widehat{\mathcal{E}}^{(1,2)}_{\lambda,n} \\ \Delta\widehat{\mathcal{E}}^{(2,1)}_{\lambda,n} & \Delta\widehat{\mathcal{E}}^{(2,2)}_{\lambda,n} \end{pmatrix} \quad \text{and} \quad \Delta\overline{\boldsymbol{\mathcal{E}}}_{\boldsymbol{\lambda}n} = \begin{pmatrix} \Delta\overline{\mathcal{E}}^{(1,1)}_{\lambda,n} & \Delta\overline{\mathcal{E}}^{(1,2)}_{\lambda,n} \\ \Delta\overline{\mathcal{E}}^{(2,1)}_{\lambda,n} & \Delta\overline{\mathcal{E}}^{(2,2)}_{\lambda,n} \end{pmatrix}, \tag{3.3.9}$$

corresponding to (3.1.13).

3.3.1 Validation of the predicted error

We validate the predicted quadrature error (3.3.6), by quantified discrepancies (3.3.7) and (3.3.8), in a series of test problems. In both this section and the remainder of the chapter we will use the test FIE2

$$U(T) = F(T) + \Lambda \int_a^b |S-c|^\alpha \exp(-T^2 S) U(S)\, dS, \tag{3.3.10}$$

where given a known exact solution $U(S) = \exp(S)\cos(S)$, the forcing function is defined by

$$F(T) = \exp(T)\cos(T) - \Lambda \int_a^b |S-c|^\alpha \exp(-T^2 S)\exp(S)\cos(S)\, dS. \tag{3.3.11}$$

The theory is tested for $n = 2$ and parameters $[a,b] = [-\frac{5}{4}, \frac{5}{4}]$, $c = \frac{1}{2}(a+b)$ and $\alpha = \frac{1}{2}$ in FIE2 (3.3.10). A comparison of the predicted error discrepancy $\Delta\overline{\mathcal{E}}^{(i,j)}_{\lambda,n} u_j(t)$ against its true counterpart $\Delta\widehat{\mathcal{E}}^{(i,j)}_{\lambda,n} u_j(t, s^*)$ is depicted in Fig 3.3.1 for *both* solutions, $u_1(t)$ and $u_2(t)$, of system (3.0.25). Each sub-figure in Fig 3.3.1 are for the different values of $i, j = 1, 2$ that correspond to the four Gaussian quadrature approximated integrals in the system (3.2.28). Fig 3.3.1 demonstrates three facts: first, $\Delta\overline{\boldsymbol{\mathcal{E}}}_{\boldsymbol{\lambda}n}\overline{\boldsymbol{u}}_n$ is both more uniform and smaller in modulus than the true error discrepancy $\Delta\widehat{\boldsymbol{\mathcal{E}}}_{\boldsymbol{\lambda}n}\overline{\boldsymbol{u}}_n$; second, the error discrepancies are converging to zero as n is increased in agreement with (3.2.5), and; third, $\Delta\overline{\boldsymbol{\mathcal{E}}}_{\boldsymbol{\lambda}n}\overline{\boldsymbol{u}}_n$ is closer to the exact global error discrepancy $Delta\boldsymbol{\mathcal{E}}_{\boldsymbol{\lambda}n}\overline{\boldsymbol{u}}_n = \mathbf{0}$ than $\Delta\widehat{\boldsymbol{\mathcal{E}}}_{\boldsymbol{\lambda}n}\overline{\boldsymbol{u}}_n$.

Fig. 3.3.2 compares the individual components of the actual error $(\mathcal{E}^{(i,j)}_{\lambda,n} u_j)$ in (3.1.8) with the predicted error $(\overline{\mathcal{E}}^{(i,j)}_{\lambda,n} u_j)$ in (3.3.8), for only $n = 2$ in both solutions $u_1(t)$ and $u_2(t)$. Divergences occur between $\mathcal{E}^{(i,j)}_{\lambda,n}$ and $\overline{\mathcal{E}}^{(i,j)}_{\lambda,n}$ in Fig. 3.3.2 due to the latter having an error of order $\mathcal{O}(\beta_n \widehat{\epsilon}^{(j)}_n)$, which decreases exponentially with n, from the integral mean-value estimation (3.3.4). The results in Figs. 3.3.1 and 3.3.2 reflect those seen in the validations of §2.2 (Figs. 2.4.1 and 2.4.2), and show a close correlation between that of the exact error and the predicted error. This is a demonstration

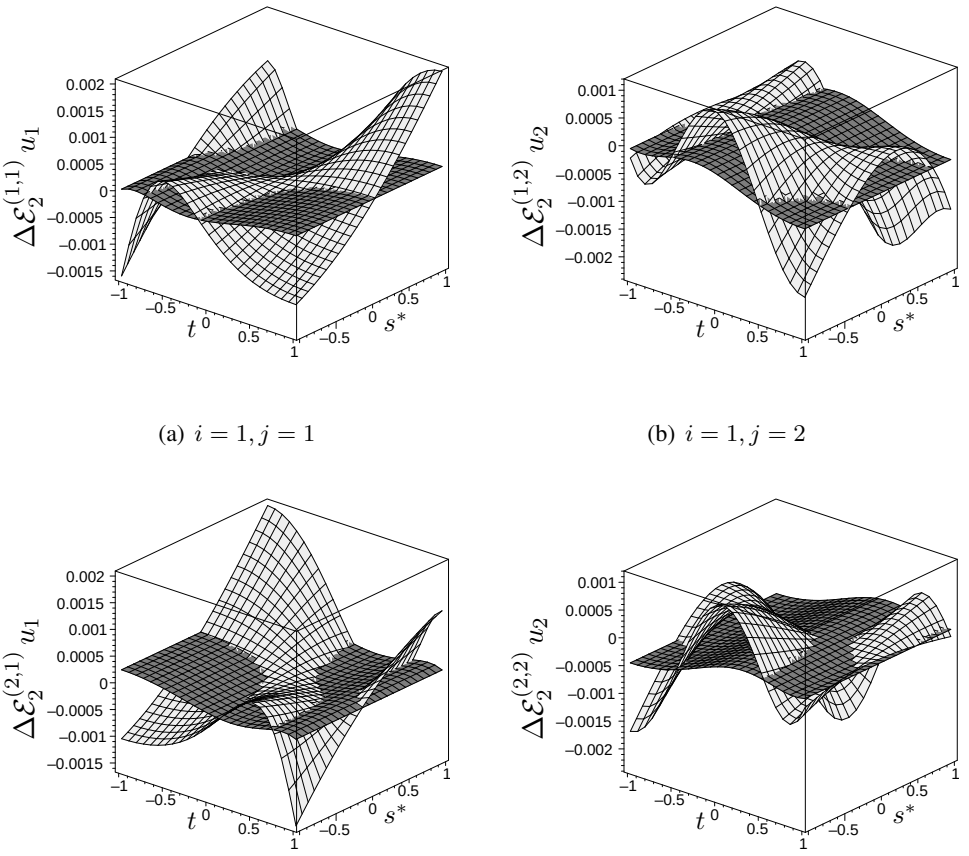

(a) $i = 1, j = 1$ (b) $i = 1, j = 2$

(c) $i = 2, j = 1$ (d) $i = 2, j = 2$

Figure 3.3.1: *True error discrepancy* $\Delta\widehat{\mathcal{E}}_{\lambda,n}^{(i,j)}u_j(t,s^*)$ *(light) and predicted error discrepancy* $\Delta\overline{\mathcal{E}}_{\lambda,n}^{(i,j)}u_j(t)$ *(dark) for* $i,j = 1,2$ *and* $n = 2$ *in* (3.3.7) *and* (3.3.8) *for a singular kernel function using Gauss-Jacobi quadrature with* $[a,b] = [-\frac{5}{4},\frac{5}{4}]$, $c = \frac{1}{2}(a+b)$ *and* $\alpha = \frac{1}{2}$ *in test FIE2* (3.3.10).

of the justification to employ the predicted error operator $\overline{\mathcal{E}}_{\lambda,n}^{(i,j)}$ as an approximation to $\widetilde{\mathcal{E}}_{\lambda,n}^{(i,j)}$ in the application of modified vector-Nyström method. With a validation prediction in place, we may now define the composition of the terms $\left(\overline{\boldsymbol{\mathcal{E}}}_{\boldsymbol{\lambda}n}^{(M)}\boldsymbol{\mathcal{K}}_{\boldsymbol{\lambda}n}\right)_{ik}$ and $\left(\overline{\boldsymbol{\mathcal{E}}}_{\boldsymbol{\lambda}n}^{(M)}\boldsymbol{f}\right)_i$ in (3.2.49), i.e. the components of the CEM (3.2.47) and the components of the CEV (3.2.48). The operator matrix $\overline{\boldsymbol{\mathcal{E}}}_{\boldsymbol{\lambda}n}^{(M)}\boldsymbol{\mathcal{K}}_{\boldsymbol{\lambda}n}$ comprise a series of products of $\overline{\mathcal{E}}_{\lambda,n}^{(i,j)}$ acting upon $\mathcal{K}_{\lambda,n}^{(l,m)}$, relative to quadrature based

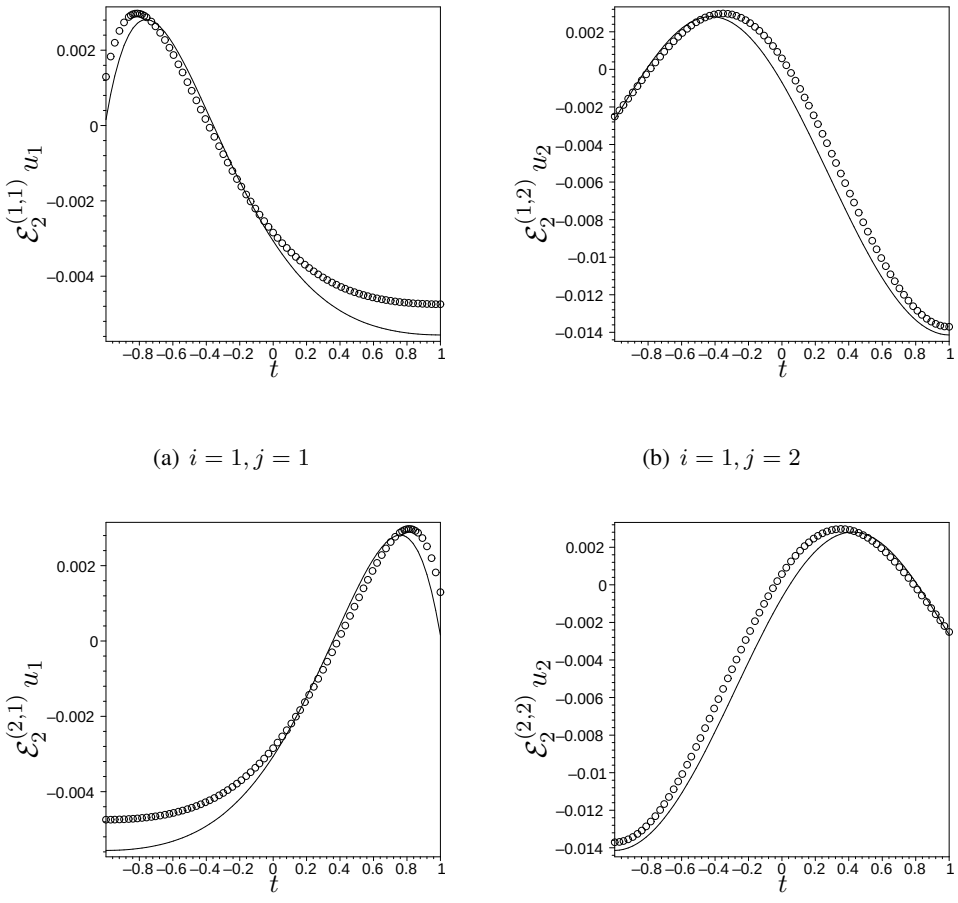

(a) $i = 1, j = 1$ (b) $i = 1, j = 2$

(c) $i = 2, j = 1$ (d) $i = 2, j = 2$

Figure 3.3.2: *Actual error* $\mathcal{E}_{\lambda,n}^{(i,j)} u_j(t)$ *(line) and predicted error* $\overline{\mathcal{E}}_{\lambda,n}^{(i,j)} u_j(t)$ *(circles) for* $i, j = 1, 2$ *and* $n = 2$ *in* (3.1.8) *and* (3.3.6)*, for a singular kernel function computed using Gauss-Jacobi quadrature* (3.0.27)*. The test problem is same as that used in Fig. 3.3.1. It is evident that the discrepancy between the curves results from the omission of* $\widehat{\epsilon}_n^{(j)}$ *in* (3.3.6)*: this discrepancy decreases rapidly with increasing* n*, and is not visible on this scale for* $n = 3$*.*

on the Jacobi polynomial $P_n(s; \mu_m, \nu_m)$. Defining

$$\mathcal{H}_{n,r}\left[F(s_r)\right] \equiv \frac{\beta_n}{2} \frac{\partial^{2n-1}}{\partial s_r^{2n-1}} \left[F(s_r)\right]\Big|_{s_r=-1}^{s_r=1}, \tag{3.3.12}$$

then, by (3.3.6), the direct action of $\overline{\mathcal{E}}_{\lambda,n}^{(i,j)}$ upon $\mathcal{K}_{\lambda,n}^{(l,m)}$ becomes

$$\begin{cases} \left(\overline{\mathcal{E}}_{\lambda,n}^{(i,j)}\mathcal{K}_{\lambda,n}^{(l,1)}\right)(t) = \mathcal{H}_{n,1}\lambda_j\left[k^{(i,j)}(t,s_1)\displaystyle\sum_{k=1}^{n}k^{(l,1)}(s_1,\sigma_k)\lambda_1 c_{k,n}^{(1)}\right] & m=1, \\ \left(\overline{\mathcal{E}}_{\lambda,n}^{(i,j)}\mathcal{K}_{\lambda,n}^{(l,2)}\right)(t) = \mathcal{H}_{n,1}\lambda_j\left[k^{(i,j)}(t,s_1)\displaystyle\sum_{k=1}^{n}k^{(l,2)}(s_1,\rho_k)\lambda_2 c_{k,n}^{(2)}\right] & m=2, \end{cases} \tag{3.3.13}$$

where $i,j,l=1,2$. Eqn. (3.3.13) is extendible to the direct action of N error operators $\overline{\mathcal{E}}_{\lambda,n}^{(p_j,q_j)}$, $j=1,\ldots,N$, acting upon $\mathcal{K}_{\lambda,n}^{(l,m)}$, required for implementing $\overline{\boldsymbol{\mathcal{E}}}_{\boldsymbol{\lambda}n}^{(M)}$ in (3.2.20), e.g. when $m=1$

$$\begin{aligned}\left(\prod_{j=1}^{N}\overline{\mathcal{E}}_{\lambda,n}^{(p_j,q_j)}\mathcal{K}_{\lambda,n}^{(l,1)}\right)(t) =& \mathcal{H}_{n,1}\Bigg[\lambda_{q_1}k^{(p_1,q_1)}(t,s_1)\mathcal{H}_{n,2}\Bigg[\lambda_{q_2}k^{(p_2,q_2)}(s_1,s_2)\ldots \\ & \mathcal{H}_{n,N}\left[\lambda_{q_N}k^{(p_N,q_N)}(s_{N-1},s_N)\sum_{k=1}^{n}k^{(l,1)}(s_N,\sigma_k)\lambda_1 c_{k,n}^{(1)}\right]\ldots\Bigg]\Bigg],\end{aligned} \tag{3.3.14}$$

where $p_j,q_j=1,2$ for all j and $N=1,\ldots,M$. A similar expression is obtainable when $m=2$ from extending the second expression in (3.3.13).

By (3.3.6) and (3.3.12), the direct action of $\overline{\mathcal{E}}_{\lambda,n}^{(p_j,q_j)}$, $j=1,\ldots,N$, upon f_m is

$$\begin{aligned}\left(\prod_{j=1}^{N}\overline{\mathcal{E}}_{\lambda,n}^{(p_j,q_j)}f_m\right)(t) =& \mathcal{H}_{n,1}\Bigg[\lambda_{q_1}k^{(p_1,q_1)}(t,s_1)\mathcal{H}_{n,2}\Bigg[\lambda_{q_2}k^{(p_2,q_2)}(s_1,s_2)\ldots \\ & \mathcal{H}_{n,N}\left[\lambda_{q_N}k^{(p_N,q_N)}(s_{N-1},s_N)f_m(s_N)\right]\ldots\Bigg]\Bigg], \quad m=1,2,\end{aligned} \tag{3.3.15}$$

where $p_j,q_j=1,2$ for all j and $N=1,\ldots,M$. Evaluating (3.3.14) and (3.3.15) at $t=\sigma_i$ or $t=\rho_i$, $i=1,\ldots,n$, depending upon the integral equation in the system of FIE2s, the collocated forms for $\left(\widetilde{\boldsymbol{\mathcal{E}}}_{\boldsymbol{\lambda}n}^{(M)}\boldsymbol{\mathcal{K}}_{\boldsymbol{\lambda}n}\right)_{ik}$ and $\left(\widetilde{\boldsymbol{\mathcal{E}}}_{\boldsymbol{\lambda}n}^{(M)}\boldsymbol{f}\right)_i$ can be acquired.

The key attribute of expressions (3.3.14) and (3.3.15) lies in the demonstration of the increasing powers of β_n with increasing M, owing to the definition of $\mathcal{H}_{n,r}$ in (3.3.12). Consequently, due to the aforementioned exponential convergence of β_n in (3.3.3), the M-term truncation $\widetilde{\boldsymbol{\mathcal{E}}}_{\boldsymbol{\lambda}n}^{(M)}$ in (3.2.20) should closely approximate the action of $\overline{\boldsymbol{\mathcal{E}}}_{\boldsymbol{\lambda}n}$ for relatively low values of M; a maximum of $M=2$ shall be imposed in the subsequent numerical implementations.

3.4 Comparison of numerical schemes

The standard and modified vector-Nyström method will now be validated for the test FIE2 (3.3.10) with known exact solution $U(S) = \exp(S)\cos(S)$ and constant Λ prescribed over interval $[a, b]$. The corresponding forcing function $F(T)$ and quadrature rule $\mathcal{K}_{\lambda,n}^{(i,j)}$ are generated from (3.3.11) and (3.1.3)-(3.1.7) respectively.

To proceed, we define a modified Nyström system *error*,

$$e_{n,i}^{(M)} u_i(t) \equiv \left\| u_i - \overline{u}_{n,i}^{(M)} \right\|_\infty, \quad M \geq 0. \tag{3.4.1}$$

The test problems, assimilated for low values of M and n to agree with our original aim, present both solutions u_1 and u_2 of the system of FIE2s (3.0.25) unless otherwise stated. With this in mind, Figs. 3.4.1-3.4.5 show the modified Nyström error (3.4.1) for low orders of quadrature. In Figs. 3.4.1 and 3.4.2 we have the modified vector-Nyström error in the approximate solutions $\overline{u}_{n,1}^{(M)}$ and $\overline{u}_{n,2}^{(M)}$ respectively for $\alpha = 0.5$ and only $n = 2$ quadrature nodes, where each sub-figure is for a fixed value of Λ and the separate curves on each sub-figure are for different values of M. The key feature of the results in Figs. 3.4.1 and 3.4.2 are the smallest errors in the modified method when $|\Lambda| \ll 1$ and the largest when $|\Lambda| \to 1$. The reason for such behaviour is due to truncation condition matrix (3.2.24) consisting of products of $M + 1$ error terms that are dependent upon $\lambda_j \beta_n$, which is approximately $\frac{\Lambda}{2}\beta_n$ by (3.0.19) and (3.0.20), hence when $|\Lambda| \to 1$ the four truncation conditions present in the system are violated.

Since

$$\lim_{\alpha \to -1} |\lambda_j| = |\Lambda|, \quad \forall j, \tag{3.4.2}$$

the prescribed value of $|\Lambda|$ also significantly affects the modified Nyström error (3.4.1) when the weight function $w_j(s)$ becomes hypersingular, i.e. $\alpha \to -1$. In Fig. 3.4.3 $\alpha \to -1$ and Λ is taken as $|\Lambda| = 0.1$ or $|\Lambda| = 0.001$, the former of which yields a converging modified Nyström error with increasing M when $\alpha = 0.5$ in Fig. 3.4.1. However, when $|\Lambda| = 0.1$ and $\alpha \approx -1$ Fig. 3.4.3(e) shows the modified Nyström error for $M = 2$ is uniformly larger than that for $M = 1$. A reduction in $|\Lambda|$ by two orders of magnitude, i.e. taking $|\Lambda| = 0.001$ (Fig. 3.4.3(f)), recovers the accuracy in the modified Nyström error yet causes a negligible effect when $M > 1$. This is a result of the product series (3.3.14) and (3.3.15) being a power series in $\lambda_j \beta_n$, which by λ_j in

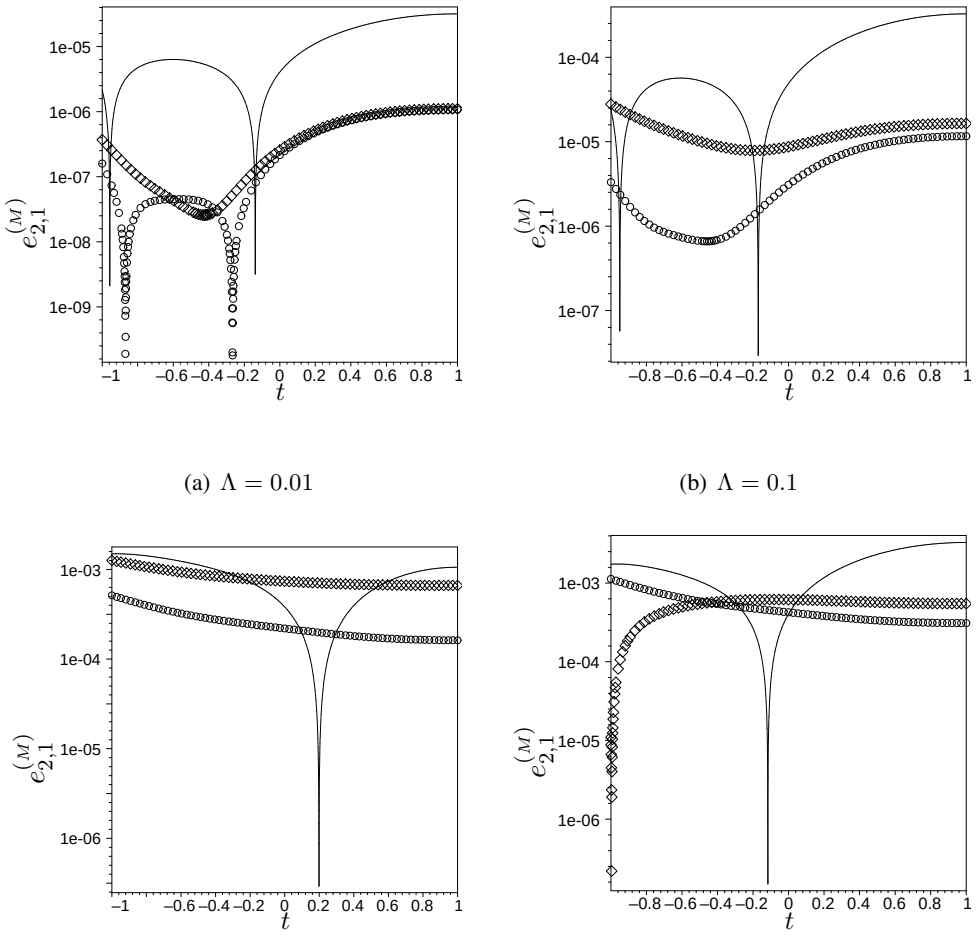

(a) $\Lambda = 0.01$ (b) $\Lambda = 0.1$

(c) $\Lambda = 0.5$ (d) $\Lambda = 1$

Figure 3.4.1: *The modified Nyström errors* $e_{n,i}^{(M)} u_i(t)$ (3.4.1) *for fixed* $n = 2$ *and* $i = 1$ *and different values of* Λ*, computed using Gauss-Jacobi quadrature of Eqn.* (3.1.3)*. The above numerical experiment uses* $[a, b] = [-\frac{5}{4}, \frac{5}{4}]$*,* $c = \frac{1}{2}(b + a)$ *and* $\alpha = 0.5$ *in the test FIE2* (3.3.10)*. Successive modifications of the standard vector-Nyström error,* $M = 0$ $(-)$*, are shown by* $M = 1$ $(\diamond)$ *and* $M = 2$ $(\circ)$*.*

(3.0.19) and (3.0.20), the convergence of $\|\widetilde{\boldsymbol{\mathcal{E}}}_{\boldsymbol{\lambda}n}^{(M)} - \overline{\boldsymbol{\mathcal{E}}}_{\boldsymbol{\lambda}n}^{(M)}\|$ is eroded as $|\Lambda|$ increases. On the other hand, by the nested operations in (3.3.14) and (3.3.15), the effect of $\overline{\boldsymbol{\mathcal{E}}}_{\boldsymbol{\lambda}n}^{(M)}$ in the modified vector-Nyström method is negligible when M increases if the magnitude of Λ is significantly small, i.e. $|\Lambda| \leq \mathcal{O}(10^{-3})$.

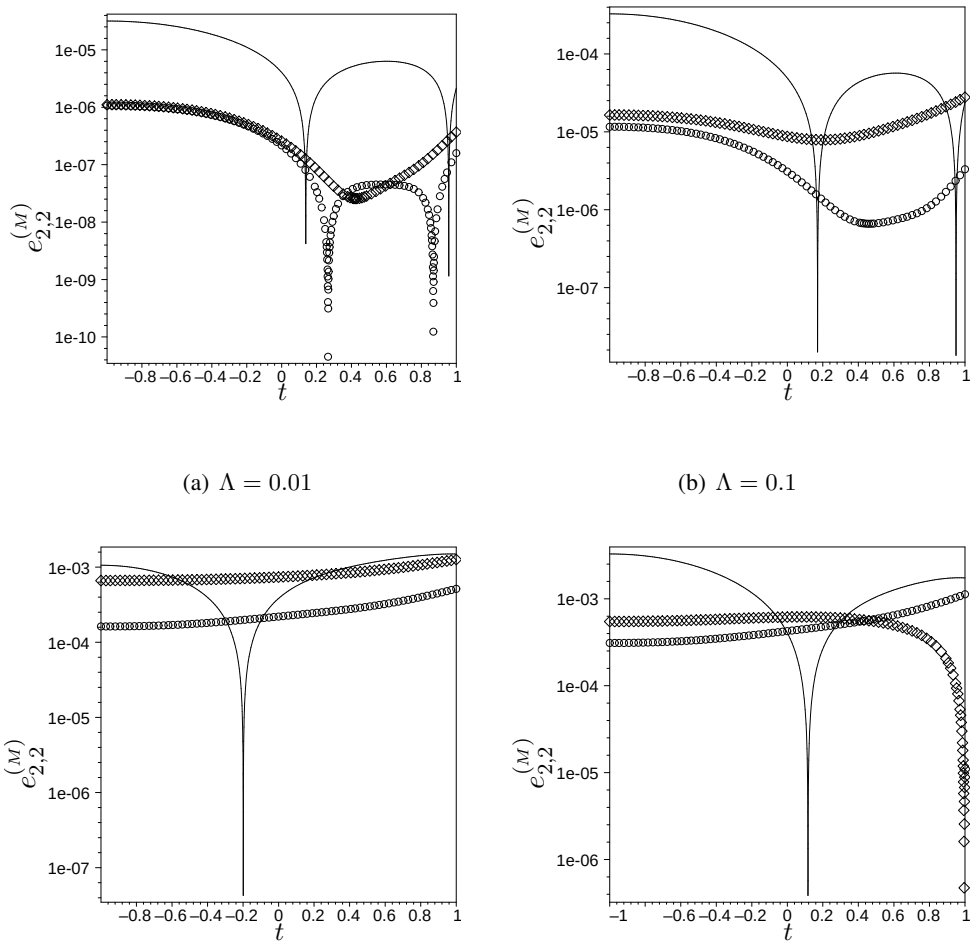

(a) $\Lambda = 0.01$

(b) $\Lambda = 0.1$

(c) $\Lambda = 0.5$

(d) $\Lambda = 1$

Figure 3.4.2: *The modified Nyström errors* $e_{n,i}^{(M)} u_i(t)$ (3.4.1) *for fixed* $n = 2$ *and* $i = 2$ *and different values of* Λ*, computed using Gauss-Jacobi quadrature of Eqn.* (3.1.4)*. The above numerical experiment uses* $[a, b] = [-\frac{5}{4}, \frac{5}{4}]$*,* $c = \frac{1}{2}(b + a)$ *and* $\alpha = 0.5$ *in the test FIE2* (3.3.10)*. Successive modifications of the standard vector-Nyström error,* $M = 0$ $(-)$*, are shown by* $M = 1$ $(\diamond)$ *and* $M = 2$ $(\circ)$.

Another fundamental aspect in determining the accuracy of the standard and modified vector-Nyström method is the positioning of the singular point c within the integration domain $[a, b]$. Further analysis of the position of c necessitates the introduction of the variable ξ, defined by the

ratio between the distance from the singular point to either end-point as

$$\xi \equiv \left(\frac{\lambda_1}{\lambda_2}\right) = \left(\frac{c-a}{b-c}\right)^{\alpha+1}. \tag{3.4.3}$$

Clearly if $c \to a$ then $\xi \to 0$ and similarly if $c \to b$ then $\xi \to \infty$ as $\alpha > -1$. In Fig 3.4.4 both solutions of the FIE2 (3.0.25) are presented for different positions of c in the domain and fixed $\alpha = 0$, so that the test problem matches that used in Fig. 2.4.1 in §2.4. As $\xi \to \infty$ in Fig 3.4.4 the modified Nyström error of $\overline{u}_{n,1}^{(M)}(t)$ in (3.2.28) matches that of $\overline{u}_n^{(M)}(t)$ in (2.2.26) for a single FIE2 because of the scalings (3.0.19) and (3.0.20). The modified Nyström error of $\overline{u}_{n,2}^{(M)}(t)$ in Fig 3.4.4, however, is fixed for all $M > 0$ owing to the dependency of the operator $\overline{\mathcal{E}}_{\lambda,n}^{(i,2)}$ upon λ_2 ($\ll 1$ as $|b-c| \ll 1$) in (3.3.6) causing $\overline{\boldsymbol{\mathcal{E}}}_{\boldsymbol{\lambda}n}^{(M)}$ in the modified method to be negligible. On the other hand, if $|c-a| \gg 1$ or $|b-c| \gg 1$, the subintervals (3.0.4) must be divided into smaller subintervals to prevent the divergence of the power series (3.3.14) and (3.3.15) by ensuring $\lambda_j \beta_n < 1$.

A disadvantage to approximating systems of FIE2s is the large systems generated, e.g. (3.2.35) and (3.2.43), that must be solved to obtain $\overline{\boldsymbol{u}}_n^{(M)}$. That is, for only one interior singular point a $2n \times 2n$ system is generated and the CPU system times increase by 137% and 756% respectively for $M = 1$ and 2, compared to the CPU system time for the standard vector-Nyström method (i.e. $M = 0$). Furthermore, compared with the CPU system times discussed in chapter 2 in which the standard Nyström method solves a $n \times n$ system, even the simplest case of $M = 0$ in the vector-Nyström method requires the solution of an $2n \times 2n$ system thereby increasing the CPU system time by approximately 100%.

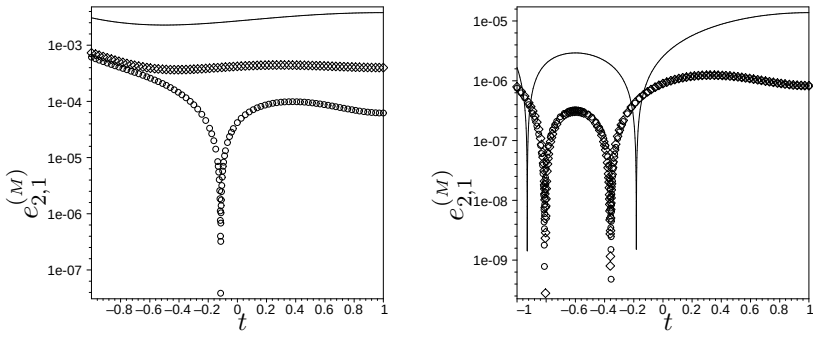

(a) $\alpha = -\frac{7}{10}, \Lambda = 0.1$

(b) $\alpha = -\frac{7}{10}, \Lambda = 0.001$

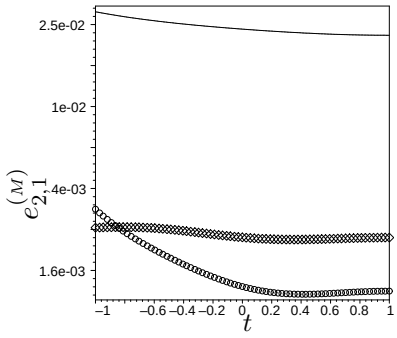

(c) $\alpha = -\frac{8}{10}, \Lambda = 0.1$

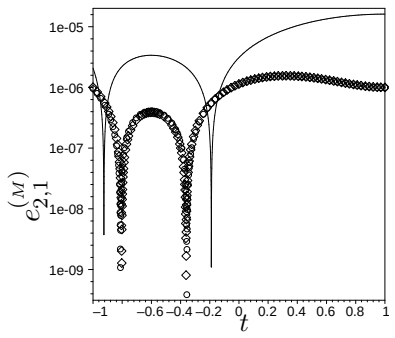

(d) $\alpha = -\frac{8}{10}, \Lambda = 0.001$

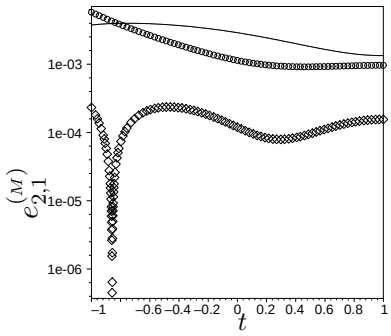

(e) $\alpha = -\frac{9}{10}, \Lambda = 0.1$

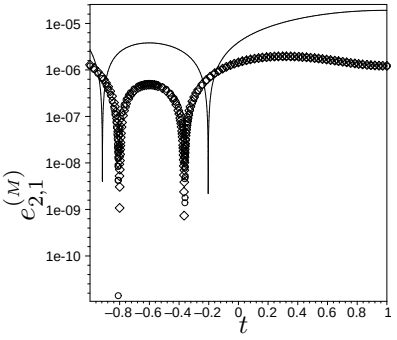

(f) $\alpha = -\frac{9}{10}, \Lambda = 0.001$

Figure 3.4.3: *The modified Nyström errors* $e_{n,i}^{(M)} u_i(t)$ *of* (3.4.1) *for fixed* $n = 2$ *and* $i = 1$ *for different* α *and* Λ*, computed using Gauss-Jacobi quadrature of* (3.1.3)*. The above numerical experiment uses* $[a, b] = [-\frac{5}{4}, \frac{5}{4}]$ *and* $c = \frac{1}{2}(b + a)$ *in the test FIE2* (3.3.10)*. Successive modifications of the standard vector-Nyström error,* $M = 0$ $(-)$*, are shown by* $M = 1$ $(\diamond)$ *and* $M = 2$ $(\circ)$*. The test problem become increasingly singular as* $\alpha \to -1$*, in which case the modified vector-Nyström method breaks down for* $|\Lambda| = \mathcal{O}(10^{-1})$*.*

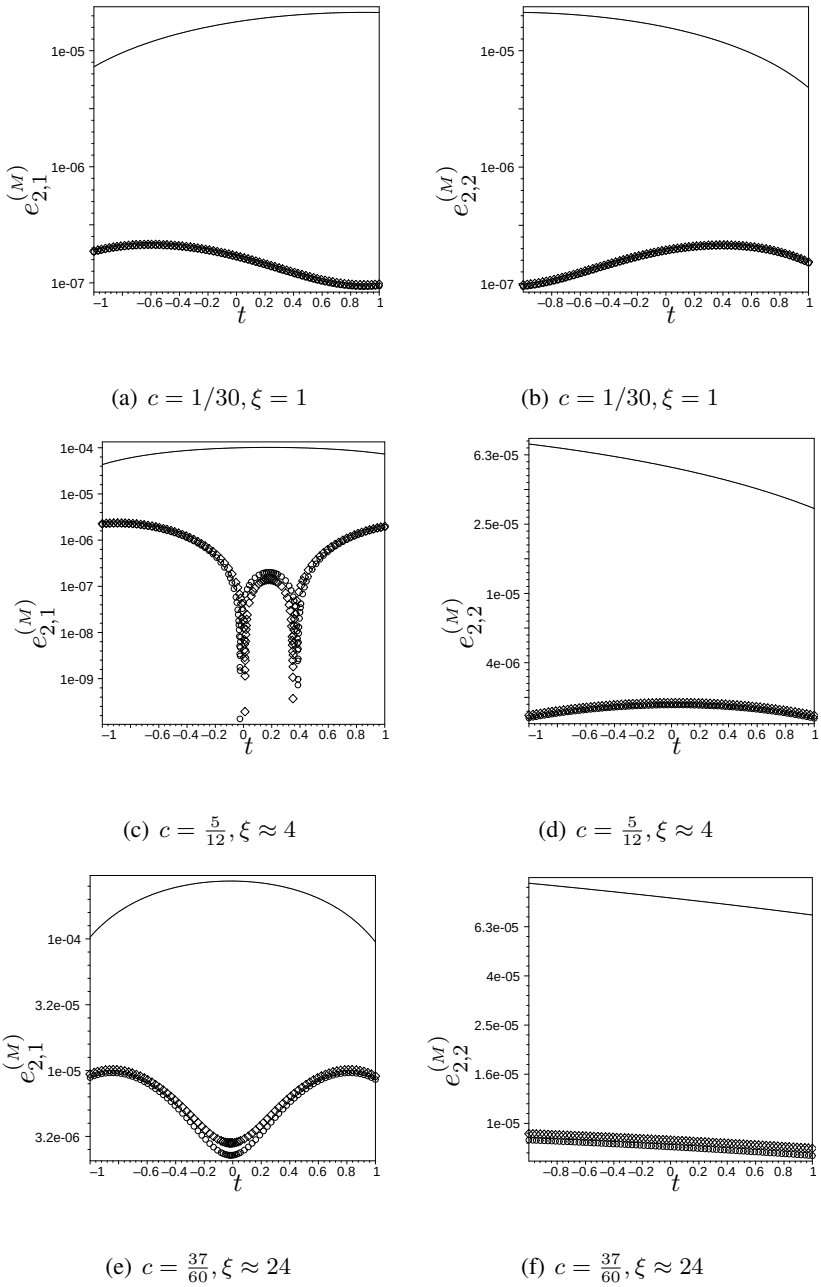

(a) $c = 1/30, \xi = 1$ (b) $c = 1/30, \xi = 1$

(c) $c = \frac{5}{12}, \xi \approx 4$ (d) $c = \frac{5}{12}, \xi \approx 4$

(e) $c = \frac{37}{60}, \xi \approx 24$ (f) $c = \frac{37}{60}, \xi \approx 24$

Figure 3.4.4: *The modified Nyström errors* $e_{n,i}^{(M)} u_i(t)$ *of* (3.4.1) *for fixed* $n = 2$ *and* $i = 1, 2$*, for different locations of* $c \in (a, b)$*, computed using Gauss-Jacobi quadrature of* (3.1.16)*. The above numerical experiment uses* $[a, b] = [-\frac{3}{5}, \frac{2}{3}]$*,* $\alpha = 0$ *and* $\Lambda = 0.1$ *in the test FIE2* (3.3.10)*. Successive modifications of the standard vector-Nyström error,* $M = 0$ $(-)$*, are shown by* $M = 1$ $(\diamond)$ *and* $M = 2$ $(\circ)$*. Comparing sub-figure* (e) *with Fig. 2.4.1*(a)*, as* $c \to b$ *the error* $e_{n,1}^{(M)} u_1(t) \to e_n^{(M)} u(t)$ *for all* t*. However, as* $\xi \to \infty$ *we have and erosion of improvement in* $e_{n,2}^{(M)} u_2(t)$ *as shown by sub-figure* (d) *and* (e)*.*

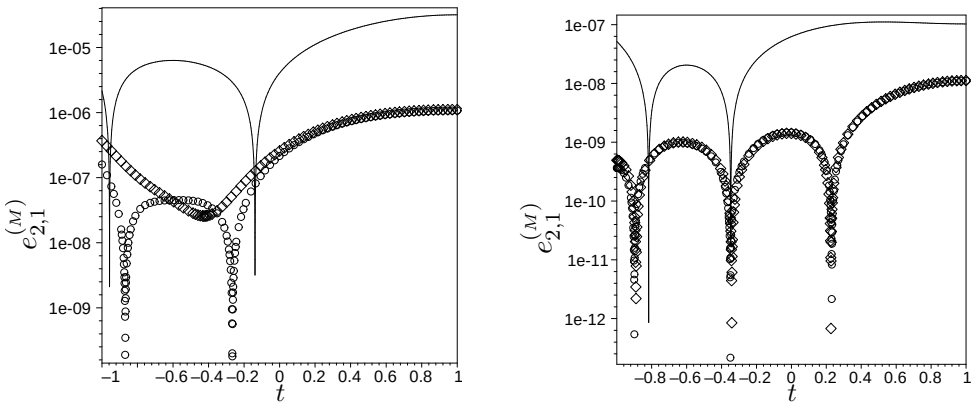

(a) $n = 2$ (b) $n = 3$

Figure 3.4.5: *The modified Nyström errors* $e_{n,i}^{(M)} u_i(t)$ *of* (3.4.1) *for fixed* $i = 1$ *and varying* $n = 2, 3$ *computed using Gauss-Jacobi quadrature of* (3.1.3)*. The above numerical experiment uses* $[a, b] = [-\frac{5}{4}, \frac{5}{4}]$*,* $c = \frac{1}{2}(b + a)$*,* $\alpha = 0.5$ *and* $\Lambda = 0.01$ *in the test FIE2* (3.3.10)*. Successive modifications of the standard vector-Nyström error,* $M = 0$ $(-)$*, are shown by* $M = 1$ $(\diamond)$ *and* $M = 2$ $(\circ)$*. Increasing* n *reduces the order of the error by up to two orders of magnitude whilst restricting the impact of* $M > 1$ *in the modified vector-Nyström method, which is in accordance with the results discussed in* §*2.2 Fig. 2.4.5.*

3.5 Summary and discussion

The aim of this chapter was to take the theory of chapter 2 for numerically approximating one-dimensional singular FIE2s and to extend it to FIE2s in which the kernels were either singular or of limited differentiability at more than one source point. In particular, this chapter was concerned with the solution of FIE2s whose kernel functions had limited differentiability at more than one point *within* the domain of integration, necessitating the solution of *systems* of FIE2s. The classical vector-Nyström method, used to approximate the solution of the *systems* of FIE2s, proceeded to be modified by a novel approach so that the accuracy in the vector-Nyström method was improved.

The theory for the modified vector-Nyström method has been conducted in the context of orthogonal-polynomial quadrature and has been validated using a series of test problems, some of which demonstrate a hundredfold error reduction for low orders of quadrature when compared with the standard vector-Nyström approach. The new modified vector-Nyström method for systems of FIE2s, albeit resembling the modified Nyström method for a single FIE2, is considerably more intricate and complex to implement. It requires the satisfaction of four truncation conditions and an implementation of a predicted error matrix, whose components are both high-degree products of the quadrature scheme and the predicted errors for each integral in the system.

This chapter was concerned with a kernel function that had limited differentiability at only one point within the domain of integration, for which the standard vector-Nyström method solution of the system containing two FIE2s increased the CPU system time for the solution of a single FIE2 by 100%. For more complicated singular kernels, i.e. taking $m > 1$ limited-differentiable points within the domain of integration, there will be a system of $(m+1)$ FIE2s to which a $(m+1)n$-point quadrature yields a system that is inverted in operations of order $\mathcal{O}((m+1)^3 n^3)$.

Further investigations in this area include combining the theory in this chapter with that of chapter 2, so that the modified vector-Nyström method may be adapted to suit FIE2s with a mixture of nonsingular and/or singular kernel functions, provided the function is factorisable into a product of "well-behaved" and "badly-behaved" parts. In the proceeding chapters 4-6, we discuss extending the theory in chapter 2 and 3 to approximate the solutions of higher-dimensional integral equations, including practical estimates of the error inherent in the numerical method.

Chapter 4

Improved Boundary Element Methods for the Solution of Nonsingular Harmonic Boundary Value Problems

Boundary-integral equations have frequently been used for the analysis of boundary values problems (BVPs), e.g., Symm [1973], Brebbia [1978], Yeung [1982], Atkinson [1997], Ang [2007]. The term boundary element method denotes any method that numerically approximates the solution of boundary-integral equations.

The boundary element methods (BEM) have the advantage over the finite-element method (FEM) and the finite-difference method (FDM) of superior convergence and reduced requirements in computer storage and code (Bush et al. [1984], Brebbia and Trevelyan [1986], Mohammadi et al. [2010]). This is because the FEM and FDM integrate the differential operator numerically, whereas the BEM integrates it numerically only after Green's formula is used to integrate the operator analytically thus reducing the dimension of a BVP by one. That is, the BEM discretises only the boundary of the domain to yield a finite-dimensional system, which is significantly smaller than that generated by a FEM or FDM.

The BEM have been applied to numerous problems in the fields of mathematics, including the solution of harmonic and biharmonic problems (Jaswon and Symm [1977], Blue [1977], Manzoor

[1984], Kelmanson [1983b], Grilli and Svendsen [1990], Mera et al. [2002], Hsiao [2006], Helsing [2009]). However, there exists only a limited amount of literature on the error analysis of the BEM, and that which does exist often defines only asymptotic error estimates or error bounds, which are not suitable for implementation (Wendland [1986], Rencis et al. [1990], Liang et al. [1999], Hsiao and Wendland [2004]). Therefore the objective in this chapter is to analyse the error in the BEM for a harmonic problem, thereby deriving practical error estimates. These practical error estimates will be used to define a new modified BEM, whereby we aim to emulate higher-order inter-element Lagrange interpolation without increasing the size of the system.

4.1 The boundary-integral equation

Partial differential equations with elliptic operators are ubiquitous in mathematics, physics, engineering, e.g., hyperbolic operators in wave problems, diffusion operators in engineering problems and Laplacian operators in static problems. Take the two-dimensional Laplace's equation, which satisfies

$$\nabla^2\phi = 0, \tag{4.1.1}$$

in a domain Ω enclosed by a boundary $\partial\Omega$. The boundary-integral equation form of (4.1.1) is derived by invoking Green's third identity (Muskhelishvili [1953], Christiansen [1974], Fairweather et al. [1979]) so that at any field point $p \in \Omega \cup \partial\Omega$

$$\int_\Omega \left[\phi(Q)\nabla^2 G(p,Q) - G(p,Q)\nabla^2\phi(Q)\right] d\Omega(Q) = \int_{\partial\Omega} \left[\phi(q)G'(p,q) - \phi'(q)G(p,q)\right]\ dq, \tag{4.1.2}$$

in which $Q \in \Omega$, $G(p,q) = \log|p-q|$, q is the source point on the boundary and dq denotes the differential increment of $\partial\Omega$ at q. The prime in (4.1.2) represents differentiation with respect to the outward normal to $\partial\Omega$ at q. Using the Dirac-Delta property of the Green's function G,

$$\nabla^2 G(p,q) = \delta(p-q), \tag{4.1.3}$$

together with its sifting property (Lighthill [1958]), (4.1.2) becomes

$$\eta(p)\phi(p) = \int_{\partial\Omega} \phi(q)G'(p,q)\ dq - \int_{\partial\Omega} \phi'(q)G(p,q)\ dq, \quad p \in \Omega \cup \partial\Omega, q \in \partial\Omega, \tag{4.1.4}$$

where

$$\eta(p) = \begin{cases} 2\pi & p \in \Omega, \\ 0 & p \notin \Omega \cup \partial\Omega, \\ \alpha & p \in \partial\Omega, \end{cases} \tag{4.1.5}$$

in which α is the internal angle between the tangents to $\partial\Omega$ on either side of p. In the case that the field point $p = \overline{q}$ lies on the boundary (4.1.4) yields

$$\int_{\partial\Omega} \phi(q) G'(\overline{q}, q)\, dq - \int_{\partial\Omega} \phi'(q) G(\overline{q}, q)\, dq - \alpha\phi(\overline{q}) = 0, \quad q, \overline{q} \in \partial\Omega, \tag{4.1.6}$$

where $\alpha = \pi$ provided that $\partial\Omega$ is smooth.

Integral equations (4.1.4) and (4.1.6) reveal the philosophy behind generalised BEMs. That is, in (4.1.4) one can only solve for the field point p given the knowledge of the Dirichlet and Neumann conditions along the entire boundary. However, we are concerned with the harmonic problem in which either Dirichlet or Neumann conditions are given along the boundary. For example, if $\partial\Omega$ is divided into two parts $\partial\Omega_\phi$ and $\partial\Omega_{\phi'}$, i.e. $\partial\Omega = \partial\Omega_\phi \cap \partial\Omega_{\phi'}$, then the Dirichlet condition $\phi(x, y)$ is prescribed along $\partial\Omega_\phi$ and the Neumann condition $\phi'(x, y)$ is prescribed along $\partial\Omega_{\phi'}$.

Eqn. (4.1.6) is essentially a closed-form equation between the potentials and their derivatives on the boundary. In other words, given one type of boundary condition on $\partial\Omega$ the other is found by (4.1.6). The completed boundary conditions can then be used in (4.1.4) to find the Laplacian anywhere in Ω. Integral equation (4.1.4) always has a unique global solution $\phi(p)$ at any point $p \in \Omega \cup \partial\Omega$ provided the boundary conditions are continuous and at least once-differentiable along $\partial\Omega$ (Jaswon [1963]).

In general the solution of (4.1.4) will not be obtainable analytically, even if the entire boundary solution is known, as it requires closed-form integrations. Therefore we need a robust numerical method for determining the solution. Currently the closed-form infinite system (4.1.6) is solved by some kind of finite-reduction method. It is an improvement upon this method that will be the focus of this chapter.

The remainder of this chapter is structured as follows. In §4.2 we outline the constant BEM and its inherent error for approximating the solution of integral equation (4.1.4). This method is validated for a nonsingular test BVP. In §4.3 we present new, modified, constant BEMs. In §4.4, we validate the modified BEM solutions of §4.3 for a nonsingular test BVP. The validation of the modified

methods highlights their superior accuracy, hence justifying their application to singular BVPs in chapter 6.

4.2 The constant boundary element method (CBEM)

For the remainder of this chapter $p \in \Omega \cup \partial\Omega$ and $q \in \partial\Omega$ unless otherwise stated. Discretising the boundary $\partial\Omega$ into n smooth elements (hence the name boundary element method), $e^{(j)}$ say, where

$$\partial\Omega = \bigcup_{j=1}^{n} e^{(j)}, \tag{4.2.1}$$

then (4.1.4) becomes

$$\eta(p)\phi(p) = \sum_{j=1}^{n} \int_{e^{(j)}} \phi(q)G'(p,q)\ dq - \int_{e^{(j)}} \phi'(q)G(p,q)\ dq. \tag{4.2.2}$$

In the constant BEM (CBEM) (Jaswon and Symm [1977], Brebbia [1978], Manzoor [1984], Ang [2007]), $\phi(q)$ and $\phi'(q)$ are respectively approximated by piecewise-constant functions $\phi_{n,j}$ and $\phi'_{n,j}$ over element $e^{(j)}$. The corresponding discretised form of (4.2.2), with approximate solution $\phi_n(p)$, is

$$\eta(p)\phi_n(p) = \sum_{j=1}^{n} \left\{ \phi_{n,j} \int_{e^{(j)}} G'(p,q)\ dq - \phi'_{n,j} \int_{e^{(j)}} G(p,q)\ dq \right\}, \tag{4.2.3}$$

in which $\phi_{n,j} \equiv \phi(q_{n,j})$ and $\phi'_{n,j} \equiv \phi'(q_{n,j})$ where $q_{n,j}$ is the mid-point of $e^{(j)}$.

By introducing the operators

$$(\mathcal{G}'_n\phi_n)(p) \equiv \sum_{j=1}^{n} \int_{e^{(j)}} \phi_{n,j}G'(p,q)\ dq \tag{4.2.4}$$

and

$$(\mathcal{G}_n\phi'_n)(p) \equiv \sum_{j=1}^{n} \int_{e^{(j)}} \phi'_{n,j}G(p,q)\ dq, \tag{4.2.5}$$

(4.2.3) can be rewritten in symbolic form as

$$(\mathcal{G}'_n - \eta\mathcal{I})\phi_n - \mathcal{G}_n\phi'_n = 0, \tag{4.2.6}$$

in which $\mathcal{I}$ is the identity operator.

For the remainder of this chapter, unless otherwise stated, indices i and j take the values $i, j =$

$1, \ldots, n$. Collocating (4.2.6) at the mid-point of each element by taking $p = q_{n,i}$ yields the system of n equations

$$\sum_{j=1}^{n} \left\{ (A_{ij} - \eta_j \delta_{ij}) \phi_{n,j} + B_{ij} \phi'_{n,j} \right\} = 0, \tag{4.2.7}$$

where $\eta_j = \eta(q_{n,j})$, δ_{ij} is the Kronecker delta function and

$$\begin{aligned} A_{ij} &= \int_{e^{(j)}} \log' |q_{n,i} - q| \, dq, \\ B_{ij} &= -\int_{e^{(j)}} \log |q_{n,i} - q| \, dq. \end{aligned} \tag{4.2.8}$$

The integrals in (4.2.8) may be evaluated analytically when element $e^{(j)}$ is a straight-line segment (see Appendix B). Otherwise, integrals (4.2.8) may be evaluated using Gaussian quadrature with a logarithmic weighting function (Mason and Smith [1982]) when $e^{(j)}$ is not linear.

Taking

$$\widehat{A}_{ij} = \begin{cases} A_{ij} & \text{if} \quad i \neq j, \\ A_{ij} - \eta_j & \text{if} \quad i = j, \end{cases} \tag{4.2.9}$$

(4.2.7) is equivalent to

$$\sum_{j=1}^{n} \widehat{A}_{ij} \phi_{n,j} = -\sum_{j=1}^{n} B_{ij} \phi'_{n,j}, \quad i = 1, \ldots, n. \tag{4.2.10}$$

Linear system (4.2.10) can alternatively be denoted by $\widehat{\mathbf{A}}\boldsymbol{\phi} = \mathbf{B}\boldsymbol{\phi'}$ in which, by (4.2.7), only some of the elements of ϕ and ϕ' are known; hence (4.2.10) must be recast into the form $\mathbf{H}\mathbf{x}_C = \mathbf{g}$ where the vector $\mathbf{x}_C$ contains the unknown mid-element nodal values of $\phi_{n,j}$ on $\partial\Omega_{\phi'}$ and $\phi'_{n,j}$ on $\partial\Omega_{\phi}$. The dense system $\mathbf{H}\mathbf{x}_C = \mathbf{g}$ is then solved using the NAG routine F07AAF. With all nodal boundary data now prespecified or approximated, $\phi_n(p)$ in (4.2.3) can be computed directly from the complete boundary distributions of ϕ and ϕ'.

When the boundary conditions are spatially dependent on the domain, the accuracy to which they will be represented in the BEM depends upon the degree of the piecewise-polynomial interpolation. However, whenever possible, the boundary conditions in (4.2.3) should be computed exactly.

There are two distinct types of solutions for the CBEM, the *theoretical discretised solution* ϕ_n in (4.2.3) and the *numerical discretised solution* $\widetilde{\phi}_n$. The theoretical discretised solution is generated without having to go through the two-stage process, i.e. is simply based upon (4.1.4), whereas for the numerical discretised solution you have to go through (4.1.6) and then (4.1.4). That is, the

theoretical discretised solution enables the subsequent quantification of the error in the Lagrangian interpolation, which we assume dominates the error in the BEM, whereas the numerical solution includes both Lagrangian interpolation and matrix inversion errors. Throughout the remainder of this thesis the theoretically and numerically derived solutions (and their corresponding errors) for each numerical method will be defined in a similar format.

Based upon the theoretical discretised solution in (4.2.3), the numerical discretised solution $\widetilde{\phi}_n$ of the CBEM satisfies

$$\eta(p)\widetilde{\phi}_n(p) = \sum_{j=1}^{n} \left\{ \int_{e^{(j)}} \widetilde{\phi}_{n,j}\, G'(p,q)\, dq - \int_{e^{(j)}} \widetilde{\phi}'_{n,j}\, G(p,q)\, dq \right\}, \tag{4.2.11}$$

in which

$$\widetilde{\phi}_{n,j} = \begin{cases} \phi(q_{n,j}) & \text{if } e^{(j)} \subseteq \partial\Omega_\phi, \\ \widetilde{\phi}(q_{n,j}) & \text{otherwise,} \end{cases} \quad \text{and} \quad \widetilde{\phi}'_{n,j} = \begin{cases} \phi'(q_{n,j}) & \text{if } e^{(j)} \subseteq \partial\Omega_{\phi'}, \\ \widetilde{\phi}'(q_{n,j}) & \text{otherwise.} \end{cases} \tag{4.2.12}$$

Recalling the operators defined in (4.2.4) and (4.2.5), the symbolic form of (4.2.11) is

$$(\mathcal{G}'_n - \eta\mathcal{I})\widetilde{\phi}_n - \mathcal{G}_n\widetilde{\phi}'_n = 0. \tag{4.2.13}$$

In the case that the CBEM applies piecewise-constant polynomial interpolation with nodes separated by a constant spacing h, the error $\|\phi - \widetilde{\phi}_n\|$ is $O(h^2)$ (Atkinson [1989], Ralston and Rabinowitz [2001]). In the remainder of this chapter the CBEM is modified in such a way as to reduce these errors to $O(h^m)$ where $m \geq 2$ is chosen *a priori*. Before attempting this, however, we first analyse the error inherent in the constant BEM.

4.2.1 Error analysis of the CBEM

To recap we have $\phi(p)$ is the exact solution, ϕ_n is the theoretical discretised solution that satisfies

$$\phi_n(p) = \frac{1}{\eta(p)} \sum_{j=1}^{n} \left\{ \phi_{n,j} \int_{e^{(j)}} G'(p,q)\, dq - \phi'_{n,j} \int_{e^{(j)}} G(p,q)\, dq \right\}, \tag{4.2.14}$$

and $\widetilde{\phi}_n$ is the numerical discretised solution that satisfies

$$\widetilde{\phi}_n(p) = \frac{1}{\eta(p)} \sum_{j=1}^{n} \left\{ \widetilde{\phi}_{n,j} \int_{e^{(j)}} G'(p,q)\, dq - \widetilde{\phi}'_{n,j} \int_{e^{(j)}} G(p,q)\, dq \right\}. \tag{4.2.15}$$

The *numerical CBEM error* is defined as

$$\widetilde{\epsilon}_n(p) \equiv \phi(p) - \widetilde{\phi}_n(p) \tag{4.2.16}$$

which, by the linearity of (4.2.2) and (4.2.11), satisfies Green's integral formulae, i.e.

$$\eta(p)\widetilde{\epsilon}_n(p) = \sum_{j=1}^{n} \left\{ \int_{e^{(j)}} \widetilde{\epsilon}_{n,j}(q)\ G'(p,q)\ dq - \int_{e^{(j)}} \widetilde{\epsilon}'_{n,j}(q)\ G(p,q)\ dq \right\}, \tag{4.2.17}$$

where

$$\widetilde{\epsilon}_{n,j}(q) = \begin{cases} \phi(q) - \phi_{n,j} & \text{if } e^{(j)} \subseteq \partial\Omega_\phi, \\ \phi(q) - \widetilde{\phi}_{n,j} & \text{otherwise,} \end{cases} \tag{4.2.18}$$

and

$$\widetilde{\epsilon}'_{n,j}(q) = \begin{cases} \phi(q) - \phi_{n,j} & \text{if } e^{(j)} \subseteq \partial\Omega_{\phi'}, \\ \phi'(q) - \widetilde{\phi}'_{n,j} & \text{otherwise.} \end{cases} \tag{4.2.19}$$

On the other hand, the *theoretical CBEM error* is defined as

$$\epsilon_n(p) \equiv \phi(p) - \phi_n(p) \tag{4.2.20}$$

which, by (4.2.3), satisfies

$$\eta(p)\epsilon_n(p) = \sum_{j=1}^{n} \left\{ \int_{e^{(j)}} \epsilon_{n,j}(q)\ G'(p,q)\ dq - \int_{e^{(j)}} \epsilon'_{n,j}(q)\ G(p,q)\ dq \right\}, \tag{4.2.21}$$

where

$$\epsilon_{n,j}(q) = \phi(q) - \phi_{n,j} \tag{4.2.22}$$

and

$$\epsilon'_{n,j}(q) = \phi'(q) - \phi'_{n,j}. \tag{4.2.23}$$

The symbolic form of (4.2.21) is

$$(\mathcal{G}'_n - \eta\mathcal{I})\epsilon_n - \mathcal{G}_n\epsilon'_n = 0, \tag{4.2.24}$$

in which we use the predefined operators $\mathcal{G}'_n$ in (4.2.4) and $\mathcal{G}_n$ in (4.2.5), so that

$$(\mathcal{G}'_n\epsilon_n)(p) \equiv \sum_{j=1}^{n} \int_{e^{(j)}} \epsilon_{n,j}(q) G'(p,q)\ dq \tag{4.2.25}$$

and

$$(\mathcal{G}_n\epsilon'_n)(p) \equiv \sum_{j=1}^{n} \int_{e^{(j)}} \epsilon'_{n,j}(q)G(p,q)\ dq. \tag{4.2.26}$$

Consider now the Taylor expansion for ϕ and ϕ' about node $q_{n,j}$, namely

$$\phi(q) = \phi_{n,j} + \sum_{k=1}^{\infty} \frac{(q-q_{n,j})^k}{k!} \frac{\partial^k}{\partial q^k} \left[\phi(q)\right]_{q=q_{n,j}} \tag{4.2.27}$$

and

$$\phi'(q) = \phi'_{n,j} + \sum_{k=1}^{\infty} \frac{(q-q_{n,j})^k}{k!} \frac{\partial^k}{\partial q^k} \left[\phi'(q)\right]_{q=q_{n,j}}. \tag{4.2.28}$$

Letting

$$J_{k,j}(p) \equiv \int_{e^{(j)}} (q-q_{n,j})^k\ G'(p,q)\ dq \tag{4.2.29}$$

and

$$K_{k,j}(p) \equiv \int_{e^{(j)}} (q-q_{n,j})^k\ G(p,q)\ dq, \tag{4.2.30}$$

then both $J_{k,j}(p)$ and $K_{k,j}(p)$ may be determined exactly (see Appendix C). By (4.2.21),(4.2.22) and (4.2.23) the infinite-series form of the theoretical error $\epsilon_n(p)$ satisfies

$$\eta(p)\epsilon_n(p) = \sum_{j=1}^{n}\sum_{k=1}^{\infty} \frac{1}{k!} \left\{ \frac{\partial^k}{\partial q^k} \left[\phi(q)\right]_{q=q_{n,j}} J_{k,j}(p) - \frac{\partial^k}{\partial q^k} \left[\phi'(q)\right]_{q=q_{n,j}} K_{k,j}(p) \right\}. \tag{4.2.31}$$

We first utilise (4.2.31) to deduce the well-known $O(h^2)$ error of the CBEM. The nodally evaluated k^{th} differentials of ϕ and ϕ' are constant, therefore only the integrals $J_{k,j}$ and $K_{k,j}$ affect the order of the CBEM error. Initially let $q_{An,j}$ and $q_{Bn,j}$ be points on $\partial\Omega$ marking the ends of boundary segment $e^{(j)}$. For a general field point $p \in \partial\Omega \cup \Omega$, if

$$\begin{aligned} a &= |p - q_{An,j}|, \\ b &= |p - q_{Bn,j}|, \\ h &= |q_{An,j} - q_{Bn,j}|, \\ \beta &= \angle q_{Bn,j} q_{An,j} p, \\ \psi &= \angle q_{An,j} p q_{Bn,j}, \end{aligned} \tag{4.2.32}$$

we have the geometry as shown in Fig. 4.2.1. By (4.2.32), we have

$$J_{k,j}(p) = \int_{-a\cos\beta}^{h-a\cos\beta} \left(x - \frac{h}{2} + a\cos\beta\right)^k \frac{a\sin\beta}{x^2 + a^2\sin^2\beta}\ dx \tag{4.2.33}$$

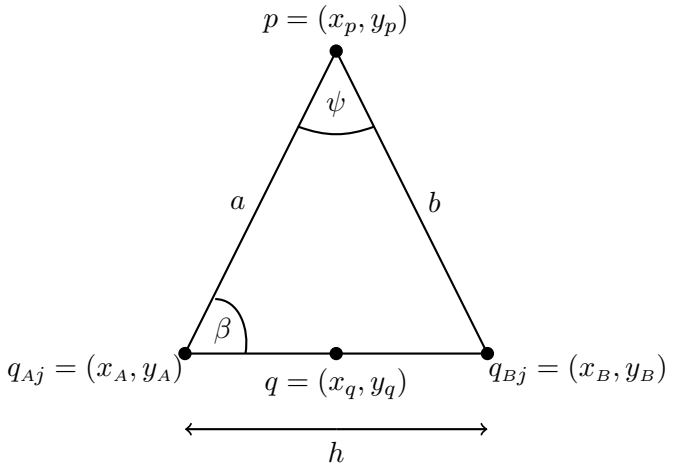

Figure 4.2.1: *Notation for the analytic evaulation of the integrals A_{ij} and B_{ij} over element $e^{(j)}$*

and

$$K_{k,j}(p) = \int_{-a\cos\beta}^{h-a\cos\beta} \left(x - \frac{h}{2} + a\cos\beta\right)^k \log\left(x^2 + a^2\sin^2\beta\right)^{\frac{1}{2}}\, dx, \tag{4.2.34}$$

which can be evaluated exactly: when $k = 1$, (4.2.33) implies

$$J_{1,j}(p) = a\sin\beta\log\left(\frac{a^2 - 2ah\cos\beta + h^2}{a^2}\right)^{\frac{1}{2}} + \psi a\cos\beta - \frac{\psi h}{2}, \tag{4.2.35}$$

and (4.2.34) implies

$$\begin{aligned} K_{1,j}(p) = {} & \frac{a^2\psi\sin 2\beta}{2} - \frac{a^2\cos 2\beta}{2}\log\left(\frac{a^2 - 2ah\cos\beta + h^2}{a^2}\right)^{\frac{1}{2}} \\ & - \frac{\psi h\sin\beta}{2a} + \frac{h\cos\beta}{2a}\left(\log\left(\frac{a^2 - 2ah\cos\beta + h^2}{a^2}\right)^{\frac{1}{2}} - 1\right) + \frac{h^2}{4a}. \end{aligned} \tag{4.2.36}$$

The analytic expressions (4.2.33) and (4.2.34) were derived by Kelmanson (private communication, 2011), who also obtained exact expressions for $J_{k,j}$ and $K_{k,j}$ for higher values of k; these are presented in Appendix C.

An analysis of the exact forms of the integrals $J_{k,j}$ and $K_{k,j}$, e.g. (4.2.35) and (4.2.36), define the leading behaviour of the error of the CBEM. However, particular consideration must be taken into the behaviour of these integrals at specific field-point locations. When the field point is not close to segment $e^{(j)}$, i.e. $h/a \ll 1$ in (4.2.32), the integrals (4.2.33) and (4.2.34) have a leading order of $O(h^3)$. Furthermore, it can be shown (Kelmanson, private communication, 2011) that the order

of (4.2.33) and (4.2.34) increase indefinitely with increasing k in a period two-cycle, e.g.

$$J_{k,j}(p), K_{k,j}(p) = \begin{cases} O(h^3) & \text{when } k = 1, \\ O(h^5) & \text{when } k = 2, 3, \\ O(h^7) & \text{when } k = 4, 5, \\ O(h^9) & \text{when } k = 6, 7. \end{cases} \tag{4.2.37}$$

Alternatively, if the field point p is close to element $e^{(j)}$ the orders of $J_{k,j}(p)$ in (4.2.33) and $K_{k,j}(p)$ in (4.2.34) are affected. For example, if the field point approaches the mid-point of $e^{(j)}$, we have

$$\lim_{p \to q_{n,j}} J_{k,j}(p) = 0, \quad \forall k, \tag{4.2.38}$$

and

$$\lim_{p \to q_{n,j}} K_{1,j}(p) = O(h^3). \tag{4.2.39}$$

However, if the field point approaches either end-point of element $e^{(j)}$, we have

$$\lim_{p \to q_{An,j}, q_{Bn,j}} K_{1,j}(p) = O(h^2), \tag{4.2.40}$$

or, if it lies close to the element, i.e. $h/a = O(1)$, we have

$$K_{1,j}(p) = O(h^2), \tag{4.2.41}$$

or, if the field point is in close proximity to a corner in the domain *both* $J_{1,j}$ and $K_{1,j}$ are $O(h^2)$. When collocating the CBEM at the mid-points $p = q_{n,i}$ a system of n equations is generated in which each coefficient has a local error of $O(h^3)$, therefore the inversion of the system will have an expected order of $O(h^2)$ overall as n is proportional to $1/h$. However, by (4.2.38)-(4.2.41), we expect the error to be lower than $O(h^2)$ because the local $O(h^3)$ coefficients go to $O(h^2)$ in the corners and at points along the boundary thus reducing the overall $O(h^2)$ nature.

4.2.2 Test case: nonsingular boundary value problem

As a test problem, we take the harmonic function

$$\phi(x, y) = e^x \sin(y), \tag{4.2.42}$$

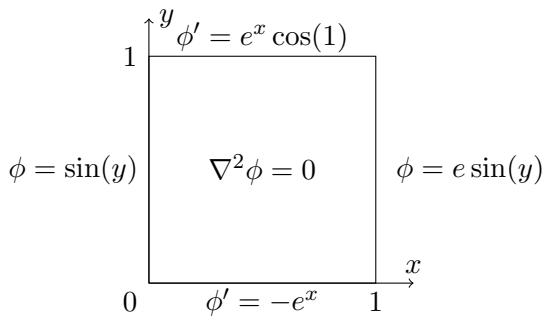

Figure 4.2.2: *Graphical representation of the nonsingular test BVP.*

in the unit square that satisfies Laplace's equation (4.1.1) with the Dirichlet and Neumann boundary conditions illustrated in Fig. 4.2.2.

The error in the numerical CBEM solution of the test BVP (Fig. 4.2.2) is depicted in Fig. 4.2.3. The key aspects of Fig. 4.2.3 are: the convergence of the error with increasing number of elements n and the prominently large errors at the corner points of the domain. The large errors at the corner points reflect the theoretically predicted $O(h^2)$ behaviour of the integrals $J_{j,k}$ in (4.2.33) and $K_{k,j}$ in (4.2.34) as the field point approaches the corners. It is also a direct result of the Maximum principle (Jaswon and Symm [1977]) inherent in the solution of contained harmonic BVPs.

To give an insight into the behaviour of the CBEM error when $n > 48$, the three surfaces in Fig. 4.2.3 are depicted on individual contour plots for $n = 48, 72$ and 108 in Fig. 4.2.4. The contour plots show a clear reduction in the CBEM error as n increases as per Fig. 4.2.3, however, the contours also demonstrate the converging behaviour of the error peaks at the corners. As predicted by the Maximum principle, Fig. 4.2.4 shows the largest of the error peaks occurs at the corner furthest from the origin.

The CBEM error is furthermore analysed by computing its root-mean-square error (RMSE) and its convergence rate. The former of these, the RMSE, is defined by

$$\widetilde{\sigma}_n \equiv \sqrt{\frac{1}{M}\sum_{j=1}^{M}\left(\widetilde{\epsilon}_n(p_{M,j})\right)^2}, \tag{4.2.43}$$

where M is the number of mesh points, chosen so that the mesh is not finer than the boundary resolution. Note in the remainder of this chapter we take $M = (\frac{n}{4} + 1)^2$ for the given test BVP.

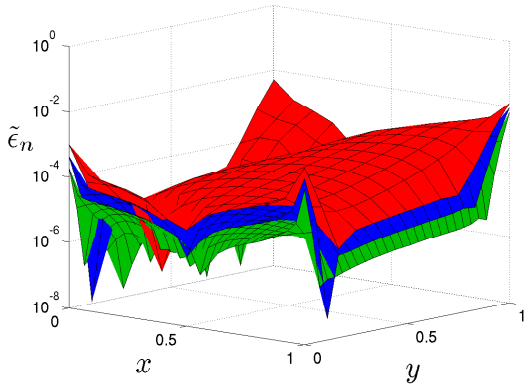

Figure 4.2.3: *Log plot of the error in the CBEM solution of the test BVP in Fig. 4.2.2,* $\widetilde{\epsilon}_n(p)$ *in* (4.2.16)*, where* p *is defined on the unit square. Here* $n = 48$ *(red),* $n = 72$ *(blue) and* $n = 108$ *(green). The CBEM error is converging to zero with increasing* n*, the rate of which is shown in Table 4.2.1. Furthermore, the error* $\widetilde{\epsilon}_n$ *demonstrates the effect of the theoretically predicted localised* $O(h)$ *pollution when the field point approaches any corner.*

The convergence rate on the other hand, is defined using Richardson's extrapolation (Ralston and Rabinowitz [2001]).

Richardson's extrapolation

Richardson's extrapolation determines the rate of convergence from numerical data generated on two or more refined meshes. It assumes that the approximate solution ϕ_h to the exact answer ϕ depends on the mesh size h according to

$$\phi \sim \phi_h + Ah^p, \tag{4.2.44}$$

where the three unknowns ϕ, A and p can be estimated by using (4.2.44) for three different values of h. Increasing h by a factor of α or $\alpha\beta$ the two respective approximate solutions are

$$\phi \sim \phi_{\alpha h} + A\left(\frac{h}{\alpha}\right)^p \quad \text{and} \quad \phi \sim \phi_{\alpha\beta h} + A\left(\frac{h}{\alpha\beta}\right)^p \tag{4.2.45}$$

which, in combination with (4.2.44), yields the ratios

$$\frac{\phi - \phi_n}{\phi - \phi_{\alpha n}} = \alpha^p \tag{4.2.46}$$

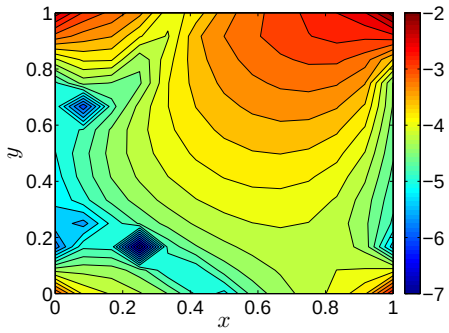

(a) $n = 48$ (red)

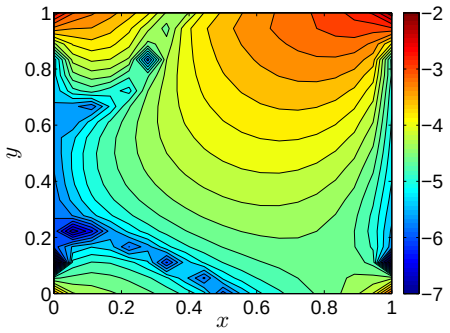

(b) $n = 72$ (blue)

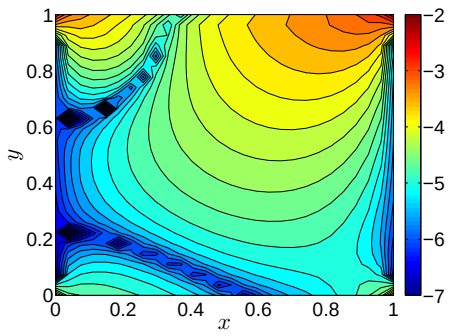

(c) $n = 108$ (green)

Figure 4.2.4: *Contour plots of* $\log|\widetilde{\epsilon}_n(p)|$*, the logarithm of the error in the CBEM solution of the test BVP in Fig. 4.2.2, for* $n = 48, 72$ *and* 108*. These plots separate and quantify the three error surfaces given in Fig. 4.2.3.*

and

$$\frac{\phi - \phi_{\alpha n}}{\phi - \phi_{\alpha\beta n}} = \beta^p. \tag{4.2.47}$$

Therefore,

$$\frac{\phi_n - \phi_{\alpha n}}{\phi_{\alpha n} - \phi_{\alpha\beta n}} = \frac{(\alpha\beta)^p - \beta^p}{\beta^p - 1} \equiv \rho, \tag{4.2.48}$$

say. Eqn. (4.2.48) can be used to predict the order p. For example if $\alpha = \beta = 2$ (i.e. $\rho = 4$) then (4.2.48) gives $p = 2$, i.e. second-order convergence is predicted.

By Richardson's extrapolation (4.2.48), the RMSE, error convergence rate ρ and error order p in the approximate CBEM solution $\widetilde{\phi}_n$ is defined in Table 4.2.1 where $\alpha = \beta = 1.5$ (identical α and

n	$\widetilde{\sigma}_n$	ρ	p
48	0.0012	2.0357	1.7531
72	6.0309×10^{-4}	2.0595	1.7818
108	2.9283×10^{-4}		

Table 4.2.1: *The RMSE $\widetilde{\sigma}_n$, error convergence rate ρ and error order p in the CBEM solution of the test BVP in Fig. 4.2.2, for $n = 48, 72, 108$ and $\alpha = 1.5$ $(= \beta)$. The results correspond to the error depicted in Figs. 4.2.3 and 4.2.4. The CBEM error does not exhibit the expected $O(h^2)$ behaviour (i.e. $p \neq 2$), due to the pollution at the corner points in the interpolation error. There is also an error introduced by interpolating (using low order polynomials) the exact form of the specified boundary conditions, and that the effect is exasperated as you go into the corners of the domain where you get a geometric change in derivative.*

β taken in Fig. 4.2.3). Theoretically we expect $\rho = 2.25$, so that the overall error in the CBEM is $O(h^2)$, i.e. $p = 2$, however, $p < 2$ in Table 4.2.1. The reason for such an occurrence is due to two factors: first, the $O(h)$ pollution when the field point approaches a corner from integrals $J_{j,k}$ in (4.2.33) and $K_{k,j}$ in (4.2.34); second, the interpolation error within the pre-inversion of the system of equations (4.2.10), in itself, produces an error post-inversion in the approximated boundary data $\widetilde{\phi}_{n,j}$ and $\widetilde{\phi}'_{n,j}$ used to determine the numerical discretised solution $\widetilde{\phi}_n$ in (4.2.11).
Our aim for the remainder of this chapter is to modify the standard CBEM, by reducing the interpolation error within the pre-inversion of the system, so that the $O(h^2)$ error is recovered without compromising on computational expense.

4.3 The modified constant boundary element method

Recall $\epsilon_n(p)$ in (4.2.20) is the true error of the CBEM that is expressible as an infinite-series in accordance with (4.2.31). The modified method, with solution $\overline{\phi}_n(p)$, is based upon taking the leading terms in the theoretically deduced error ϵ_n and building them into the standard CBEM *a priori*. That is, if $\overline{\epsilon}_n$ contains the leading terms of ϵ_n then we have

$$\overline{\phi}_n(p) = \phi_n(p) + \overline{\epsilon}_n(p). \tag{4.3.1}$$

The *difference* between the true and approximated errors, defined by the *discrepancy*

$$(\Delta\overline{\epsilon}_n)(p) \equiv (\epsilon_n - \overline{\epsilon}_n)(p), \tag{4.3.2}$$

means that, by (4.2.20) and (4.3.1), the *modified CBEM error* satisfies

$$\begin{aligned} \phi - \overline{\phi}_n &= \phi - (\phi_n + \overline{\epsilon}_n) \\ &= \epsilon_n - \overline{\epsilon}_n \\ &= \Delta\overline{\epsilon}_n. \end{aligned} \tag{4.3.3}$$

Thus the modified CBEM error is less than the standard CBEM error, owing to the former being composed of an error discrepancy rather than the error itself, i.e.

$$\|\phi - \overline{\phi}_n\|_\infty \ll \|\phi - \phi_n\|_\infty \tag{4.3.4}$$

as, by construction, $\|\Delta\overline{\epsilon}_n\|_\infty \ll \|\epsilon_n\|_\infty$. Consistent with (2.2.19) and (3.2.16) in the previous chapters, Eqn. (4.3.4) demonstrates the philosophy behind finding improved methods: the error of the improved method should be minimal in comparison to the error of the original method. We now modify the CBEM in §4.2 by deriving an explicit form of the approximate error $\overline{\epsilon}_n$ in (4.3.1) because, once known, we can implement a modified CBEM whose solution $\overline{\phi}_n$ satisfies (4.3.4).

4.3.1 Approximations of the CBEM error

Truncating the infinite-series of the CBEM error ϵ_n in (4.2.31) to *order* m, the *truncated-series error* $\epsilon_n^{(m)}$ satisfies

$$\eta(p)\epsilon_n^{(m)}(p) = \sum_{j=1}^{n} \left\{ \int_{e^{(j)}} \epsilon_{n,j}^{(m)}(q)\; G'(p,q)\; dq - \int_{e^{(j)}} \epsilon_{n,j}^{\prime(m)}(q)\; G(p,q)\; dq \right\}, \tag{4.3.5}$$

where

$$\epsilon_{n,j}^{(m)}(q) \equiv \sum_{k=1}^{m} \frac{(q - q_{n,j})^k}{k!} \frac{\partial^k}{\partial q^k} \left[\phi(q)\right]_{q=q_{n,j}} \tag{4.3.6}$$

and

$$\epsilon_{n,j}^{\prime(m)}(q) \equiv \sum_{k=1}^{m} \frac{(q - q_{n,j})^k}{k!} \frac{\partial^k}{\partial q^k} \left[\phi'(q)\right]_{q=q_{n,j}}. \tag{4.3.7}$$

The symbolic form of (4.3.5) is

$$(\mathcal{G}'_{n,m} - \eta\mathcal{I})\epsilon_n^{(m)} - \mathcal{G}_{n,m}\epsilon_n'^{(m)} = 0, \tag{4.3.8}$$

in which, by the definitions of $J_{k,j}$ and $K_{k,j}$ in (4.2.29) and (4.2.30),

$$\begin{aligned}(\mathcal{G}'_{n,m}\epsilon_n^{(m)})(p) &\equiv \sum_{j=1}^{n}\int_{e^{(j)}} \epsilon_{n,j}^{(m)}(q)G'(p,q)\,dq \\ &= \sum_{j=1}^{n}\sum_{k=1}^{m}\frac{1}{k!}\frac{\partial^k}{\partial q^k}\left[\phi(q)\right]_{q=q_{n,j}} J_{k,j}(p)\end{aligned} \tag{4.3.9}$$

and

$$\begin{aligned}(\mathcal{G}_{n,m}\epsilon_n'^{(m)})(p) &\equiv \sum_{j=1}^{n}\int_{e^{(j)}} \epsilon_{n,j}'^{(m)}(q)G(p,q)\,dq \\ &= \sum_{j=1}^{n}\sum_{k=1}^{m}\frac{1}{k!}\frac{\partial^k}{\partial q^k}\left[\phi'(q)\right]_{q=q_{n,j}} K_{k,j}(p).\end{aligned} \tag{4.3.10}$$

The constant error analysis only allows the CBEM error to be expressed in terms of the solution, which is of course, unknown *a priori*. The following approach circumvents this problem by using estimates based not upon unknown derivatives, but rather on increasingly complex molecules of existing Dirichlet and Neumann data to simulate those derivatives. Of course the number of points that can be included in the molecule will be restricted by n: this restriction will be quantified later. A finite-difference molecule is a closed-form expression defined by the order of the error a and the degree of differentiation d, such that it has N points. By (4.3.9) and (4.3.10) we require derivatives of order $d = 1, \ldots, m$, hence the number of atoms in each finite-difference molecule will range from $N = a + 1$ to $N = a + m - 1$ if m is even or $N = a + m$ if m is odd, each of which will be centred on the n *base points* $q = q_{n,j}$ along each side of the domain. Thus standard central-difference molecules can be applied at the base points that are further than $a - m$ nodes from each corner. For the remaining points, special asymmetric, ultimately one-sided, formulae must be derived. An example is given in Fig. 4.3.1 in which $m = 2$ and $a = 4$.

By applying asymmetric central-difference molecules our finite-difference method will require a minimum of only N points along each edge, whereas a standard central difference molecule would require a higher number of forward and backward differences thus requiring a minimum of $N + (a - 2)$ points along each edge in order to maintain an error of order a. Note that although the

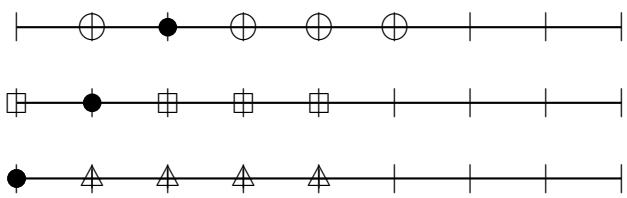

Figure 4.3.1: *Schematic representation of 4^{th}-order finite-difference molecules for the second derivative. Base points are indicated in black. The first molecule is centrally symmetric and applies at all base points further than 2 from the corner (◯); the second is asymmetric (□) and the third is one-sided (△).*

applied finite-difference molecules are restricted to evenly spaced elements for the purpose of the test BVP, they can be easily modified to cope with arbitrary spaced grids if required, e.g. Fornberg [1988, 1998].

By the use of finite-difference methods, the partial differential equations in (4.3.9) and (4.3.10) are re-expressed as linear combinations of the nodal boundary data $\phi_{n,j}$ and $\phi'_{n,j}$. Let $c^{(m)}_{k,j}(p)$ and $d^{(m)}_{k,j}(p)$, which consist of combinations of finite-difference coefficients and integrals $J_{k,j}$ and $K_{k,j}$, $k = 1, \ldots, m$, respectively define the coefficients of the nodal data $\phi_{n,j}$ and $\phi'_{n,j}$. Then the *finite-difference-series error* $\epsilon^{(m,F)}_n$ satisfies

$$(\mathcal{G}'_{n,m} - \eta\mathcal{I})\epsilon^{(m,F)}_n - \mathcal{G}_{n,m}\epsilon'^{(m,F)}_n = 0, \tag{4.3.11}$$

where, by (4.3.9) and (4.3.10),

$$\begin{aligned}(\mathcal{G}'_{n,m}\epsilon^{(m,F)}_n)(p) &\equiv \sum_{j=1}^{n}\int_{e^{(j)}} \epsilon'^{(m,F)}_{n,j}(q)G'(p,q)\,dq \\ &= \sum_{j=1}^{n}\sum_{k=1}^{m} c^{(m)}_{k,j}(p)\phi_{n,j} \\ &\equiv (\mathcal{C}_{n,m}\phi_n)(p)\end{aligned} \tag{4.3.12}$$

and

$$\begin{aligned}(\mathcal{G}_{n,m}\epsilon_n'^{(m,F)})(p) &\equiv \sum_{j=1}^{n}\int_{e^{(j)}} \epsilon_{n,j}^{(m,F)}(q)G(p,q)\ dq \\ &= \sum_{j=1}^{n}\sum_{k=1}^{m} d_{k,j}^{(m)}(p)\phi_{n,j}' \\ &\equiv (\mathcal{D}_{n,m}\phi_n')(p). \end{aligned} \tag{4.3.13}$$

Consistent with the true error of the CBEM (4.2.20), the discrepancies in the truncated-series error and the finite-difference-series error are defined by

$$\Delta\epsilon_n^{(m)}(p) \equiv \epsilon_n(p) - \epsilon_n^{(m)}(p) \tag{4.3.14}$$

and

$$\Delta\epsilon_n^{(m,F)}(p) \equiv \epsilon_n(p) - \epsilon_n^{(m,F)}(p). \tag{4.3.15}$$

4.3.2 Validation of the error approximations

The approximate truncated-series CBEM errors $\epsilon_n^{(m)}$ and $\epsilon_n^{(m,F)}$ are validated using discrepancies (4.3.14) and (4.3.15) for the nonsingular test BVP in Fig. 4.2.2. This experiment is first conducted for $\epsilon_n^{(m)}$, where we do know the solution *a priori*, so that it can be compared with the numerical approximated $\epsilon_n^{(m,F)}$ for which the solution is not required.

In Fig. 4.3.2 the discrepancy in the truncated-series error $\Delta\epsilon_n^{(m)}$ is depicted for different values of n and m, which demonstrates two facts: first, as the truncation order m increases, $\epsilon_n^{(m)}$ converges to the exact error ϵ_n, i.e.

$$\Delta\epsilon_n^{(m)}(p) \to 0, \quad n, m \to \infty; \tag{4.3.16}$$

second, there is a close agreement between the error discrepancy surfaces when $m = 2$ and $m = 3$ regardless of n as the truncated-series error $\epsilon_n^{(m)}$ in (4.2.37) consists of integrals $J_{k,j}$ and $K_{k,j}$ that are order $O(h^5)$ for both values of m.

The RMSE of $\epsilon_n^{(m)}$ is defined by

$$\sigma_{n,m} = \sqrt{\frac{1}{M}\sum_{j=1}^{M}\left(\epsilon_n^{(m)}(p_{M,j}\right)^2}, \tag{4.3.17}$$

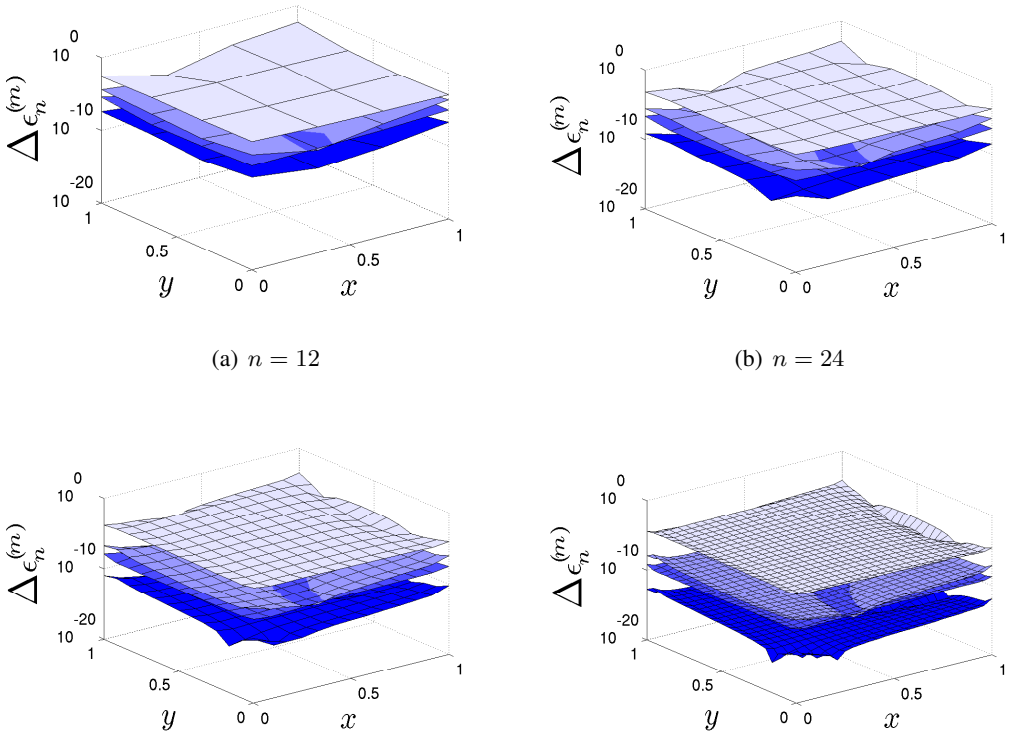

(a) $n = 12$ (b) $n = 24$

(c) $n = 48$ (d) $n = 96$

Figure 4.3.2: *Log plots of the discrepancy between the truncated-series error* $\epsilon_n^{(m)}$ *and the true error* ϵ_n*,* $\Delta\epsilon_n^{(m)}(p)$*, in the CBEM solution of the test BVP in Fig. 4.2.2, for* $n = 12, 24, 48, 96$ *and different values of* m*. The varying shades in the surfaces from light to dark correspond to* $m = 1, 2, 3$ *and* 4 *respectively. The truncated-series error is converging to the true error with increasing* m *and* n*, reflected by the decrease in the absolute values of* $\Delta\epsilon_n^{(m)}$ *on each sub-figure.*

where M is the number of mesh points.

In Table 4.3.1 the RMSE and the rate of convergence of the truncated-series error $\epsilon_n^{(m)}$ are presented for the test BVP (Fig. 4.2.2) with different values of m and n. The RMSE of the truncated-series error is fixed when $m > 3$ due to the convergence of the Taylor-series, therefore a maximum of $m = 4$ will be imposed in the implementation of $\epsilon_n^{(m)}$. As for the rate of convergence in truncated-series error, $\sigma_{n,m}/\sigma_{2n,m}$, Table 4.3.1 shows it is tending to second order (i.e. $\rho = 4$) with increasing n thus recovers the predicted $O(h^2)$ convergence. Although, most interestingly we have $\sigma_{n,m}/\sigma_{2n,m} \to 4^+$, which is not reflecting the $O(h^2)$ pollution, due to the construction of the

m	n	$\sigma_{n,m}$	$\sigma_{n,m}/\sigma_{2n,m}$
1	12	0.0201	5.1475
	24	0.0039	4.8112
	48	8.1234×10^{-4}	4.3623
	96	1.8622×10^{-4}	
2	12	0.0190	5.0946
	24	0.0037	4.7370
	48	7.8670×10^{-4}	4.3057
	96	1.8271×10^{-4}	
3	12	0.0189	5.0816
	24	0.0037	4.7348
	48	7.8668×10^{-4}	4.3055
	96	1.8271×10^{-4}	
4	12	0.0189	5.0817
	24	0.0037	4.7348
	48	7.8668×10^{-4}	4.3055
	96	1.8271×10^{-4}	

Table 4.3.1: *The RMSE $\sigma_{n,m}$ and convergence rate $\sigma_{n,m}/\sigma_{2n,m}$ of the truncated error $\epsilon_n^{(m)}(p)$ in the CBEM solution of the test BVP in Fig. 4.2.2, for $n = 12, 24, 48, 96$ and $m = 1, 2, 3, 4$. By the nomenclature of Richardson's extrapolation in* (4.2.48)*, for $O(h^2)$ error $\rho = \sigma_{n,m}/\sigma_{2n,m} = 4$, however, here $\rho \to 4^+$ as $n \to \infty$ due to the mesh points being taken at the end-points of the boundary elements.*

mesh points. For example, recall $J_{k,j}$ and $K_{k,j}$ define the leading behaviour of the truncated-series error $\epsilon_n^{(m)}$ in (4.3.9) and (4.3.10). When the field point p is situated at either end-point of element $e^{(j)}$ (denoted by $q_{An,j}$ and $q_{Bn,j}$ in Fig. 4.2.1), by (4.2.37) and (4.2.40), $J_{k,j}(p) = O(h^3)$ and $K_{k,j}(p) = O(h^2)$, as

$$K_{k,j}(p = q_{An,j}) = \frac{1}{4}h^2 + \left(\frac{1}{12}\log(h) - \frac{1}{9}\right)h^3 + \frac{1}{24}h^4 + \dots \tag{4.3.18}$$

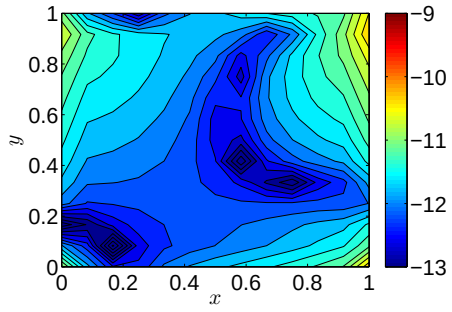

Figure 4.3.3: *Contour plots of* $\log|\Delta\epsilon_n^{(m)}(p)|$*, the logarithm of the discrepancy in the truncated-series error in the CBEM solution of the test BVP in Fig. 4.2.2, for* $n = 48$ *and* $m = 4$*. The contour plot corresponds to the dark surface in Fig. 4.3.2*(c) *and is used as a quantitative comparator for the finite-difference-series error in Fig. 4.3.4.*

and

$$K_{k,j}(p = q_{Bn,j}) = -\frac{1}{4}h^2 + \left(\frac{1}{12}\log(h) - \frac{1}{9}\right)h^3 - \frac{1}{24}h^4 + \dots. \tag{4.3.19}$$

However, over the n end-points along the boundary, where the mesh is defined, the coefficients of the even powers of h in $K_{k,j}$ cancel so that $K_{k,j} = O(h^3)$ and hence we recover $\sigma_{n,m}/\sigma_{2n,m} \to 4^+$.

In the finite-difference method we chose the order of accuracy *a priori* so that its error is of order $O(h^a)$. Although, the choice of the order of accuracy a, which determines the number of points in the molecule, is restricted by n in the finite-difference-series error $\epsilon_n^{(m,F)}$: for the nonsingular test BVP in Fig. 4.2.2

$$a \leq \frac{n}{4} - m, \tag{4.3.20}$$

where m is truncation limit. With this in mind, the discrepancy in the finite-difference-series error $\Delta\epsilon_n^{(m,F)}(p)$ is depicted in Fig. 4.3.4 for $a = 2, 4, 6, 8$ and fixed $n = 48$ and $m = 4$. Fig. 4.3.4 demonstrates that $\epsilon_n^{(m,F)}$ converges to the exact error ϵ_n as the order of accuracy increases, i.e.

$$\|\Delta\epsilon_n^{(m,F)}\| \to 0, \quad a \to \infty. \tag{4.3.21}$$

Also, by comparing Fig. 4.3.4 with the truncated-series error discrepancy equivalent in Fig. 4.3.3 where $n = 48$ and $m = 4$,

$$\Delta\epsilon_n^{(m,F)} \to \Delta\epsilon_n^{(m)}, \quad a \to \infty. \tag{4.3.22}$$

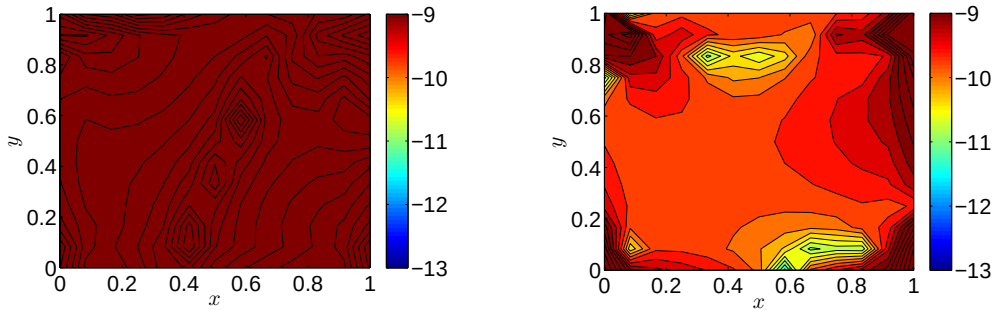

(a) $a = 2$

(b) $a = 4$

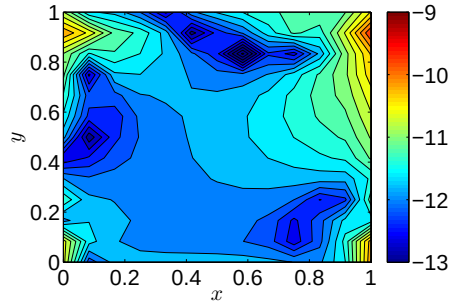

(c) $a = 6$

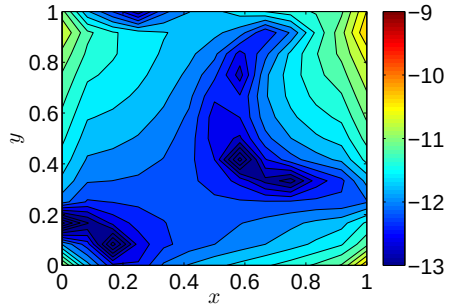

(d) $a = 8$

Figure 4.3.4: *Contour plots of* $\log|\Delta\epsilon_n^{(m,F)}(p)|$*, the logarithm of the discrepancy in the finite-difference-series error in the CBEM solution of the test BVP in Fig. 4.2.2, where the error has been predicted using only linear combinations of nodal boundary values. Here* $n = 48$*,* $m = 4$ *and the accuracy order* a *is varied as* $a = 2, 4, 6, 8$*. The contour plots are a quantitative comparison with the discrepancy in the truncated-series error* $\Delta\epsilon_n^{(m)}(p)$ *that is depicted in Fig. 4.3.3 for the same* n *and* m*.*

That is, when $a \geq 8$ the finite-difference-series $\epsilon_n^{(m,F)}$ approximates the truncated-series error $\epsilon_n^{(m)}$ to at least eighth-order accuracy which, for the test problem considered in Fig. 4.3.3 and Fig. 4.3.4, proves to be sufficient. For example, given the truncated-series error $\epsilon_n^{(4)}$ approximates the true error ϵ_n to $O(10^{-17})$ degrees of accuracy in the test BVP, which is more than sufficient for real-life applications, the finite-difference-truncated-series error $\epsilon_n^{(4,F)}$ also approximates ϵ_n to $O(10^{-17})$ degrees of accuracy when $a \geq 8$. Moreover, provided the accuracy is taken to be greater

than or equal to eighth-order, $\epsilon_n^{(m,F)}$ will be $O(h^2)$, consistent with $\epsilon_n^{(m)}$ in Table 4.3.1. Hence the truncated-series error $\epsilon_n^{(m)}$ and its finite-difference equivalent $\epsilon_n^{(m,F)}$ will be used to approximate $\bar{\epsilon}_n$ in the modified method of (4.3.1).

4.3.3 Implementation of the modified CBEMs

Given the validations of the error predictions in §4.3.2, we now build the error predictions into the CBEM using the modified approach of (4.3.1). There will be two types of modified methods: one dependent upon the truncated-series error $\epsilon_n^{(m)}$ and the other upon the finite-difference-series error $\epsilon_n^{(m,F)}$. First, the truncated-series modified CBEM (MCBEM) with solution $\phi_n^{(m)}$ incorporates $\epsilon_n^{(m)}$, an approximate of the true error ϵ_n. Following (4.3.1), we therefore reformulate the standard CBEM for ϕ_n using

$$\phi_n^{(m)}(p) = \phi_n(p) + \epsilon_n^{(m)}(p). \tag{4.3.23}$$

Recalling the predefined $\epsilon_{n,j}^{(m)}$ in (4.3.6) and $\epsilon_{n,j}^{\prime(m)}$ in (4.3.7), by Green's integral formula, (4.3.23) is expressible in integral form as

$$\eta(p)\phi_n^{(m)}(p) = \sum_{j=1}^{n} \left\{ \int_{e^{(j)}} \left[\phi_{n,j} + \epsilon_{n,j}^{(m)}(q)\right] \; G'(p,q)\; dq - \int_{e^{(j)}} \left[\phi'_{n,j} + \epsilon_{n,j}^{\prime(m)}(q)\right] \; G(p,q)\; dq \right\}, \tag{4.3.24}$$

where, following §4.2, $\phi_n^{(m)}$ is the *theoretical discretised MCBEM solution*. Using (4.2.6), the symbolic form of (4.3.24) is

$$\left(\mathcal{G}'_n - \eta\mathcal{I}\right)\phi_n^{(m)} + \mathcal{G}'_{n,m}\epsilon_n^{(m)} - \mathcal{G}_n\phi_n^{\prime(m)} - \mathcal{G}_{n,m}\epsilon_n^{\prime(m)} = 0 \tag{4.3.25}$$

which, upon applying (4.3.8), is equivalent to

$$\left(\mathcal{G}'_n - \eta\mathcal{I}\right)\phi_n^{(m)} - \mathcal{G}_n\phi_n^{\prime(m)} + \eta\mathcal{I}\epsilon_n^{(m)} = 0. \tag{4.3.26}$$

Second, the finite-difference-modified CBEM (FDMCBEM) with solution $\phi_n^{(m,F)}$ incorporates $\epsilon_n^{(m,F)}$, an approximate of the truncated-series error $\epsilon_n^{(m)}$. As per (4.3.23), we reformulate the standard CBEM using

$$\phi_n^{(m,F)}(p) = \phi_n(p) + \epsilon_n^{(m,F)}(p), \tag{4.3.27}$$

where, by definition of the finite-difference-series error $\epsilon_n^{(m,F)}$ in (4.3.12) and (4.3.13), $\phi_n^{(m,F)}$ satisfies the discretised boundary-integral equation

$$\eta(p)\phi_n^{(m,F)}(p) = \sum_{j=1}^{n}\left\{\phi_{n,j}\left[\int_{e^{(j)}} G'(p,q)\ dq + \sum_{k=1}^{m} c_{k,j}^{(m)}(p)\right] - \phi'_{n,j}\left[\int_{e^{(j)}} G(p,q)\ dq + \sum_{k=1}^{m} d_{k,j}^{(m)}(p)\right]\right\}. \tag{4.3.28}$$

To match with the nomenclature of §4.2, $\phi_n^{(m,F)}$ in (4.3.28) is the *theoretical discretised FDMCBEM solution*. The symbolic form of (4.3.28) is

$$\left(\mathcal{G}'_n - \eta\mathcal{I}\right)\phi_n^{(m,F)} + \mathcal{G}'_{n,m}\epsilon_n^{(m,F)} - \mathcal{G}_n\phi_n'^{(m,F)} - \mathcal{G}_{n,m}\epsilon_n'^{(m,F)} = 0 \tag{4.3.29}$$

which, by (4.3.12) and (4.3.13), may be alternatively expressed in the form

$$\left(\mathcal{G}'_n + \mathcal{C}_{n,m} - \eta\mathcal{I}\right)\phi_n^{(m,F)} - (\mathcal{G}_n + \mathcal{D}_{n,m})\phi_n'^{(m,F)} = 0. \tag{4.3.30}$$

Note when $\mathcal{C}_{n,m} = \mathcal{D}_{n,m} = 0$ (4.3.30) reduces to the standard CBEM in (4.2.6). Eqn. (4.3.30) demonstrates that the FDMCBEM is a *perturbation* of the standard CBEM (4.2.6), whereby an approximation of the error in the CBEM is included over each element $e^{(j)}$.

4.3.4 Collocation equations

To recap, the standard CBEM has a system of n collocated equations (4.2.10) expressible in the form $\mathbf{H}\mathbf{x}_C = \mathbf{g}$, where $\mathbf{g}$ contains all prescribed boundary conditions. Now, collocating the MCBEM (4.3.26) at the n mid-points $p = q_{n,i}$ defines a system $\mathbf{H}\mathbf{x}_{MC} = \mathbf{g} + \mathbf{e}$, where $\mathbf{e}$ is the n-dimensional error vector with components

$$e_i = \sum_{j=1}^{n}\left\{\int_{e^{(j)}} \epsilon_{n,j}^{(m)}(q)\ G'(q_{n,i},q)\ dq - \int_{e^{(j)}} \epsilon_{n,j}'^{(m)}(q)\ G(q_{n,i},q)\ dq\right\}. \tag{4.3.31}$$

In system $\mathbf{H}\mathbf{x}_{MC} = \mathbf{g} + \mathbf{e}$ the vector $\mathbf{x}_{MC}$ contains the unknown mid-element nodal values of $\phi_{n,j}$ on $\partial\Omega_{\phi'}$ and $\phi'_{n,j}$ on $\partial\Omega_\phi$ which, once determined, can be used to compute $\phi_n^{(m)}$ in (4.3.26) directly thus defining the numerical discretised solution. That is, by linearity with the numerical discretised CBEM solution in (4.2.11), the *numerical discretised MCBEM solution* $\widetilde{\phi}_n^{(m)}$ satisfies

$$\eta(p)\widetilde{\phi}_n^{(m)}(p) = \sum_{j=1}^{n}\left\{\int_{e^{(j)}}\left[\widetilde{\phi}_{n,j} + \epsilon_{n,j}^{(m)}(q)\right]\ G'(p,q)\ dq - \int_{e^{(j)}}\left[\widetilde{\phi}'_{n,j} + \epsilon_{n,j}'^{(m)}(q)\right]\ G(p,q)\ dq\right\}, \tag{4.3.32}$$

in which

$$\widetilde{\phi}_{n,j} = \begin{cases} \phi(q_{n,j}) & \text{if } e^{(j)} \subseteq \partial\Omega_\phi, \\ \widetilde{\phi}(q_{n,j}) & \text{otherwise,} \end{cases} \quad \text{and} \quad \widetilde{\phi}'_{n,j} = \begin{cases} \phi'(q_{n,j}) & \text{if } e^{(j)} \subseteq \partial\Omega_{\phi'}, \\ \widetilde{\phi}'(q_{n,j}) & \text{otherwise,} \end{cases} \tag{4.3.33}$$

where $\widetilde{\phi}(q_{n,j})$ and $\widetilde{\phi}'(q_{n,j})$ are defined from the solution of the dense system $\mathbf{H}\mathbf{x}_{MC} = \mathbf{g} + \mathbf{e}$. As is evident from (4.3.30), the FDMCBEM is a variation of the CBEM, hence a collocation of the FDMCBEM at the mid-points $p = q_{n,i}$ results in a discretised system $(\mathbf{H} + \delta\mathbf{H})\mathbf{x}_{FC} = \mathbf{g}$ with solution $\mathbf{x}_{FC}$ containing the unknown mid-element nodal values of $\phi_{n,j}$ on $\partial\Omega_{\phi'}$ and $\phi'_{n,j}$ on $\partial\Omega_\phi$. In the dense system $(\mathbf{H} + \delta\mathbf{H})\mathbf{x}_{FC} = \mathbf{g}$ the $n \times n$ matrix $\delta\mathbf{H}$ has components

$$\delta H_{i,j} = \begin{cases} \displaystyle\sum_{k=1}^{m} c_{k,j}^{(m)}(q_{n,i}) & \text{if } e^{(j)} \in \partial\Omega_{\phi'}, \\ \displaystyle\sum_{k=1}^{m} d_{k,j}^{(m)}(q_{n,i}) & \text{if } e^{(j)} \in \partial\Omega_\phi. \end{cases} \tag{4.3.34}$$

Given the CBEM solution $\mathbf{x}_C$ along with

$$\mathbf{x}_{FC} = (\mathbf{I} + \mathbf{H}^{-1}\delta\mathbf{H})^{-1}\mathbf{H}^{-1}\mathbf{g}, \tag{4.3.35}$$

where $\mathbf{I}$ is the identity matrix,

$$\mathbf{x}_C - \mathbf{x}_{FC} = \left[\mathbf{I} - (\mathbf{I} + \mathbf{H}^{-1}\delta\mathbf{H})^{-1}\right]\mathbf{x}_C \tag{4.3.36}$$

whose norm satisfies

$$\|\mathbf{x}_C - \mathbf{x}_{FC}\| \leq \left\|\left[\mathbf{I} - (\mathbf{I} + \mathbf{H}^{-1}\delta\mathbf{H})^{-1}\right]\right\| \|\mathbf{x}_C\|. \tag{4.3.37}$$

By the geometric series theorem (Appendix A), $(\mathbf{I} + \mathbf{H}^{-1}\delta\mathbf{H})^{-1}$ in (4.3.35) exists and is bounded if and only if (Golub and Van Loan [1996])

$$\|\mathbf{H}^{-1}\delta\mathbf{H}\| < 1, \tag{4.3.38}$$

i.e.

$$\|(\mathbf{I} + \mathbf{H}^{-1}\delta\mathbf{H})^{-1}\| \leq \frac{1}{1 - \|\mathbf{H}^{-1}\delta\mathbf{H}\|}. \tag{4.3.39}$$

The solution of $(\mathbf{H} + \delta\mathbf{H})\mathbf{x}_{FC} = \mathbf{g}$, which is known as the *numerical discretised solution*, completes the boundary distributions of ϕ and ϕ', hence $\phi_n^{(m,F)}$ in (4.3.28) can be computed

directly. In other words, by analogy with (4.2.11), the solution of $(\mathbf{H}+\delta\mathbf{H})\mathbf{x}_{FC}=\mathbf{g}$, defined by $\widetilde{\phi}(q_{n,j})$ and $\widetilde{\phi}'(q_{n,j})$, are elements of the *numerical discretised FDMCBEM solution* $\widetilde{\phi}_n^{(m,F)}$ that satisfies

$$\eta(p)\widetilde{\phi}_n^{(m,F)}(p)=\sum_{j=1}^{n}\left\{\widetilde{\phi}_{n,j}\left[\int_{e^{(j)}}G'(p,q)\,dq+\sum_{k=1}^{m}c_{k,j}^{m}(p)\right]\right.$$
$$\left.-\widetilde{\phi}'_{n,j}\left[\int_{e^{(j)}}G(p,q)\,dq+\sum_{k=1}^{m}d_{k,j}^{m}(p)\right]\right\}, \tag{4.3.40}$$

where

$$\widetilde{\phi}_{n,j}=\begin{cases}\phi(q_{n,j}) & \text{if } e^{(j)}\subseteq\partial\Omega_{\phi},\\ \widetilde{\phi}(q_{n,j}) & \text{otherwise,}\end{cases}\quad\text{and}\quad \widetilde{\phi}'_{n,j}=\begin{cases}\phi'(q_{n,j}) & \text{if } e^{(j)}\subseteq\partial\Omega_{\phi'},\\ \widetilde{\phi}'(q_{n,j}) & \text{otherwise.}\end{cases} \tag{4.3.41}$$

4.3.5 Error analysis of the modified CBEMs

Comparing the theoretical discretised MCBEM solution $\phi_n^{(m)}$ in (4.3.24) with the exact solution $\phi(p)$, the *theoretical MCBEM error* is defined as

$$\varepsilon_{n,m}(p)=\phi(p)-\phi_n^{(m)}(p) \tag{4.3.42}$$

where, by (4.3.2), (4.3.3), (4.3.14) and (4.3.23), we obtain

$$\begin{aligned}\varepsilon_{n,m}(p)&=\phi(p)-\left(\phi_n(p)+\epsilon_n^{(m)}(p)\right)\\ &=\epsilon_n(p)-\epsilon_n^{(m)}(p)\\ &=\Delta\epsilon_n^{(m)}(p).\end{aligned} \tag{4.3.43}$$

Similarly, by comparing the theoretical discretised FDMCBEM solution $\phi_n^{(m,F)}$ in (4.3.28) with the exact solution $\phi(p)$, the *theoretical FDMCBEM error* is defined as

$$\varepsilon_{n,m}^{(F)}(p)=\phi(p)-\phi_n^{(m,F)}(p) \tag{4.3.44}$$

which, by (4.3.15) and (4.3.27), we obtain

$$\begin{aligned}\varepsilon_{n,m}^{(F)}(p)&=\phi(p)-\left(\phi_n(p)+\epsilon_n^{(m,F)}(p)\right)\\ &=\phi(p)-\left(\phi_n(p)+\epsilon_n^{(m)}(p)-\Delta\epsilon_n^{(m,F)}(p)\right)\\ &=\Delta\epsilon_n^{(m)}(p)+\Delta\epsilon_n^{(m,F)}(p).\end{aligned} \tag{4.3.45}$$

Thus, by (4.3.43), we have

$$\|\varepsilon_{n,m}\|_\infty = \|\Delta\epsilon_n^{(m)}\|_\infty, \tag{4.3.46}$$

and, by (4.3.45), we have

$$\|\varepsilon_{n,m}^{(F)}\|_\infty \leq \|\Delta\epsilon_n^{(m)}\|_\infty + \|\Delta\epsilon_n^{(m,F)}\|_\infty. \tag{4.3.47}$$

In other words, the MCBEM error (4.3.46) and the FDMCBEM error (4.3.47) are theoretically proportional to error discrepancies and, as the standard CBEM error in (4.2.20) is proportional to an error, we have

$$\|\varepsilon_{n,m}\|_\infty \ll \|\varepsilon_{n,m}^{(F)}\|_\infty \ll \|\epsilon_n\|_\infty. \tag{4.3.48}$$

By construction, the MCBEM and FDMCBEM are methods that reduce the overall error of the standard CBEM.

Alternatively, by respectively comparing the numerical discretised MCBEM solution $\widetilde{\phi}_n^{(m)}$ in (4.3.32) and the numerical discretised FDMCBEM solution $\widetilde{\phi}_n^{(m,F)}$ in (4.3.40) with the exact solution $\phi(p)$, the *numerical MCBEM error* is defined as

$$\widetilde{\varepsilon}_{n,m}(p) = \phi(p) - \widetilde{\phi}_n^{(m)}(p), \tag{4.3.49}$$

and the *numerical FDMCBEM error* is defined as

$$\widetilde{\varepsilon}_{n,m}^{(F)}(p) = \phi(p) - \widetilde{\phi}_n^{(m,F)}(p). \tag{4.3.50}$$

Therefore, by (4.3.48), we predict

$$\|\widetilde{\varepsilon}_{n,m}\|_\infty \ll \|\widetilde{\varepsilon}_{n,m}^{(F)}\|_\infty \ll \|\widetilde{\epsilon}_n\|_\infty, \tag{4.3.51}$$

thereby achieving the aim of the modifications in (4.3.4).

4.4 Comparison of the modified numerical schemes

Before computing the numerical errors of both the MCBEM and FDMCBEM, we first consider their theoretical behaviours. By (4.3.43) and (4.3.45), the MCBEM error and the FDMCBEM error are respectively dependent upon $\epsilon_n^{(m)}$ and $\epsilon_n^{(m,F)}$ that comprise the integrals $J_{k,j}$ in (4.2.29)

and $K_{k,j}$ in (4.2.30), as seen in §4.3.2. Thus it is the behaviour of $J_{k,j}$ and $K_{k,j}$ that determines the overall behaviour of the MCBEM and FDMCBEM errors. For example, in accordance with (4.3.23) and (4.3.43),

$$\varepsilon_{n,m} = \phi - \phi_n^{(m)} = \phi - \phi_n - \epsilon_n^{(m)}, \tag{4.4.1}$$

in which the first two terms on the right-hand side are $O(h^2)$, therefore the order of the MCBEM error $\varepsilon_{n,m}$ is determined by the truncated-series error $\epsilon_n^{(m)}$. As the truncated-series error is defined by the integrals $J_{k,j}$ and $K_{k,j}$, whose orders increase indefinitely with k in a two-cycle, as discussed in (4.2.37), over n elements we have

$$\varepsilon_{n,m} = \begin{cases} O(h^2) & m = 1, \\ O(h^4) & m = 2, 3, \\ O(h^6) & m = 4, 5, \\ O(h^8) & m = 6, 7. \end{cases} \tag{4.4.2}$$

In §4.3.2 the finite-difference-truncated-series error recovered the behaviour of the truncated-series error when the accuracy in the finite-difference scheme was taken to be sufficiently large, e.g. an eighth-order accuracy in the finite-difference scheme was sufficient when $m = 4$. Therefore, the order of the finite-difference-truncated-series error $\varepsilon_{n,m}^{(F)}$ will match the order of $\varepsilon_{n,m}$ in (4.4.2), provided the accuracy in the finite-difference scheme is sufficiently high, although a quantification into the exact order of accuracy required is deferred until later.

Both the modified CBEMs of §4.3 are validated for the test BVP of Fig. 4.2.2 by a combination of graphical and data analysis. Using (4.3.49) and (4.3.50), we define the RMSEs as

$$\widetilde{\sigma}_{n,m} \equiv \sqrt{\frac{1}{M}\sum_{j=1}^{M}\left(\widetilde{\varepsilon}_{n,m}(p_{M,j})\right)^2} \quad \text{for the MCBEM,} \tag{4.4.3}$$

and

$$\widetilde{\sigma}_{n,m}^{(F)} \equiv \sqrt{\frac{1}{M}\sum_{j=1}^{M}\left(\widetilde{\varepsilon}_{n,m}^{(F)}(p_{M,j})\right)^2} \quad \text{for the FDMCBEM,} \tag{4.4.4}$$

where M is the number of mesh points $p_{M,j}$ over the internal grid. The convergence rate and order of the MCBEM error and the FDMCBEM error are determined by Richardson's extrapolation formula (4.2.48), as discussed in §4.2.2.

Similar to the CBEM error $\widetilde{\epsilon}_n$ in §4.2.2, the MCBEM and FDMCBEM errors are computed for

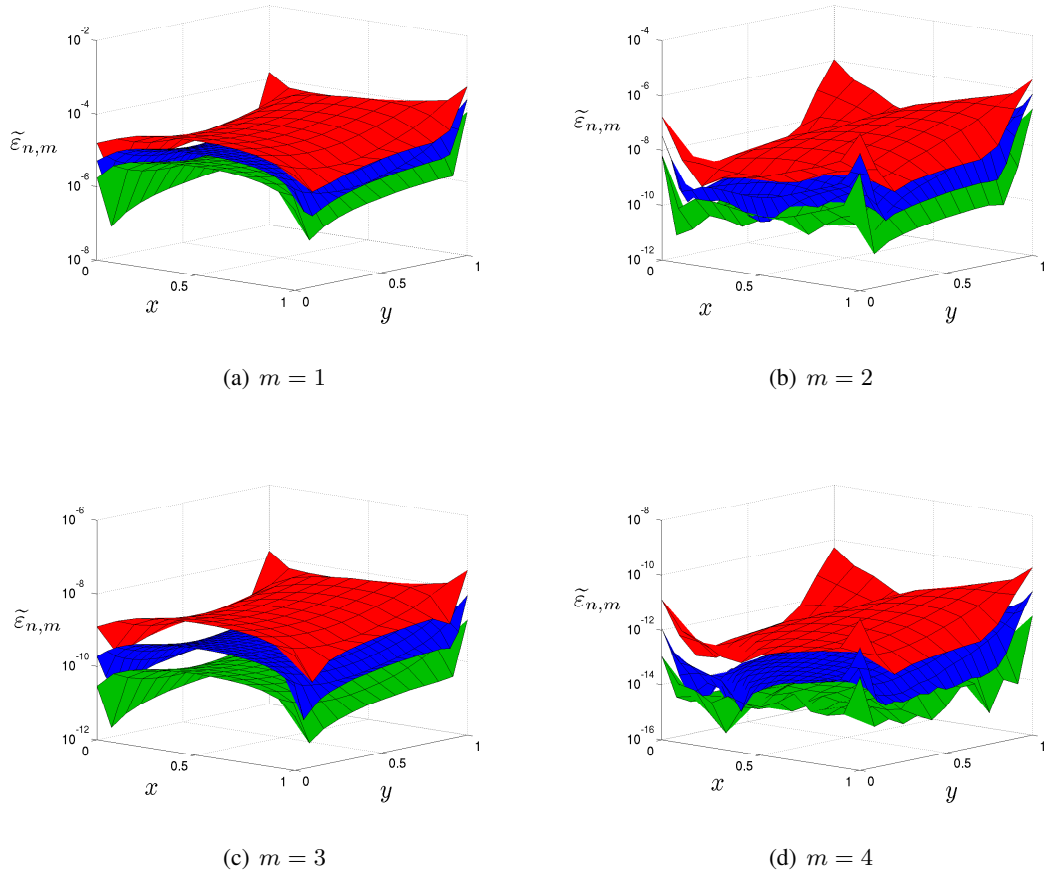

(a) $m = 1$ (b) $m = 2$

(c) $m = 3$ (d) $m = 4$

Figure 4.4.1: *Log plots of the error in the MCBEM solution of the test problem in Fig. 4.2.2,* $\widetilde{\varepsilon}_{n,m}(p)$*, for different values of* n *and truncation limits* $m = 1, 2, 3, 4$*. Each surface corresponds to* $n = 48$ *(red),* $n = 72$ *(blue) and* $n = 108$ *(green). The MCBEM errors are converging to zero with increasing* n*, and furthermore, by comparison with the CBEM errors in Fig. 4.2.3, reduce the overall error by up to eight orders of magnitude.*

different values of n. To simplify the implementation of the modified methods, however, the computations take a maximum of $m = 4$ only.

The MCBEM error $\widetilde{\varepsilon}_{n,m}$ in the test BVP (Fig. 4.2.2) is depicted in Fig. 4.4.1. By comparison with the standard CBEM error in Fig 4.2.3, Fig. 4.4.1 shows an impressive reduction in the MCBEM error, even for the simplest case of $m = 1$. Furthermore, Fig. 4.4.1 demonstrates two features of the MCBEM error: first, prominent error peaks at the corner points due to the $O(h^2)$ behaviour of $J_{k,j}$ and $K_{k,j}$; second, the error is converging to zero with increasing n, although further analysis

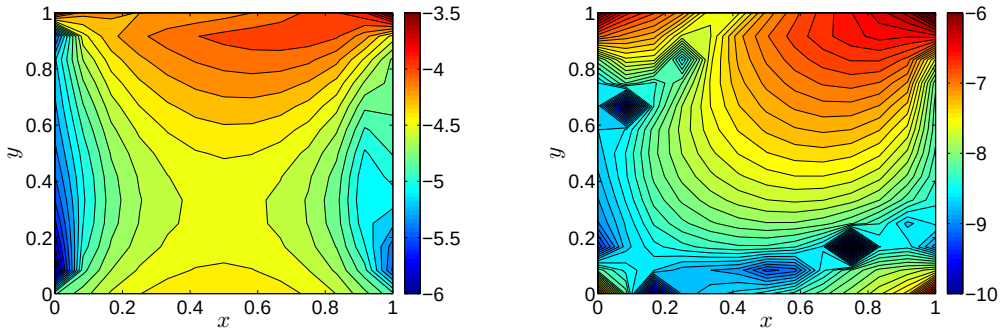

(a) $m = 1$

(b) $m = 2$

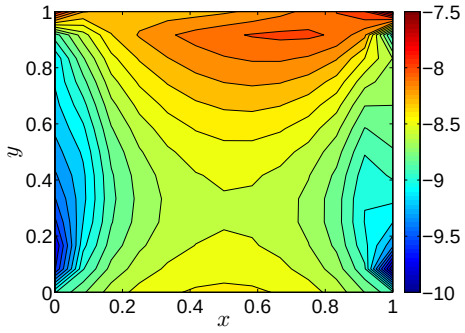

(c) $m = 3$

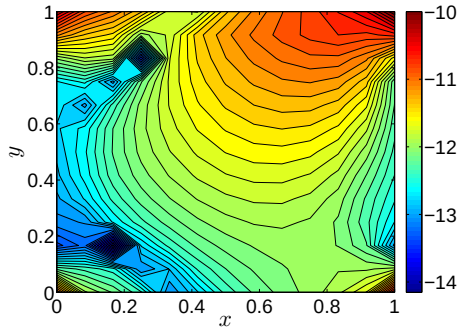

(d) $m = 4$

Figure 4.4.2: *Contour plots of* $\log(\widetilde{\varepsilon}_{n,m}(p))$*, the logarithm of the relative error in the MCBEM solution of the test BVP in Fig. 4.2.2, for* $n = 48$ *and different values of* m*. Here we have a detailed quantification of the red error surfaces given in Fig. 4.4.1 for* $m = 1, \ldots, 4$*. By comparison with the CBEM error in Fig. 4.2.4*(a)*, the scaling of the colour maps show the superior accuracy gained by the MCBEM method when* $m > 1$*.*

into its rate and order is deferred until after the errors of the FDMCBEM have been computed and discussed.

As a quantification of the $n = 48$ error surfaces in Fig. 4.4.1, the MCBEM errors are also depicted in four contour plots in Fig. 4.4.2 with fixed $n = 48$ and varying m. Compared with Fig. 4.4.1, the contour plots in Fig. 4.4.2 provide a greater extent of detail of the behaviour of the errors over the whole domain. In particular, the contours show the error converging to zero with increasing m and prominent error peaks at the corners, the largest of which is at $(x, y) = (1, 1)$ due the Maximum

m	n	Exact $\widetilde{\sigma}_{n,m}$	Approximate $\widetilde{\sigma}^{(F)}_{n,m}$			
			2nd Order	4th Order	6th Order	8th Order
1	48	5.8686×10^{-5}	6.0706×10^{-5}	5.9828×10^{-5}	6.0003×10^{-5}	6.0124×10^{-5}
	72	2.4105×10^{-5}	2.4437×10^{-5}	2.4336×10^{-5}	2.4372×10^{-5}	2.4397×10^{-5}
2	48	2.4885×10^{-7}	3.5340×10^{-6}	3.1080×10^{-7}	3.1105×10^{-7}	3.2030×10^{-7}
	72	5.0907×10^{-8}	7.1107×10^{-7}	6.2389×10^{-8}	6.3710×10^{-8}	6.5621×10^{-8}
3	48	5.0121×10^{-9}	3.2867×10^{-6}	1.5171×10^{-8}	5.1945×10^{-9}	5.1945×10^{-9}
	72	9.3238×10^{-10}	6.6054×10^{-7}	1.6921×10^{-9}	9.4754×10^{-10}	9.4901×10^{-10}
4	48	1.2476×10^{-11}	3.2890×10^{-6}	1.2967×10^{-8}	9.0726×10^{-11}	1.8043×10^{-11}
	72	1.2129×10^{-12}	6.6121×10^{-7}	1.2425×10^{-9}	4.6511×10^{-12}	1.6704×10^{-12}

Table 4.4.1: *The RMSE of the MCBEM (exact) $\widetilde{\sigma}_{n,m}$ and the FDMCBEM (approximate) $\widetilde{\sigma}^{(F)}_{n,m}$ in the solution of the test BVP in Fig. 4.2.2, taking $\alpha = 1.5$ in* (4.2.48)*, $n = 48, 72$, $m = 1, 2, 3, 4$ and order of accuracy $a = 2, 4, 6, 8$ in the finite-difference method. Here the RMSEs are quantifications of the error surfaces in Fig. 4.4.1 and Fig. 4.4.3 ($n = 48$ (red), $n = 72$ (blue)). When eighth-order accuracy is taken in the FDMCBEM, the difference between the approximate RMSE and the exact RMSE is the least for all m and n, which is in agreement with Fig. 4.3.4.*

principle. Furthermore, by comparison with the contour plot of the CBEM error in Fig. 4.2.4(a), the scaling of the colour maps show the superior accuracy gained by the MCBEM method when $m > 1$.

For the FDMCBEM to closely approximate the MCBEM, we require the error in the finite-difference molecule, which is dependent upon its chosen size, to be less than the new error that we are seeking to find in the improvement, namely the MCBEM error. Although, in accordance with in (4.3.20) of §4.2.1, the size of the molecule in the finite-difference method is restricted by n and m in $\epsilon_n^{(m,F)}$. Bearing this restriction in mind, the effect of the error in the molecule upon the accuracy of the FDMCBEM is depicted in Table 4.4.1, in which the size of the molecule (i.e. the accuracy of order $O(h^a)$) is varied.

When $a = 2$ in Table 4.4.1, i.e. the finite-difference method is taken to second-order accuracy, the order of the FDMCBEM RMSE (approximate) only matches that of the MCBEM RMSE (exact)

when $m = 1$. For $m > 1$, taking $a = 2$ in the finite-difference method adversely affects the overall FDMCBEM error, as the finite-difference error is greater than that we are seeking to find thus dominating the behaviour of $\widetilde{\varepsilon}^{(F)}_{n,m}$. Hence we require the accuracy of the finite-difference method to be greater than second-order when $m > 1$.

Table 4.4.1 provides another interesting observation: when $m = 1$ the difference between the approximate error $\widetilde{\varepsilon}^{(F)}_{n,m}$ and the exact error $\widetilde{\varepsilon}_{n,m}$ is the least when fourth-order accuracy is taken in the finite-difference scheme. This follows since, by (4.4.2), $\widetilde{\varepsilon}_{n,1}$ is of $O(h^2)$ therefore fourth-order accuracy is enough to recover $O(h^2)$ in $\widetilde{\varepsilon}^{(F)}_{n,1}$, i.e. the error in the molecule of the finite-difference method is less than the new error. However, Table 4.4.1 also shows that no further benefit is gained for increasing the accuracy above fourth-order, as the errors from the integrals $J_{k,j}$ and $K_{k,j}$ in $\epsilon^{(m,F)}_n$ will be the most dominant. Similarly, when $m = 3$, by (4.4.2), $\widetilde{\varepsilon}_{n,m}$ is of $O(h^4)$ therefore we expect no further improvement in $\widetilde{\varepsilon}^{(F)}_{n,3}$ when the accuracy is above sixth-order, as confirmed by Table 4.4.1. That is, Table 4.4.1 shows no monotonic improvement between the degree of the FDMCBEM error and the accuracy of the finite-difference approximation. Instead there is a staggered improvement, because the inclusion of larger numbers of $J_{k,j}$ and $K_{k,j}$ does not always compensate for the error in the finite-difference approximation.

For varying values of m, Table 4.4.1 quantifies the degree of accuracy required in the FDMCBEM. For example, when $a = 8$ in the finite-difference method, Table 4.4.1 shows $|\widetilde{\sigma}_{n,m} - \widetilde{\sigma}^{(F)}_{n,m}|$ is the least for all n and m, hence eighth-order accuracy is taken in the subsequent implementation of the FDMCBEM.

The errors of the FDMCBEM are depicted in Fig. 4.4.3 for the test BVP in Fig. 4.2.2. By adopting eighth-order accuracy in the finite-difference scheme, the FDMCBEM errors in Fig. 4.4.3 are indistinguishable from the MCBEM errors in Fig. 4.4.1 for all n and m. Moreover, by comparing the FDMCBEM errors in Fig. 4.4.3 with the CBEM errors in Fig. 4.2.3, we note an impressive error reduction in the FDMCBEM (up to eight-orders of magnitude), therefore achieving the original aim of the modification in (4.3.51).

The orders (and convergence rates) of the MCBEM and FDMCBEM errors in Figs. 4.4.1 and 4.4.3 are presented in Table 4.4.2. Using the nomenclature of Richardson's extrapolation in §4.2.2, the convergence rates are denoted by ρ and orders by p. The errors of the modified numerical schemes in Table 4.4.2 are converging to the theoretically predicted in orders in (4.4.2) with increasing n,

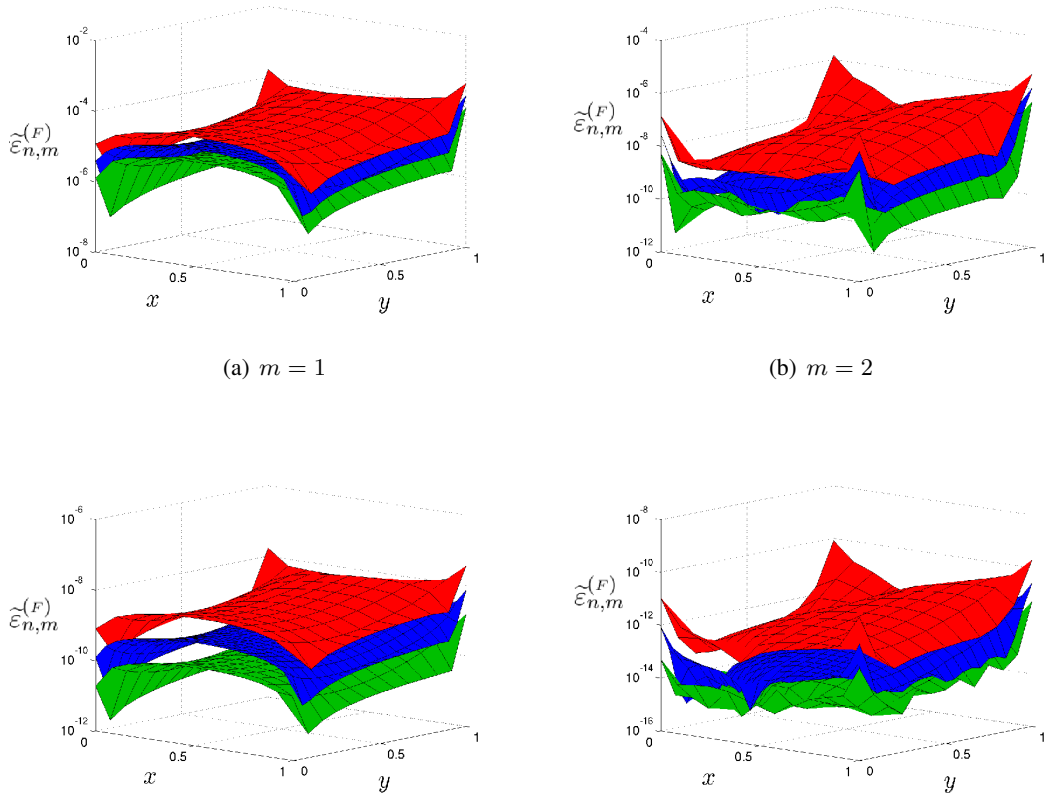

(a) $m = 1$ (b) $m = 2$

(c) $m = 3$ (d) $m = 4$

Figure 4.4.3: *Log plot of the error in the FDMCBEM solution of the test BVP in Fig. 4.2.2,* $\widetilde{\varepsilon}^{(F)}_{n,m}(p)$*, for* $m = 1, 2, 3, 4$*, fixed eighth-order accuracy in the finite-difference scheme and different values of* n*. Each surface corresponding to* $n = 48$ *(red),* $n = 72$ *(blue) and* $n = 108$ *(green). By comparison with Fig. 4.4.3, the FDMCBEM errors and the MCBEM are indistinguishable for all* n *and* m *when* $a = 8$*.*

i.e. $O(h^2)$ when $m = 1$, $O(h^4)$ when $m = 2, 3$ and $O(h^6)$ when $m = 4$. The orders are not exactly as predicted in (4.4.2) owing to two reasons: first, the imposed truncation m in $\epsilon_n^{(m)}$ and $\epsilon_n^{(m,F)}$ that respectively define the MCBEM error in (4.3.43) and FDMCBEM error in (4.3.45), and; second, the $O(h)$ pollution at the corners which, as demonstrated by the CBEM errors in Table 4.2.1, affects the overall accuracy of the numerical solution.

In addition, the results in Table 4.4.2 show the orders of the MCBEM and FDMCBEM errors are alternating between converging to the predicted value from above and below as m increases. The

m	$n, \alpha n$	ρ			p		
		Predicted	Exact	Approx	Predicted	Exact	Approx
1	$48, 72$	2.25	2.4346	2.4644	2	2.1945	2.2245
	$72, 108$	2.25	2.3412	2.3570	2	2.0980	2.1146
2	$48, 72$	5.0625	4.8884	4.8811	4	3.9137	3.9100
	$72, 108$	5.0625	4.9681	4.9599	4	3.9535	3.9495
3	$48, 72$	5.0625	5.3756	5.4735	4	4.1480	4.1925
	$72, 108$	5.0625	5.2416	5.2942	4	4.0857	4.1104
4	$48, 72$	11.3906	10.2861	10.8018	6	5.7484	5.8691
	$72, 108$	11.3906	10.7969	10.9647	6	5.8680	5.9060

Table 4.4.2: *The error convergence rate ρ and error order p in the MCBEM $\widetilde{\phi}_n^{(m)}$ (exact) and the FDMCBEM $\widetilde{\phi}_n^{(m,F)}$ (approximated) solution of the test BVP in Fig. 4.2.2, for eighth-order accuracy in the finite difference method, $\alpha = 1.5(= \beta)$ in* (4.2.48)*, $n = 48, 72, 108$ and $m = 1, 2, 3, 4$. The error orders in the MCBEM and FDMCBEM are approximately $O(h^2)$ for $m = 1$, $O(h^4)$ for $m = 2, 3$ and $O(h^6)$ behaviour for $m = 4$ as predicted in* (4.4.2)*.*

reason for such behaviour is due to the errors $\epsilon_n^{(m)}$ and $\epsilon_n^{(m,F)}$, which define the MCBEM error in (4.3.43) and the FDMCBEM error in (4.3.45), comprise the integrals $J_{k,j}$ in (4.2.29) and $K_{k,j}$ in (4.2.30) where $k = 1, \ldots, m$. Then (4.2.37) shows that we require only $m = 1$ to capture all of the $O(h^2)$ behaviour of the error in both the MCBEM and the FDMCBEM. The interesting case is $m = 2$ because we still expect $O(h^4)$ behaviour from the $m = 3$ term. This suggests that we have a incomplete representation of the $O(h^4)$ behaviour when $m = 2$, and in practise we get an under-specification. On the other hand, when $m = 3$ we get an over-specification of the $O(h^4)$ behaviour (consistent with the over-specification in Table 4.3.1) and this repeats in a period-two cycle in accordance with the period-two cycle implied by (4.2.37).

The $O(h^4)$ error in the MCBEM (and the FDMCBEM), which was recovered when $m = 2$ or $m = 3$, is equivalent to the order of the error for a piecewise-quadratic BEM. However, the modified methods are augmenting a piecewise-constant BEM, thus require only a n-dimensional collocation system, whereas a quadratic BEM would require a $2n$-dimensional collocation system.

n	RMSE ($\widetilde{\sigma}$)		
	CBEM	MCBEM	FDMCBEM
48	1.2001×10^{-03}	1.2476×10^{-11}	1.8043×10^{-11}
72	6.0309×10^{-04}	1.2129×10^{-12}	1.6704×10^{-12}

Table 4.4.3: *An overview of the RMSEs in the CBEM, the MCBEM and the FDMCBEM solution of the test BVP in Fig. 4.2.2 for* $\alpha = 1.5$ *in* (4.2.48)*,* $n = 48, 72$*,* $m = 4$ *and order of accuracy* $a = 8$ *in the finite-difference method. Evidently both modified methods are superior in accuracy over the standard CBEM for each value of* n*.*

In other words, we have emulated the behaviour of higher-order Lagrangian interpolation without increasing the size of the system, thereby achieving the aim of the modification.

In general, the order of the error in the MCBEM varies with m as

$$\begin{cases} O(h^{m+1}) & \text{if } m \text{ is odd,} \\ O(h^{m+2}) & \text{if } m \text{ is even,} \end{cases} \tag{4.4.5}$$

where m is chosen *a priori*, thus the error order can be enhanced beyond quadratic accuracy. The accuracy of the error in the FDMCBEM on the other hand, which must be taken to a higher degree if m is to be increased beyond $m = 4$, is restricted due to the accuracy in the finite-difference method.

Increasing m in the modified methods, however, results in an increase in the required CPU system time. For example, by comparison with the simplest case of $m = 1$, the MCBEM CPU system time increases by 22%, 47% and 71% by increasing m to $2, 3$ or 4 respectively. Similarly, by comparison with the simplest case of $m = 1$, the FDMCBEM CPU system time increases by 28%, 77% and 92% by increasing m to $2, 3$ or 4 respectively. Furthermore, by construction, the required FDMCBEM CPU system time will be greater than the MCBEM CPU system time as the FDMCBEM requires the derivation of the finite-difference molecules, e.g., an increase of 2% when $m = 4$ and eighth-order accuracy is imposed.

Essentially, for any m, the required CPU system time in the MCBEM (and FDMCBEM) is less than the required CPU system time for a standard BEM of an equivalent order of accuracy. For example, the time taken to invert a $n \times n$ matrix in the MCBEM and FDMCBEM, which are

of order $O(h^m)$, is $2n^3/3$. However, the time taken to invert a $(m/2)n \times (m/2)n$ matrix in a BEM using higher-order Lagrangian interpolation, which is also $O(h^m)$, is $2(mn)^3/24$. Therefore, because the modified methods require only the solution of a $n \times n$ system, they are computationally superior over the standard BEMs that are based on higher-order Lagrangian interpolation, e.g. the piecewise-quadratic BEM (Manzoor [1984]).

For the simplest case of $m = 1$ the CPU system time for the MCBEM is an increase from the CBEM time by 222% when $n = 48$, although this increase in CPU system time is justified by the higher order gained in the MCBEM over that in the CBEM. In practice, to obtain a solution of higher accuracy one usually increases the number of elements taken in a BEM. If we apply this principle to the CBEM, then only by taking $n = 164$ elements do we recover a RMSE of an equivalent order to that in MCBEM in the case when $m = 1$ and $n = 48$. However, as the MCBEM requires a substantially smaller number of elements, the CBEM will increase the CPU system time by 784% in order to match the accuracy in the new improved BEM, thus demonstrating that the MCBEM is the superior BEM for solving (and improving) the accuracy of regular BVPs.

4.5 Summary and discussion

In this chapter we have demonstrated the use of numerical methods to approximate the solution of a nonsingular two-dimensional harmonic boundary value problem. This involved implementing a piecewise-constant boundary element method, which was subsequently modified in a novel way, so that the order of the error in the numerical solution could be chosen *a priori*.

The modification was based on an in-depth analysis of the behaviour of the piecewise-constant boundary-element-method error, in which the unpredicted $O(h)$ error peaks occurring in at the corners of a domain were highlighted. The error peaks, which could be reduced by taking higher-order Lagrangian interpolation, are subsequently reduced by a modified method without increasing the size of the system.

For the test BVP considered, the error in the modified methods was shown to emulate the rate of convergence normally associated with piecewise-quadratic boundary element methods (Brebbia and Dominguez [1989], Manzoor [1984]) *without* the need to solve a larger system. In other words, the modified methods require only a n-point collocation unlike the piecewise-quadratic boundary element method that require a $2n$-point collocation; the corresponding smaller dense system requiring substantially less time to invert, and so making the modified methods computationally advantageous. Moreover, by construction of the modified methods, the order of the error in these methods can be further increased to emulate the order in Lagrangian interpolation of a degree higher than second-order, again without increasing the size of the system.

The modified methods demonstrated a significant reduction (up to eight orders of magnitude) in the error of the approximated solution in comparison to the standard piecewise-constant boundary element method. However, this reduction is achieved at a cost of an increase in the CPU system time of at least 222% upon that in the piecewise-constant boundary element method. On the other hand, in order to match the superior accuracy of the modified method, the piecewise-constant boundary element method would require a substantial increase in the number of elements thus increasing the CPU system time, e.g. a 784% increase in CPU time is required to match the accuracy of the modified method when $m = 1$ and $n = 48$.

Further investigations into the theory covered in this chapter involve finding improved estimates of the exact piecewise-constant boundary element method error ϵ_n in order to reduce the error in the

approximated $\bar{\epsilon}_n$ that defines the modified method. We proceed by utilising the theory outlined in chapter 4 to analyse the solution of singular harmonic boundary value problems in chapters 5 and 6.

Chapter 5

Pseudo-Analytic Solution of a Singular Harmonic Boundary Value Problem

Previously, in chapter 4 we considered improving the accuracy of the numerical solution of BVPs that contained no additional difficulties. Now, we consider problems with inherent difficulties, i.e. BVPs with the presence of a boundary singularity, otherwise known as singular BVPs.

Singular BVPs (SBVP), have attracted much attention (Whiteman and Papamichael [1971], Symm [1973], Jaswon and Symm [1977], Blue [1977], Crank and Furzeland [1978], Xanthis et al. [1981], Kelmanson [1984], Manzoor [1984], Mason et al. [1985], Aitchison and Karageorghis [1988], Atkinson and Chandler [1990], Hansen and Kelmanson [1994], Elliotis et al. [2002], Li et al. [2005], Elliotis et al. [2006], Helsing [2009], Xenophontos et al. [2010]): they arise in the mathematical modelling of many real-world problems drawn from applied maths, physics and engineering. Most commonly, the singularities are those arising from a sudden change in boundary conditions, e.g. changes in dielectric properties (Daly [1973]), or a sudden change in boundary geometry, e.g. in stress analysis in regions with cracks (Mason and Smith [1982]) and flow near sharp corners (Kelmanson [1983a]). SBVPs can generally not be solved explicitly, therefore numerical procedures are necessary.

To be able to quantify the accuracy of a given numerical procedure, one must be able to validate the approximate solution against either existing results or an analytic solution. In the present work, we consider the latter of these. That is, we present a method whereby we can derive the analytic

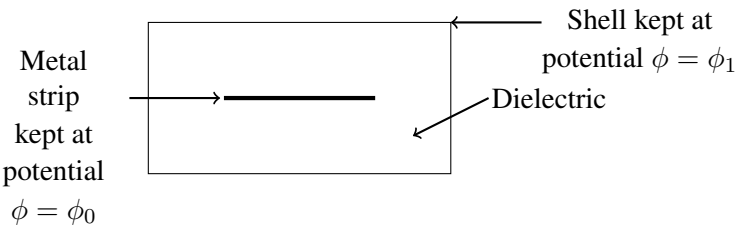

Figure 5.1.1: *Schematic diagram of the physical origin of the stripline problem.*

solution of a given singular BVP.

The remainder of this chapter is as follows. In §5.1 we present a singular harmonic BVP, considered in this and the proceeding chapter. In §5.2 we outline the conformal transformation method, by the analogy of Whiteman and Papamichael [1971] and Rosser and Papamichael [1975], for determining a pseudo-analytic solution. Finally, in §5.3 we determine a pseudo-analytic (series) solution of the singular harmonic BVP.

5.1 Singular harmonic boundary value problems

We consider BVPs with the presence of boundary singularities arising from a sudden change in boundary conditions, as these occur in the vast majority of problems where we have no control over the boundary conditions. An example of such a SBVP is seen in the analysis of transmission-line singularities (Daly [1973], Postoyalko [1986]), such as the stripline problem. The solution of the stripline problem is essential in electrical engineering owing to its many practical applications, particularly its use in electromagnetic compatibility testing due to its ability to reduce random fluctuations in electrical signals, i.e. noise. The physical stripline problem consists of a flat strip of conducting metal that is contained within insulating material (forming a dielectric), all of which is inside a grounded rectangular shell, as shown in Fig. 5.1.1.

The SBVP for the stripline (Ingham et al. [1981c], Postoyalko [1986]), summarised pictorially in Fig. 5.1.2, results from considering only the upper-right quadrant of the dually symmetric physical problem in Fig. 5.1.1. The stripline SBVP comprises solution of Laplace's equation, $\nabla^2\phi = 0$, for the electrostatic potential ϕ in a two-dimensional domain. Moreover, the stripline SBVP in Fig.

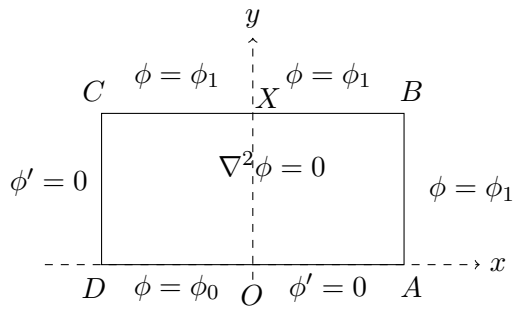

Figure 5.1.2: *A pictorial summary of the stripline singular boundary value problem.*

5.1.2 has a boundary singularity at O (the origin) due to a discontinuity between Neumann and Dirichlet boundary conditions either side of O.

The stripline problem is an adaptation of the classical SBVP, which is known as the Motz problem (Motz [1946]), presented in Fig. 5.1.3. The computation of approximate solutions of the Motz problem has invited extensive research into a variety of techniques, some pseudo-analytic and others numerical, e.g. Whiteman and Papamichael [1971, 1972], Papamichael and Symm [1975], Blue [1977], Crank and Furzeland [1978], Wigley [1988], Karageorghis et al. [1996], Li and Lu [2000], Hu [2003], Li et al. [2005] and, Li et al. [2006]. Utilising the near-identical geometrical resemblance between the Motz and stripline problem, the research techniques developed for the solution of the Motz problem can be extended to the stripline problem, subject to only minor adaptations. For example, in §5.2 the pseudo-analytic solution of the stripline problem will be derived using an adaptation of the conformal transformation method for the Motz problem.

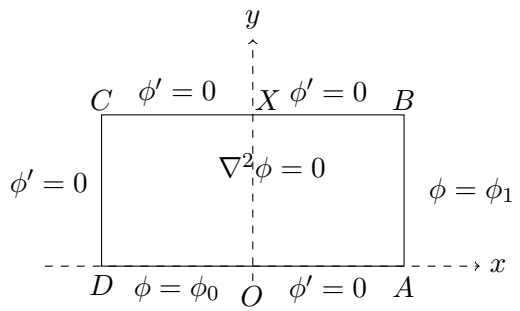

Figure 5.1.3: *A pictorial summary of the Motz singular boundary value problem.*

The analytical solution of the stripline (and Motz) problem is expressible as an explicit series obtained via separation of variables in polar coordinates (r, θ) centred at O in Fig. 5.1.3 and 5.1.2. For either the Motz or stripline problem, the boundary conditions on $\theta = 0$ and $\theta = \pi$ yield the harmonic potential for $(x, y) \in [ABCD]$

$$\phi(r, \theta) = \phi_0 + \sum_{i=1}^{\infty} a_i r^{i-\frac{1}{2}} \cos\left[\left(i - \frac{1}{2}\right)\theta\right], \tag{5.1.1}$$

where a_i are expansion coefficients yet to be determined. The validity of (5.1.1) holds throughout the entire domain (Rosser and Papamichael [1975]).

Several different approaches have been developed to approximate the unknown expansion coefficients a_i in (5.1.1), the conformal transformation method (Whiteman and Papamichael [1971]) being one of the original. Other methods include: the Trefftz method (Trefftz [1926], Lu et al. [2004]); the global element method (Hendry and Delves [1979], Kermode and McKerrell [1985]); the least squares method (Li et al. [1987]); the singular basis function method (Olson et al. [1991]); the block-grid method (Dosiyev [2005]); the boundary approximation method (Li et al. [2006]), and; the hybrid BEM (Pashos et al. [2010]). In order to obtain "near-exact" (Papamichael [1989], Arad et al. [1998], Hu [2003]) estimates of the coefficients a_i in (5.1.1), we employ the conformal transformation method (CTM), not least of which because it yields information that forms a baseline comparator against which we test the results of our numerical methods in the proceeding chapter.

5.2 The conformal transformation method (CTM)

The CTM is well-established and has been successfully applied to many types of boundary value problems, e.g. Whiteman and Papamichael [1971, 1972], Papamichael and Sideridis [1979] and Li and Lu [2000]. Because of the non-transparency of implementing the CTM, we take this opportunity to describe the steps of the CTM in some detail, particularly because some of the process has not yet been described in the literature.

The CTM is based on applying a sequence of conformal mappings, which preserves the angles in a domain, to transform a complex harmonic BVP into a harmonic BVP for which there

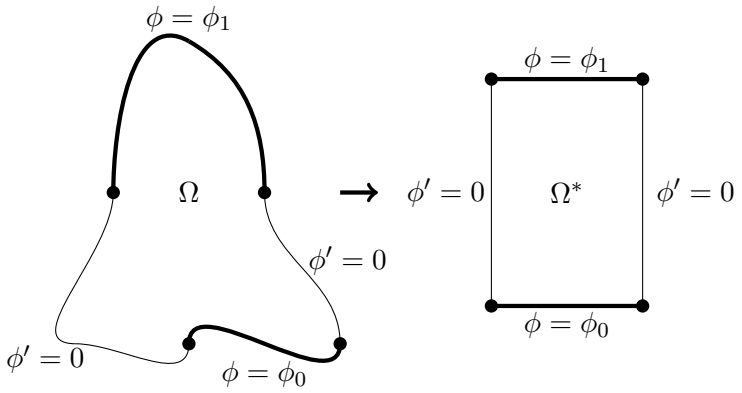

Figure 5.2.1: *The mapping of a generalised polygon in Ω, through a sequence of conformal transformations, to a quadrilateral Ω^* with a unique aspect ratio. The distribution of the Dirichlet and Neumann conditions along the boundary of the polygon in Ω must be split in a two-two fashion as shown. The heavy and thin lines denote boundary sub-arcs on which Dirichlet and Neumann conditions are respectively applied.*

exists a simple analytic solution. The CTM has been applied to many problems in mathematical physics, e.g. aerodynamics, hydrodynamics, electromagnetism, acoustics, and thermal equilibrium (Schinzinger and Laura [2003]). The application of the CTM, however, usually deals with solutions of Laplace's equation, as the harmonic function remains invariant under a CTM, i.e. the solution is still harmonic after being transformed by a conformal map.

We are particularly interested in the CTM, because of its use in transforming a SBVP with a mixture of Neumann and Dirichlet boundary conditions, to yield a final nonsingular BVP defined on a quadrilateral (Whiteman and Papamichael [1971]). For example, provided the boundary distributions ϕ and ϕ' are split in a two-two fashion, as shown in Fig. 5.2.1, the transformation is achieved through a sequence of conformal mappings. The boundary conditions in the final transformed domain (right-hand side of Fig. 5.2.1) occur in two sets of pairs on opposite faces, e.g. Dirichlet conditions on the north and south face and Neumann conditions on the east and west face. The (linear) solution in the final domain space, after inverting the sequence of transformations back to the original domain, defines the analytic solution of the SBVP.

We will illustrate the CTM by transforming a rectangular domain, consistent with the stripline

problem in Fig. 5.1.2, with discontinuous boundary data into a quadrilateral with continuous boundary data. To begin with, the generalised *Schwarz-Christoffel* mapping, used in the sequence of transformations, is outlined; this includes the definition of complete and incomplete elliptic functions of the second kind and the their inverses. Using the Schwarz-Christoffel mapping, the aim is to provide a schematic overview of the sequence of transformations in the CTM, specific for the stripline problem, thus determining the analytic solution (5.1.1).

5.2.1 Schwarz-Christoffel mapping: rectangular domains

The CTM comprises a sequence of Schwarz-Christoffel mappings (SCM). The SCM is used to map vertices in a upper-half plane to the corners of a polygon in a complex domain. Let Ω be the region in the complex plane bounded by a polygon P with vertices $w_1, w_2, \ldots, w_n$, given in a counter-clockwise order, and interior angles $a_1\pi, a_2\pi, \ldots, a_n\pi$. Assuming Ω is bounded and without any cusps or slits, i.e. $\alpha_j \in (0, 2)$ for each j, then f denotes the conformal map of the upper-half plane, Ω^* say, onto Ω with k^{th} *prevertex* $z_j = f^{-1}(w_j)$. If the n distinct points z_j in the real axis are such that $|z_j| < \infty$ for all j, then the Schwarz-Christoffel mapping is given by the formula (Driscoll and Trefethen [2002][1])

$$w = f(z) = c_1 \int_{z_0}^{z} \prod_{j=1}^{n} (\zeta - z_j)^{(a_j - 1)} d\zeta + c_2, \tag{5.2.1}$$

where z_0 is a fixed lower limit, c_1 and c_2 are constants and $w_j = f(z_j)$ for $j = 1, \ldots, n$.
As we are concerned with the simple case of a rectangular polygon (to match with the stripline problem), with length $2a$ and height b, the Schwarz-Christoffel mapping is as follows. Taking $n = 4$ in (5.2.1), by Copson [1946], Nehari [1952] and Bowman [1953], the Schwarz-Christoffel prevertices are $z_1 = (1, 0), z_2 = (1/k, 0), z_3 = (-1/k, 0)$ and $z_4 = (-1, 0)$, where the parameter k is the *elliptic modulus* satisfying $0 < k^2 < 1$. Moreover, we have $a_j = 1/2$ for all $j = 1, \ldots, n$, so that the Schwarz-Christoffel function $f(z)$ in (5.2.1) maps z_1, z_2, z_3 and z_4 in the complex $z \equiv u + iv$ upper half-plane to the corners of a rectangle w_1, w_2, w_3 and w_4 in the complex plane, $w \equiv x + iy$, as depicted in Fig. 5.2.2.

[1]The reference by Driscoll and Trefethen [2002] is given in preference to earlier/classic work on the Schwarz-Christoffel method because of the level of detail presented.

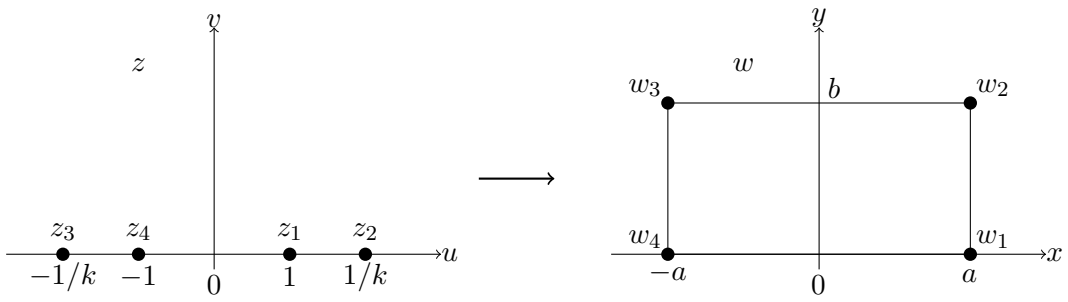

Figure 5.2.2: *A Schwarz-Christoffel mapping* $w_j = f(z_j)$ *from* $z = u + iv$ *upper half-plane to complex plane* $w = x + iy$ *when* $n = 4$ *in* (5.2.1). *Here* k *the elliptic modulus, representing the degrees of freedom in the prevertices* $\{z_j\}$.

Eqn. (5.2.1) may be written as an *elliptic integral of the first kind*[2]:

$$\begin{aligned} w = f(z) &= c_1 \int_0^z \prod_{j=1}^{4} (\zeta - z_j)^{(a_j - 1)} d\zeta + c_2, \\ &= c \int_0^z \frac{1}{[(1-\zeta^2)(1-k^2\zeta^2)]^{\frac{1}{2}}} d\zeta, \\ &= F(z,k) \end{aligned} \tag{5.2.2}$$

where $c = kc_1$ and $c_2 = 0$ (since the origin is mapped to itself). By (5.2.2), each vertex $\{w_j\}$ in the rectangle in the w-plane on the right-hand side of Fig. 5.2.2 is related to $\{z_j\}$ in the z-plane by

$$a + i0 = c \int_0^1 \frac{1}{[(1-\zeta^2)(1-k^2\zeta^2)]^{\frac{1}{2}}} d\zeta, \tag{5.2.3}$$

$$a + ib = c \int_0^{1/k} \frac{1}{[(1-\zeta^2)(1-k^2\zeta^2)]^{\frac{1}{2}}} d\zeta, \tag{5.2.4}$$

$$-a + ib = c \int_0^{-1/k} \frac{1}{[(1-\zeta^2)(1-k^2\zeta^2)]^{\frac{1}{2}}} d\zeta, \tag{5.2.5}$$

$$-a + i0 = c \int_0^{-1} \frac{1}{[(1-\zeta^2)(1-k^2\zeta^2)]^{\frac{1}{2}}} d\zeta. \tag{5.2.6}$$

Substituting $\zeta = -\widehat{\zeta}$ in (5.2.6) results in (5.2.3) and, by subtracting (5.2.3) from (5.2.4), the height of the rectangle b satisfies

$$b = c \int_1^{1/k} \frac{1}{[(\zeta^2-1)(1-k^2\zeta^2)]^{\frac{1}{2}}} d\zeta \tag{5.2.7}$$

[2]Sometimes m is used in place of the elliptic modulus k where $m = k^2$ (Abramowitz and Stegun [1972]).

which, by the substitution $\zeta = 1/(1-k_1^2x^2)^{\frac{1}{2}}$, where $k_1^2 + k^2 = 1$, (5.2.7) becomes

$$b = c\int_0^1 \frac{1}{\left[(1-x^2)(1-k_1^2x^2)\right]^{\frac{1}{2}}}dx. \tag{5.2.8}$$

The *complete elliptic function of the first kind* (Abramowitz and Stegun [1972]) is

$$K(k) = F(1,k) \equiv \int_0^1 \frac{1}{[(1-\zeta^2)(1-k^2\zeta^2)]^{\frac{1}{2}}}d\zeta, \tag{5.2.9}$$

where, by (5.2.3) and (5.2.8),

$$a = cK(k), \quad b = cK(\sqrt{1-k^2}), \tag{5.2.10}$$

so that

$$\frac{a}{b} = \frac{K(k)}{K(\sqrt{1-k^2})}, \tag{5.2.11}$$

which defines the value of the elliptic modulus k for known dimensions a and b.

When $c = 1$ in the integral (5.2.2), i.e.

$$F(z,k) = \int_0^z \frac{1}{[(1-\zeta^2)(1-k^2\zeta^2)]^{\frac{1}{2}}}d\zeta, \tag{5.2.12}$$

$F(z,k)$ is a *incomplete elliptic function of the first kind* which, when k is fixed, gives a one-to-one relation between the complex z-plane and its mapped w-plane (the geometry of the rectangle).

Introducing the parameter $m = k^2$, the incomplete elliptic function (5.2.12) can be equivalently denoted by

$$F(\sin\phi, m) = F(\phi|m) = \int_0^\phi \frac{1}{\left(1-m\sin^2\theta\right)^{\frac{1}{2}}}d\theta, \tag{5.2.13}$$

where $\phi \equiv \arcsin z$ corresponds to the *amplitude* (Rosser and Papamichael [1975]). In defining F in (5.2.13), we have used the comma to imply that the argument preceding it is the sine of the amplitude and the vertical line to imply the proceeding argument is the amplitude itself: this notation is consistent with Abramowitz and Stegun [1972]. The elliptic function (5.2.13) is said to be *complete* when the amplitude ϕ is $\pi/2$, i.e. $K(m) = F\left(\frac{\pi}{2}|m\right) = F(1,k)$.

We define the complementary parameter m' by

$$m' \equiv 1 - m, \tag{5.2.14}$$

whence the complete elliptic integral (5.2.9) is

$$K(m') = K'(m) \equiv \int_0^{\pi/2} \frac{1}{\left(1 - m' \sin^2\theta\right)^{\frac{1}{2}}} d\theta. \tag{5.2.15}$$

Eqns. (5.2.9) and (5.2.15) are used to define the *nome* and the *complementary nome* respectively by

$$q(m) \equiv \exp(-\pi K'(m)/K(m)), \tag{5.2.16}$$

$$q'(m) = \ q(m') \equiv \exp(-\pi K(m)/K'(m)), \tag{5.2.17}$$

as well as the supplementary functions

$$R(q) = \frac{2\pi}{K\sqrt{m}}, \tag{5.2.18}$$

$$R'(q) = \ R(q') = \frac{2\pi}{K'\sqrt{m'}}. \tag{5.2.19}$$

Note, (5.2.15)-(5.2.19) are consistent with Rosser and Papamichael [1975], whereby the prime does not denote a differential, but rather the dependence of a function upon the complementary parameter m'. Observing that $K(m)$ is a increasing function in (5.2.9) and, conversely, that $K'(m)$ is a decreasing function in (5.2.15) then, by construction of the nomes (5.2.16) and (5.2.17), $q(m)$ is a increasing function of m, whereas $q'(m)$ is a decreasing function of m.

Since the stripline problem is defined on a rectangular domain, we require the inverse of the Schwarz-Christoffel function in order to map the rectangle onto the complex line, i.e.

$$\phi = F^{-1}(w|m) \equiv \mathrm{sn}(w, m), \tag{5.2.20}$$

where sn is the Jacobi elliptic sine function. The Jacobi elliptic sine function (5.2.20) can be expressed in the series form (Abramowitz and Stegun [1972]) as

$$\mathrm{sn}(v, m) = \frac{2\pi}{K(m)\sqrt{m}} \sum_{n=0}^{\infty} \frac{q^{n+\frac{1}{2}}}{1 - q^{2n+1}} \sin(2n+1)\left(\frac{\pi v}{2K(m)}\right), \tag{5.2.21}$$

where q is defined in (5.2.16). By using (5.2.18) and $\sin(x) = \sum_{n=0}^{\infty}(-1)^n(x^{2n+1}/(2n+1)!)$, (5.2.21) yields

$$\begin{aligned}\mathrm{sn}(v,m) &= \frac{2\pi}{K\sqrt{m}}\sum_{r=0}^{\infty}\frac{(-1)^r}{(2r+1)!}\sum_{n=0}^{\infty}\frac{q^{n+\frac{1}{2}}(2n+1)^{2r+1}}{1-q^{2n+1}}\left(\frac{\pi v}{2K}\right)^{2r+1}\\ &= \frac{2\pi}{K\sqrt{m}}\sum_{r=0}^{\infty}A_r(q)\left(\frac{\pi v}{2K}\right)^{2r+1}\\ &= R(q)\sum_{r=0}^{\infty}A_r(q)\left(\frac{\pi v}{2K}\right)^{2r+1}, \end{aligned} \tag{5.2.22}$$

where

$$A_r(q) = \frac{(-1)^r}{(2r+1)!}\sum_{n=0}^{\infty}\frac{q^{n+\frac{1}{2}}(2n+1)^{2r+1}}{1-q^{2n+1}}. \tag{5.2.23}$$

Series (5.2.23) of the Jacobian elliptic sine function is essential in the following implementation of the CTM.

5.2.2 The sequence of transformations in the CTM

Whiteman and Papamichael [1971] first used the CTM to reduce, by a sequence of transformations, a complicated harmonic BVP into a simpler harmonic BVP whose solution could be deduced by inspection. The explicit solution of the simpler harmonic BVP, however, transpires to be in terms of elliptic functions (and their inverses) that, in practice, require numerical evaluation. Consequently, we derive a "near-exact" solution in the CTM in the sense that the solution is restricted by only machine precision.

Both the Motz and the stripline problem are specific cases of general harmonic BVPs that are amenable to the CTM (Whiteman and Papamichael [1972]), the general form of which is

$$\begin{cases} \nabla^2\phi = 0, & \text{in } \Omega,\\ \phi & \text{known on } \Gamma_1, \Gamma_3,\\ \phi' & \text{known on } \Gamma_2, \Gamma_4, \end{cases} \tag{5.2.24}$$

where Ω is a simply connected open domain with closed boundary $\partial\Omega \equiv \cup_{i=1}^{4}\Gamma_i$ in which Γ_1 is the adjacent sub-arc of Γ_2, Γ_2 is the adjacent sub-arc of Γ_3, Γ_3 is the adjacent sub-arc of Γ_4 and Γ_4 is the adjacent sub-arc of Γ_1. That is, the Dirichlet and Neumann boundary conditions on the

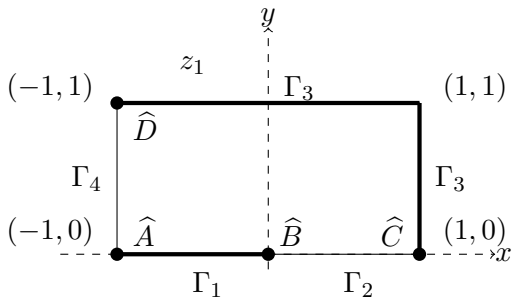

Figure 5.2.3: *The z_1-plane for the stripline SBVP in Fig. 5.1.2. The heavy and thin lines denote boundary sub-arcs on which Dirichlet and Neumann conditions are respectively applied.*

polygonal boundary are split in a two-two fashion, in accordance with Fig. 5.2.1. Specifically, for the stripline problem of Fig. 5.1.2, the Dirichlet and Neumann boundary sub-arcs are shown in Fig. 5.2.3.

The idea behind the CTM is to apply a succession of four transformations, T_1, T_2, T_3 and T_4 say, which include the Schwarz-Christoffel mapping (see §5.2.1), to transform an original SBVP in the $z_1 \equiv x + iy$ plane onto a nonsingular harmonic BVP with solution $\overline{\phi}$ in the $z_5 \equiv \xi + i\eta$ plane where if $z_5 = (\xi, \eta) \in \Omega^*$ then

$$\nabla^2 \overline{\phi} = 0, \quad \text{in } \Omega^*. \tag{5.2.25}$$

The composite transformation $T = T_4 \circ T_3 \circ T_2 \circ T_1$ is constructed so that, in the z_5-plane, (5.2.25) has an *exact* (linear in ξ or η) solution. Hence defining a the solution of the Motz and the stripline problem, $\phi(p) = \overline{\phi}(p')$, where $p \xrightarrow{T} p'$, $p \in \Omega$ and $p' \in \Omega^*$. Thus the goal is to determine the (sequence of) conformal mappings T that transform the original BVP into (5.2.25).

The conformal mappings in T that transform the original BVP into (5.2.25) have already been defined for the Motz problem (Whiteman and Papamichael [1971, 1972], Li and Lu [2000]), therefore in this thesis we outline the conformal mappings for the stripline problem so that they are readily available for others to use. In Fig. 5.2.3 each point of the rectangular domain of the stripline SBVP (Fig. 5.1.2) in the (x, y)-plane is a complex number $z_1 = x + iy$. In particular, the points $\widehat{A}$, $\widehat{B}$, $\widehat{C}$ and $\widehat{D}$ in Fig. 5.2.3, located where there is a change in boundary conditions, are $-1, 0, 1$ and $-1 + i$. The boundary conditions in Fig. 5.2.3 are a zero normal derivative on the line segment from $\widehat{D}$ to $\widehat{A}$ and from $\widehat{B}$ to $\widehat{C}$, value ϕ_0 on the line segment from $\widehat{A}$ to $\widehat{B}$, and the value

of ϕ_1 on the line segment from $\widehat{C}$ around to $\widehat{D}$ along the right and top side of the rectangle.
The mapping of the rectangular domain of the stripline problem onto an upper half-plane is achieved using the theory of the Schwarz-Christoffel mapping in §5.2.1. Here we first take

$$k = \frac{1}{\sqrt{2}}, \tag{5.2.26}$$

i.e. $a = b = 1$ in (5.2.11): then, because $m = k^2$, we have $m = \frac{1}{2}$, for which value, (5.2.14) yields $m' = m$ and, by (5.2.9) and (5.2.15),

$$K(m) = K'(m). \tag{5.2.27}$$

Therefore, (5.2.16) implies

$$q(m) = q'(m) = \exp(-\pi). \tag{5.2.28}$$

Through (5.2.10), Eqn. (5.2.26) also implies that $c = 1/K(k)$ and so, by (5.2.2), we have

$$\begin{aligned} z_1 &= \frac{1}{K(k)} \int_0^{z_2} \frac{1}{[(1-\zeta^2)(1-k^2\zeta^2)]^{\frac{1}{2}}} d\zeta \\ &= \frac{1}{K(k)} F(z_2, k). \end{aligned} \tag{5.2.29}$$

Thus the inverse of (5.2.29) defines the first transformation in the sequence, T_1, from z_1 to the upper-half plane z_2 shown in Fig. 5.2.4, in which the points $\widehat{A}$, $\widehat{B}$, $\widehat{C}$ and $\widehat{D}$ on the rectangle map to points $\widehat{A}' = -1$, $\widehat{B}' = 0$, $\widehat{C}' = 1$ and $\widehat{D}' = -\sqrt{2}$. Note, the red arrows in the right-hand diagram in Fig. 5.2.4 denote the connection of the Dirichlet conditions at infinity in the transformed domain that correspond to the same physical connection of the Dirichlet conditions in the original domain in the left-hand diagram. That is, even though the boundary along the top of the rectangle and the right-hand side of the rectangle share the same boundary condition type property, they do not share the same geometric property, thus the transformed plane (right-hand diagram in Fig. 5.2.4) is a manifestation of this disjointness.
By definition of the Jacobian elliptic sine function (5.2.20), the transformation $T_1 : z_1 \to z_2$ in the CTM is

$$z_2 = \text{sn}(Kz_1, m). \tag{5.2.30}$$

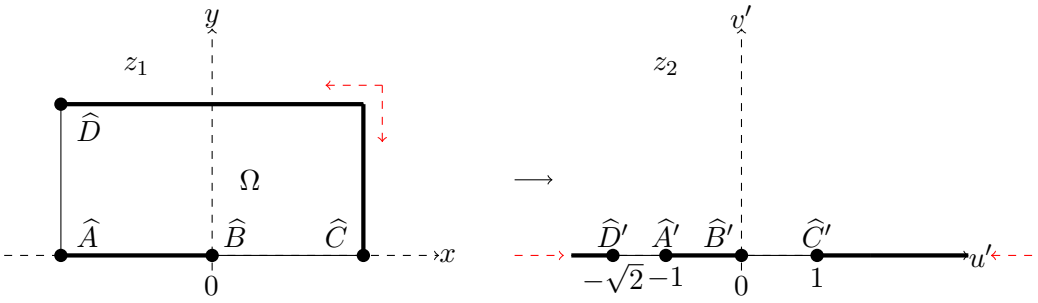

Figure 5.2.4: *Schematic representation of the transformation $T_1 : z_1 \to z_2$ from the full complex plane $z_1 = x + iy$ to the upper half-plane z_2. The heavy lines represent Dirichlet boundary conditions otherwise they are Neumann. The points $\widehat{A}$,$\widehat{B}$,$\widehat{C}$ and $\widehat{D}$ map to points $\widehat{A}'$, $\widehat{B}'$, $\widehat{C}'$ and $\widehat{D}'$ by the inverse of a Schwarz-Christoffel mapping (Fig. 5.2.2), e.g. $\widehat{A}' = f^{-1}(\widehat{A})$. That is, the five different sections of the original quadrilateral in the left-hand figure are mapped into five different sections on the real line in the upper half-plane in the right-hand figure. The red arrows in the right-hand diagram in Fig. 5.2.4 denote the connection of the Dirichlet conditions at infinity in the transformed domain that correspond to the same physical connection of the Dirichlet conditions in the original domain in the left-hand diagram.*

The next step in the CTM is bilinear transformation $T_2 : z_2 \to z_3$ that transforms the upper-half plane in z_2 onto the upper half-plane z_3, shown in Fig. 5.2.5. The bilinear transformation for the stripline SBVP is (Whiteman and Papamichael [1971])

$$z_3 = \frac{2z_2}{1 + z_2}, \tag{5.2.31}$$

in which the points $\widehat{A}'$, $\widehat{B}'$, $\widehat{C}'$ and $\widehat{D}'$ in the z_2-plane map to points $\widehat{A}'' = -\infty$, $\widehat{B}'' = 0$, $\widehat{C}'' = 1$ and $\widehat{D}'' = 4/(2 - \sqrt{2})$ in the z_3-plane.

The third transformation $T_3 : z_3 \to z_4$ in the CTM, fixed for any BVP, is

$$z_4 = \sqrt{z_3}, \tag{5.2.32}$$

which corresponds to a mapping from the upper half-plane z_3 onto the first quadrant in the z_4-plane, shown in Fig. 5.2.6. The points $\widehat{A}''$, $\widehat{B}''$, $\widehat{C}''$ and $\widehat{D}''$ in the z_3-plane map to points $\widehat{A}''' = \infty i$, $\widehat{B}''' = 0$, $\widehat{C}''' = 1$ and $\widehat{D}''' = \sqrt{4/(2 - \sqrt{2})}$ in the z_4-plane.

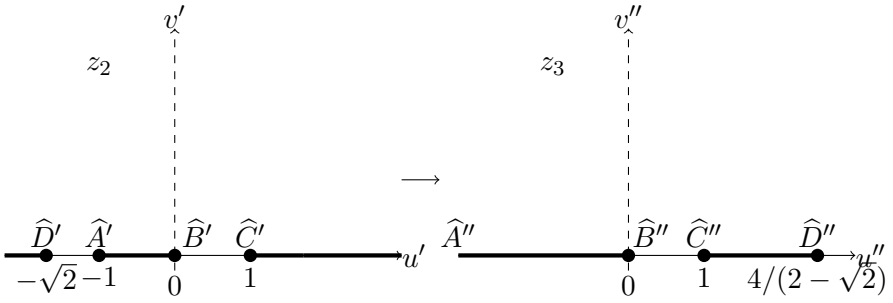

Figure 5.2.5: *Schematic representation of the transform $T_2 : z_2 \to z_3$ from the upper half-plane z_2 to the upper half-plane z_3 by bilinear transformation* (5.2.31)*. The heavy lines represent Dirichlet boundary conditions otherwise they are Neumann. Transform T_2 maps the five different sections on the real line in the upper-half plane in the left-hand figure into only four sections on the real line in the upper-half plane in the right-hand figure.*

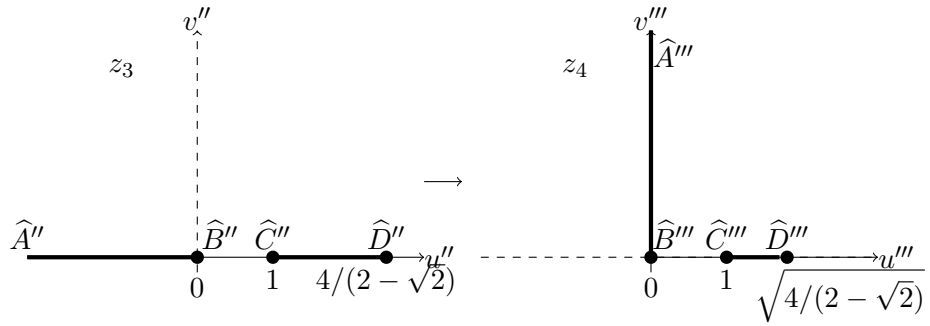

Figure 5.2.6: *Schematic representation of the transform $T_3 : z_3 \to z_4$ from the upper half-plane z_3 onto the first quadrant in the z_4-plane by* (5.2.32)*. The heavy lines represent Dirichlet boundary conditions otherwise they are Neumann. Transform T_3 is the beginning of "folding" the four sections into the closed final domain.*

We now take a new variable, $\overline{m}$ say, defined explicitly by the bilinear transformation (5.2.31) as

$$\overline{m} = \frac{(2-\sqrt{2})}{4}. \tag{5.2.33}$$

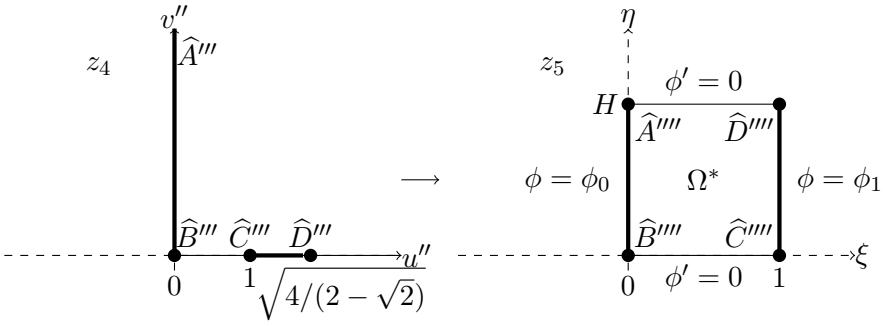

Figure 5.2.7: *Schematic representation of the transform $T_4 : z_4 \to z_5$ from the first quadrant z_4 onto the rectangle in the z_5-plane by* (5.2.34)*. The boundary conditions on the quadrilateral are defined in* (5.2.38) *and its H is defined in* (5.2.39)*. The heavy lines represent Dirichlet boundary conditions otherwise they are Neumann. Transform T_4 is the final "folding" to give a regular BVP and an immediate recognition that the closed final domain admits an analytic harmonic-solution that is linear in ξ.*

From (5.2.15) and (5.2.29), we have

$$\begin{aligned} z_5 &= \frac{1}{K(\overline{m})} \int_0^{z_4} \frac{1}{[(1-\zeta^2)(1-\overline{m}\zeta^2)]^{\frac{1}{2}}}\, d\zeta \\ &= \frac{1}{K(\overline{m})} F(z_4, \overline{m}) \\ &= \frac{1}{K} \mathrm{sn}^{-1}(z_4, \overline{m}), \end{aligned} \tag{5.2.34}$$

where

$$\overline{K} = K(\overline{m}). \tag{5.2.35}$$

The last transformation $T_4 : z_4 \to z_5$ in the CTM, shown in Fig. 5.2.7, maps the first quadrant z_4 into a rectangle in the z_5-plane. The rectangle of the z_5-plane has corners at $0, 1, i(\overline{K}'/\overline{K})$ and $1 + i(\overline{K}'/\overline{K})$ where, analogously with (5.2.35),

$$\overline{K}' = K'(\overline{m}). \tag{5.2.36}$$

The points $\widehat{A}'''$, $\widehat{B}'''$, $\widehat{C}'''$ and $\widehat{D}'''$ in the z_4-plane maps to points $\widehat{A}'''' = i(\overline{K}'/\overline{K})$, $\widehat{B}'''' = 0$, $\widehat{C}'''' = 1$ and $\widehat{D}'''' = 1 + i(\overline{K}'/\overline{K})$ in the z_5-plane.

By the sequence of composite transformations $\{T_i\}_{i=1}^4$ the original domain $z_1 = (x, y) \in \Omega$ has

Name of transformation	Action of transformation	Initial domain	Final domain
T_1	$z_1 \to z_2$	Quadrilateral in a full complex plane	Complex line on a upper half-plane
T_2	$z_2 \to z_3$	Complex line on a upper half-plane	Complex line on a upper half-plane
T_3	$z_3 \to z_4$	Complex line on a upper half-plane	First quadrant in a complex plane
T_4	$z_4 \to z_5$	First quadrant in a complex plane	Quadrilateral in the first quadrant of a complex plane

Table 5.2.1: *Summary of composite transformations* $\{T_i\}_{i=1}^4$ *in the CTM.*

been mapped onto a new closed domain $z_5 = (\xi, \eta) \in \Omega^*$, in which the transformed BVP has an exact solution $\overline{\phi}(p)$. In Ω^* the stripline problem satisfies the PDE

$$\nabla^2 \overline{\phi} = 0 \quad 0 < \xi < 1, 0 < \eta < H, \tag{5.2.37}$$

subject to the boundary conditions

$$\begin{aligned} \overline{\phi}(0, \eta) &= \phi_0, \\ \overline{\phi}(1, \eta) &= \phi_1, \\ \overline{\phi}'(\xi, 0) = \overline{\phi}'(\xi, H) &= 0, \end{aligned} \tag{5.2.38}$$

in which H is the height of the rectangle (see Fig. 5.2.7) defined by

$$H = \frac{K(\sqrt{1 - \overline{m}^2})}{K(\overline{m})}. \tag{5.2.39}$$

The *nonsingular* BVP (5.2.37) and (5.2.38) in Ω^* (there are now no discontinuous boundary conditions) has the general solution

$$\overline{\phi}(\xi, \eta) = \overline{\phi}(\xi) = (\phi_1 - \phi_0)\xi + \phi_0, \tag{5.2.40}$$

which is symmetrical about the line $\eta = H/2$ over domain Ω^*.

	z_1	z_2	z_3	z_4	z_5
$\widehat{A}$	$(-1,0)$	$(-1,0)$	$(-\infty,0)$	$(0,\infty)$	$(0,H)$
$\widehat{B}$	$(0,0)$	$(0,0)$	$(0,0)$	$(0,0)$	$(0,0)$
$\widehat{C}$	$(1,0)$	$(1,0)$	$(1,0)$	$(1,0)$	$(1,0)$
$\widehat{D}$	$(-1,1)$	$(-\sqrt{2},0)$	$(2\sqrt{2}/(\sqrt{2}-1),0)$	$((2\sqrt{2}/(\sqrt{2}-1)^{\frac{1}{2}},0)$	$(1,H)$

Table 5.2.2: *Composite transformations* $\{T_i\}_{i=1}^4$ *of the vertices* $(x,y) \in \Omega$ *in the* z_1*-plane onto* $(\xi,\eta) \in \Omega^*$ *in the* z_5*-plane for the stripline SBVP where* H *is defined in* (5.2.39)*.*

Although the outlined CTM theory corresponds to the stripline problem, Li and Lu [2000] showed it can be applied to the Motz problem, subject to adaptations of the composite transformations $\{T_i\}_{i=1}^4$.

5.2.3 Power-series solution of the CTM

In order to connect the final solution in the simplified domain $z_5 = (\xi,\eta)$ with the original solution in domain $z_1 = (x,y)$, it is necessary to determine z_5, z_4, z_3, z_2 and z_1 as power series. To this end, we proceed to determine $\{z_i\}_{i=2}^5$ as power series in z_1 by the method of Rosser and Papamichael [1975]. However, the corresponding solution $\phi(z_1)$ will be referred to as the "near-exact" solution: although this is an analytic solution, it is referred to as near-exact in the sense that some of the infinite-power series will need to be truncated, and also, because of its restriction by the degree of precision in the computer.

Introduced by Rosser and Papamichael [1975], the exact details of the power-series CTM solution of a harmonic BVP are now difficult to obtain[1]. We aim to bring this method back into the light in a form that is more detailed than the original, so that it can be used in related problems to generate quasi-analytic solutions against which the results of numerical methods can be validated.

The power-series method is based on the harmonic series solution of the stripline problem (Fig. 5.2.3), namely

$$\phi(z_1) = \phi_0 + \sum_{i=0}^{\infty} a_i z_1^{i+\frac{1}{2}}, \tag{5.2.41}$$

[1]The author obtained a hard copy of Professor Papamichael's rare paper directly through private communication

where $z_1 = x + iy$. By taking the real part of both sides of (5.2.41), we obtain

$$\phi(r\cos\theta, r\sin\theta) = \phi_0 + \sum_{i=0}^{\infty} a_i r^{i+\frac{1}{2}} \cos\left(i + \frac{1}{2}\right)\theta, \tag{5.2.42}$$

in which the object of the exercise is to determine the coefficients a_i as accurately as possible.
In order to calculate the coefficients a_i we introduce the series $F(x)$ defined by

$$F(x) \equiv \sum_{n=1}^{\infty} F_n x^n, \tag{5.2.43}$$

whose j^{th} power defines the coefficients $F_n^{(j)}$ of x^{n+j-1} in $(F(x))^j$. That is,

$$(F(x))^j = \sum_{n=1}^{\infty} F_n^{(j)} x^{n+j-1}. \tag{5.2.44}$$

By comparing powers of x in (5.2.44), (5.2.43) gives

$$F_n^{(1)} = F_n \tag{5.2.45}$$

and

$$F_n^{(j+1)} = \sum_{r=1}^{n} F_r F_{n+1-r}^{(j)}. \tag{5.2.46}$$

Hence, provided F_n is known for $1 \le n \le N$, $F_n^{(j)}$ can be calculated for all j and $1 \le n \le N$.
If only the values for $F_n^{(J)}$ are required for $1 \le n \le N$, one can derive them without finding $F_n^{(j)}$ for $1 \le j \le J$ (Rosser and Papamichael [1975], Nijenhuis and Wilf [1975]). Taking the logarithm of both sides of (5.2.44) yields

$$J \log F(x) = \log \sum_{n=1}^{\infty} F_n^{(J)} x^{n+J-1} \tag{5.2.47}$$

which, after differentiating and rearranging, gives

$$J \log \sum_{n=1}^{\infty} F_n^{(J)} x^{n+J-1} \sum_{k=1}^{\infty} k F_k x^{k-1} = \sum_{n=1}^{\infty} (n + J - 1) F_n^{(J)} x^{n+J-2} \sum_{k=1}^{\infty} F_k x^k. \tag{5.2.48}$$

Equating the coefficients of x^{M+J} on both sides of (5.2.48) gives

$$J \log \sum_{n=1}^{M+1} F_n^{(J)} (M + 2 - n) F_{M+2-n} = \sum_{n=1}^{M+1} (n + J - 1) F_n^{(J)} F_{M+2-n}, \tag{5.2.49}$$

hence, for $M \geq 1$,

$$MF_{M+1}^{(J)}F_1 = \sum_{n=1}^{M}(J(M+1-n)-n+1)F_n^{(J)}F_{M+2-n}. \tag{5.2.50}$$

If $F_1 \neq 0$ then (5.2.50) defines $F_n^{(J)}$, beginning with

$$F_1^{(J)} = (F_1)^J. \tag{5.2.51}$$

Now, referring back to (5.2.41), let

$$G_i = a_{i-1}, \quad i \geq 1, \tag{5.2.52}$$

so that

$$\phi(z_1)z_1^{\frac{1}{2}} = \sum_{i=1}^{\infty} G_i z_1^i \tag{5.2.53}$$

from which, by (5.2.43), the j^{th} power satisfies

$$\begin{aligned}(\phi(z_1))^j &= \sum_{i=1}^{\infty} {G_i}^{(j)} {z_1}^{i-1+j} {z_1}^{-\frac{j}{2}} \\ &= \sum_{i=1}^{\infty} {G_i}^{(j)} {z_1}^{i-1+\frac{j}{2}},\end{aligned} \tag{5.2.54}$$

where ${G_i}^{(j)}$ is defined analogously to $F_i^{(j)}$ in (5.2.46).

In order to match the power-series solution (5.2.53) with the CTM solution $\overline{\phi}$ in (5.2.40), we must express the transformations $\{T_i\}_{i=1}^4$ in power-series form. The first of these transformations T_1 in (5.2.30), by sine series (5.2.22), can be expressed as

$$\begin{aligned}z_2 &= \text{sn}(Kz_1, m) \\ &= R(q)\sum_{r=0}^{\infty} A_r(q)\left(\frac{\pi z_1}{2K}\right)^{2r+1} \\ &= \sum_{n=0}^{\infty} C_n {z_1}^{2n+1},\end{aligned} \tag{5.2.55}$$

where the coefficients C_n are determined by the explicit definition of $A_r(q)$ in (5.2.23). By T_2 in (5.2.31), we have

$$z_3 = \frac{2\sum_{n=0}^{\infty} C_n {z_1}^{2n+1}}{1+\sum_{n=0}^{\infty} C_n {z_1}^{2n+1}} = \sum_{n=0}^{\infty} B_n {z_1}^{n+1}, \tag{5.2.56}$$

where the coefficients B_n are determined from C_n. Then, by T_3 in (5.2.32),

$$z_4 = z_1^{\frac{1}{2}} \left(\sum_{n=0}^{\infty} B_n {z_1}^n \right)^{\frac{1}{2}}, \tag{5.2.57}$$

in which the coefficients B_n are those in the power series

$$B(z_1) = \sum_{n=0}^{\infty} B_n z_1^n, \quad B_0 \neq 0, \tag{5.2.58}$$

so that, because of (5.2.43), $F(z_1)$ and $B(z_1)$ are related by

$$B(z_1) = B_0(1 + F(z_1)), \tag{5.2.59}$$

so that $F_n = B_n/B_0$ for $n \geq 1$.

By construction of z_4 in (5.2.57) the series expansion of $[B(z_1)]^{\frac{1}{J}}$ is required for $J \geq 1$ where, by (5.2.59),

$$[B(z_1)]^{\frac{1}{J}} = B_0^{\frac{1}{J}} (1 + F(z_1))^{\frac{1}{J}}, \tag{5.2.60}$$

and hence a new series, with coefficients D_n, is introduced that satisfies

$$\left(1 + \sum_{n=1}^{\infty} D_n z_1^n \right) = (1 + F(z_1))^{\frac{1}{J}}. \tag{5.2.61}$$

Following (5.2.47)-(5.2.50), we take the logarithm of (5.2.61)

$$\log \left(1 + \sum_{n=1}^{\infty} D_n z_1^n \right) = \frac{1}{J} \log \left(1 + \sum_{k=1}^{\infty} F_k z_1^k \right), \tag{5.2.62}$$

then differentiate (5.2.62) with respect to z_1 and clear all fractions to obtain

$$J \sum_{n=1}^{\infty} n D_n z_1^{n-1} \left(1 + \sum_{k=1}^{\infty} F_k z_1^k \right) = \sum_{k=1}^{\infty} k F_k z_1^{k-1} \left(1 + \sum_{n=1}^{\infty} D_n z_1^n \right), \tag{5.2.63}$$

which may be simplified as

$$\begin{aligned} & J \left[\sum_{n=0}^{\infty} (n+1) D_{n+1} z_1^n + \sum_{m=1}^{\infty} \sum_{n=1}^{m} n D_n F_{m-n+1} z_1^m \right] \\ & = \sum_{n=0}^{\infty} (n+1) F_{n+1} z_1^n + \sum_{m=1}^{\infty} \sum_{n=1}^{m} (m-n+1) D_n F_{m-n+1} z_1^m. \end{aligned} \tag{5.2.64}$$

Matching the coefficients of z_1^M in (5.2.64) yields explicit expressions for the coefficients D_n, namely

$$D_1 = \frac{F_1}{J} \tag{5.2.65}$$

and

$$D_M = \frac{1}{JM}\left[MF_M + \sum_{n=1}^{M-1}(M - n(J+1))D_n F_{M-n}\right], \quad M \geq 2. \tag{5.2.66}$$

By combining (5.2.57), (5.2.58) and (5.2.60), and by taking $J = 2$ because of the transformation T_3 in (5.2.32), we have

$$z_4 = [B(z_1)z_1]^{\frac{1}{2}} \tag{5.2.67}$$

$$= z_1^{\frac{1}{2}} B_0^{\frac{1}{2}} [1 + F(z_1)]^{\frac{1}{2}} \tag{5.2.68}$$

which, as the series form of z_4 is known from the definition (5.2.22) of the elliptic sn function, defines F_j for all $j \geq 1$ and, in effect, D_j through (5.2.65) and (5.2.66).

The first three transformations in the CTM have been defined in a power-series form with known coefficients. The inverse for the final mapping T_4 in (5.2.34), however, requires the parametric inversion and comparisons of the coefficients of two infinite series. Instead, consistent with Rosser and Papamichael [1975], we use the following. By the sn series (5.2.22) and T_4 in (5.2.34),

$$z_4 = \text{sn}(\overline{K} z_5, \overline{m}) \tag{5.2.69}$$

$$= \sum_{n=1}^{\infty} E_n z_5^{2n-1} \tag{5.2.70}$$

$$= \sum_{n=1}^{\infty} E_n (\phi(z_1))^{2n-1}, \tag{5.2.71}$$

this last result arising because z_5 is the required solution ϕ. The coefficients E_n in (5.2.71) are determined by matching the series in (5.2.71) with the known expression for the sn series (5.2.22), i.e.

$$E_n = \overline{R} A_{n-1}(\overline{q}) \left(\frac{\pi}{2}\right)^{2n-1}, \tag{5.2.72}$$

where $\overline{R} = R(\overline{q})$ is dependent upon nome $\overline{q}$ and parameter $\overline{m}$ defined in (5.2.16), (5.2.18) and (5.2.33).

We now have two expressions for z_4, i.e. (5.2.67) and (5.2.71), that by definition must match,

therefore

$$\sum_{n=1}^{\infty} E_n(\phi(z_1))^{2n-1} = [B(z_1)z_1]^{\frac{1}{2}}. \tag{5.2.73}$$

The combination of (5.2.53), (5.2.54), (5.2.60) and (5.2.73) yields

$$\sum_{n=1}^{\infty} E_n \sum_{m=1}^{\infty} G_m^{(2n-1)} z_1^{m+n-\frac{3}{2}} = z_1^{\frac{1}{2}} B_0^{\frac{1}{2}} \left(1 + \sum_{n=1}^{\infty} D_n z_1^n\right), \tag{5.2.74}$$

in which, by (5.2.45), $G_m^{(1)} \equiv G_m$ and (5.2.74) implies

$$E_1 \sum_{m=1}^{\infty} G_m z_1^{m-1} + \sum_{r=2}^{\infty} \sum_{m=1}^{\infty} E_r G_m^{(2r-1)} z_1^{m-2+r} = B_0^{\frac{1}{2}} \left(1 + \sum_{m=1}^{\infty} D_m z_1^m\right). \tag{5.2.75}$$

By equating the coefficient of z_1^M when $M = 0$, we have

$$G_1 = \frac{B_0^{\frac{1}{2}}}{E_1}. \tag{5.2.76}$$

Hence (5.2.75) simplifies to

$$E_1 \sum_{m=2}^{\infty} G_m z_1^{m-1} = B_0^{\frac{1}{2}} \sum_{m=1}^{\infty} D_m z_1^m - \sum_{r=2}^{\infty} \sum_{m=1}^{\infty} E_r G_m^{(2r-1)} z_1^{m-2+r}. \tag{5.2.77}$$

By considering the coefficient of z_1^M for $M \geq 1$ in (5.2.75), G_M is deduced to be

$$G_M = \frac{1}{E_1} \left[B_0^{\frac{1}{2}} D_{M-1} - \sum_{r=2}^{M} E_r G_{M+1-r}^{(2r-1)} \right], \quad M \geq 2 \tag{5.2.78}$$

which, by the relation $a_{i-1} = G_i$ in (5.2.52), determines the coefficients in the expansion (5.2.41) of the solution of the stripline problem, thereby solving the original SBVP. However, in practice only a finite truncation, defined as ϕ_M, of the series in (5.2.41) is used, from which (5.2.41) is approximated by

$$\phi_M(z_1) = \phi_0 + \sum_{i=0}^{M} a_i z_1^{i+\frac{1}{2}}. \tag{5.2.79}$$

A summary of the power-series method described in this section is given in the flowchart of Fig. 5.2.8, which is subsequently implemented to derive a "near-exact" (i.e. truncated power-series) solution of the stripline SBVP.

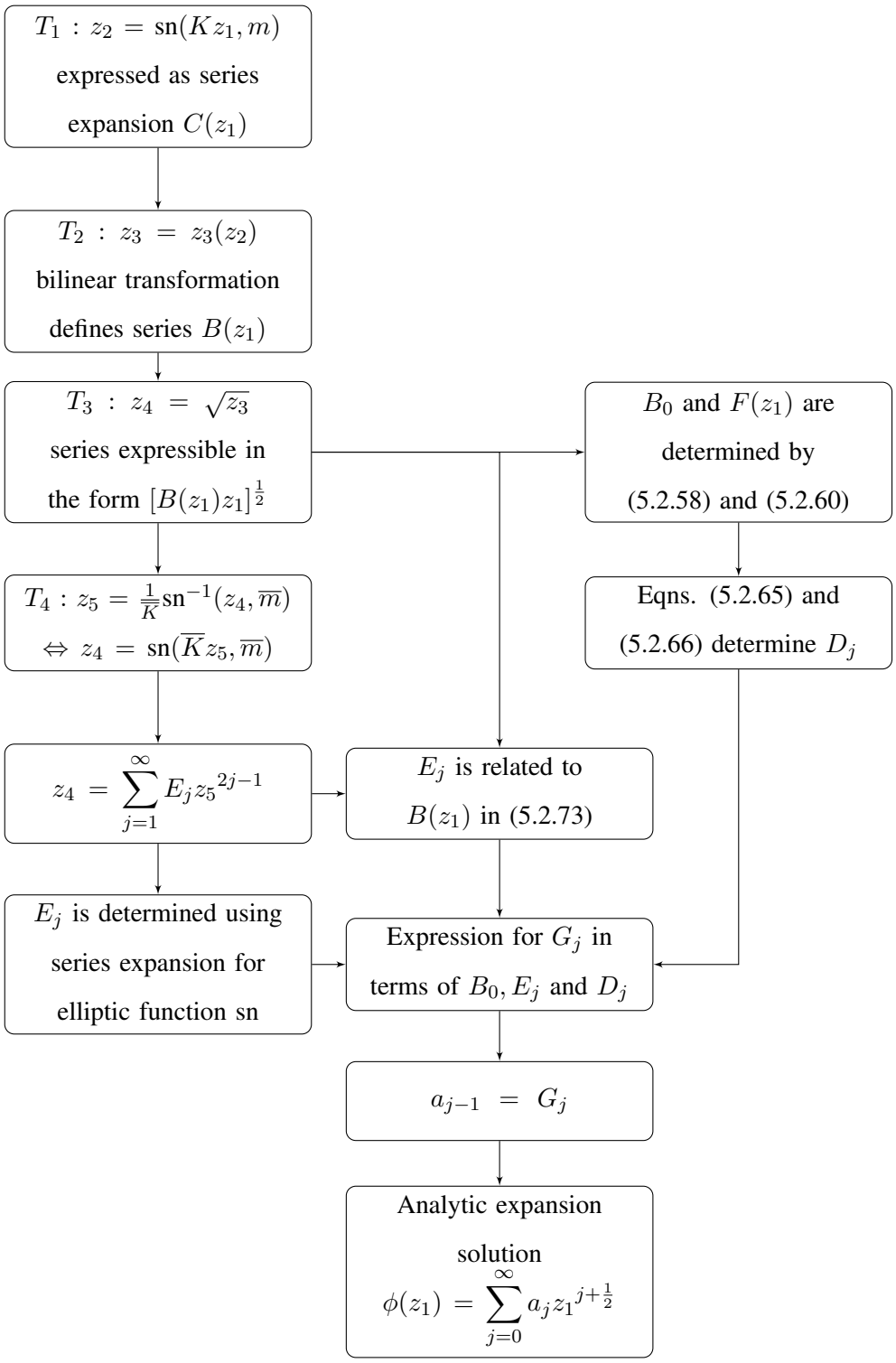

Figure 5.2.8: *Flowchart summary of the power-series solution of the CTM. For implementation, the infinite limits of the summations are truncated to M, in accordance with* (5.2.79).

5.3 Analytic solution of the stripline problem by the CTM

Recall, for the stripline SBVP in Fig. 5.1.2 that, by (5.2.26), we have $m = 1/2$ for which the complete elliptic function (5.2.15) can be evaluated numerically as

$$K(m) = 1.85407467730 \tag{5.3.1}$$

and, by (5.2.33), we also have

$$\overline{m} = \frac{2-\sqrt{2}}{4}. \tag{5.3.2}$$

Thus (5.2.9), (5.2.15), (5.2.18) and (5.2.28) are respectively evaluated (here using Maple 12) to be

$$\overline{K} \quad = K(\overline{m}) \quad = 1.63358630746, \tag{5.3.3}$$

$$\overline{K}' \quad = K'(\overline{m}) \quad = 2.40009445913, \tag{5.3.4}$$

$$\overline{R} \quad = R(\overline{q}) \quad = \frac{2\pi}{\overline{K}\sqrt{\overline{m}}} = 10.0507419612, \tag{5.3.5}$$

$$\overline{q} \quad = q(\overline{m}) \quad = \exp\left(-\pi\frac{\overline{K}'}{\overline{K}}\right) = 0.00989540694, \tag{5.3.6}$$

all to 12 significant figures. Note that in the works of Rosser and Papamichael [1975], (5.3.3)-(5.3.6) had to be approximated by highly-accurate computations of the truncated series, whereas this feature is inbuilt in Maple in which the number of digits can be chosen *a priori*.

The power series for each of the transformations $\{T_i\}_{i=1}^4$ can be explicitly defined. For example (5.2.55) becomes, for $m = 1/2$,

$$\begin{aligned} z_2 = 2\Bigg[v - v^3 + \frac{11}{10}v^5 - \frac{13}{10}v^7 + \frac{181}{120}v^9 - \frac{351}{200}v^{11} + \frac{31861}{15600}v^{13} \\ - \frac{185363}{78000}v^{15} + \frac{9777931}{3536000}v^{17} - \frac{2625613}{816000}v^{19} + \ldots\Bigg], \end{aligned} \tag{5.3.7}$$

where

$$v = \frac{Kz_1}{2}. \tag{5.3.8}$$

Similarly, applying the binomial theorem or Padé approximants to (5.3.7), the power-series form of the bilinear transformation (5.2.31) for the stripline problem is

$$\begin{aligned} z_3 = 4v\Bigg[1 - 2v + 3v^2 - 4v^3 + \frac{51}{10}v^4 - \frac{32}{5}v^5 + \frac{79}{10}v^6 \\ - \frac{48}{5}v^7 + \frac{1381}{120}v^8 - \frac{1024}{75}v^9 + \frac{3213}{200}v^{10} + \ldots\Bigg], \end{aligned} \tag{5.3.9}$$

where v is as defined in (5.3.8).

By the definition of transformation T_3, the square root of (5.3.9) yields

$$z_4 = 2\sqrt{v}\left[1 - 2v + 3v^2 - 4v^3 + \frac{51}{10}v^4 - \frac{32}{5}v^5 + \frac{79}{10}v^6 - \frac{48}{5}v^7 + \frac{1381}{120}v^8 - \frac{1024}{75}v^9 + \frac{3213}{200}v^{10} + \ldots\right]^{\frac{1}{2}}. \tag{5.3.10}$$

Comparing (5.3.10) with (5.2.68), we explicitly determine that

$$B_0 = 2K, \tag{5.3.11}$$

$$F(z_1) = -Kz_1 + \frac{3K^2{z_1}^2}{4} - \frac{K^3{z_1}^3}{2} + \ldots. \tag{5.3.12}$$

Therefore, by the construction of $F(z_1)$ in (5.2.43), we have

$$F_1 = -K, F_2 = \frac{3}{4}K^2, F_3 = -\frac{1}{2}K^3, \ldots, \tag{5.3.13}$$

thus (5.2.65) gives

$$D_1 = -\frac{K}{2} \tag{5.3.14}$$

and D_j for $j \geq 2$ is defined by (5.2.66).

Now, by (5.2.78) and the summary in Fig. 5.2.8, the computed D_j, E_j and B_0 yield G_j for $j = 1, \ldots, M$ and (5.2.52) yields approximations of the coefficients a_i; the first ten a_i are presented in Table 5.3.1. The coefficients a_i in the analytical expansion solution of the stripline problem are presented, as they will affect subsequent discussions on both the accuracy of the CTM and the numerical methods employed to solve the stripline SBVP.

Thus armed with a near-analytic solution, which was computed using 100 working digits, the CTM solution ϕ_M of the stripline SBVP in (5.2.79) can be computed, along with its normal derivative on all boundaries. To this end, Fig. 5.3.1 depicts the computed forms of ϕ_M, $\partial\phi_M/\partial x$ and $\partial\phi_M/\partial y$. In Fig. 5.3.1, the finite nature of the jump at the origin in both derivatives of ϕ_M is a result of computing data on a finite mesh: in reality these jumps are infinite. Moreover, the discontinuities occur only in terms of the normal derivatives of ϕ_M and not in terms of ϕ_M itself, from which it is clear that discontinuous boundary data will adversely affect the performance of standard BEMs.

Using the power-series form of the CTM (Rosser and Papamichael [1975]), we have thus computed a near-exact approximation of the solution of the singular stripline SBVP against which numerical approximation techniques can be validated.

i	E_i	a_{i-1}
1	1.63358630746	589.395110654
2	−0.83296899732	−128.785658529
3	0.29778845257	25.3262556623
4	−0.14579375616	11.8583749967
5	0.06898886628	2.11607464631
6	−0.03159457003	−0.48639180785
7	0.01463391823	0.40467751314
8	−0.00678919036	0.12772352310
9	0.00314429524	0.04937289333
10	−0.00145646174	−0.02260300040

Table 5.3.1: *The first ten coefficients E_i and a_i in the stripline problem computed to* 12 *significant figures, using* (5.2.52) *and* (5.2.72) *in Maple 12. The a_i coefficients are presented because these are the required coefficients in the original solution* (5.2.79) *in the $z_1 = (x, y)$-plane. The E_i coefficients on the other hand, are presented in keeping with Rosser and Papamichael [1975] so that subsequent implementations, by other authors, of the CTM for the stripline problem can be verified against these.*

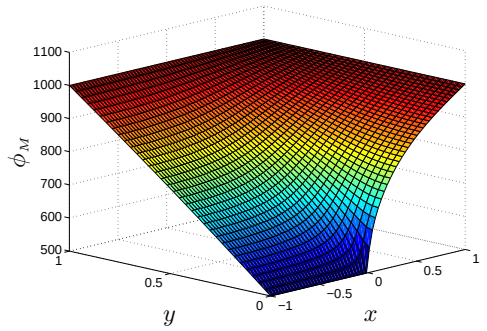

(a) $\phi_M(p)$

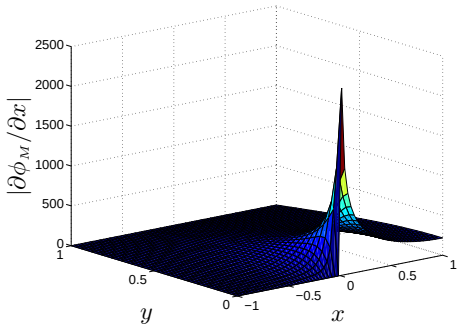

(b) $|\partial\phi_M(p)/\partial x|$

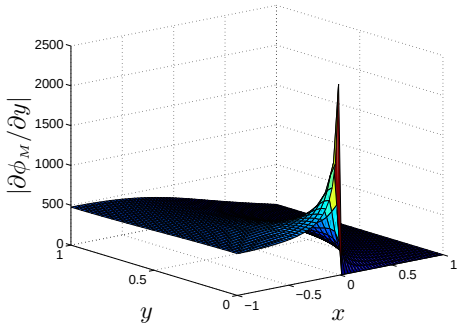

(c) $|\partial\phi_M(p)/\partial y|$

Figure 5.3.1: *The near-exact analytic solution ϕ_M and its normal derivatives, $|\partial\phi_M/\partial x|$ and $|\partial\phi_M/\partial y|$, on all boundaries of the stripline problem as derived by the power-series CTM for $\phi_0 = 500$, $\phi_1 = 1000$ and $M = 60$. The finite nature of the jump at the origin in both derivatives of ϕ_M is a result of computing data on a finite mesh: in reality these jumps are infinite.*

5.4 Summary and discussion

This chapter was based on the derivation of an pseudo-analytic solution of a two-dimensional singular harmonic BVP using a conformal transformation method (CTM).

The CTM, although well-established, was extensively outlined owing to parts of the details being difficult to obtain. The CTM maps the original bounded (singular) domain into quadrilateral containing no singularities, and to which a quasi-analytic solution is known. Although the mapping technique produces an analytic solution to the original problem, it involves elliptic functions and integrals which have to be evaluated numerically, so that in practice only a near-exact solution can be obtained.

The implementation of the CTM was achieved through a power-series method, which approximates the solution to a pre-defined accuracy, by the analogy of Rosser and Papamichael [1975]. In this chapter we outlined CTM and power-series for only the stripline problem, however, the theory is applicable to more general BVPs (Whiteman and Papamichael [1971], Li and Lu [2000]).

Whiteman and Papamichael [1972] showed that the results by the CTM compare favourably with those obtained previously by other methods, such as the (discrete) finite-difference and finite-element method. Two obvious advantages of the CTM, over a discrete method, are: first, that the original problem itself rather than some approximating problem is solved, and; second, that the same technique produces the solution at all points right up to the singularities. The solution can also be obtained at any desired point in the domain without the need to interpolate between the values at mesh points.

The near-exact analytic solution derived in this chapter using the CTM, will serve as a basis to which all numerical methods are validated against in the subsequent chapter.

Chapter 6

Numerical Solutions of Singular Harmonic Boundary Value Problems by Improved Boundary Element Methods

In chapter 5 we derived a near-exact analytic solution of a singular harmonic BVP, known as the stripline problem (see Fig. 5.1.2). Now, numerical methods are considered for solving the singular stripline problem.

The boundary element method (BEM) has proved to be a successful tool for the numerical solution of two-dimensional harmonic SBVPs (Symm [1973], Ingham et al. [1981a], Manzoor [1984]). However, it is well-known that the presence of a boundary singularity tends to decrease the rate of convergence of the numerical solution with decreasing element size (Motz [1946], Woods [1953]). There exist numerous modified numerical schemes devised to cope with the presence of boundary singularities. For example, Symm [1973] rendered the singular problem into a regular one by employing the singularity subtraction method, in which the singularity's known analytical form, in terms of a series expansion, was subtracted from the entire solution before the numerical procedure was employed. Xanthis et al. [1981] on the other hand, used the analytic nature of the singularity to build in the singular behaviour on only those elements closest to the singularity, i.e. the singularity incorporation method. More recently, Kelmanson and Lonsdale [1995] employed

a singularity annihilation method which, by utilising a suitable Green's function in the boundary-integral equation reformulation, the boundary singularities are placed in a region in which the Green's function are asymptotically small, therefore annihilating most of the singular behaviour.
In this chapter, the aim is to illustrate the application of the singularity subtraction and singularity incorporation method for the stripline SBVP using the constant BEM. The novel feature is that modified BEM techniques, defined and applied in chapter 4, will be developed in order to improve the accuracy of both the singularity subtraction and singularity incorporation methods. The pseudo-analytic solution of stripline SBVP, which was derived in chapter 5 using a CTM, will be used to validate the numerical methods.
The remainder of this chapter is as follows. In §6.1 we present the boundary-integral-equation form of an harmonic BVP. In §6.2 we present BEMs for approximating the solution of a boundary-integral equation for the stripline SBVP. In §6.5 we use the near-exact analytic solution of the stripline problem of chapter 5 to validate the BEM solutions of §6.2. Finally, in accordance with the modified technique of chapter 4, new, modified BEMs are defined in §6.6, that are validated for the stripline SBVP in §6.7.

6.1 The boundary-integral equation

The stripline problem, which is defined in §5.1, satisfies Laplace's equation, i.e.

$$\nabla^2\phi = 0, \tag{6.1.1}$$

in the simply connected domain Ω enclosed by boundary $\partial\Omega$. To recap on chapter 4, we derive the boundary-integral-equation form of (6.1.1) as follows. First, for the remainder of this chapter, the field point $p \in \Omega \cup \partial\Omega$ and the source point $q \in \partial\Omega$ unless otherwise stated. Then using Green's third identity, the elliptic partial differential equation (6.1.1) can be expressed as a boundary-integral equation in terms of ϕ and its (outward) normal derivative ϕ'. That is,

$$\eta(p)\phi(p) = \int_{\partial\Omega} \phi(q)G'(p,q)\ dq - \int_{\partial\Omega} \phi'(q)G(p,q)\ dq, \tag{6.1.2}$$

where $G(p,q) = \log|p-q|$ and

$$\eta(p) = \begin{cases} 2\pi & p \in \Omega, \\ 0 & p \notin \Omega \cup \partial\Omega, \\ \alpha & p \in \partial\Omega, \end{cases} \tag{6.1.3}$$

in which α is the internal angle between the tangents to $\partial\Omega$ on either side of p.

The data prescribed along $\partial\Omega$ in the stripline problem of Fig. 5.1.2 is a mixture of Dirichlet and Neumann conditions. Namely $\phi(x,y)$ is prescribed on $\partial\Omega_\phi$ and $\phi'(x,y)$ on $\partial\Omega_{\phi'}$, where $\partial\Omega_\phi \cap \partial\Omega_{\phi'} = \partial\Omega$. When $p = \overline{q}$ lies on the boundary, (6.1.2) becomes a closed-form equation between the potentials and their derivatives on the boundary, and one can solve for the unknown boundary data using

$$\int_{\partial\Omega} \phi(q) G'(\overline{q},q)\, dq - \int_{\partial\Omega} \phi'(q) G(\overline{q},q) - \alpha\phi(\overline{q}) = 0, \quad \overline{q} \in \partial\Omega, \tag{6.1.4}$$

provided that $\partial\Omega$ is everywhere smooth. Approximate solutions of (6.1.4) completes the boundary data, whereafter (6.1.2) can be used to find the harmonic function anywhere in Ω. In this chapter we use boundary element methods (BEMs) to determine the approximate solutions of (6.1.4).

6.2 The constant boundary element method (CBEM)

In the BEM we first discretise the boundary $\partial\Omega$ into n smooth elements, $e^{(j)}$ say, where

$$\partial\Omega = \bigcup_{j=1}^{n} e^{(j)}, \tag{6.2.1}$$

so that (6.1.2) becomes

$$\eta(p)\phi(p) = \sum_{j=1}^{n} \int_{e^{(j)}} \phi(q) G'(p,q)\, dq - \int_{e^{(j)}} \phi'(q) G(p,q)\, dq. \tag{6.2.2}$$

The constant BEM (CBEM) approximates $\phi(q)$ and $\phi'(q)$ by the piecewise-constant functions $\phi_{n,j}$ and $\phi'_{n,j}$ over each element. As the derivation of a the CBEM was discussed at length in §4.2 of chapter 4, only the basic outline is reviewed in this chapter.

The discretised form of (6.2.2) with piecewise-constant solution ϕ_n is

$$\eta(p)\phi_n(p) = \sum_{j=1}^{n} \left\{ \phi_{n,j} \int_{e^{(j)}} G'(p,q)\, dq - \phi'_{n,j} \int_{e^{(j)}} G(p,q)\, dq \right\}, \tag{6.2.3}$$

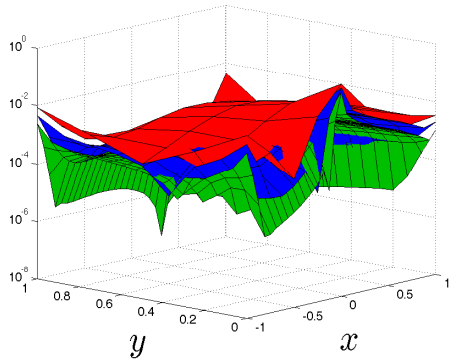

Figure 6.2.1: *Log plot of the relative error in the CBEM solution of the stripline SBVP,* $|\widetilde{\epsilon}_n/\phi|$*, for different values of* n*. The singular point is located at* $(x, y) = (0, 0)$ *and each surface corresponds to* $n = 24$ *(red),* $n = 48$ *(blue) and* $n = 96$ *(green). The relative errors increase near the corners owing to the* $O(h)$ *pollution (theoretically predicted using* (4.2.31) *in §4.2.1), although this is overshadowed by the large error in the neighbourhood of the singular point; this is an example of the CBEM failing to model the singular behaviour.*

in which $\phi_{n,j} \equiv \phi(q_{n,j})$ and $\phi'_{n,j} \equiv \phi'(q_{n,j})$ where $q_{n,j}$ is the mid-point of $e^{(j)}$. Collocating (6.2.3) at the mid-point of each element, by taking $p = q_{n,i}$, $i = 1, \ldots, n$, yields a system of n equations (defined in (4.2.10)), whose solution yields approximations of the unknown boundary data $\phi_{n,j}$ on $\partial\Omega_{\phi'}$ and $\phi'_{n,j}$ on $\partial\Omega_{\phi}$. Using the approximated boundary conditions to complete all the nodal data, $\phi_n(p)$ in (6.2.3) can be determined everywhere on Ω: this is referred to as the *numerical discretised solution* $\widetilde{\phi}_n$ in (4.2.11).

Using the nomenclature of §4.2, the *numerical CBEM error* is defined by

$$\widetilde{\epsilon}_n(p) \equiv \phi(p) - \widetilde{\phi}_n(p), \tag{6.2.4}$$

and it is presented for the stripline SBVP in Fig. 6.2.1 and, in an alternative form, in Fig. 6.2.2. Figs. 6.2.1 and 6.2.2 both show a large error in the neighbourhood of the singular point in comparison with the error over the remainder of Ω: this demonstrates the inability of the piecewise-constant boundary representation to model the singularity arising from the discontinuity in boundary conditions. The effect of the singularity is also evident in the root-mean-square error (RMSE) $\widetilde{\sigma}_n$ (defined in (4.2.43)), the error convergence rate ρ and the error order p of the CBEM

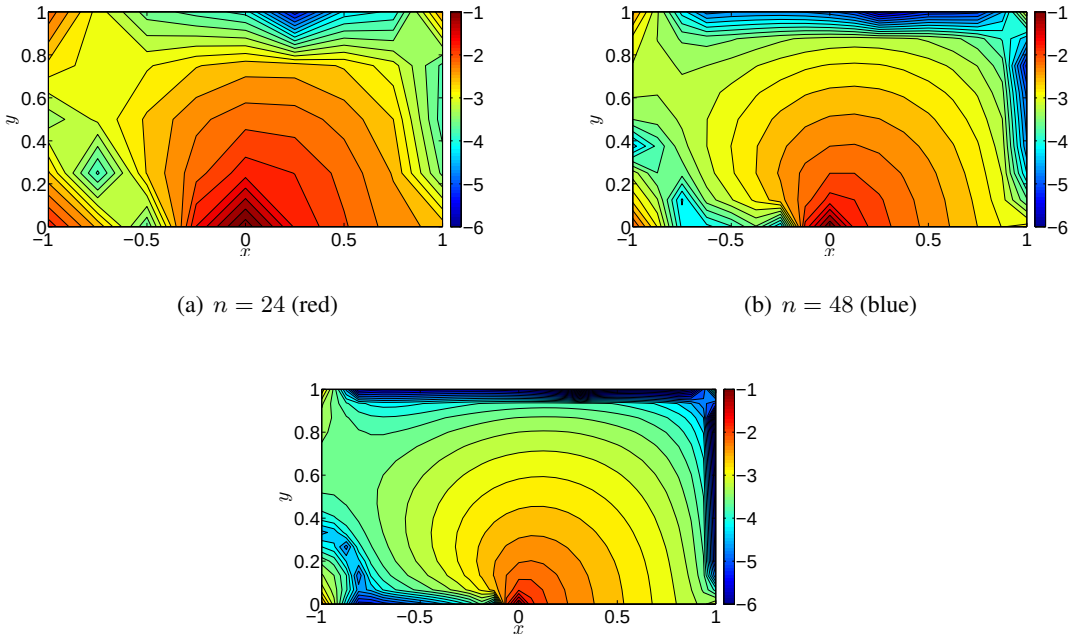

(a) $n = 24$ (red)

(b) $n = 48$ (blue)

(c) $n = 96$ (green)

Figure 6.2.2: *Contour plots of* $\log|\widetilde{\epsilon}_n/\phi|$*, the logarithm of the relative error in the CBEM solution of the stripline SBVP, for* $n = 24, 48$ *and* 96*. The singular point is located at* $(x, y) = (0, 0)$*. These plots separate and quantify the three error surfaces given in Fig. 6.2.1. By comparing sub-figure* (b) *with Fig. 6.2.1*(a)*, the effect of the singularity is evidenced from the large errors about the origin.*

solution for the stripline SBVP in Table 6.2.1. By comparison with the corresponding CBEM quantities for a nonsingular BVP in Table 4.2.1, Table 6.2.1 shows an increase in the RMSE and a decrease in both the error convergence rate and order. In other words, the presence of a singularity in a BVP has adversely affected the convergence of the CBEM with decreasing mesh size.

The CBEM errors for the stripline SBVP evidence the well-known adverse affect upon the accuracy in any numerical method when that fails to model the behaviour of a singularity (Motz [1946], Woods [1953], Ingham et al. [1981c]). As taking higher-order Lagrangian interpolation approximations are ineffective at recovering the accuracy when computing the solution of a singular problem, there are numerous techniques that modify the existing CBEM (Jaswon and Symm [1977], Ingham et al. [1981a,b], Manzoor [1984], Kelmanson [1983a,b, 1984]). These

n	$\widetilde{\sigma}_n$	ρ	p
24	0.0336	2.4938	1.3183
48	0.0135	2.5489	1.3499
96	0.0053		

Table 6.2.1: *The RMSE $\widetilde{\sigma}_n$, error convergence rate ρ and the error order p in the CBEM solution of the stripline SBVP, for $n = 24, 48, 96$ and $\alpha = 2$ $(= \beta)$. These results correspond to the errors depicted in Fig. 6.2.2. Due to the singularity in the BVP, the error convergence rate and the error order are a reduction upon that in the CBEM for a nonsingular BVP. For example, using Table 4.2.1, when $n = 48$, we find $p \approx 1.75$ in the CBEM for a nonsingular BVP, whereas for a SBVP the CBEM error is $p \approx 1.35$.*

techniques, however, are often based on approximating the harmonic function ϕ near the singular point by the introduction of special functions displaying the required singular behaviour. In this chapter, we consider two such techniques: the singularity incorporation method (SIM) and the singularity subtraction method (SSM). In the SSM, the analytic form of the singularity is subtracted throughout, yielding a uniformly nonsingular BVP (Symm [1973]), and in the SIM, the analytic form of the singularity is built into only those boundary elements closest to the singularity (Xanthis et al. [1981]). Hence the SSM yields a non-physical solution, which requires post-processing, of a nonsingular BVP in which all physical boundary conditions are pre-processed, whereas the SIM is used to compute a physical solution of a singular BVP in which the form of the singularity is included as accurately as possible. Both methods necessitate determination of unknown coefficients of eigenfunctions in the analytic form of the singularity.

Separable solutions of (6.1.1) in polar coordinates centred at $(0, 0)$, give the analytic form of the singularity as

$$\phi_s(r, \theta) = \phi_0 + \sum_{i=1}^{\infty} \alpha_i r^{\lambda_i} f_i(r, \theta), \quad (r, \theta) \in \Omega, \tag{6.2.5}$$

where α_i are unknown eigenfunction coefficients, λ_i are constants (which may be complex in a biharmonic problem, Poullikkas et al. [1998]) and $f_i(\lambda, \theta)$ represents the θ-dependence of the eigensolution. Following (5.1.1), we have

$$f_i(\lambda, \theta) = \cos(\lambda_i \theta), \quad i \in \mathbb{N}, \tag{6.2.6}$$

and, by the boundary conditions either side of $(0,0)$ on $y=0$,

$$\lambda_i = \frac{(2i-1)}{2}, \quad i \in \mathbb{N}. \tag{6.2.7}$$

That is, (6.2.7) reveals that ϕ has leading order $O(r^{\frac{1}{2}})$, and so ϕ' has leading order $O(r^{-\frac{1}{2}})$, which is the most dominant form of a singularity possible for harmonic problems. Hence if the SIM and the SSM methods are effective on this type of boundary singularity they will readily cope with weaker forms. The SIM and the SSM are now implemented and their results are compared with one another, as well as the analytic solution generated by the CTM in §5.2.

6.3 The singularity incorporation constant boundary element method (SICBEM)

Following Kelmanson [1983a], the elements $e^{(j)}$ in the domain discretisation (6.2.1) are numbered anticlockwise from the singular point, as illustrated in Fig. 6.3.1. The SIM takes $\phi \approx \phi_s$ and $\phi' \approx \phi'_s$ over the M elements either side of the singular point. Over the remaining $(n-M)$ elements, ϕ and ϕ' are approximated by piecewise Lagrangian interpolation. For example, the singularity incorporated constant BEM (SICBEM), with approximate solution $\phi_n^{(SI,M)}$, uses piecewise-constant Lagrangian approximations over $(n-M)$ elements, as per the CBEM, so that

$$\begin{aligned}\eta(p)\phi_n^{(SI,M)}(p) = &\sum_{j=1}^{M}\int_{e^{(j)}} \phi_s^{(M)}(q)G'(p,q)\,dq + \sum_{j=M+1}^{n}\int_{e^{(j)}} \phi_{n,j}G'(p,q)\,dq \\ &- \sum_{j=1}^{n-M}\int_{e^{(j)}} \phi'_{n,j}G(p,q)\,dq - \sum_{j=n-M+1}^{n}\int_{e^{(j)}} \phi_s'^{(M)}(q)G(p,q)\,dq,\end{aligned} \tag{6.3.1}$$

where $\phi_{n,j} \equiv \phi(q_{n,j})$ and $\phi'_{n,j} \equiv \phi'(q_{n,j})$. The function $\phi_s^{(M)}$ denotes the M^{th}-order truncation of ϕ_s in (6.2.5), i.e. (Manzoor [1984])

$$\phi_s^{(M)}(r,\theta) = \phi_0 + \sum_{i=1}^{M}\alpha_i r^{\lambda_i} f_i(\lambda,\theta), \quad (r,\theta) \in \Omega, \tag{6.3.2}$$

whereby the number of unknowns in (6.3.1) is equal to n.

Without loss of generality, we take $M = 2$ in the SICBEM, as this is sufficient to illustrate the

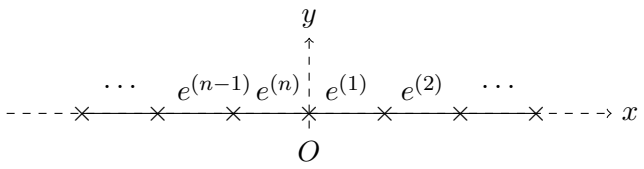

Figure 6.3.1: *Anticlockwise numbering of the boundary elements in the discretised boundary from the singularity point O, consistent with the stripline problem in Fig. 5.1.2.*

impact of the singularity incorporation without complicating the issue with over-complex algebra. Thus, by (6.2.6) and (6.2.7), $\phi_s^{(M)}$ becomes

$$\phi_s^{(2)}(r,\theta) = \phi_0 + \alpha_1 r^{\frac{1}{2}} \cos\left(\frac{\theta}{2}\right) + \alpha_2 r^{\frac{3}{2}} \cos\left(\frac{3\theta}{2}\right), \tag{6.3.3}$$

which is applied to the *two* elements either side of the singularity, $e^{(1)}$ and $e^{(n)}$, in accordance with Fig. 6.3.1. On $e^{(n)}$ the outward normal derivative of $\phi_s^{(M)}$ is fixed in plane polar coordinates as

$$\phi_s'^{(M)}(r,\theta) = \frac{1}{r}\frac{\partial \phi_s^M}{\partial \theta}, \tag{6.3.4}$$

so that, by (6.3.3), we have

$$\phi_s'^{(2)}(r,\theta) = -\frac{1}{2}\left\{\alpha_1 r^{-\frac{1}{2}} \sin\left(\frac{\theta}{2}\right) + 3\alpha_2 r^{\frac{1}{2}} \sin\left(\frac{3\theta}{2}\right)\right\}. \tag{6.3.5}$$

Note, the first term on the right-hand side of (6.3.5) contains the highly-singular behaviour as $r \to 0$. In the stripline SBVP, $\phi_s^{(2)}$ and $\phi_s'^{(2)}$ are applied only along $y = 0$, i.e. $\theta = 0$ or $\theta = \pi$, thus (6.3.3) and (6.3.5) reduce to

$$\begin{aligned} \phi_s^{(2)}|_{\theta=0} &= \phi_0 + \alpha_1 r^{\frac{1}{2}} + \alpha_2 r^{\frac{3}{2}}, \\ \phi_s'^{(2)}|_{\theta=\pi} &= -\frac{1}{2}\alpha_1 r^{-\frac{1}{2}} + \frac{3}{2}\alpha_2 r^{\frac{1}{2}}, \end{aligned} \tag{6.3.6}$$

so that (6.3.1) becomes

$$\begin{aligned} \eta(p)\phi_n^{(SI,2)}(p) = &\int_{e^{(1)}} \left(\phi_0 + \alpha_1 r^{\frac{1}{2}} + \alpha_2 r^{\frac{3}{2}}\right) G'(p,q)\, dq + \sum_{j=2}^{n} \int_{e^{(j)}} \phi_{n,j} G'(p,q)\, dq \\ &- \sum_{j=1}^{n-1} \int_{e^{(j)}} \phi'_{n,j} G(p,q)\, dq - \int_{e^{(n)}} \left(-\frac{1}{2}\alpha_1 r^{-\frac{1}{2}} + \frac{3}{2}\alpha_2 r^{\frac{1}{2}}\right) G(p,q)\, dq. \end{aligned} \tag{6.3.7}$$

For the remainder of this chapter, unless otherwise stated, indices i and j take the values $1, \ldots, n$. Discretising (6.3.7) at the mid-points $p = q_{n,i}$ yields the system of n equations

$$\begin{aligned} &\phi_0 A_{i1} + \alpha_1 C_{i1} + \alpha_2 D_{i1} + \sum_{j=2}^{n} \phi_{n,j} A_{ij} + \sum_{j=1}^{n-1} \phi'_{n,j} B_{ij} + \frac{\alpha_1}{2} E_{in} + \frac{3\alpha_2}{2} F_{in} \\ &= \begin{cases} \eta_1 \left(\phi_0 + \alpha_1 r_1{}^{\frac{1}{2}} + \alpha_2 r_1{}^{\frac{3}{2}} \right) & i = 1, \\ \eta_i \phi_{n,i} & i = 2, \ldots, n, \end{cases} \end{aligned} \tag{6.3.8}$$

where $r_1 = r(q_{n,1}) = |x_1|$ is the mid-point of $e^{(1)}$, the coefficients are given by

$$C_{ij} = \int_{e^{(j)}} r^{\frac{1}{2}} G'(q_{n,i}, q)\, dq, \tag{6.3.9}$$

$$D_{ij} = \int_{e^{(j)}} r^{\frac{3}{2}} G'(q_{n,i}, q)\, dq, \tag{6.3.10}$$

$$E_{ij} = \int_{e^{(j)}} r^{-\frac{1}{2}} G(q_{n,i}, q)\, dq, \tag{6.3.11}$$

$$F_{ij} = -\int_{e^{(j)}} r^{\frac{1}{2}} G(q_{n,i}, q)\, dq, \tag{6.3.12}$$

and the integrals A_{ij} and B_{ij} are defined as in (4.2.8). In (6.3.9)-(6.3.12) r is the distance from the origin to point q and the integrals may be evaluated analytically provided each element $e^{(j)}$ is a straight-line segment (see Appendix D).

Using $\widehat{A}_{ij}$ in (4.2.9), system (6.3.8) is equivalent to

$$\begin{aligned} &\phi_0 \widehat{A}_{i1} + \alpha_1 \left(C_{i1} + \frac{1}{2} E_{in} - \eta_1 \delta_{i1} r_1{}^{\frac{1}{2}} \right) + \sum_{j=2}^{n} \phi_{n,j} \widehat{A}_{ij} \\ &= -\alpha_2 \left(D_{i1} + \frac{3}{2} F_{in} - \eta_1 \delta_{i1} r_1{}^{\frac{3}{2}} \right) - \sum_{j=1}^{n-1} \phi'_{n,j} B_{ij}. \end{aligned} \tag{6.3.13}$$

Eqn. (6.3.13) can be cast into the form $\mathbf{M}\mathbf{x}_{SI} = \mathbf{t}$, in which the vector $\mathbf{x}_{SI}$ contains the $(n-2)$ unknown mid-nodal values of $\phi_{n,j}$ on $\partial\Omega_{\phi'}$ and $\phi'_{n,j}$ on $\partial\Omega_{\phi}$ and the two unknown singularity coefficients α_1 and α_2. The vector $\mathbf{t}$ contains the prescribed boundary conditions, i.e. ϕ on $\partial\Omega_{\phi}$, ϕ' on $\partial\Omega_{\phi'}$ and $\phi_0 \widehat{A}_{i1}$.

The collocated SICBEM (6.3.13) is a minor variation upon the corresponding CBEM system

$\mathbf{Hx}_C = \mathbf{g}$, where

$$M_{ij} = \begin{pmatrix} (C_{11} - \frac{1}{2}E_{1n} - \eta_1 r_1{}^{\frac{1}{2}}) & H_{12} & \dots & H_{1(n-1)} & (D_{11} - \frac{3}{2}F_{1n} - \eta_1 r_1{}^{\frac{3}{2}}) \\ (C_{21} - \frac{1}{2}E_{2n}) & H_{22} & \dots & H_{2(n-1)} & (D_{21} - \frac{3}{2}F_{2n}) \\ \vdots & & \ddots & & \vdots \\ (C_{n1} - \frac{1}{2}E_{nn}) & H_{n2} & \dots & H_{n(n-1)} & (D_{n1} - \frac{3}{2}F_{nn}) \end{pmatrix}, \quad (6.3.14)$$

$$x_{SI,i} = \begin{pmatrix} \alpha_1 \\ x_{C,2} \\ x_{C,3} \\ \vdots \\ x_{C,n-1} \\ \alpha_2 \end{pmatrix} \quad (6.3.15)$$

and

$$t_i = g_i + e_i = g_i - \phi_0 \widehat{A}_{i1}. \quad (6.3.16)$$

The dense system $\mathbf{Mx}_{SI} = \mathbf{t}$ is solved using the NAG routine F07AAF, thus completing the unknown boundary data in (6.1.4). With all nodal boundary data now prespecified or approximated, $\phi_n^{(SI,2)}$ in (6.3.7) can be computed directly.

By analogy with the CBEM in chapter 4, there are two types of solutions for the SICBEM: the *theoretical discretised solution* $\phi_n^{(SI,2)}$ in (6.3.7) and the *numerical discretised solution*, the latter of which is defined by $\widetilde{\phi}_n^{(SI,2)}$. Consistent with the theoretical and numerical discretised solutions of the CBEM, $\phi_n^{(SI,2)}$ is defined by a fully specified boundary solution whereas $\widetilde{\phi}_n^{(SI,2)}$ is defined by a partly specified (partly approximated) boundary solution. In other words, the theoretical discretised solution is generated without having to go through the two-stage process, i.e. is simply based upon (6.1.2), whereas the numerical discretised solution is defined by both (6.1.2) and (6.1.4). Therefore the theoretical solution enables a quantification of the error in the Lagrangian interpolation, which dominates the error in the BEM, whereas the numerical solution includes both Lagrangian interpolation and matrix inversion errors. Throughout the remainder of this chapter, we will define the theoretically and numerically derived solutions (and their corresponding errors) in the same way.

Based on $\phi_n^{(SI,2)}$ in (6.3.7), the numerical discretised solution $\widetilde{\phi}_n^{(SI,2)}$ satisfies

$$\widetilde{\phi}_n^{(SI,2)}(p) = \frac{1}{\eta(p)} \left\{ \int_{e^{(1)}} \left(\phi_0 + \widetilde{\alpha}_1 r^{\frac{1}{2}} + \widetilde{\alpha}_2 r^{\frac{3}{2}} \right) G'(p,q)\, dq + \sum_{j=2}^{n} \int_{e^{(j)}} \widetilde{\phi}_{n,j} G'(p,q)\, dq \right.$$
$$\left. - \sum_{j=1}^{n-1} \int_{e^{(j)}} \widetilde{\phi}'_{n,j} G(p,q)\, dq - \int_{e^{(n)}} \left(-\frac{1}{2}\widetilde{\alpha}_1 r^{-\frac{1}{2}} + \frac{3}{2}\widetilde{\alpha}_2 r^{\frac{1}{2}} \right) G(p,q)\, dq \right\}, \quad (6.3.17)$$

in which $\widetilde{\alpha}_i$ are the numerically computed forms of α_i from solving (6.3.13), and

$$\widetilde{\phi}_{n,j} = \begin{cases} \phi(q_{n,j}) & \text{if } e^{(j)} \subseteq \partial\Omega_\phi, \\ \widetilde{\phi}(q_{n,j}) & \text{otherwise,} \end{cases} \quad \text{and} \quad \widetilde{\phi}'_{n,j} = \begin{cases} \phi'(q_{n,j}) & \text{if } e^{(j)} \subseteq \partial\Omega_{\phi'}, \\ \widetilde{\phi}'(q_{n,j}) & \text{otherwise.} \end{cases} \quad (6.3.18)$$

6.3.1 Error analysis of the SICBEM

By comparing $\widetilde{\phi}_n^{(SI,2)}(p)$ with the exact solution $\phi(p)$, the *numerical SICBEM error* is defined by

$$\widetilde{\epsilon}_n^{(SI,2)}(p) \equiv \phi(p) - \widetilde{\phi}_n^{(SI,2)}(p), \quad (6.3.19)$$

which, by the linearity of (6.1.2) and (6.3.17), satisfies Green's integral formulae, i.e.

$$\eta(p)\widetilde{\epsilon}_n^{(SI,2)}(p) = \sum_{j=1}^{n} \left\{ \int_{e^{(j)}} \widetilde{\epsilon}_{n,j}^{(SI,2)}(q)\, G'(p,q)\, dq - \int_{e^{(j)}} \widetilde{\epsilon}_{n,j}'^{(SI,2)}(q)\, G(p,q)\, dq \right\}, \quad (6.3.20)$$

where

$$\widetilde{\epsilon}_{n,j}^{(SI,2)}(q) = \begin{cases} \phi(q) - \widetilde{\phi}_s^{(2)}(q) & j = 1, \\ \phi(q) - \widetilde{\phi}_{n,j} & j = 2, \ldots, n \end{cases} \quad (6.3.21)$$

and

$$\widetilde{\epsilon}_{n,j}'^{(SI,2)}(q) = \begin{cases} \phi'(q) - \widetilde{\phi}'_{n,j} & j = 1, \ldots, n-1, \\ \phi'(q) - \widetilde{\phi}_s'^{(2)}(q) & j = n. \end{cases} \quad (6.3.22)$$

Note that in (6.3.21) and (6.3.22), $\widetilde{\phi}_s^{(2)}$ is the numerical form of $\phi_s^{(2)}$ with singular coefficients $\widetilde{\alpha}_i$ computed from solving $\mathbf{M}\mathbf{x}_{SI} = \mathbf{t}$. Therefore, by (5.1.1), we have

$$\phi(q) - \widetilde{\phi}_s^{(2)}(q) = \sum_{j=1}^{2} (a_j - \widetilde{\alpha}_j) r^{j-\frac{1}{2}} \cos\left[\left(j - \frac{1}{2} \right) \theta \right]$$
$$+ \sum_{j=3}^{\infty} a_j r^{j-\frac{1}{2}} \cos\left[\left(j - \frac{1}{2} \right) \theta \right] \quad (6.3.23)$$

and

$$\phi'(q) - \widetilde{\phi}_s'^{(2)}(q) = \sum_{j=1}^{2}(a_j - \widetilde{\alpha}_j)\left(j-\frac{1}{2}\right) r^{j-\frac{3}{2}} \sin\left[\left(j-\frac{3}{2}\right)\theta\right] + \sum_{j=3}^{\infty}\left(j-\frac{1}{2}\right) a_j r^{j-\frac{3}{2}} \sin\left[\left(j-\frac{3}{2}\right)\theta\right]. \tag{6.3.24}$$

Similarly, by comparing $\phi_n^{(SI,2)}(p)$ with the exact solution $\phi(p)$, the *theoretical SICBEM error* is defined by

$$\epsilon_n^{(SI,2)}(p) \equiv \phi(p) - \phi_n^{(SI,2)}(p). \tag{6.3.25}$$

To simplify the following error analysis, we define the functions

$$\phi^{(\alpha,\beta)}(q) \equiv \sum_{j=\alpha}^{\beta} a_j r^{j-\frac{1}{2}} \cos\left[\left(j-\frac{1}{2}\right)\theta\right] \tag{6.3.26}$$

and

$$\phi'^{(\alpha,\beta)}(q) \equiv \sum_{j=\alpha}^{\beta}\left(j-\frac{1}{2}\right) a_j r^{j-\frac{3}{2}} \sin\left[\left(j-\frac{3}{2}\right)\theta\right], \tag{6.3.27}$$

so that $\phi(p) = \phi_0 + \phi^{(1,\infty)}(p)$ recovers solution (5.1.1). Then, by linearity of (6.1.2) and (6.3.7), the theoretical error of the SICBEM (6.3.7) satisfies Green's integral formulae, i.e.

$$\eta(p)\epsilon_n^{(SI,2)}(p) = \sum_{j=1}^{n}\left\{\int_{e^{(j)}} \epsilon_{n,j}^{(SI,2)}(q)\, G'(p,q)\, dq - \int_{e^{(j)}} \epsilon_{n,j}'^{(SI,2)}(q)\, G(p,q)\, dq\right\}, \tag{6.3.28}$$

where

$$\epsilon_{n,j}^{(SI,2)}(q) = \begin{cases} \phi^{(3,\infty)}(q) & j=1, \\ \phi(q) - \phi_{n,j} & j=2,\ldots,n \end{cases} \tag{6.3.29}$$

and

$$\epsilon_{n,j}'^{(SI,2)}(q) = \begin{cases} \phi'(q) - \phi'_{n,j} & j=1,\ldots,n-1, \\ \phi'^{(3,\infty)}(q) & j=n. \end{cases} \tag{6.3.30}$$

In (6.3.29) we have $\phi^{(3,\infty)}(q)$ applied only on $q \in e^{(1)}$, where $\theta = 0$ and $r = x$, hence, by (5.1.1) and (6.3.26), $\epsilon_{n,1}^{(SI,2)}(q)$ is equivalent to

$$\phi^{(3,\infty)}(q) = \sum_{j=3}^{\infty} a_j x^{j-\frac{1}{2}}, \quad q=(x,y) \in e^{(1)}. \tag{6.3.31}$$

Similarly, in (6.3.30) we have $\phi'^{(3,\infty)}(q)$ applied only on $q \in e^{(n)}$, where $\theta = \pi$ and $r = -x$, hence, by (5.1.1) and (6.3.27), $\epsilon'^{(SI,2)}_{n,n}(q)$ is equivalent to

$$\phi'^{(3,\infty)}(q) = \sum_{j=3}^{\infty} \left(j - \frac{1}{2}\right) a_j (-1)^j (-x)^{j-\frac{3}{2}}, \quad q = (x, y) \in e^{(n)}. \tag{6.3.32}$$

By comparison with the components of the CBEM error in (4.2.22) and (4.2.23), the SICBEM error components (6.3.29) and (6.3.30) differ on the first and last element only; this is depicted in Fig. 6.3.2 for the stripline SBVP. Fig. 6.3.2 reiterates the results of the CBEM error in Fig. 6.2.1, namely the CBEMs inability to model the true behaviour of ϕ and its derivative ϕ' in the neighbourhood of the singular point. Another feature of the results in Fig. 6.3.2 is that the SICBEM error is smaller than the CBEM error. That is, on $e^{(1)}$

$$\|\epsilon^{(SI,2)}_{n,1}\|_\infty \ll \|\epsilon_{n,1}\|_\infty \tag{6.3.33}$$

and, on $e^{(n)}$,

$$\|\epsilon'^{(SI,2)}_{n,n}\|_\infty \ll \|\epsilon'_{n,n}\|_\infty. \tag{6.3.34}$$

Therefore, by (6.3.33) and (6.3.34), we have

$$\|\epsilon^{(SI,2)}_{n}\|_\infty \ll \|\epsilon_{n}\|_\infty, \tag{6.3.35}$$

i.e. theoretically the SICBEM error $\epsilon^{(SI,2)}_n$ is smaller than the standard CBEM error ϵ_n.
When the computed $\widetilde{\alpha}_j$ in the numerical discretised SICBEM satisfy

$$|a_j - \widetilde{\alpha}_j| \ll |a_j|, \tag{6.3.36}$$

where a_j are the coefficients in the analytic solution (5.1.1), we have

$$\phi(q) - \widetilde{\phi}^{(2)}_s(q) \approx \phi^{(3,\infty)}(q) \tag{6.3.37}$$

and

$$\phi'(q) - \widetilde{\phi}'^{(2)}_s(q) \approx \phi'^{(3,\infty)}(q). \tag{6.3.38}$$

Hence (6.2.4), (6.3.20), (6.3.35) and (6.3.36) imply

$$\|\widetilde{\epsilon}^{(SI,2)}_{n}\|_\infty \ll \|\widetilde{\epsilon}_{n}\|_\infty, \tag{6.3.39}$$

where $\widetilde{\epsilon}^{(SI,2)}_n$ is the numerical discretised SICBEM error and $\widetilde{\epsilon}_n$ is the numerical discretised CBEM. That is, the aim of reducing the error by using the SICBEM has been achieved.

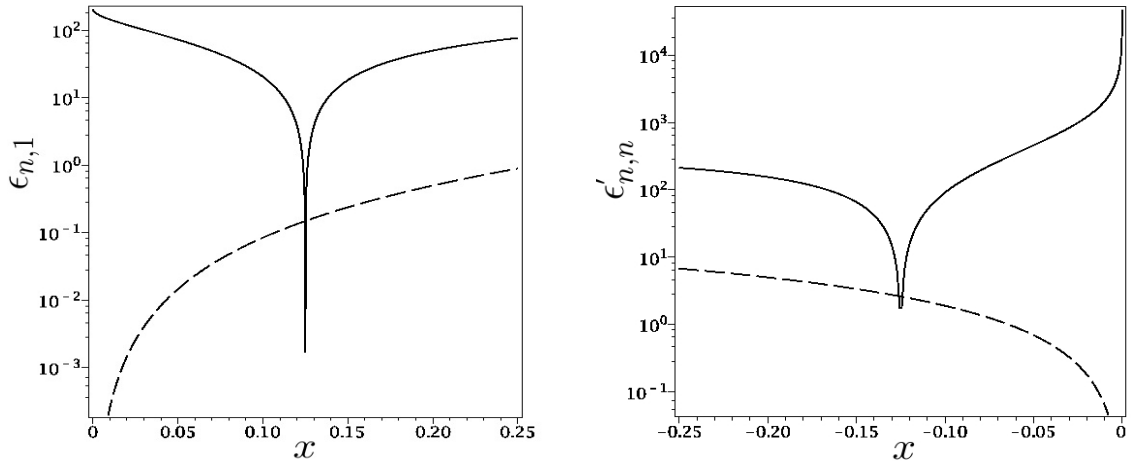

(a) $j = 1$ (b) $j = n$

Figure 6.3.2: *Log plot of $\epsilon_{n,1}(q)$ on $e^{(1)}$ and $\epsilon'_{n,n}(q)$ on $e^{(n)}$ for the stripline SBVP for $n = 24$. Here we have the SICBEM error (dashed line) and the CBEM error (solid line). As the elements are adjacent to singular point the piecewise-constant approximations in the CBEM error are poorly modelling the behaviour of ϕ and ϕ', as demonstrated by the vertical scalings. Furthermore, the peaks in the CBEM result from the error changing sign: in reality these peaks are infinite yet appear finite because they are computed on a finite mesh.*

6.4 The singularity subtraction constant boundary element method (SSCBEM)

The SSM, which differs from the SIM by removing the analytic form of the singularity throughout, transforms the SBVP into a uniformly nonsingular BVP. Following Symm [1973], we define $\psi^{(M)}$ by

$$\psi^{(M)}(p) \equiv \phi(p) - \phi_s^{(M)}(p) \tag{6.4.1}$$

so that, by (6.3.2), the *regular* function $\psi^{(M)}$ satisfies

$$\psi^{(M)}(p) = \phi(p) - \phi_0 - \sum_{k=1}^{M} \alpha_k r^{\lambda_k} f_k(\lambda, \theta), \tag{6.4.2}$$

in which we ignore terms of order $O(r^{\lambda_{M+1}})$ and higher. The series solution (5.1.1) of ϕ implies, that near the singular point, we expect a residual behaviour of the form

$$\psi^{(M)}(p) = \sum_{k=M+1}^{\infty} \alpha_k r^{\lambda_k} f_k(\lambda, \theta). \tag{6.4.3}$$

As the right-hand side of (6.4.1) satisfies Green's integral formula, the same must hold for the left-hand side of (6.4.1), i.e. $\psi^{(M)}$ is harmonic and so, by (4.1.4),

$$\eta(p)\psi^{(M)}(p) = \int_{\partial\Omega} \psi^{(M)}(q)\ G'(p,q)\ dq - \int_{\partial\Omega} \psi'^{(M)}(q)\ G(p,q)\ dq. \tag{6.4.4}$$

By (4.2.3), the CBEM approximation $\psi_n^{(M)}$ of $\psi^{(M)}$ satisfies

$$\eta(p)\psi_n^{(M)}(p) = \sum_{j=1}^{n} \left\{ \psi_{n,j}^{(M)} \int_{e^{(j)}} G'(p,q)\ dq - \psi_{n,j}'^{(M)} \int_{e^{(j)}} G(p,q)\ dq \right\}, \tag{6.4.5}$$

where $\psi_{n,j}^{(M)} \equiv \psi^{(M)}(q_{n,j})$, $\psi_{n,j}'^{(M)} \equiv \psi'^{(M)}(q_{n,j})$ and $q_{n,j}$ is the mid-point of $e^{(j)}$. In accordance with the notation of the SIM, we define $\psi_n^{(M)}$ in (6.4.5) as the *theoretical discretised solution* of $\psi^{(M)}$, namely defined by a fully specified boundary solution. Thus, by a rearrangement of (6.4.1), the singularity subtracted CBEM (SSCBEM), with solution $\phi_n^{(SS,2)}$ approximating the exact solution ϕ, is given by

$$\phi_n^{(SS,M)}(p) = \psi_n^{(M)}(p) + \phi_s^{(M)}(p). \tag{6.4.6}$$

The boundary data for $\psi^{(M)}$ in (6.4.2) is computed from $\phi_s^{(M)}$ and the prescribed boundary data for ϕ (and ϕ') in the stripline SBVP. That is, owing to the dependency of $\psi^{(M)}$ upon the analytic form of the singularity $\phi_s^{(M)}$, the boundary data for $\psi^{(M)}$ will be dependent upon the unknown coefficients α_i. For example, for the stripline SBVP in Fig. 5.1.2, by (6.2.6) and (6.2.7),

$$\psi_n^{(M)}(x < 0, 0) = 0, \tag{6.4.7}$$

$$\psi_n'^{(M)}(x > 0, 0) = 0, \tag{6.4.8}$$

$$\psi_n^{(M)}(x = 1, y) = \phi_1 - \phi_0 - \sum_{k=1}^{M} \alpha_k r^{k-\frac{1}{2}} \cos\left[\left(k - \frac{1}{2}\right)\theta\right], \tag{6.4.9}$$

$$\psi_n^{(M)}(x, y = 1) = \phi_1 - \phi_0 - \sum_{k=1}^{M} \alpha_k r^{k-\frac{1}{2}} \cos\left[\left(k - \frac{1}{2}\right)\theta\right], \tag{6.4.10}$$

$$\psi_n'^{(M)}(x = -1, y) = -\sum_{k=1}^{M} \alpha_k \left(k - \frac{1}{2}\right) r^{k-\frac{3}{2}} \sin\left[\left(k - \frac{3}{2}\right)\theta\right]. \tag{6.4.11}$$

Contrary to the constant boundary data for ϕ and ϕ' in the stripline SBVP, the boundary data for $\psi^{(M)}$ in (6.4.9)-(6.4.11) are spacially dependent on the domain. Therefore, the accuracy to which the boundary condition of $\psi^{(M)}$ will be represented in the BEM, depends upon both the degree of the piecewise-polynomial interpolation and the index M.

Discretising (6.4.5) at the mid-point of each element by taking $p = q_{n,i}$ yields the system of n equations

$$\sum_{j=1}^{n} \widehat{A}_{ij}\psi_{n,j}^{(M)} = -\sum_{j=1}^{n} B_{ij}\psi_{n,j}^{\prime(M)}, \tag{6.4.12}$$

where $\widehat{A}_{ij}$ and B_{ij} are respectively defined in (4.2.9) and (4.2.8). System (6.4.12) contains $M+n$ unknowns: M singularity coefficients α_k and n unknown mid-element nodal boundary data $\psi_{n,j}^{(M)}$ on $\partial\Omega_{\phi'}$ and $\psi_{n,j}^{\prime(M)}$ on $\partial\Omega_{\phi}$. Taking $M = 2$ in the remainder of this section, so that the SSCBEM can be validated against the SICBEM of §6.3, (6.4.2) becomes

$$\psi_n^{(2)}(p) = \phi(p) - \phi_0 - \left(\alpha_1 r^{\frac{1}{2}} \cos\left(\frac{\theta}{2}\right) + \alpha_2 r^{\frac{3}{2}} \cos\left(\frac{3\theta}{2}\right)\right). \tag{6.4.13}$$

Boundary conditions (6.4.7) and (6.4.8) imply that $\psi_n^{(2)}$ in (6.4.13) is zero in the locality of the singular point, as is its normal derivative $\psi_n^{\prime(2)}$. Thus, by (6.4.7) and (6.4.8), we take $\psi_{n,1}^{(2)} = 0$ and $\psi_{n,n}^{\prime(2)} = 0$, which are known as the *balancing approximations*, and the number of unknowns in system (6.4.12) is reduced from $M+n$ to n.

Eqn. (6.4.12) can be cast into the form $\mathbf{P}\mathbf{x}_{SS} = \mathbf{q}$ where the n-dimensional vector $\mathbf{x}_{SS}$ contains the $(n-2)$ unknown mid-element values $\psi_{n,j}^{(2)}$ on $\partial\Omega_{\phi'}$ and $\psi_{n,j}^{\prime(2)}$ on $\partial\Omega_{\phi}$ and the two unknown singularity coefficients α_1 and α_2. The vector $\mathbf{q}$ contains the balancing approximations and the elements of the prescribed boundary data that do not depend on α_k, e.g. ϕ_0 and ϕ_1 in (6.4.9) and (6.4.10).

The dense system $\mathbf{P}\mathbf{x}_{SS} = \mathbf{q}$, solved using the NAG routine F07AAF, yields the discretised boundary data to supplement the original boundary data in (6.4.7)-(6.4.11). Then using the completed boundary data, we can compute $\psi_n^{(2)}$ in (6.4.5) directly, which is defined as the *numerical discretised solution*: to distinguish it from the theoretical discretised solution in (6.4.5), we denote the numerical discretised solution by $\widetilde{\psi}_n^{(2)}$ that satisfies

$$\widetilde{\psi}_n^{(2)}(p) = \frac{1}{\eta(p)} \sum_{j=1}^{n} \left\{ \int_{e^{(j)}} \widetilde{\psi}_{n,j}^{(2)}\, G'(p,q)\, dq - \int_{e^{(j)}} \widetilde{\psi}_{n,j}^{\prime(2)}\, G(p,q)\, dq \right\}, \tag{6.4.14}$$

where

$$\widetilde{\psi}_{n,j}^{(2)} = \begin{cases} \psi^{(2)}(q_{n,j}) & \text{if } e^{(j)} \subseteq \partial\Omega_{\phi}, \\ \widetilde{\psi}^{(2)}(q_{n,j}) & \text{otherwise,} \end{cases} \quad \text{and} \quad \widetilde{\psi}_{n,j}^{\prime(2)} = \begin{cases} \psi^{\prime(2)}(q_{n,j}) & \text{if } e^{(j)} \subseteq \partial\Omega_{\phi^{\prime}}, \\ \widetilde{\psi}^{\prime(2)}(q_{n,j}) & \text{otherwise.} \end{cases} \tag{6.4.15}$$

Consistent with the SICBEM of §6.3, $\widetilde{\phi}_s^{(2)}$ is the numerical form of $\phi_s^{(2)}$ with singular coefficients $\widetilde{\alpha}_i$ computed from solving $\mathbf{P}\mathbf{x}_{SS} = \mathbf{q}$.

Finally, by (6.4.6) and (6.4.14), the *numerical discretised solution* of the SSCBEM, $\widetilde{\phi}_n^{(SS,2)}$ approximating the exact solution ϕ, is given by

$$\widetilde{\phi}_n^{(SS,2)}(p) = \widetilde{\psi}_n^{(2)}(p) + \widetilde{\phi}_s^{(2)}(p). \tag{6.4.16}$$

Eqn. (6.4.16) shows that the singularity behaviour, which was subtracted throughout to yield a non-physical solution, is re-included post-processing to recover the physical solution.

6.4.1 Error analysis of the SSCBEM

By comparing the numerical SSCBEM solution $\widetilde{\phi}_n^{(SS,2)}$ in (6.4.16) with the exact solution ϕ, the *numerical SSCBEM error* is defined by

$$\widetilde{\epsilon}_n^{(SS,2)}(p) \equiv \phi(p) - \widetilde{\phi}_n^{(SS,2)}(p). \tag{6.4.17}$$

Whereas comparing the theoretical SSCBEM solution $\phi_n^{(SS,2)}$ in (6.4.6) with the exact solution ϕ yields the *theoretical SSCBEM error* defined by

$$\epsilon_n^{(SS,2)}(p) \equiv \phi(p) - \phi_n^{(SS,2)}(p). \tag{6.4.18}$$

Considering the right-hand side of (6.4.18), by (6.4.5) and (6.4.6) we have

$$\begin{aligned} \phi(p) - \phi_n^{(SS,2)}(p) &= \phi(p) - (\psi_n^{(2)} + \phi_s^{(2)}(p)) \\ &= \phi(p) - \left[\frac{1}{\eta(p)} \sum_{j=1}^{n} \left\{ \int_{e^{(j)}} \psi_{n,j}^{(2)}\, G^{\prime}(p,q)\, dq \right. \right. \\ &\quad \left. \left. - \int_{e^{(j)}} \psi_{n,j}^{\prime(2)}\, G(p,q)\, dq \right\} + \phi_s^{(2)}(p) \right] \end{aligned} \tag{6.4.19}$$

which, after applying the balancing approximations, becomes

$$\phi(p) - \phi_n^{(SS,2)}(p) = \phi(p) - \frac{1}{\eta(p)} \left\{ \sum_{j=2}^{n} \int_{e^{(j)}} \left[\phi_{n,j} - \phi_s^{(2)}(q_{n,j}) \right] \, G'(p,q) \, dq \right.$$
$$\left. + \sum_{j=1}^{n-1} \int_{e^{(j)}} \left[\phi'_{n,j} - \phi_s'^{(2)}(q_{n,j}) \right] \, G(p,q) \, dq \right\} - \phi_s^{(2)}(p). \tag{6.4.20}$$

Using the functions $\phi^{(\alpha,\beta)}$ and $\phi'^{(\alpha,\beta)}$ in (6.3.26) and (6.3.27), (6.4.20) is equivalent to

$$\begin{aligned} \phi(p) - \phi_n^{(SS,2)}(p) = \frac{1}{\eta(p)} \Bigg\{ & \int_{e^{(1)}} \phi^{(3,\infty)}(q) \, G'(p,q) \, dq \\ & + \sum_{j=2}^{n} \int_{e^{(j)}} \left[\phi^{(3,\infty)}(q) - \phi^{(3,\infty)}(q_{n,j}) \right] \, G'(p,q) \, dq \\ & - \sum_{j=1}^{n-1} \int_{e^{(j)}} \left[\phi'^{(3,\infty)}(q) - \phi'^{(3,\infty)}(q_{n,j}) \right] \, G(p,q) \, dq \\ & - \int_{e^{(n)}} \phi'^{(3,\infty)}(q) \, G(p,q) \, dq \Bigg\}. \end{aligned} \tag{6.4.21}$$

In other words, the theoretical error $\epsilon_n^{(SS,2)}$ in (6.4.18) satisfies

$$\eta(p)\epsilon_n^{(SS,2)}(p) = \sum_{j=1}^{n} \left\{ \int_{e^{(j)}} \epsilon_{n,j}^{(SS,2)}(q) \, G'(p,q) \, dq - \int_{e^{(j)}} \epsilon_{n,j}'^{(SS,2)}(q) \, G(p,q) \, dq \right\}, \tag{6.4.22}$$

where

$$\epsilon_{n,j}^{(SS,2)}(q) = \begin{cases} \phi^{(3,\infty)}(q) & j = 1, \\ \phi^{(3,\infty)}(q) - \phi^{(3,\infty)}(q_{n,j}) & j = 2, \ldots, n \end{cases} \tag{6.4.23}$$

and

$$\epsilon_{n,j}'^{(SS,2)}(q) = \begin{cases} \phi'^{(3,\infty)}(q) - \phi'^{(3,\infty)}(q_{n,j}) & j = 1, \ldots, n-1, \\ \phi'^{(3,\infty)}(q) & j = n. \end{cases} \tag{6.4.24}$$

By comparing the components of the SSCBEM error in (6.4.23) and (6.4.24) with the components of the SICBEM error in (6.3.29) and (6.3.30), we have $\epsilon_{n,1}^{(SS,2)} = \epsilon_{n,1}^{(SI,2)}$ and $\epsilon_{n,n}'^{(SS,2)} = \epsilon_{n,n}'^{(SI,2)}$ thus, by (6.3.33) and (6.3.34),

$$\|\epsilon_{n,1}^{(SS,2)}\|_\infty \ll \|\epsilon_{n,1}\|_\infty \tag{6.4.25}$$

and

$$\|\epsilon_{n,n}'^{(SS,2)}\|_\infty \ll \|\epsilon'_{n,n}\|_\infty, \tag{6.4.26}$$

where $\epsilon_{n,j}$ and $\epsilon'_{n,j}$ are the components of the CBEM error ϵ_n in (4.2.20).

To facilitate comparison of the remaining components in the SSCBEM error with those in the SICBEM error and the CBEM error, we use the functions $\phi^{(\alpha,\beta)}$ and $\phi'^{(\alpha,\beta)}$ in (6.3.26) and (6.3.27) to define the theoretical components of the CBEM error and the SICBEM error as

$$\phi(q) - \phi_{n,j} \equiv \phi^{(1,\infty)}(q) - \phi^{(1,\infty)}(q_{n,j}) \tag{6.4.27}$$

and

$$\phi'(q) - \phi'_{n,j} \equiv \phi'^{(1,\infty)}(q) - \phi'^{(1,\infty)}(q_{n,j}). \tag{6.4.28}$$

The coefficients of $\phi^{(1,\infty)}(q)$ in the series solution (5.1.1) are such that $|a_i| > |a_{i+1}|$ for all i in the stripline SBVP (as shown in Table 5.3.1), therefore $\|\phi^{(1,\infty)}\| \gg \|\phi^{(3,\infty)}\|$ and $\|\phi'^{(1,\infty)}\| \gg \|\phi'^{(3,\infty)}\|$. Thus, by comparing the theoretical error components in the CBEM ((6.4.27) and (6.4.28)), the SICBEM ((6.3.29) and (6.3.30)) and the SSCBEM ((6.4.23) and (6.4.24)), we have

$$\|\epsilon_n^{(SS,2)}\|_\infty \ll \|\epsilon_n^{(SI,2)}\|_\infty \ll \|\epsilon_n\|_\infty, \tag{6.4.29}$$

i.e. the SSCBEM error is uniformly smaller than the SICBEM error that is uniformly smaller then the CBEM. Eqn. (6.4.29) is an extension of (6.3.39), and furthermore, it acts as a basis for the hypothesis

$$\|\widetilde{\epsilon}_n^{(SS,2)}\|_\infty \ll \|\widetilde{\epsilon}_n^{(SI,2)}\|_\infty \ll \|\widetilde{\epsilon}_n\|_\infty, \tag{6.4.30}$$

through which we achieve the original aim of the SIM and SSM.

By definition of the theoretical errors in each of the BEMs, we can alternatively express (6.4.29) as

$$\|\phi - \phi_n^{(SS,2)}\|_\infty \ll \|\phi - \phi_n^{(SI,2)}\|_\infty \ll \|\phi - \phi_n\|_\infty, \tag{6.4.31}$$

in which the modified methods (the SICBEM and the SSCBEM) have a minimal error in comparison to the standard method (the CBEM), thereby providing a link with (2.2.19), (3.2.16) and (4.3.4) in previous chapters. Also in agreement with the previous chapters, we now aim to modify each of the new BEMs in such a way that we improve upon the existing errors. However, before doing so, we require the analysis of the errors in both the standard SICBEM and SSCBEM prior to any modification.

6.5 Comparison of the numerical schemes for the stripline problem

We validate the SICBEM and SSCBEM against the standard CBEM by comparing the numerical solutions of the stripline problem with the pseudo-analytic solution derived using the CTM chapter 5.

The relative errors of the SICBEM solution, depicted in Fig. 6.5.1, show a impressive reduction in the localised peak about the singularity in comparison with the CBEM error in Fig. 6.2.2. Furthermore, as the SICBEM is based on piecewise-constant approximations, then similar to the CBEM it also has large errors at the corner points; for justification of this phenomenon we refer the reader to the error analysis of the CBEM in §4.2.1. Unique to the SICBEM error, are the new localised error peaks that occur at the left-hand end-point of the n^{th} element. These are due to the change between the incorporation of the analytic singular behaviour and the piecewise-constant approximations.

The relative errors in the SSCBEM for the stripline SBVP are shown in Fig. 6.5.2. The SSCBEM error peaks about the singular point when n is relatively low, e.g. $n = 24$ in Fig. 6.5.2. Although the magnitude of the peak is significantly smaller than that in the CBEM error in Fig. 6.2.2 for an equivalent n due to the improved modelling of the singular behaviour in the SSCBEM. However, as the SSCBEM is based on piecewise-constant approximations, then similar to the CBEM, it also has large errors at the corner points. Furthermore, the SSCBEM errors in Fig. 6.5.2 are a (ten-fold) reduction on both the CBEM and SICBEM errors in Figs. 6.2.2 and 6.5.1.

A quantitative comparison of the BEMs errors in Figs. 6.2.2, 6.5.1 and 6.5.2 are given in Fig. 6.5.3, where all the errors as presented over the same range. Fig. 6.5.3 is confirmation of (6.4.29) and hypothesis (6.4.30), i.e. the SSCBEM error is uniformly smaller than the SICBEM error, which in turn is uniformly smaller than the CBEM error. Alternatively, we could use the data in Table 6.5.1, where the error in the coefficients of the SICBEM and SSCBEM are smaller than the errors in the coefficients of the analytic series solution, i.e. $|\widetilde{\alpha}_i - a_i| \ll |a_i|$ for $i = 1, 2$, to prove the validity of condition (6.3.36), thus confirming hypothesis (6.4.30).

Further analysis of the BEM results in Figs. 6.5.1 and 6.5.2 is achieved via Richardson's extrapolation of §4.2 which, by the nomenclature of (4.2.48), defines the rate of convergence ρ and the order p of the error. Recall that Table 4.2.1 revealed that the CBEM error for a nonsingular

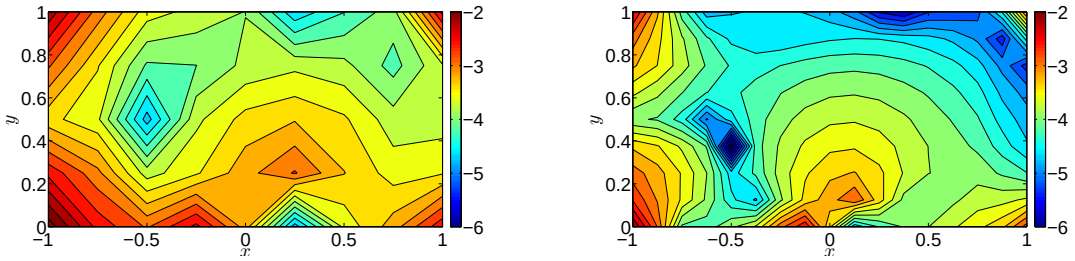

(a) $n = 24$

(b) $n = 48$

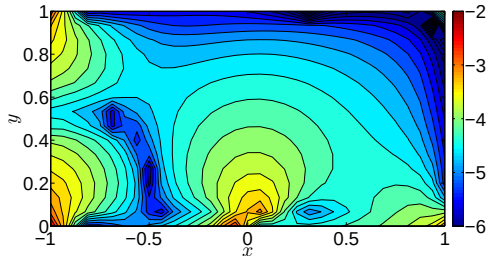

(c) $n = 96$

Figure 6.5.1: *Contour plots of* $\log|\widetilde{\epsilon}_n^{(SI,M)}/\phi|$*, the logarithm of the relative error in the SICBEM solution of the stripline SBVP, for* $M = 2$ *and* $n = 24, 48, 96$*. The singular point is located at* $(x, y) = (0, 0)$*. The SICBEM errors are an improvement upon the CBEM errors in Fig. 6.2.2 since the incorporation of the analytic form of the singularity is the correct functional form, rather than the piecewise-constant interpolation of the CBEM.*

BVP was of order $O(h^{1.75})$, whereas in Table 6.2.1 the order of the CBEM error for a singular BVP was shown to have been eroded to $O(h^{1.3})$. It is precisely this effect that the new methods are designed to combat.

In Table 6.5.2 the rate of convergence and order of both the SICBEM and SSCBEM errors are presented. Table 6.5.2 shows that although the convergence rate (and orders) of the errors in the SICBEM and the SSCBEM are faster than those in the CBEM in Table 6.2.1, it is the SICBEM error that is closer to the expected behaviour of $O(h^{1.75})$. This phenomenon is due to the rate of convergence of the SICBEM being based upon the rate of $\phi_n^{(SI,2)}$, whereas in the SSCBEM, it is based upon the rate of $\psi_n^{(2)}$, the latter of which is zero everywhere near the singularity by definition in (6.4.1). Therefore we cannot directly compare the rates of convergence in the SSCBEM to that

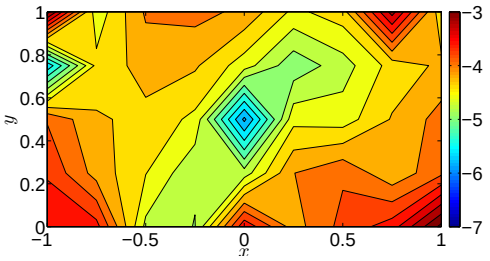

(a) $n = 24$

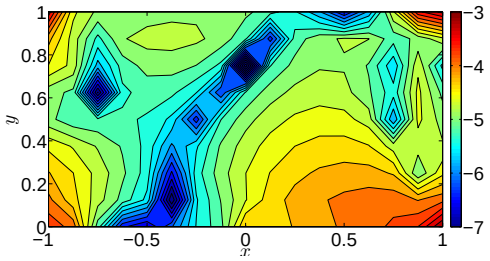

(b) $n = 48$

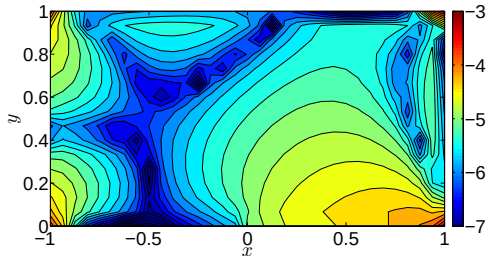

(c) $n = 96$

Figure 6.5.2: *Contour plots of* $\log|\widetilde{\epsilon}_n^{(SS,M)}/\phi|$*, the logarithm of the relative error in the SSCBEM solution of the stripline SBVP, for* $M = 2$ *and* $n = 24, 48, 96$*. The singular point is located at* $(x, y) = (0, 0)$*. The SSCBEM errors are an improvement upon the CBEM errors in Fig. 6.2.2 since its solution is computed by solving a regular BVP.*

		$\lvert\widetilde{\alpha}_i - a_i\rvert$	
i	$\lvert a_i\rvert$	SICBEM	SSCBEM
1	589.3951	1.2235	0.7313
2	128.7857	8.9141	2.3576

Table 6.5.1: *The error in the computed eigenfunction coefficients in the SICBEM and SSCBEM solutions of the stripline problem, for* $M = 2$ *and* $n = 24$*. Here* a_i *are the coefficients of the pseudo-analytic series solution, as computed in chapter 5 for the stripline problem using the CTM. The errors in the coefficients satisfy* $|\widetilde{\alpha}_i - a_i| \ll |a_i|$ *for* $i = 1, 2$*. That is, condition* (6.3.36) *for the error hypothesis* (6.4.30) *is satisfied. The error in the eigenfunction coefficients of the SSCBEM is smaller than that in the SICBEM owing to the SSM being computed on a nonsingular BVP.*

in the SICBEM.

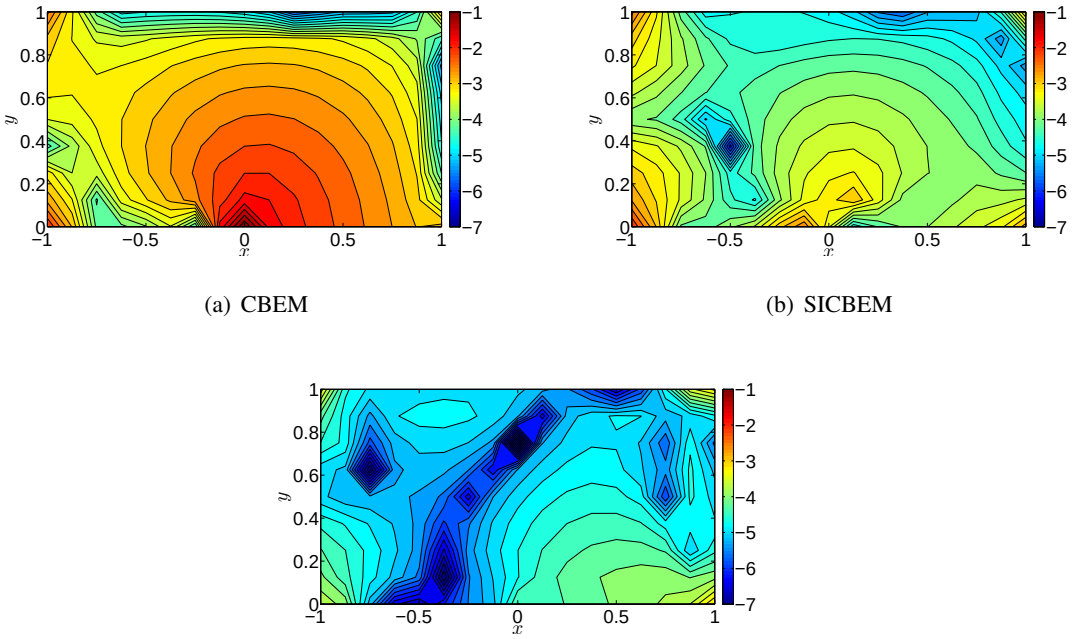

(a) CBEM

(b) SICBEM

(c) SSCBEM

Figure 6.5.3: *A comparison of the logarithm of the relative errors in the CBEM, SICBEM and SSCBEM solutions of the stripline SBVP, for* $n = 48$ *and* $M = 2$ *where the singular point is located at* $(x, y) = (0, 0)$*. The relative errors in the SSCBEM are uniformly smaller over* Ω *than both the SICBEM and the CBEM.*

	SICBEM		SSCBEM	
$n, 2n$	ρ	p	ρ	p
$24, 48$	3.4895	1.8030	2.9550	1.5632
$48, 96$	3.3939	1.7629	3.0807	1.6233

Table 6.5.2: *The convergence rate* ρ *and order* p *of the error in the SICBEM and SSCBEM solutions of the stripline problem, for* $M = 2$ *and* $n = 24, 48, 96$*. The results correspond to the errors depicted in Figs. 6.5.1 and 6.5.2. Compared with the standard CBEM error convergence rates in Table 6.2.1, both the SICBEM and SSCBEM errors have improved the convergence rate by* 37% *and* 20% *respectively. In fact, particularly for the SICBEM, the error order resembles that in the CBEM for a nonsingular BVP in Table 4.2.1.*

Another feature of the data in Table 6.5.2 is the deceleration in the convergence rate in the SICBEM error as n increases. By construction of the SICBEM, the size of the elements over which the analytic form of the singular behaviour is incorporated is dependent on n. Thus with increasing n, the region over which the correct functional form $\phi_s^{(M)}$ is incorporated is reduced and therefore its convergence rate decelerates. In other words, SICBEM error varies with n, so that, empirically at least, we postulate that there exists a significantly large $N \in \mathbb{N}$ such that when $n \geq N$

$$\widetilde{\epsilon}_n^{(SI,2)} = \widetilde{\epsilon}_n, \tag{6.5.1}$$

where $\widetilde{\epsilon}_n$ is the CBEM error, as shown in Fig. 6.2.2. A proof of (6.5.1) is beyond the scope of the present work.

By construction of the SICBEM, the size of the elements over which the analytical behaviour of the singularity is incorporated may be varied. For example, in Fig. 6.5.4 the first and last elements over which the analytical behaviour of the singularity $\phi_s^{(M)}$ in (6.3.2) is incorporated in the SICBEM are of length 0.25 (the standard length of an element when $n = 24$) for all n. By comparison with the standard SICBEM error in Fig. 6.5.4, fixing the length of the two elements reduces the localised error peak that occurs when there is a change between piecewise-constant approximations and the incorporation of the analytic behaviour of the singularity. This phenomenon suggests that the region over which the singular behaviour is incorporated is sufficiently large to model all the singular behaviour absent in the piecewise-constant method. Furthermore, by taking the two elements to be of length 0.25 the order of the error in SICBEM, which is defined in Table 6.5.3, no longer erodes when $n > 24$. That is, fixing the element length prevents the convergence rate in the SICBEM error from decelerating as n increases whilst requiring no extra analysis or programming. However, the *optimum* size of the elements over which the singularity behaviour is incorporated can be determined for each BVP only by experimentation.

Our aim for the remainder of this chapter is to modify each of the outlined BEMs, using the method of chapter 4, in such a way that the order of the error in the numerical solution of the stripline problem is increased beyond the existing $O(h^{1.8})$. Furthermore, by doing so we would be demonstrating that the modified method of chapter 4 can: first, be extended to BEMs other than the CBEM, and; second, be used to accurately solve singular BVPs.

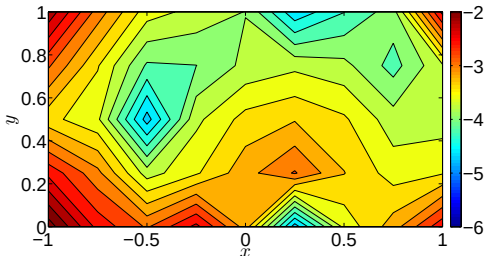

(a) $n = 24$

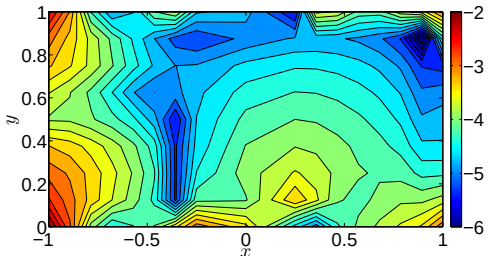

(b) $n = 48$

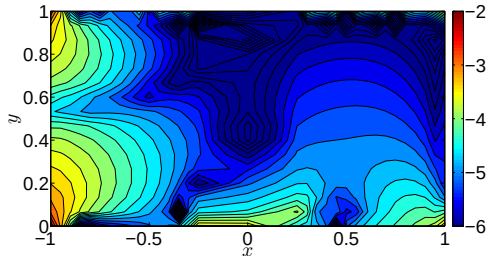

(c) $n = 96$

Figure 6.5.4: *Contour plots of* $\log|\widetilde{\epsilon}_n^{(SI,M)}/\phi|$*, the logarithm of the relative error in the SICBEM solution of the stripline SBVP, for* $M = 2$ *and* $n = 24, 48, 96$*. The elements* $e^{(1)}$ *and* $e^{(n)}$ *over which the singular behaviour is incorporated are of length* 0.25 *for all* n *and the singular point is located at* $(x, y) = (0, 0)$*. Compared with the standard SICBEM error in Fig. 6.5.1, fixing the lengths of the two elements reduces the localised peaks near the singular point, although it requires a non-uniform element distribution when* $n \neq 24$*.*

6.6 Modified boundary element methods

In this section we obtain explicit expressions for the error incurred in the BEM, with the aim of incorporating them *a priori* into the BEM to produce a method with a higher order of error convergence. Hence the following modification technique is based on the modified CBEM in §4.3. Namely, for any standard BEM with solution ϕ_n^* and corresponding theoretical error defined by ϵ_n^*, the modified method with solution $\overline{\phi}_n$ incorporates the leading behaviour of the error ϵ_n^* into the standard BEM *a priori*. For example, if $\overline{\epsilon}_n$ contains the leading behaviour of ϵ_n^*, then

$$\overline{\phi}_n = \phi_n^* + \overline{\epsilon}_n, \tag{6.6.1}$$

$n, 2n$	ρ	p
$24, 48$	3.3333	1.7370
$48, 96$	3.5129	1.8127

Table 6.5.3: *The convergence rate ρ and order p in the error of the SICBEM solution of the stripline SBVP, for $M = 2$ and $n = 24, 48, 96$. The results correspond to the errors depicted in Fig. 6.5.4. The element $e^{(1)}$ and $e^{(n)}$ over which the singular behaviour is incorporated are of length 0.25 for all n. By comparison with the original SICBEM error orders in Table 6.5.2, fixing the length of the elements over which the singular behaviour is incorporated prevents the rate of convergence from decelerating as n increases.*

so that, letting the difference between the true error ϵ_n^* and the approximation $\overline{\epsilon}_n$ be defined by the *discrepancy*

$$\Delta\overline{\epsilon}_n(p) \equiv \epsilon_n^*(p) - \overline{\epsilon}_n(p), \tag{6.6.2}$$

the *modified BEM error* satisfies, by (6.6.1),

$$\begin{aligned} \phi - \overline{\phi}_n &= \phi - (\phi_n^* + \overline{\epsilon}_n) \\ &= \epsilon_n^* - \overline{\epsilon}_n \\ &= \Delta\overline{\epsilon}_n. \end{aligned} \tag{6.6.3}$$

Thus the error of the modified BEM is proportional to an error discrepancy which, as $\|\Delta\overline{\epsilon}_n\| \ll \|\epsilon_n^*\|$, the modified BEM error is less than the standard BEM error, i.e. consistent with (4.3.4), we have

$$\|\phi - \overline{\phi}_n\|_\infty \ll \|\phi - \phi_n^*\|_\infty. \tag{6.6.4}$$

Considering the CBEM then, following (6.2.3), the *theoretical CBEM error* ϵ_n is defined by

$$\epsilon_n(p) \equiv \phi(p) - \phi_n(p) \tag{6.6.5}$$

which, by (6.2.2), satisfies

$$\eta(p)\epsilon_n(p) = \sum_{j=1}^{n} \left\{ \int_{e^{(j)}} (\phi(q) - \phi_{n,j})\, G'(p,q)\, dq - \int_{e^{(j)}} (\phi'(q) - \phi'_{n,j})\, G(p,q)\, dq \right\}. \tag{6.6.6}$$

As per the CBEM in (6.2.2)-(6.2.4), the derivation of the MCBEM was discussed at length in §4.3 therefore only a basic outline is reviewed in this chapter. Considering the Taylor expansions for ϕ and ϕ' about node $q_{n,j}$, and defining the functions

$$J_{k,j}(p) \equiv \int_{e^{(j)}} (q - q_{n,j})^k \; G'(p,q) \; dq \tag{6.6.7}$$

and

$$K_{k,j}(p) \equiv \int_{e^{(j)}} (q - q_{n,j})^k \; G(p,q) \; dq, \tag{6.6.8}$$

then the infinite-series form of (6.6.6) is

$$\eta(p)\epsilon_n(p) = \sum_{j=1}^{n} \sum_{k=1}^{\infty} \frac{1}{k!} \left\{ \frac{\partial^k}{\partial q^k} \left[\phi(q)\right]_{q=q_{n,j}} J_{k,j} - \frac{\partial^k}{\partial q^k} \left[\phi'(q)\right]_{q=q_{n,j}} K_{k,j} \right\}. \tag{6.6.9}$$

Following (6.6.1)-(6.6.4), by the nomenclature of chapter 4, the modified CBEM (MCBEM) with solution $\phi_n^{(m)}$ incorporates $\epsilon_n^{(m)}$, the approximate of the true error ϵ_n. That is, the MCBEM solution is given by

$$\phi_n^{(m)}(p) = \phi_n(p) + \epsilon_n^{(m)}(p), \tag{6.6.10}$$

where

$$\eta(p)\epsilon_n^{(m)}(p) = \sum_{j=1}^{n} \sum_{k=1}^{m} \frac{1}{k!} \left\{ \frac{\partial^k}{\partial q^k} \left[\phi(q)\right]_{q=q_{n,j}} J_{k,j} - \frac{\partial^k}{\partial q^k} \left[\phi'(q)\right]_{q=q_{n,j}} K_{k,j} \right\}. \tag{6.6.11}$$

A rigorous analysis and validation of the error prediction $\epsilon_n^{(m)}$ to the true error ϵ_n was presented in §4.3.2. By comparing $\phi_n^{(m)}$ in (6.6.10) with the exact solution ϕ, the *theoretical MCBEM error* is defined by

$$\varepsilon_{n,m}(p) \equiv \phi(p) - \phi_n^{(m)}(p) \tag{6.6.12}$$

which, by (4.3.2), (6.6.3) and (6.6.5), satisfies

$$\begin{aligned} \varepsilon_{n,m}(p) &= \phi(p) - \left(\phi_n(p) + \epsilon_n^{(m)}(p) \right) \\ &= \epsilon_n(p) - \epsilon_n^{(m)}(p) \\ &= \Delta\epsilon_n^{(m)}(p). \end{aligned} \tag{6.6.13}$$

Thus the error of the MCBEM (6.6.13) is proportional to an error discrepancy, in accordance with the MCBEM error (4.3.43), which since $\|\Delta\epsilon_n^{(m)}\| \ll \|\epsilon_n\|$, is less than the standard CBEM error. By (6.6.4), we therefore have

$$\|\varepsilon_{n,m}\|_\infty \ll \|\epsilon_n\|_\infty. \tag{6.6.14}$$

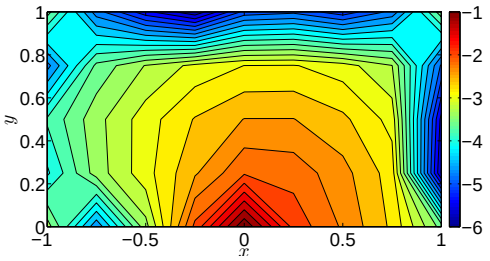

(a) $n = 24$

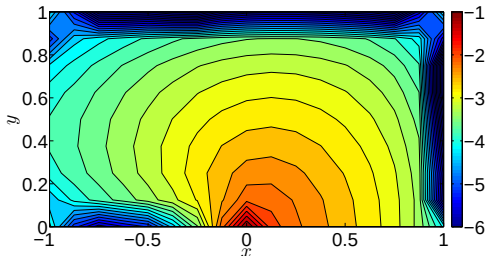

(b) $n = 48$

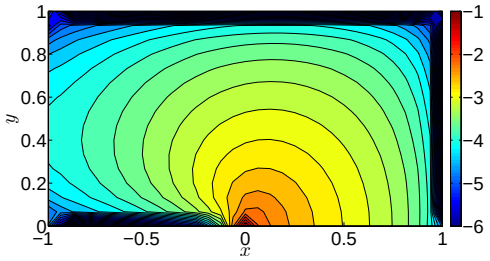

(c) $n = 96$

Figure 6.6.1: *Contour plots of* $\log|\widetilde{\varepsilon}_{n,m}/\phi|$*, the logarithm of the relative error in the MCBEM solution of the stripline SBVP, for* $n = 24, 48, 96$*. The singular point is located at* $(x, y) = (0, 0)$ *and* $m = 4$*, consistent with the MCBEM error for a nonsingular BVP in Fig. 4.4.2*(d)*. The most prominent error in the MCBEM remains in the neighbourhood of the singularity due to the MCBEM failing to model the singular behaviour.*

In keeping with the CBEM error in (6.2.4), the *numerical MCBEM error* is defined by

$$\widetilde{\varepsilon}_{n,m}(p) \equiv \phi(p) - \widetilde{\phi}_n^{(m)}(p), \tag{6.6.15}$$

in which $\widetilde{\phi}_n^{(m)}$ is the *numerical discretised* form of $\phi_n^{(m)}$ in (6.6.10), determined by the computed boundary data from solving the collocated MCBEM in §4.3.4.

The numerical MCBEM error $\widetilde{\varepsilon}_{n,m}$ is depicted in Fig. 6.6.1 for the singular stripline problem. By comparison with the standard CBEM error in Fig. 6.2.2, Fig. 6.6.1 shows that the prominent error peak in the neighbourhood of the singularity also occurs in the MCBEM. That is, by construction of the MCBEM, the method fails to model the singular behaviour in the stripline SBVP. The reason for such behaviour is that although we are building in the leading behaviour of the error in the piecewise-constant approximations, the effect of the singularity remains, which in turn effects the

	Standard			Modified		
n	$\widetilde{\sigma}_n$	ρ	p	$\widetilde{\sigma}_{n,m}$	ρ	p
24	0.0336	2.4938	1.3183	0.0232	2.5375	1.3434
48	0.0135	2.5489	1.3499	0.0091	2.6028	1.3800
96	0.0053			0.0035		

Table 6.6.1: *The RMSE, error convergence rate ρ and error order p in the CBEM (standard) and MCBEM (modified) solutions of the stripline SBVP, for $m = 4$ and $n = 24, 48, 96$. The results correspond to the errors depicted in Figs. 6.2.2 and 6.6.1. Although the order in the MCBEM error is higher than that in the standard CBEM error, it remains significantly lower than the order in the MCBEM for a nonsingular BVP in Table 4.4.2.*

accuracy of the MCBEM.

For further quantification of the behaviour of the MCBEM error, we consider two approaches: first, finding the root-mean-square error (RMSE), and; second, using Richardson's extrapolation in (4.2.48) to define the convergence rate ρ and order p. Consistent with (4.2.43) and (4.4.3), the RMSEs are defined by

$$\widetilde{\sigma}_n \equiv \sqrt{\frac{1}{M_p}\sum_{j=1}^{M_p}\left(\widetilde{\epsilon}_n(p_{M_p,j})\right)^2} \quad \text{for the CBEM} \tag{6.6.16}$$

and

$$\widetilde{\sigma}_{n,m} \equiv \sqrt{\frac{1}{M_p}\sum_{j=1}^{M_p}\left(\widetilde{\varepsilon}_{n,m}(p_{M_p},j)\right)^2} \quad \text{for the MCBEM,} \tag{6.6.17}$$

where M_p is the number of mesh points over the internal grid that is not finer than the boundary resolution. Note for the stripline BVP we take $M_p = (\frac{n}{3}+1)(\frac{n}{6}+1)$.

Extending from the original data for the CBEM in Table 6.2.1, Table 6.6.1 presents the RMSE, order and convergence rate of both the CBEM error and the MCBEM error. The data in Table 6.6.1 shows two features: first, the MCBEM error is smaller than the CBEM, as $\widetilde{\sigma}_{n,m} \ll \widetilde{\sigma}_n$ for all n, and; second, there is only a small deviation between the order (and convergence rate) in the MCBEM error and the standard CBEM error, because both methods fail to model the singular behaviour.

Recall in §6.5, we showed that the SICBEM and SSCBEM were successful modifications of

the CBEM, whereby the error in the neighbourhood of the singular point could be significantly reduced. Therefore, the culmination is achieved when joining the methods that incorporate the singular behaviour with an augmentation by the predicted error.

6.6.1 The modified singularity incorporation method (MSICBEM)

In order to modify the SICBEM, we first establish the leading behaviour of its theoretical error $\epsilon_n^{(SI,M)}$, so that $\bar{\epsilon}_n$ in (6.6.1) can be determined. Given that the SICBEM is based upon the CBEM, then the leading behaviour of $\epsilon_n^{(SI,M)}$ is based upon the leading behaviour of the CBEM error, defined as $\epsilon_n^{(m)}$ in (6.6.11). That is, recalling the SICBEM error in (6.3.28), we have $(2n-2)$ components $\epsilon_{n,j}^{(SI,2)}$ and $\epsilon_{n,j}^{\prime(SI,2)}$ of $\epsilon_n^{(SI,2)}$, defined by

$$\epsilon_{n,j}^{(SI,2)} \equiv \phi(q) - \phi_{n,j}, \quad j = 2, \ldots, n \tag{6.6.18}$$

and

$$\epsilon_{n,j}^{\prime(SI,2)} \equiv \phi'(q) - \phi'_{n,j}, \quad j = 1, \ldots, n-1, \tag{6.6.19}$$

from taking piecewise-constant interpolation. We again use Taylor expansions of ϕ and ϕ' about the node $q_{n,j}$ so that, by (6.6.7) and (6.6.8), the theoretical SICBEM error $\epsilon_n^{(SI,2)}$ in (6.3.28) satisfies

$$\begin{aligned}\eta(p)\epsilon_n^{(SI,2)}(p) = &\int_{e^{(1)}} \phi^{(3,\infty)}(q)\; G'(p,q)\; dq + \sum_{j=2}^{n}\sum_{k=1}^{\infty} \frac{1}{k!}\frac{\partial^k}{\partial q^k}\left[\phi(q)\right]_{q=q_{n,j}} J_{k,j} \\ &- \sum_{j=1}^{n-1}\sum_{k=1}^{\infty} \frac{1}{k!}\frac{\partial^k}{\partial q^k}\left[\phi'(q)\right]_{q=q_{n,j}} K_{k,j} - \int_{e^{(n)}} \phi'^{(3,\infty)}(q)\; G(p,q)\; dq. \end{aligned} \tag{6.6.20}$$

Truncating the infinite-series in the SICBEM error $\epsilon_n^{(SI,2)}$ in (6.6.20) to order m yields the *truncated-series SICBEM error* $\epsilon_{n,m}^{(SI,2)}$ that satisfies

$$\eta(p)\epsilon_{n,m}^{(SI,2)}(p) = \sum_{j=1}^{n}\left\{\int_{e^{(j)}} \epsilon_{n,m,j}^{(SI,2)}(q)\; G'(p,q)\; dq - \int_{e^{(j)}} \epsilon_{n,m,j}^{\prime(SI,2)}(q)\; G(p,q)\; dq\right\}, \tag{6.6.21}$$

where

$$\epsilon_{n,m,j}^{(SI,2)}(q) = \begin{cases} \phi^{(3,\infty)}(q) & j = 1, \\ \displaystyle\sum_{k=1}^{m} \frac{(q-q_{n,j})^k}{k!}\frac{\partial^k}{\partial q^k}\left[\phi(q)\right]_{q=q_{n,j}} & j = 2, \ldots, n \end{cases} \tag{6.6.22}$$

and

$$\epsilon'^{(SI,2)}_{n,m,j}(q) = \begin{cases} \displaystyle\sum_{k=1}^{m} \frac{(q-q_{n,j})^k}{k!} \frac{\partial^k}{\partial q^k} \left[\phi'(q)\right]_{q=q_{n,j}} & j = 1, \ldots, n-1, \\ \phi'^{(3,\infty)}(q) & j = n. \end{cases} \tag{6.6.23}$$

Since the error $\epsilon^{(SI,2)}_{n,m}$ is the leading behaviour of the true error in the SICBEM $\epsilon^{(SI,2)}_{n}$, we take $\epsilon^{(SI,2)}_{n,m}$ in (6.6.1) and then the modified singularity incorporated CBEM (MSICBEM) with solution $\phi^{(MSI,2)}_{n,m}$ is given by

$$\phi^{(MSI,2)}_{n,m}(p) = \phi^{(SI,2)}_{n}(p) + \epsilon^{(SI,2)}_{n,m}(p). \tag{6.6.24}$$

Recall that in §6.3 we showed that collocating the standard SICBEM at the mid-points $p = q_{n,i}$ generated a system of n equations (6.3.8) expressible in the form $\mathbf{M}\mathbf{x}_{SI} = \mathbf{t}$, where $\mathbf{x}_{SI}$ contained the unknown boundary data. Now, collocating the MSICBEM (6.6.24) at the same mid-points $p = q_{n,i}$ yields a system of n equations, which is similarly expressible in the form $\mathbf{M}\mathbf{x}_{MSI} = \mathbf{t} + \mathbf{e}^{MSI}$, i.e. augmented by an error vector. The solution vector $\mathbf{x}_{MSI}$ now contains the unknown mid-element nodal values of $\phi_{n,j}$ on $\partial\Omega_{\phi'}$ and $\phi'_{n,j}$ on $\partial\Omega_{\phi}$ and the two unknown singularity coefficients α_1 and α_2. In the system $\mathbf{M}\mathbf{x}_{MSI} = \mathbf{t} + \mathbf{e}^{MSI}$, the error vector $\mathbf{e}^{MSI}$ has components

$$e^{MSI}_{i} = \sum_{j=1}^{n} \left\{ \int_{e^{(j)}} \epsilon^{(SI,2)}_{n,m,j}\, G'(q_{n,i}, q)\, dq - \epsilon'^{(SI,2)}_{n,m,j}\, G(q_{n,i}, q)\, dq \right\}, \tag{6.6.25}$$

in which $\epsilon^{(SI,2)}_{n,m,j}$ and $\epsilon'^{(SI,2)}_{n,m,j}$ are defined in (6.6.22) and (6.6.23). The solution of $\mathbf{M}\mathbf{x}_{MSI} = \mathbf{t} + \mathbf{e}^{MSI}$ yields the unknown boundary data that supplements the original boundary conditions in the stripline SBVP. With a complete set of boundary data $\phi^{(MSI,2)}_{n,m}$ in (6.6.24) can be computed at any point in the domain which, in accordance with §6.3, we define as the *numerical discretised MSICBEM solution*. Given $\phi^{(MSI,2)}_{n,m}$ in (6.6.24) is the theoretical discretised solution, we define the numerical discretised solution as $\widetilde{\phi}^{(MSI,2)}_{n,m}$, which satisfies

$$\widetilde{\phi}^{(MSI,2)}_{n,m}(p) = \widetilde{\phi}^{(SI,2)}_{n}(p) + \epsilon^{(SI,2)}_{n,m}(p), \tag{6.6.26}$$

where $\widetilde{\phi}^{(SI,2)}_{n}$ is the numerical discretised solution of the SICBEM obtained by (6.3.17) and (6.3.18).

6.6.2 The modified singularity subtraction method (MSSCBEM)

In contrast to the MCBEM and the MSICBEM, the modification of the SSCBEM does not use the leading behaviour of the theoretical SSCBEM error $\epsilon_n^{(SS,2)}$. In fact we require only the leading behaviour of the error incurred in $\psi_n^{(M)}$ in (6.4.5).

The error in $\psi_n^{(M)}$, defined by $\epsilon_n^{(\psi,M)}$, satisfies

$$\eta(p)\epsilon_n^{(\psi,M)}(p) = \sum_{j=1}^{n}\left\{\int_{e^{(j)}}\left(\psi^{(M)}(q)-\psi_{n,j}^{(M)}\right)G'(p,q)\,dq - \int_{e^{(j)}}\left(\psi'^{(M)}(q)-\psi_{n,j}'^{(M)}\right)G(p,q)\,dq\right\}. \tag{6.6.27}$$

Note that in the present form of (6.6.27), the balancing approximations imposed in the SSCBEM are not accounted for as they are specific to the BVP to which the BEM is applied.

As discussed in §6.4, the two balancing approximations for the stripline problem are $\psi_{n,1}^{(2)}=0$ and $\psi_{n,n}'^{(2)}=0$, in which case $(2n-2)$ of the integrands in (6.6.27) contain the error resulting from piecewise-constant interpolation. Therefore, using Taylor expansions of ψ and ψ' about the node $q_{n,j}$, the terms $\psi^{(2)}(q)-\psi_{n,j}^{(2)}$ and $\psi'^{(2)}(q)-\psi_{n,j}'^{(2)}$ are expressible as infinite series so that (6.6.27) becomes

$$\eta(p)\epsilon_n^{(\psi,2)}(p) = \sum_{j=1}^{n}\left\{\int_{e^{(j)}}\epsilon_{n,j}^{(\psi,2)}(q)\,G'(p,q)\,dq - \int_{e^{(j)}}\epsilon_{n,j}'^{(\psi,2)}(q)\,G(p,q)\,dq\right\}, \tag{6.6.28}$$

where

$$\epsilon_{n,j}^{(\psi,2)}(q) = \begin{cases} \psi^{(2)}(q) & j=1, \\ \displaystyle\sum_{k=1}^{\infty}\frac{(q-q_{n,j})^k}{k!}\frac{\partial^k}{\partial q^k}\left[\psi^{(2)}(q)\right]_{q=q_{n,j}} & j=2,\ldots,n \end{cases} \tag{6.6.29}$$

and

$$\epsilon_{n,j}'^{(\psi,2)}(q) = \begin{cases} \displaystyle\sum_{k=1}^{\infty}\frac{(q-q_{n,j})^k}{k!}\frac{\partial^k}{\partial q^k}\left[\psi'^{(2)}(q)\right]_{q=q_{n,j}} & j=1,\ldots,n-1, \\ \psi'^{(2)}(q) & j=n. \end{cases} \tag{6.6.30}$$

Truncating the infinite series of (6.6.29) and (6.6.30) to order m yields $\epsilon_n^{(\psi,2,m)}$, which is the m^{th} order truncation of $\epsilon_n^{(\psi,2)}$, that satisfies

$$\eta(p)\epsilon_n^{(\psi,2,m)}(p) = \sum_{j=1}^{n}\left\{\int_{e^{(j)}}\epsilon_{n,j}^{(\psi,2,m)}(q)\,G'(p,q)\,dq - \int_{e^{(j)}}\epsilon_{n,j}'^{(\psi,2,m)}(q)\,G(p,q)\,dq\right\}, \tag{6.6.31}$$

where

$$\epsilon_{n,j}^{(\psi,2,m)}(q) = \begin{cases} \psi^{(2)}(q) & j = 1, \\ \displaystyle\sum_{k=1}^{m} \frac{(q-q_{n,j})^k}{k!} \frac{\partial^k}{\partial q^k} \left[\psi^{(2)}(q)\right]_{q=q_{n,j}} & j = 2, \ldots, n \end{cases} \tag{6.6.32}$$

and

$$\epsilon_{n,j}^{\prime(\psi,2,m)}(q) = \begin{cases} \displaystyle\sum_{k=1}^{m} \frac{(q-q_{n,j})^k}{k!} \frac{\partial^k}{\partial q^k} \left[\psi^{\prime(2)}(q)\right]_{q=q_{n,j}} & j = 1, \ldots, n-1, \\ \psi^{\prime(2)}(q) & j = n. \end{cases} \tag{6.6.33}$$

Thus, given that $\epsilon_n^{(\psi,2,m)}$ is an approximation of the true error $\epsilon_n^{(\psi,2)}$, we have

$$\psi_{n,m}^{(2)} = \psi_n^{(2)}(p) + \epsilon_n^{(\psi,2,m)} \tag{6.6.34}$$

which, following (6.6.1), the modified SSCBEM (MSSCBEM) with solution $\phi_{n,m}^{(MSS,2)}$ is given by

$$\begin{aligned} \phi_{n,m}^{(MSS,2)}(p) &= \psi_{n,m}^{(2)}(p) + \phi_s^{(2)}(p) \\ &= \left(\psi_n^2(p) + \epsilon_n^{(\psi,2,m)}(p)\right) + \phi_s^{(2)}(p) \\ &= \phi_n^{(SS,2)}(p) + \epsilon_n^{(\psi,2,m)}(p). \end{aligned} \tag{6.6.35}$$

In other words, the MSSCBEM in (6.6.35) is derived by incorporating $\epsilon_n^{(\psi,2,m)}$ into the standard SSCBEM *a priori*.

Recall that collocating $\psi_n^{(2)}(p)$ in the SSCBEM at the mid-points $p = q_{n,i}$ generated a system of n equations (6.4.12) expressible in the form $\mathbf{P}\mathbf{x}_{SS} = \mathbf{q}$, where $\mathbf{x}_{SS}$ contained the unknown boundary data, as discussed in §6.4. Now, collocating $\psi_{n,m}^{(2)}(p)$ in (6.6.31) at the mid-points $p = q_{n,i}$ yields a system of n equations expressible as $\mathbf{P}\mathbf{x}_{MSS} = \mathbf{q} + \mathbf{e}^{MSS}$, where $\mathbf{x}_{MSS}$ contains the unknown mid-element nodal values of $\psi_{n,j}^{(2)}$ on $\partial\Omega_{\phi'}$ and $\psi_{n,j}^{\prime(2)}$ on $\partial\Omega_{\phi}$ and the two unknown singularity coefficients α_1 and α_2. By the argument preceding (6.6.25) the error vector $\mathbf{e}^{MSS}$ has components

$$e_i^{MSS} = \sum_{j=1}^{n} \left\{ \int_{e^{(j)}} \epsilon_{n,j}^{(\psi,2,m)}(q)\, G'(q_{n,i}, q)\, dq - \int_{e^{(j)}} \epsilon_{n,j}^{\prime(\psi,2,m)}(q)\, G(q_{n,i}, q)\, dq \right\}, \tag{6.6.36}$$

in which $\epsilon_{n,j}^{(\psi,2,m)}$ and $\epsilon_{n,j}^{\prime(\psi,2,m)}$ are respectively defined in (6.6.32) and (6.6.33).

The solution of $\mathbf{P}\mathbf{x}_{MSS} = \mathbf{q} + \mathbf{e}^{MSS}$ yields the unknown boundary data that supplements the original boundary conditions in the stripline SBVP. Using the complete boundary data $\psi_{n,m}^{(2)}$ in

(6.6.31) can be determined at any point in the domain which, in accordance with (6.4.14) and (6.4.15), we define as the *numerical discretised solution* $\widetilde{\psi}_{n,m}^{(2)}$. To distinguish this from the theoretical discretised $\psi_{n,m}^{(2)}$ in (6.6.34), $\widetilde{\psi}_{n,m}^{(2)}$ is given by

$$\widetilde{\psi}_{n,m}^{(2)} = \widetilde{\psi}_{n}^{(2)}(p) + \epsilon_{n}^{(\psi,2,m)}, \tag{6.6.37}$$

in which $\widetilde{\psi}_{n}^{(2)}$ in (6.4.14) is the numerical discretised form of $\psi_{n}^{(2)}$ in the SSCBEM. Finally, by (6.6.37), the *numerical discretised MSSCBEM solution* is

$$\begin{aligned}\widetilde{\phi}_{n,m}^{(MSS,2)}(p) &= \widetilde{\psi}_{n,m}^{(2)}(p) + \widetilde{\phi}_{s}^{(2)}(p) \\ &= \widetilde{\phi}_{n}^{(SS,2)}(p) + \epsilon_{n}^{(\psi,2,m)}(p),\end{aligned} \tag{6.6.38}$$

where, in keeping with (6.4.16), $\widetilde{\phi}_{n}^{(SS,2)}(p) = \widetilde{\psi}_{n}^{(2)}(p) + \widetilde{\phi}_{s}^{(2)}(p)$ and $\widetilde{\phi}_{s}^{(2)}$ is the series $\phi_{s}^{(2)}$ with computed coefficients $\widetilde{\alpha}_{i}$.

6.6.3 Error analysis of the MSICBEM and MSSCBEM

Comparing the theoretical discretised MSICBEM solution $\phi_{n,m}^{(MSI,2)}$ in (6.6.24) with the exact solution ϕ and following (4.3.42), the *theoretical MSICBEM error* is defined by

$$\varepsilon_{n,m}^{(MSI,2)}(p) \equiv \phi(p) - \phi_{n,m}^{(MSI,2)}(p), \tag{6.6.39}$$

where, by (6.6.24) and (6.6.3), $\varepsilon_{n,m}^{(MSI,2)}$ is proportional to an error discrepancy. Namely, taking the *discrepancy*

$$\Delta\epsilon_{n,m}^{(SI,2)}(p) \equiv \epsilon_{n}^{(SI,2)}(p) - \epsilon_{n,m}^{(SI,2)}(p), \tag{6.6.40}$$

by (6.6.24), (6.6.3) and (6.6.39), we have

$$\begin{aligned}\varepsilon_{n,m}^{(MSI,2)}(p) &= \phi(p) - \left(\phi_{n}(p) + \epsilon_{n,m}^{(MSI,2)}(p)\right) \\ &= \epsilon_{n}(p) - \epsilon_{n,m}^{(MSI,2)}(p) \\ &= \Delta\epsilon_{n,m}^{(MSI,2)}(p).\end{aligned} \tag{6.6.41}$$

Similarly, by comparing the MSSCBEM theoretical solution $\phi_{n,m}^{(MSS,2)}$ in (6.6.35) with the exact solution ϕ, the *theoretical MSSCBEM error* is defined by

$$\varepsilon_{n,m}^{(MSS,2)}(p) \equiv \phi(p) - \phi_{n,m}^{(MSS,2)}(p). \tag{6.6.42}$$

The MSSCBEM error in (6.6.42) is also proportional to an error discrepancy. That is, letting the difference between the truncated error $\epsilon_n^{(\psi,2,m)}$ and the exact error $\epsilon_n^{(\psi,2)}$ be defined by the *discrepancy*

$$\Delta\epsilon_{n,m}^{(\psi,2)}(p) \equiv \epsilon_n^{(\psi,2)}(p) - \epsilon_n^{(\psi,2,m)}(p), \tag{6.6.43}$$

then (6.4.1), (6.4.6), (6.6.35) and (6.6.42) yield

$$\begin{aligned}
\varepsilon_{n,m}^{(MSS,2)}(p) &= \phi(p) - (\phi_n^{(SS,2)}(p) + \epsilon_n^{(\psi,2,m)}(p)) \\
&= \psi^{(2)}(p) + \phi_s^{(2)}(p) - (\psi_n^{(2)}(p) + \phi_s^{(2)}(p)) - \epsilon_n^{(\psi,2,m)}(p) \\
&= \epsilon_n^{(\psi,2)}(p) - \epsilon_n^{(\psi,2,m)}(p) \\
&= \Delta\epsilon_{n,m}^{(\psi,2)}(p).
\end{aligned} \tag{6.6.44}$$

Thus, by (6.6.41), we have

$$\|\varepsilon_{n,m}^{(MSI,2)}\|_\infty = \|\Delta\epsilon_{n,m}^{(MSI,2)}\|_\infty, \tag{6.6.45}$$

and, by (6.6.44), we have

$$\|\varepsilon_{n,m}^{(MSS,2)}\|_\infty = \|\Delta\epsilon_{n,m}^{(\psi,2)}\|_\infty. \tag{6.6.46}$$

In other words, the errors in the MSICBEM (6.6.41) and the MSSCBEM (6.6.44), which are proportional to error discrepancies, are smaller than the errors in both the SICBEM in (6.3.25) and the SSCBEM in (6.4.18) as they are proportional to an error. Hence

$$\|\varepsilon_{n,m}^{(MSI,2)}\|_\infty \ll \|\epsilon_n^{(SI,2)}\|_\infty \tag{6.6.47}$$

and

$$\|\varepsilon_{n,m}^{(MSS,2)}\|_\infty \ll \|\epsilon_n^{(SS,2)}\|_\infty. \tag{6.6.48}$$

Recall that in (6.4.29) we had

$$\|\epsilon_n^{(SS,2)}\|_\infty \ll \|\epsilon_n^{(SI,2)}\|_\infty \ll \|\epsilon_n\|_\infty, \tag{6.6.49}$$

where ϵ_n is the error in the standard CBEM. By (6.6.47) and (6.6.48), we now have

$$\|\varepsilon_{n,m}^{(MSI,2)}\|_\infty \ll \|\epsilon_n^{(SI,2)}\|_\infty \ll \|\epsilon_n\|_\infty \tag{6.6.50}$$

and

$$\|\varepsilon_{n,m}^{(MSS,2)}\|_\infty \ll \|\epsilon_n^{(SS,2)}\|_\infty \ll \|\epsilon_n\|_\infty, \tag{6.6.51}$$

thereby achieving the aim of modifying the SICBEM and SSCBEM. However, in contrast to the original hypothesis in (6.4.29), we cannot theoretically quantify which of the MSICBEM and MSSCBEM are of superior accuracy.

6.7 Comparison of the modified numerical schemes for the stripline problem

To recap over §4.4, for a nonsingular BVP the modified CBEM recovered an error of order $O(h^m)$, where m could be chosen *a priori*. For example, in accordance with (4.4.2), the order of the error in the MCBEM was theoretically predicted as

$$\begin{cases} O(h^2) & m = 1, \\ O(h^4) & m = 2, 3, \\ O(h^6) & m = 4, 5, \\ O(h^8) & m = 6, 7. \end{cases} \tag{6.7.1}$$

The basis of the error order prediction in (6.7.1) for the modified CBEM is as follows. By (6.6.1)-(6.6.3), for a modified BEM with solution $\overline{\phi}$ the error $\overline{\varepsilon}_n$ is given by

$$\overline{\varepsilon}_n = \phi - \overline{\phi} = \phi - \phi^* - \overline{\epsilon}_n, \tag{6.7.2}$$

where ϕ^* is the solution of a standard BEM, ϵ_n^* is its error and $\overline{\epsilon}_n$ contains the leading order of the error ϵ_n^*. Provided the first two terms on the right-hand side of (6.7.2) are of an equal order, the order of the modified BEM was determined by the order of the incorporated error $\overline{\epsilon}_n$. However, for a singular BVP the first two terms on the right-hand side of (6.7.2) are not of an equal order. This is because the presence of a singularity adversely effects the convergence rate of a given numerical BEM, as pictorially demonstrated by the error in the CBEM solution of the stripline problem in Fig. 6.2.2 and in the MCBEM solution of the stripline problem in Fig. 6.6.1.

We applied the SICBEM and SSCBEM to recover the rate of convergence when a singularity exists. However, as only the leading behaviour of the singularity is taken into account in the SICBEM and SSCBEM, because $\phi_s^{(M)}$ is implemented for finite values of M, the singularity affects the numerical methods. That is, we do not recover the theoretically predicted $O(h^2)$ in Table 6.5.2 for either

method. Similarly, by construction of the MSICBEM and MSSCBEM, although they improve the accuracy in the SICBEM and SSCBEM, we expect the error orders to be lower than the predicted $O(h^m)$ error in (6.7.1). In the remainder of this chapter, we provide a quantification of the error orders in the MSICBEM and the MSSCBEM for the stripline SBVP of Fig. 5.1.2 by a mixture of graphical and data analysis.

Following (6.6.16) and (6.6.17), we define the RMSEs by

$$\widetilde{\sigma}_n^{(SI,M)} \equiv \sqrt{\frac{1}{M_p}\sum_{j=1}^{M_p}\left(\widetilde{\epsilon}_n^{(SI,M)}(p_{M,j})\right)^2} \quad \text{for the SICBEM} \tag{6.7.3}$$

and

$$\widetilde{\sigma}_n^{(SS,M)} \equiv \sqrt{\frac{1}{M_p}\sum_{j=1}^{M_p}\left(\widetilde{\epsilon}_n^{(SS,M)}(p_{M,j})\right)^2} \quad \text{for the SSCBEM,} \tag{6.7.4}$$

then similarly for the modified counterparts by

$$\widetilde{\sigma}_n^{(MSI,M)} \equiv \sqrt{\frac{1}{M_p}\sum_{j=1}^{M_p}\left(\widetilde{\varepsilon}_{n,m}^{(MSI,M)}(p_{M,j})\right)^2} \quad \text{for the MSICBEM} \tag{6.7.5}$$

and

$$\widetilde{\sigma}_n^{(MSS,M)} \equiv \sqrt{\frac{1}{M_p}\sum_{j=1}^{M_p}\left(\widetilde{\varepsilon}_{n,m}^{(MSS,M)}(p_{M,j})\right)^2} \quad \text{for the MSSCBEM,} \tag{6.7.6}$$

where M_p are the number of mesh points taken over the internal grid. The convergence rate and order of the error in each of the BEMs will be defined using Richardson's extrapolation in (4.2.48). A depiction of the error in the MSICBEM solution of the stripline problem is given in Fig. 6.7.1 for $n = 24, 48, 96$ and fixed $m = 4$. By comparing Fig. 6.7.1 with the SICBEM counterpart in Fig. 6.5.1, it is evident from the scalings of the contour colour mappings that the MSICBEM error is substantially smaller than the SICBEM error, in accordance with (6.6.50). Moreover, in the MSICBEM error of Fig. 6.7.1, the dominant error, which now exists in the neighbourhood of the origin, is a demonstration of the $O(r^{\lambda_{M+1}})$ error in the MSICBEM due to the finite truncation of the correct functional form $\phi_s^{(M)}$ in (6.3.3).

The order of the errors in the SICBEM and MSICBEM solutions of the stripline problem in Figs. 6.5.1 and 6.7.1 are given in Table 6.7.1, along with the RMSEs and convergence rates for $n = 24, 48$ and 96. Along with its graphical counterpart, Fig. 6.7.1, Table 6.7.1 demonstrates three features: first, taking only $m = 4$ leading terms in $\epsilon_{n,m}^{(SI,2)}$ in the MSICBEM of (6.6.26) produces

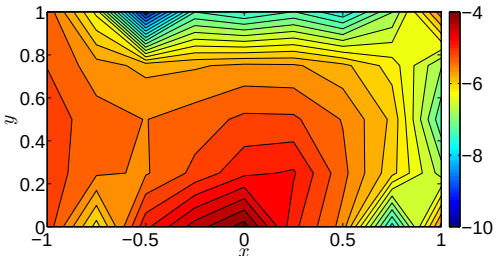

(a) $n = 24$

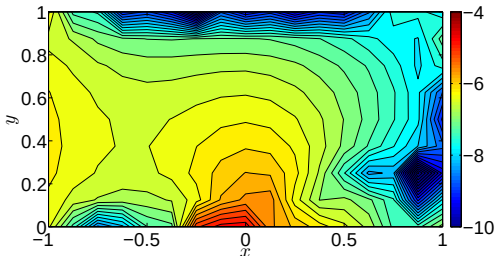

(b) $n = 48$

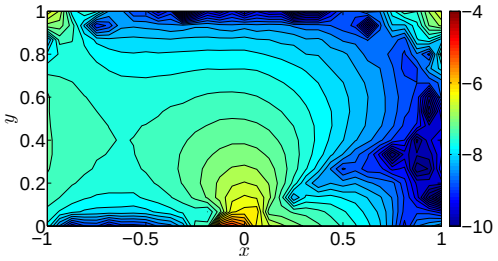

(c) $n = 96$

Figure 6.7.1: *Contour plots of* $\log|\widetilde{\varepsilon}_{n,m}^{(MSIC,M)}/\phi|$*, the logarithm of the relative error in the MSICBEM solution of the stripline SBVP, for* $M = 2$*,* $m = 4$ *and* $n = 24, 48, 96$*. The singular point is located at* $(x, y) = (0, 0)$*. Although a prominent localised error peak is occurring at the singular point, its magnitude is prominently smaller than in the SICBEM error in Fig. 6.5.1. Moreover, by comparison with Fig. 6.5.1, the scaling in the colour mapping shows that the MSICBEM errors are smaller than the standard SICBEM errors, in accordance with* (6.6.50)*.*

a significantly smaller RMSE than in the standard SICBEM. Second, although a localised peak remains about the singularity in the MSICBEM error, its magnitude is prominently smaller than in the SICBEM error, e.g. an error of third order is obtained in the MSICBEM for only $n = 24$. Third, the convergence rate in the MSICBEM error decelerates when $n > 24$ (consistent with the SICBEM error in Table 6.7.1), due to the region of in which the correct functional $\phi_s^{(M)}$ is incorporated being dependent upon n.

In the standard SICBEM the length of the first and last elements were varied to prevent the eroding order of the SICBEM error with increasing n. However, such a remedy is no longer plausible in the MSICBEM owing to the modified method requiring a uniform element distribution. For example,

	Standard			Modified		
n	$\widetilde{\sigma}_n^{(SI,2)}$	ρ	p	$\widetilde{\sigma}_{n,m}^{(MSI,2)}$	ρ	p
24	0.0037	3.4895	1.8030	2.0788×10^{-5}	7.9977	2.9996
48	0.0010	3.3939	1.7629	2.5992×10^{-6}	4.3751	2.1293
96	3.0904×10^{-4}			5.9409×10^{-7}		

Table 6.7.1: *The RMSE σ, error order p and error convergence rate ρ of the SICBEM (standard) and MSICBEM (modified) solutions of the stripline SBVP, for $M = 2$, $m = 4$ and $n = 24, 48, 96$. The results correspond to the errors depicted in Figs. 6.5.1 and 6.7.1. We achieve an increase in the rate of convergence (up to third order) by applying the MSICBEM. However, the convergence rate rapidly decelerates with increasing n, due to the dependence of region over which the correct functional $\phi_s^{(M)}$ is incorporated upon n.*

if n is doubled after fixing the length of an element then the discretised system in the MSICBEM contains an error of $O(8h^3)$ instead of $O(h^3)$, thus resulting in a fixed maximum error, dependent upon the length of the element, and minimal variation in the relative error for differing values of n; this is demonstrated in the error of MSICBEM in Fig. 6.7.2.

As for the error in the MSSCBEM solution of the stripline problem, this is depicted in Fig. 6.7.3 for $n = 24, 48, 96$ and $m = 4$. By comparing Fig. 6.7.3 with the standard SSCBEM errors in Fig. 6.5.2, the MSSCBEM has reduced only the localised error peaks that occur in the corners of the domain in the standard SSCBEM error. That is, the SSCBEM has dealt with the singularity therefore Fig. 6.7.3 is a manifestation of the dominance of the $O(r^{\lambda_{M+1}})$ singular behaviour in the MSSCBEM.

For a quantification into the effect of applying a MSSCBEM, we require the RMSE, error order and error convergence rate of both the MSSCBEM and the standard SSCBEM solution of the stripline problem for different values of n: this is presented in Table 6.7.2. Table 6.7.2 shows two features: first, the MSSCBEM error is smaller than the standard SCCBEM error, as the MSSCBEM RMSE is a reduction (up to a hundredfold) upon the SSCBEM RMSE, and; second, the order of the MSSCBEM error is approximately double that of the SSCBEM error. That is, the error in the MSSCBEM is of third order and, contrary to the MSICBEM error in Table 6.7.1, this does not erode as n increases.

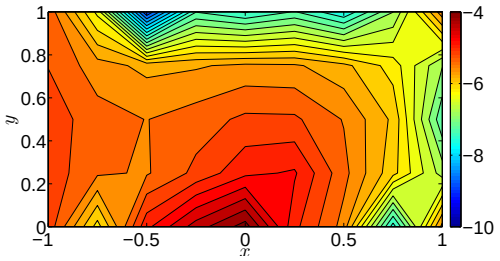

(a) $n = 24$

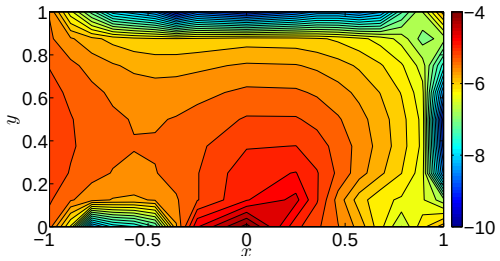

(b) $n = 48$

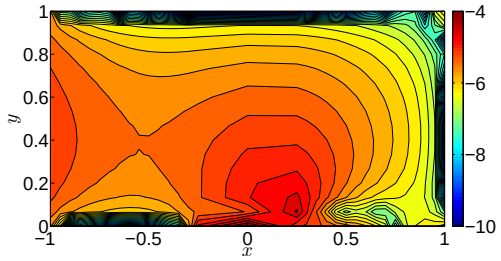

(c) $n = 96$

Figure 6.7.2: *Contour plots of* $\log|\widetilde{\varepsilon}_{n,m}^{(MSIC,M)}/\phi|$*, the logarithm of the relative error in the MSICBEM solution of the stripline SBVP, for* $M = 2$*,* $m = 4$ *and* $n = 24, 48, 96$*. The singular point is located at* $(x, y) = (0, 0)$ *and the first and last elements are of length* $e^{(1)} = e^{(n)} = 0.25$ *to match with Fig. 6.5.4. The maximum error in each of the sub-figures is fixed, regardless of the choice of* n*, due the large error being built into the pre-inversion of the MSICBEM.*

Although errors of order $O(h^3)$ are shown in Tables 6.7.1 and 6.7.2 for $m = 4$ in the MSICBEM and MSSCBEM solution of the stripline problem, we do not recover the theoretically predicted error orders. That is, we do not recover an error of order $O(h^6)$ when $m = 4$, which was obtained for a nonsingular BVP in chapter 4, in either modified method. The same is true for other values m, as demonstrated in Table 6.7.3. This phenomenon is a demonstration of the $O(r^{\lambda_{M+1}})$ truncation of $\phi_s^{(M)}$, that is incorporated/subtracted from the CBEM in both the MSICBEM and MSSCBEM. Thus it is the choice of M that determines the magnitude of the residual singular behaviour of order $O(r^{\lambda_{M+1}})$ which, in turn, determines the order of the error in the modified BEMs. Hence to further increase the order of the error in the numerical methods, we require a higher number of terms M to be taken in the correct functional $\phi_s^{(M)}$ in (6.3.2) in both the MSICBEM and the MSSCBEM.

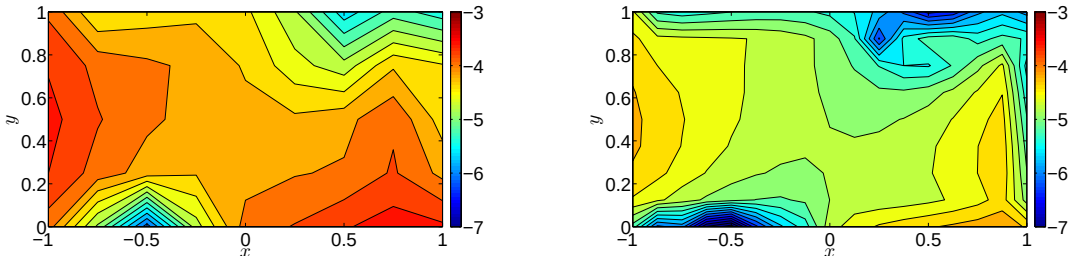

(a) $n = 24$

(b) $n = 48$

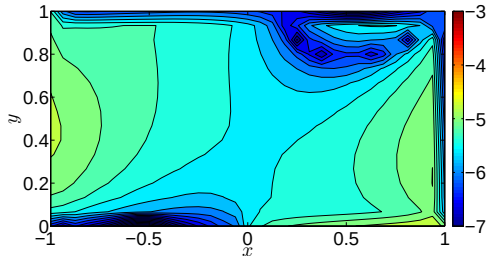

(c) $n = 96$

Figure 6.7.3: *Contour plots of* $\log|\widetilde{\varepsilon}_{n,m}^{(MSSC,M)}/\phi|$*, the logarithm of the relative error in the MSSCBEM solution of the stripline SBVP, for* $M = 2$*,* $m = 4$ *and* $n = 24, 48, 96$*. The singular point is located at* $(x, y) = (0, 0)$*. By comparison with the standard SSCBEM errors in Fig. 6.5.2, the MSSCBEM has significantly reduced the localised error peaks that occurred in the corners of the unmodified error domain.*

In Fig. 6.7.4 the errors of the MSICBEM and MSSCBEM solutions of the stripline problem are given where the truncation limit M in $\phi_s^{(M)}$ is $M = 4$. When $M = 4$, the analytic form of the singularity is built in over the first and last *two* elements in the MSICBEM, whereas for the MSSCBEM, we now require *four* balancing approximations. By comparing Fig. 6.7.4 with the original errors in the modified methods of Figs. 6.7.1 and 6.7.3 it is apparent, particularly in the MSICBEM, that increasing M significantly reduces the relative errors. A quantification into the error convergence rates and error orders in the MSICBEM and MSSCBEM for $M = 4$ are presented in Table 6.7.4, along with the those for $M = 2$ for comparison. It is evident from the data in Table 6.7.4, that the order in the MSICBEM error can be increased by taking higher values of M. Note that further investigations reveal that when $M = 6$ the order of the MSICBEM error

	Standard			Modified		
n	$\widetilde{\sigma}_n^{(SS,2)}$	ρ	p	$\widetilde{\sigma}_{n,m}^{(MSS,2)}$	ρ	p
24	3.7166×10^{-4}	2.9550	1.5632	1.9903×10^{-5}	9.2686	3.2124
48	1.2577×10^{-4}	3.0807	1.6233	2.1474×10^{-6}	8.2169	3.0386
96	4.0825×10^{-5}			2.6134×10^{-7}		

Table 6.7.2: *The RMSE σ, error order p and error convergence rate ρ of the SSCBEM (standard) and MSSCBEM (modified) solutions of the stripline SBVP, for $M = 2$, $m = 4$ and $n = 24, 48, 96$. The results correspond to the errors depicted in Figs. 6.5.2 and 6.7.3. The increase in the error order to $O(h^3)$ and the hundredfold decrease in the RMSE are evidence of the superiority in MSSCBEM over the standard SCCBEM. Furthermore, the decrease in p with increasing n in the MSSCBEM shows that the order its error is an over-specification, consistent with the error orders in the modified BEMs in chapter 4.*

	MSICBEM		MSSCBEM	
m	ρ	p	ρ	p
1	4.5205	2.1765	3.1323	1.6472
2	9.3615	3.2267	3.9268	1.9734
3	9.2696	3.2125	4.6078	2.2041
4	9.2696	3.2125	8.2479	3.0440

Table 6.7.3: *The convergence rate ρ and order p of the error in the MSICBEM and MSSCBEM solutions of the stripline SBVP for $m = 1, 2, 3, 4$, $n = 24$ and $M = 2$. Here we take $\alpha = \beta = 2$ in Richardson's extrapolation* (4.2.48)*. The order is increased in the errors of the MSICBEM and the MSSCBEM by increasing m, as by doing so we incorporate a truncated explicit error of higher degree of leading order within the modified methods.*

is $O(h^4)$ when $n = 24$, i.e. we recover the rate of convergence of piecewise-quadratic BEM by solving only a $n \times n$ system in the MSICBEM. Table 6.7.4 also shows that the order of the error in the MSSCBEM, which requires a higher number of balancing approximations, erodes when M is increased as the balancing approximations introduce additional errors. Thus the truncation limit M in both the SSCBEM and MSSCBEM should be kept at low as possible: this is consistent with

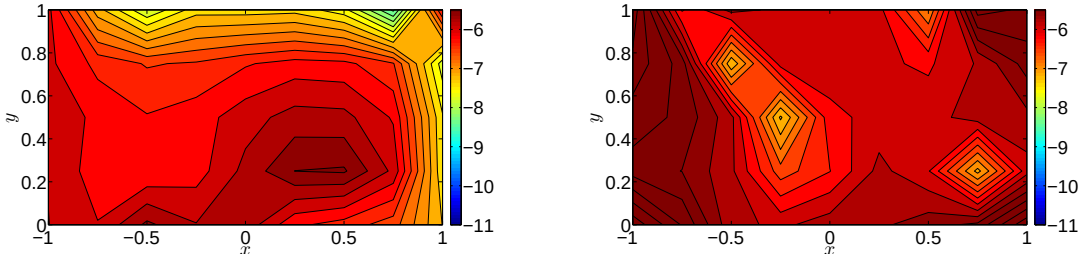

(a) MSICBEM,$n = 24$

(b) MSSCBEM,$n = 24$

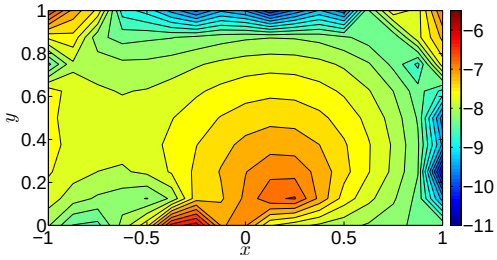

(c) MSICBEM,$n = 48$

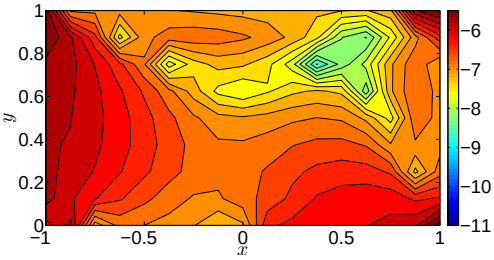

(d) MSSCBEM,$n = 48$

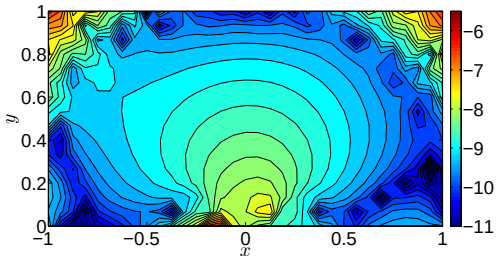

(e) MSICBEM,$n = 96$

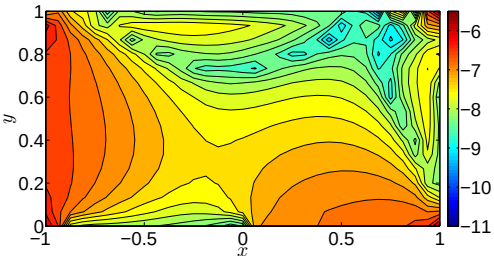

(f) MSSCBEM,$n = 96$

Figure 6.7.4: *Contour plots of* $\log|\widetilde{\varepsilon}_{n,m}^{(MSIC,M)}/\phi|$ *and* $\log|\widetilde{\varepsilon}_{n,m}^{(MSSC,M)}/\phi|$*, the respective logarithms of the relative error in the MSICBEM and MSSCBEM solutions of the stripline SBVP, for* $M = 4$*,* $m = 4$ *and* $n = 24, 48, 96$*. The MSICBEM error is less than the MSSCBEM error when* $M = 4$ *because increasing* M *in the MSICBEM increases the region over which the singular behaviour is incorporated, whereas in the MSSCBEM, a higher number of balancing approximations are required.*

the findings of Jaswon and Symm [1977] who applied a singularity subtraction BEM to the Motz problem.

Finally, an quantitative comparison of the errors in *all* the outlined BEMs in this chapter for the

	MSICBEM				MSSCBEM			
	$M=2$		$M=4$		$M=2$		$M=4$	
$n, 2n$	ρ	p	ρ	p	ρ	p	ρ	p
$24, 48$	7.9977	2.9996	13.8933	3.7963	9.2696	3.2125	8.2479	3.0440
$48, 96$	4.3751	2.1932	2.1998	1.1374	8.2169	3.0386	6.2737	2.6493

Table 6.7.4: *The convergence rate ρ and order p of the error in the MSICBEM and MSSCBEM solutions of the stripline SBVP, for $M = 2, 4$, $n = 24, 48, 96$ and $m = 4$. The results correspond to the errors depicted in Fig. 6.7.4. The order is improved in the MSICBEM error when M is increased, however, this is not the case for the MSSCBEM error due to the method requiring a higher number of balancing approximations. Although when $n > 24$ the effect of the singularity incorporation in the MSICBEM is reduced, as shown by the deceleration in its convergence rate.*

Numerical Method	RMSE ($\widetilde{\sigma}$)
CBEM	0.0135
MCBEM	0.0091
SICBEM	0.0010
MSICBEM	2.5992×10^{-6}
SSCBEM	1.2577×10^{-4}
MSSCBEM	2.1474×10^{-6}

Table 6.7.5: *Comparison of the RMSEs $\widetilde{\sigma}$ in the CBEM, SICBEM, SSCBEM, MCBEM, MSICBEM and MSSCBEM solutions of the stripline BVP, for $n = 48$, $M = 2$ and $m = 4$. The RMSEs correspond to the error surfaces depicted in Fig. 6.7.5.*

stripline SBVP is depicted in Fig. 6.7.5 and quantified in Table 6.7.5 for $n = 48$, $m = 4$ and $M = 2$. Fig. 6.7.5 and Table 6.7.5 both show three features: first, the error in each of the modified methods have smaller localised error peaks in the corners of the domain compared to their standard counterparts; second, the SICBEM and SSCBEM (and the MSICBEM and MSCBEM) are superior to the CBEM and MCBEM at modelling the singular behaviour, thus confirming (6.4.30) and (6.6.50), and; third, out of the methods presented, the MSICBEM is the most accurate method for modelling SBVPs.

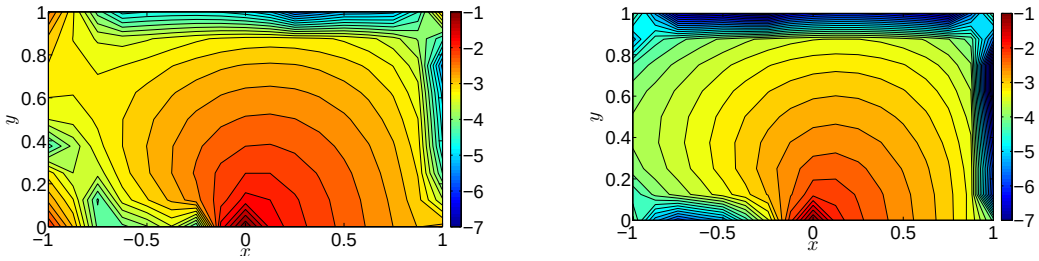

(a) CBEM

(b) MCBEM

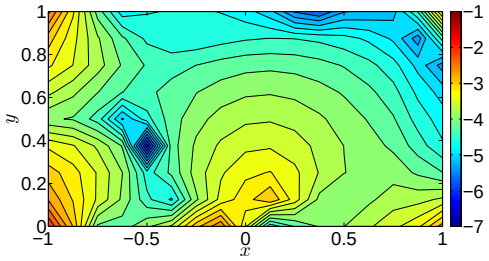

(c) SICBEM

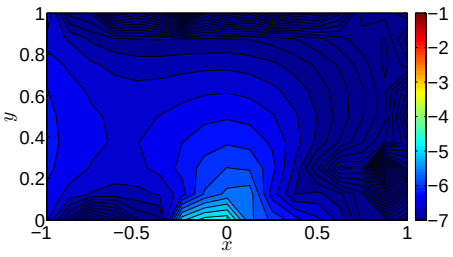

(d) MSICBEM

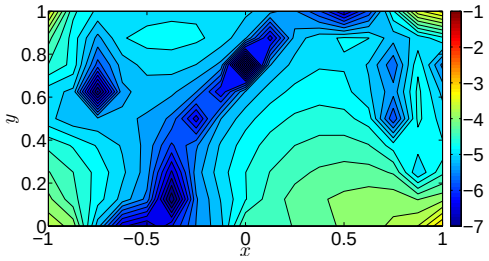

(e) SSCBEM

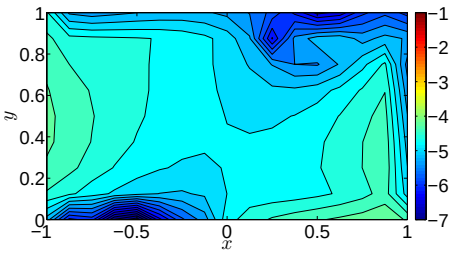

(f) MSSCBEM

Figure 6.7.5: *Comparison of the relative errors in the CBEM, SICBEM, SSCBEM, MCBEM, MSICBEM and MSSCBEM solutions of the stripline BVP, for* $n = 48$, $M = 2$ *and* $m = 4$ *(in accordance with Fig. 6.5.3).*

In general, Fig. 6.7.5 is a demonstration of the applicability of the modified approach of chapter 4 to BEMs other than the CBEM, whereby improving the convergence rate of the unmodified counterparts in the numerical solution of singular BVPs.

6.8 Summary and discussion

This chapter was based on improving numerical methods for approximating the solution of a two-dimensional singular harmonic BVP. This involved implementing modification techniques to conquer the adverse effect on the convergence with decreasing mesh size caused by boundary singularities.

The outlined work was concerned with approximating the solution of a singular stripline problem due to its geometric resemblance to the fundamental Motz problem and its applicability in electromagnetism. The near-exact analytic solution of the stripline problem, derived in chapter 5, was used to validate the numerical methods presented.

As a boundary singularity is present in the stripline problem the rate of convergence in the constant boundary element method decreased by 20% compared to its rate in chapter 4 for a nonsingular problem. Thus, following Symm [1973] and Xanthis et al. [1981], we used the analytic form of the singularity to implement two modifications of the constant boundary element method: the singularity incorporation method and the singularity subtraction method. Both the singularity incorporation and subtraction methods showed improved convergence rates for the numerical solution of the stripline problem compared to the constant boundary element method, thereby decreasing the error in the constant boundary element method by up to two orders of magnitude.

In the latter part of this chapter we further improved the convergence rates of the singularity incorporation and the singularity subtraction methods, by a modification technique based on an optimal approximation and inclusion of the explicit form of the Lagrangian-interpolation errors. In particular the modified singularity incorporation method demonstrated a significant reduction (of up to four orders of magnitude) when taking only the first two leading orders terms in the analytic form of the singularity. Furthermore, in both the modified singularity incorporation and the modified singularity subtraction methods we obtained third-order convergence rates, double that of the unmodified counterparts. The improvement in the rate of convergence of the error in modified methods was, however, not to the extent seen in the nonsingular BVP (Table (4.4.2)) due to the finite truncation of the analytic form of the singularity required for implementation.

Further investigations into the theory covered in this chapter include: defining a modified singularity incorporation or singularity subtraction method that does not depend upon the explicit

solution, e.g. using finite-difference methods as in chapter 4, and; extending the modification technique to the singularity annihilation boundary element method (Kelmanson and Lonsdale [1995, 1996]) as an alternative to the singularity incorporation and the singularity subtraction methods.

Chapter 7

Conclusions

Since brief but detailed summaries have been included at the end of each chapter, we provide here a collective overview of the numerical methods, key achievements and outcomes of this thesis.
The primary theme throughout this thesis has been to investigate the error in the numerical solutions of both one- and two-dimensional integral equations. In particular, by deriving explicit approximations of the error inherent in the numerical methods, we aimed to modify each method by including *a priori* estimates of the theoretical error, thus reducing the numerical error in the approximate solution. Chapter 2 and 3 considered the solution of one-dimensional singular Fredholm integral equations of the second kind (FIE2), whereas chapters 4, 5 and 6 concerned the solution of two-dimensional harmonic BVPs, both nonsingular and singular.

In chapters 2 and 3 it was shown that a FIE2, whose integrand exhibited singular behaviour, could be solved using a Nyström -quadrature method. The modified Nyström method enabled one to obtain significantly improved accuracy in the numerical solution compared to the standard Nyström method, particularly for low numbers of quadrature nodes. For example, for a n-point Gaussian quadrature rule, a reduction in the Nyström error of two orders of magnitude was achieved using the modified method for only $n = 2$.
The philosophy behind the first two chapters was to first define a modification technique for the Nyström method, and then to build up the complexity of the types of problems to which the modified Nyström method could be applied. The work in chapter 2 is an extension of Kelmanson

and Tenwick [2010]. The work in chapter 3, on the other hand, is an extension of the standard Nyström method for systems of FIEs presented in De Bonis and Laurita [2008]. The modification of a Nyström method for systems of FIEs, however, is substantially more intricate and complex than the modification for a single FIE; it is obtained at an expense of a large increase in analysis and computer code.

In chapters 4, 5 and 6 we considered improving the numerical solutions of higher-dimensional integral equations, namely those which were a reformulation of Laplace's equation in two-dimensions. The constant BEM in Brebbia [1978] was modified in chapter 4 by incorporating the leading behaviour of the error into the BEM *a priori*. In particular, two variations of a modified constant BEM were presented: one that used the exact boundary conditions, whereas the other used finite-differences to approximate them. Validated against a test problem in which the exact solution was known, it was shown how the modified BEMs were more accurate than the constant BEM. In the test problem considered the modified BEM achieved a rate of convergence normally associated with piecewise-quadratic Lagrangian interpolation, e.g. Ingham et al. [1981a], although without requiring the solution of a larger system of equations. For example, only a n-point collocation is required in the modified BEM whereas a $2n$-point collocation is required in a piecewise-quadratic BEM.

In chapter 6 it was shown how the modification technique of chapter 4 could be extended to singular BVPs, particularly the stripline problem. However, with no existing results to validate the numerical solutions against, the derivation of a pseudo-analytic solution was essential. Therefore, in chapter 5 a pseudo-analytic solution of the stripline problem was derived using the conformal transformation method of Whiteman and Papamichael [1971] and Rosser and Papamichael [1975]. An extensive overview of the steps in the conformal transformation method have been given, so that they can be used in future by others.

Following the work of Symm [1973] and Xanthis et al. [1981], the asymptotic nature of the singularity in the stripline problem was incorporated in to the constant BEM in chapter 6. These methods were modified by the technique of chapter 4, in that the leading behaviour of the error was incorporated into the BEMs *a priori*. Validations against the quasi-analytic conformal transformation solution illustrated the excellent accuracy in the modified BEMs. However, it was demonstrated how the modified methods were restricted in the degree of accuracy which could

be recovered in the numerical solution of a singular BVP, as only the leading behaviour of the asymptotic nature of the singularity was incorporated in Symm [1973] and Xanthis et al. [1981].

The methods of chapter 6 are applicable to the solution of a large number of physical problems in the field of electrostatics, magnetostatics, steady-fluid flow and steady-heat conduction, as demonstrated by their ability to model the singular stripline model.

There is scope for further developments into the modified methods presented in this thesis. For example, the methods of chapter 3 were illustrated for only one (interior) singular point, although the theory could be amended to cope with more complex singular problems if necessary. Alternatively, given the numerical solution of singular BVPs in chapter 6, we could consider developing modified BEMs that do not require a solution to be known *a priori*. Finally, we could consider developing the modified BEMs in 4 and 6 for biharmonic problems, e.g. hair-line cracks, although this would require dealing with coupled systems of integral equations.

Appendix

A Geometric series theorem

Let $\mathcal{A}$ be a bounded operator. For

$$\|\mathcal{A}\| < 1, \tag{A.1}$$

the Neumann series implies that $(\mathcal{I} - \mathcal{A})^{-1}$ exists and is bounded by

$$\|(\mathcal{I} - \mathcal{A})^{-1}\| \leq \frac{1}{1 - \|\mathcal{A}\|}, \tag{A.2}$$

where

$$(\mathcal{I} - \mathcal{A})^{-1} = \sum_{j=0}^{\infty} A^j. \tag{A.3}$$

B Analytic forms of $\mathbf{A_{ij}}$ and $\mathbf{B_{ij}}$

When $e^{(j)}$ is a straight-line segment, the integrals in the CBEM (4.2.3) were first evaluated analytically by Symm [1963]. His expressions are presented here for completeness.
Let $q_{Aj,n}$ and $q_{Bj,n}$ be points on $\partial\Omega$ marking the ends of boundary segment $e^{(j)}$. Given a general field point $p \in \partial\Omega \cup \Omega$ and

$$\begin{aligned} a &= |p - q_{Aj,n}|, \\ b &= |p - q_{Bj,n}|, \\ h &= |q_{Aj,n} - q_{Bj,n}|, \\ \beta &= \angle q_{Bj,n} q_{Aj,n} p, \\ \psi &= \angle q_{Aj,n} p q_{Bj,n}, \end{aligned} \tag{B.1}$$

we have the geometry as shown in Fig. 4.2.1. Using the notation of (B.1) we have the following analytic expression for the integrals A_{ij} and B_{ij} in (4.2.8): first,

$$\begin{aligned} \int_{e^{(j)}} \log|p-q| \, dq &= \int_{q_{Aj}}^{q_{Bj}} \log\left[(x_p - x_q)^2 + (y_p - y_q)^2\right]^{\frac{1}{2}} \, dx_q, \\ &= \int_{x_A}^{x_B} \log\left[(x_p - x_q)^2 + (y_p - y_q)^2\right]^{\frac{1}{2}} \, dx_q, \end{aligned} \tag{B.2}$$

where $p = (x_p, y_p)$ is the field point and $q = (x_q, y_q)$ the source point. After substituting $x = x_p - x_q$ and $y = y_p - y_q$, (B.2) is equivalent to

$$\begin{aligned} \int_{e^{(j)}} \log|p-q| \, dq &= \int_{x_A - x_p}^{x_B - x_p} \log\left[x^2 + y^2\right]^{\frac{1}{2}} \, dx, \\ &= \left[x\left(\log\left[x^2+y^2\right]^{\frac{1}{2}} - 1\right) + y\tan^{-1}\left(\frac{x}{y}\right)\right]_{x_A - x_p}^{x_B - x_p}, \\ &= h(\log(b) - 1) + a\cos(\beta)\log\left(\frac{a}{b}\right) + a\psi\sin(\beta). \end{aligned} \tag{B.3}$$

Second, using the Cauchy-Riemann equations for a complex function $w = u + iv$

$$\frac{\partial u}{\partial \underline{n}} = \frac{\partial v}{\partial \underline{s}} \tag{B.4}$$

where $\underline{n}$ and $\underline{s}$ are the unit normal and tangent vectors to $\partial\Omega$ at any given point. If ψ is the angle made by the vector $p-q$ with the outward normal to $e^{(j)}$ then $\log|p-q| = \log(r) + i\psi$, thus

$$\begin{aligned}\int_{e^{(j)}} \log'|p-q|\ dq &= \int_{e^{(j)}} \frac{\partial}{\partial \underline{n}} \log(r)\ dq \\ &= \int_{e^{(j)}} \frac{\partial}{\partial \underline{s}} \psi\ dq \\ &= \psi. \end{aligned} \tag{B.5}$$

C Analytic forms of $\mathbf{J_{k,j}}$ and $\mathbf{K_{k,j}}$

When $e^{(j)}$ is a straight-line segment, the integrals $J_{k,j}$ and $K_{k,j}$ used in the error analysis of §4.2.1 can, by extending the theory underlying Appendix B, also be derived analytically. Kelmanson (private communication, 2011) has obtained these integrals for a general k using an automated Maple process; they are presented here, for completeness, for $k = 1, \ldots, 4$.

In order to simplify the expressions, let

$$\mu = \frac{h}{a}, \tag{C.1}$$

and

$$\lambda = \log(1 - 2\mu\cos(\beta) + \mu^2), \tag{C.2}$$

by the notation of (B.1). The introduction of μ and λ facilitate the examination of the behaviour of the integrals at specific field point locations, including: corners, element end-points, element mid-point, or, collinear with the element.

Recall $J_{1,j}$ and $K_{1,j}$ were explicitly defined in §4.2.1. Therefore, by (B.1), (C.1) and (C.2), the integral expressions for $J_{k,j}$ in (4.2.29) and $K_{k,j}$ in (4.2.30) for $k = 2, 3$ and 4 are

$$\begin{aligned}
J_{2,j} &= a^2\left(\psi\cos 2\beta + \frac{\lambda\sin 2\beta}{2} + \left(-\psi\cos\beta - \frac{\lambda\sin\beta}{2} + \sin\beta + \frac{\psi\mu}{4}\right)\ \mu\right),\\
J_{3,j} &= a^3\left(\frac{\lambda\sin 3\beta}{2} + \psi\cos 3\beta + \left(\frac{-3\psi\cos 2\beta}{2} - \frac{3\lambda\sin 2\beta}{4} + \sin 2\beta\right.\right.\\
&\quad \left.\left. + \left(\frac{3\lambda\sin\beta}{8} + \frac{3\psi\cos\beta}{4} - \sin\beta - \frac{\psi\mu}{8}\right)\ \mu\right)\ \mu\right),\\
J_{4,j} &= a^4\left(\psi\cos 4\beta + \frac{\lambda\sin 4\beta}{2} + \left(\sin 3\beta - \lambda\sin 3\beta - 2\psi\cos 3\beta\right.\right.\\
&\quad + \left(\frac{-3\sin 2\beta}{2} + \frac{3\psi\cos 2\beta}{2} + \frac{3\lambda\sin 2\beta}{4}\right.\\
&\quad \left.\left.\left. + \left(\frac{-\psi\cos\beta}{2} - \frac{\lambda\sin\beta}{4} + \frac{5\sin\beta}{6} + \frac{\psi\mu}{16}\right)\ \mu\right)\ \mu\right)\ \mu\right)
\end{aligned} \tag{C.3}$$

and

$$
\begin{aligned}
K_{2,j} &= a^3 \left(\frac{\psi \sin 3\beta}{3} - \frac{\lambda \cos 3\beta}{6} + \left(-\frac{\psi \sin 2\beta}{2} + \frac{\lambda \cos 2\beta}{4} - \frac{\cos 2\beta}{3} \right.\right. \\
&\quad \left.\left. + \left(\frac{-\lambda \cos \beta}{8} + \frac{\psi \sin \beta}{4} + \frac{\cos \beta}{3} + \left(-\frac{1}{9} + \frac{\log a}{12} + \frac{\lambda}{24} \right) \mu \right) \mu \right), \mu \right) \\
K_{3,j} &= a^4 \left(\frac{-\lambda \cos 4\beta}{8} + \frac{\psi \sin 4\beta}{4} + \left(\frac{-\psi \sin 3\beta}{2} + \frac{\lambda \cos 3\beta}{4} - \frac{\cos 3\beta}{4} \right.\right. \\
&\quad \left.\left. + \left(\frac{-3\lambda \cos 2\beta}{16} + \frac{3\psi \sin 2\beta}{8} + \frac{3 \cos 2\beta}{8} + \right.\right.\right. \\
&\quad \left.\left.\left. + \left(\frac{-\psi \sin \beta}{8} + \frac{\lambda \cos \beta}{16} - \frac{5 \cos \beta}{24} + \frac{\mu}{24} \right) \mu \right) \mu \right) \mu \right), \\
K_{4,j} &= a^5 \left(\frac{\psi \sin 5\beta}{5} - \frac{\lambda \cos 5\beta}{10} + \left(\frac{-\psi \sin 4\beta}{2} + \frac{\lambda \cos 4\beta}{4} - \frac{\cos 4\beta}{5} \right.\right. \\
&\quad \left.\left. + \left(\frac{2 \cos 3\beta}{5} + \frac{\psi \sin 3\beta}{2} - \frac{\lambda \cos 3\beta}{4} \right.\right.\right. \\
&\quad \left.\left.\left. + \left(\frac{-\psi \sin 2\beta}{4} + \frac{\lambda \cos 2\beta}{8} - \frac{19 \cos 2\beta}{60} + \left(\frac{-\lambda \cos \beta}{32} + \frac{\psi \sin \beta}{16} + \frac{7 \cos \beta}{60} \right.\right.\right.\right. \\
&\quad \left.\left.\left.\left. + \left(\frac{\lambda}{160} + \frac{\log a}{80} - \frac{23}{1200} \right) \mu \right) \mu \right) \mu \right) \mu \right) \mu \right).
\end{aligned}
\tag{C.4}
$$

D Integrals $\mathbf{C_{ij}}, \mathbf{D_{ij}}, \mathbf{E_{ij}}$ and $\mathbf{F_{ij}}$

By (B.1) in Appendix B, the integrals for C_{ij}, D_{ij}, E_{ij} and F_{ij} in Eqns. (6.3.9)-(6.3.12) over the first (i.e. $j = 1$) or last (i.e. $j = n$)) elements are

$$\begin{aligned} C_{i1} &= \int_{x_1}^{x_2} \frac{x_q^{\frac{1}{2}}(y_p - y_q)}{[(x_p - x_q)^2 + (y_p - y_q)^2]}\, dx_q \\ &= \int_{-a\cos\beta}^{h-a\cos\beta} (x + a\cos\beta)^{\frac{1}{2}} \left(\frac{a\sin\beta}{x^2 + a^2\sin^2\beta}\right) dx, \end{aligned} \tag{D.1}$$

$$\begin{aligned} D_{i1} &= \int_{x_1}^{x_2} \frac{x_q^{\frac{3}{2}}(y_p - y_q)}{[(x_p - x_q)^2 + (y_p - y_q)^2]}\, dx_q \\ &= \int_{-a\cos\beta}^{h-a\cos\beta} (x + a\cos\beta)^{\frac{3}{2}} \left(\frac{a\sin\beta}{x^2 + a^2\sin^2\beta}\right) dx, \end{aligned} \tag{D.2}$$

$$\begin{aligned} E_{in} &= \int_{x_{n-1}}^{x_n} (-x_q)^{-\frac{1}{2}} \log\left[(x_p - x_q)^2 + (y_p - y_q)^2\right]^{\frac{1}{2}}\, dx_q \\ &= \int_{-a\cos\beta}^{h-a\cos\beta} (h - a\cos\beta - x)^{-\frac{1}{2}} \left(\frac{a\sin\beta}{x^2 + a^2\sin^2\beta}\right) dx \end{aligned} \tag{D.3}$$

and

$$\begin{aligned} F_{in} &= -\int_{x_{n-1}}^{x_n} (-x_q)^{\frac{1}{2}} \log\left[(x_p - x_q)^2 + (y_p - y_q)^2\right]^{\frac{1}{2}}\, dx_q \\ &= \int_{-a\cos\beta}^{h-a\cos\beta} (h - a\cos\beta - x)^{\frac{1}{2}} \left(\frac{a\sin\beta}{x^2 + a^2\sin^2\beta}\right) dx. \end{aligned} \tag{D.4}$$

Integrals (D.1)-(D.4) may be evaluated analytically provided each element $e^{(j)}$ is a straight-line segment (Kelmanson [1984]). Otherwise, these integrals must be evaluated numerically, which shall be achieved by Patterson's quadrature package D01AHF in Fortran.

Bibliography

M. Abramowitz and I. A. Stegun. *Handbook of mathematical functions*. Dover, New York, 1972.

J. M. Aitchison and A. Karageorghis. Numerical solution of a free surface problem by a boundary element method. *Int. J. Numer. Meth. Fl.*, 8(1):91–96, 1988.

A. Akyüz-Daşcıolu. Chebyshev polynomial solutions of systems of linear integral equations. *Appl. Math. Comput.*, 151(1):221–232, 2004.

W. T. Ang. *A beginner's course in boundary element methods*. Universal Publishers, USA, 2007.

P. M. Anselone. Singularity subtraction in the numerical solution of integral equations. *J. Austral. Math. Soc. Ser. B*, 22:408–418, 1981.

M. Arad, Z. Yosibash, G. Ben-Dor, and A. Yakhot. Computing flux intensity factors by a boundary method for elliptic equations with singularities. *CNME*, 14(7):657–670, 1998.

K. Atkinson. Iterative variants of the Nyström method for the numerical solution of integral equations. *Numer. Math.*, 22(1):17–31, 1974.

K. Atkinson and G. Chandler. Boundary integral equation methods for solving Laplace's equation with nonlinear boundary conditions - The smooth boundary case. *Math. Comp.*, 55(192):451–472, 1990.

K. E. Atkinson. *An introduction to numerical analysis*. J. Wiley & Sons, 1989.

K. E. Atkinson. *The numerical solution of integral equations of the second kind*. Cambridge Univ. Pr., 1997.

E. Babolian, J. Biazar, and A. R. Vahidi. The decomposition method applied to systems of Fredholm integral equations of the second kind. *Appl. Math. Comput.*, 148(2):443–452, 2004.

C. T. H. Baker. *The numerical treatment of integral equations*. Clarendon Press Oxford, 1977.

J. Bart, J. W. G. Janssen, P. J. M. Van Bentum, A. P. M. Kentgens, and J. G. E. Gardeniers. Optimization of stripline-based microfluidic chips for high-resolution nmr. *J. Magn. Reson.*, 201(2):175–185, 2009.

D. Benko, D. C. Biles, M. P. Robinson, and J. S. Spraker. Nyström methods and singular second-order differential equations. *Comp. Math. Applic.*, 56(8):1975–1980, 2008.

F. Bernal and M. Kindelan. Radial basis function solution of the Motz problem. *Eng. Computation.*, 27(5):606–620, 2010.

M. Bernkopf. The development of function spaces with particular reference to their origins in integral equation theory. *Arch. Hist. Exact Sci.*, 3(1):1–96, 1966.

J. L. Blue. *Boundary integral solutions of Laplace's equation*. Bell Telephone Laboratories, 1977.

F. Bowman. *Introduction to elliptic functions: with applications*. English Univerisities Press, 1953.

J. P. Boyd. *Chebyshev and Fourier spectral methods*. Dover, 2001.

C. Brebbia and J. Trevelyan. On the accuracy and convergence of boundary element results for the Floyd pressure vessel problem. *Comp. Struct.*, 24(3):513–516, 1986.

C. A. Brebbia. *The boundary element method for engineers*. Pentech Press, 1978.

C. A. Brebbia and J. Dominguez. *Boundary elements an introductory course*. WIT Press, 1989.

M. B. Bush, J. F. Milthorpe, and R. I. Tanner. Finite element and boundary element methods for extrusion computations. *J. Non-Newton. Fluid.*, 16(1-2):37–51, 1984.

R. S. C. Cheng. Some numerical results using the modified Nyström method to solve the 2-D potential problem. *Eng. Anal. Bound. Elem.*, 14(4):335–342, 1994.

S. Christiansen. On Green's third identity as a basis for derivation of integral equations. *ZAMM J. Appl. Math. Mech*, 54(12):185–186, 1974.

E. T. Copson. *An introduction to the theory of functions of a complex variable*. Oxford Univ. Pr., 1946.

J. Crank and R. M. Furzeland. The numerical solution of elliptic and parabolic partial differential equations with boundary singularities. *J. Comput. Phys.*, 26(3):285–296, 1978.

J. A. Crow. Quadrature of integrands with a logarithmic singularity. *Math. Comp.*, 60:297–301, 1993.

P. Daly. Singularities in transmission lines. *The Mathematics of Finite Elements and Applications*, pages 337–350, 1973.

M. C. De Bonis and C. Laurita. Numerical treatment of second kind Fredholm integral equations systems on bounded intervals. *J. Comput. Appl. Math.*, 217(1):64–87, 2008.

L. M. Delves and J. L. Mohamed. *Computational methods for integral equations*. Cambridge Univ. Pr., 1988.

J. Dick, P. Kritzer, F. Y. Kuo, and I. H. Sloan. Lattice-Nyström method for Fredholm integral equations of the second kind with convolution type kernels. *J. Complexity*, 23(4-6):752–772, 2007.

A. A. Dosiyev. The high accurate block-grid method for solving Laplace's boundary value problem with singularities. *SIAM J. Numer. Anal.*, pages 153–178, 2005.

T. A. Driscoll and L. N. Trefethen. *Schwarz-Christoffel Mapping*. Cambridge University Press, 2002.

M. Elliotis, G. Georgiou, and C. Xenophontos. The solution of Laplacian problems over L-shaped domains with a singular function boundary integral method. *CNME*, 18(3):213–222, 2002.

M. Elliotis, G. Georgiou, and C. Xenophontos. The singular function boundary integral method for a two-dimensional fracture problem. *Eng. Anal. Bound. Elem.*, 30(2):100–106, 2006.

D. Elliott. The approximate solution of singular integral equations. In M. A. Goldberg, editor, *Solution Methods for Integral Equations, Theory and Applications*, pages 83–107. Plenum, New York, 1979.

D. Elliott. A comprehensive approach to the approximate solution of singular integral equations. *J. Integral Equations Appl.*, 2(1):59–94, 1989.

G. Fairweather and A. Karageorghis. The method of fundamental solutions for elliptic boundary value problems. *Adv. Comput. Math.*, 9(1):69–95, 1998.

G. Fairweather, F. J. Rizzo, D. J. Shippy, and Y. S. Wu. On the numerical solution of two-dimensional potential problems by an improved boundary integral equation method*1. *J. Comput. Phys.*, 31(1):96–112, 1979.

R. T. Fenner. The boundary integral equation (boundary element) method in engineering stress analysis. *J. Strain. Anal. Eng.*, 18(4):199–205, 1983.

B. Fornberg. Generation of finite difference formulas on arbitrarily spaced grids. *Math. Comput.*, 51(184):699–706, 1988.

B. Fornberg. Calculation of weights in finite difference formulas. *SIAM review*, pages 685–691, 1998.

I. Fredholm. Sur une classe déquations fonctionnelles. *Acta Mathematica*, 27(1):365–390, 1903.

W. Gautschi. *Orthogonal Polynomials:Computation and Approximation*. Oxford Univ. Pr., 2004.

A. Gerasoulis and R. P. Srivastav. On the solvability of singular integral equations via Gauss-Jacobi quadrature. *International Journal of Computer Mathematics*, 12(1):59–75, 1982.

G. H. Golub and C. F. Van Loan. *Matrix computations*. Johns Hopkins Univ. Pr., 1996.

I.G. Graham, S. Joe, and I. H. Sloan. Iterated galerkin versus iterated collocation for integral equations of the second kind. *IMA J. Numer. Anal.*, 5(3):355–369, 1985.

C. D. Green. *Integral equation methods*. Nelson, 1969.

S. T. Grilli and I. A. Svendsen. Corner problems and global accuracy in the boundary element solution of nonlinear wave flows. *Eng. Anal. Bound. Elem.*, 7(4):178–195, 1990.

C. M. Groh and M. A. Kelmanson. Closed-form error estimates for the numerical solution of Fredholm integral equations of the second kind. *J. Integral Equations Appl.*, 20(4):481–505, 2008.

W. Hackbusch. *Integral equations: Theory and numerical treatment*. Birkhäuser, 1995.

E. B. Hansen and M. A. Kelmanson. An integral equation justification of the boundary conditions of the driven-cavity problem. *Comput. Fluids*, 23(1):225–240, 1994.

J. Helsing. Integral equation methods for elliptic problems with boundary conditions of mixed type. *J. Comput. Phys.*, 228(23):8892–8907, 2009.

J. A. Hendry and L. M. Delves. The global element method applied to a harmonic mixed boundary value problem. *J. Comput. Phys.*, 33(1):33–44, 1979.

G. C. Hsiao. Boundary element methodsan overview. *Appl. Numer. Math.*, 56(10):1356–1369, 2006.

G. C. Hsiao and W. L. Wendland. Boundary element methods: Foundation and error analysis. pages 339–373, 2004.

H. Y. Hu. *The Trefftz and collocation methods for elliptic equations*. PhD thesis, Doctoral dissertation, Department of Applied Mathematics, National Sun Yat-sen University, Kaohsiung, 2003.

D. B. Ingham and M. A. Kelmanson. *Boundary integral equation analyses of singular, potential, and biharmonic problems*. Springer-Verlag Berlin, 1984.

D. B. Ingham, P. J. Heggs, and M. Manzoor. The numerical solution of plane potential problems by improved boundary integral equation methods. *J. Comput. Phys.*, 42(1):77–98, 1981a.

D. B. Ingham, P. J. Heggs, and M. Manzoor. Boundary integral equation solution of non-linear plane potential problems. *IMA J. Numer. Anal.*, 1(4):415–426, 1981b.

D. B. Ingham, P. J. Heggs, and M. Manzoor. Boundary integral equation analysis of transmission-line singularities. *IEEE Trans. Microw. Theory Tech.*, 29(11):1240–1243, 1981c.

H. Jafari, H. Hosseinzadeh, and S. Mohamadzadeh. Numerical solution of system of linear integral equations by using Legendre wavelets. *Int. J. Open Problems Compt. Math*, 3(5):63–71, 2010.

M. A. Jaswon. Integral equation methods in potential theory. I. *P. Roy. Soc. Lond. A Math.*, 275 (1360):23–32, 1963.

M. A. Jaswon and G. T. Symm. *Integral equation methods in potential theory and elastostatics*. Oxford Univ. Pr., 1977.

M. Javidi and A. Golbabai. A numerical solution for solving system of Fredholm integral equations by using homotopy perturbation method. *Appl. Math. Comput.*, 189(2):1921–1928, 2007.

E. Jen and R. P. Srivastav. Cubic splines and approximate solution of singular integral equations. *Math. Comp.*, 37(156):417–423, 1981.

X. Jin, L. M. Keer, and Q. Wang. A practical method for singular integral equations of the second kind. *Eng. Fract. Mech.*, 75(5):1005–1014, 2008.

H. Kaneko and Y. Xu. Gauss-type quadratures for weakly singular integrals and their application to Fredholm integral equations of the second kind. *Math. Comput.*, 62(206):739–754, 1994.

S. Y. Kang, I. Koltracht, and G. Rawitscher. Nyström-Clenshaw-Curtis quadrature for integral equations with discontinuous kernels. *Math. Comp.*, 72(242):729–756, 2003.

L. V. Kantorovich, V. I. Krylov, and C. D. Benster. *Approximate methods of higher analysis*. Interscience Groningen, 1964.

A. Karageorghis, N. S. Stylianopoulos, and H. A. Zachariades. A numerical conformal mapping method for harmonic mixed boundary value problems. *J. Sci. Comput.*, 11(3):167–178, 1996.

L. N. Karpenko. Approximate solution of a singular integral equation by means of Jacobi polynomials. *PMM-J. Appl. Math. Mec.*, 30(3):668–675, 1966.

R. B. Kelman. Harmonic mixed boundary-value problems in composite rectangular domains. *Q. J. Mech. Appl. Math.*, 23(4):549–566, 1970.

M. A. Kelmanson. Modified integral equation solution of viscous flows near sharp corners. *Comput. Fluids*, 11(4):307–324, 1983a.

M. A. Kelmanson. Boundary integral equation solution of viscous flows with free surfaces. *J. Eng. Math.*, 17(4):329–343, 1983b.

M. A. Kelmanson. Solution of nonlinear elliptic equations with boundary singularities by an integral equation method. *J. Comput. Phys.*, 56(2):244–258, 1984.

M. A. Kelmanson. A consistency analysis for the numerical solution of boundary integral equations. *Appl. Numer. Math.*, 1(5):381–393, 1985.

M. A. Kelmanson and B. Lonsdale. Annihilation of boundary singularities via suitable Green's functions. *Comput. Math. Appl.*, 29(4):1–7, 1995.

M. A. Kelmanson and B. Lonsdale. Eddy genesis in the double-lid-driven cavity. *Q. J. Mech. Appl. Math.*, 49(4):635–655, 1996.

M. A. Kelmanson and M. C. Tenwick. A modified orthogonal-polynomial Nyström method for Fredholm integral equations of the second kind. In *Proceedings of the 7th UK conference on Boundary Integral Methods*, pages 181–192, 2009.

M. A. Kelmanson and M. C. Tenwick. Error reduction in Gauss-Jacobi-Nyström quadrature for Fredholm integral equations of the second kind. *CMES*, 1392(1):1–20, 2010.

M. Kermode and L. M. McKerrell. The calculation of singular coefficients* 1. *Comput. Method. Appl. M.*, 50(3):205–215, 1985.

R. Kress. A Nyström method for boundary integral equations in domains with corners. *Numer. Math.*, 58(1):145–161, 1990.

D. P. Laurie. Computation of Gauss-type quadrature formulas. *J. Comput. Appl. Math.*, 127: 201–217, 2001.

Z. C. Li and T. T. Lu. Singularities and treatments of elliptic boundary value problems* 1. *Math. Comput. Model.*, 31(8-9):97–145, 2000.

Z. C. Li, R. Mathon, and P. Sermer. Boundary methods for solving elliptic problems with singularities and interfaces. *SIAM J. Numer. Anal.*, 24(3):487–498, 1987.

Z. C. Li, T. T. Lu, H. Y. Hu, and A. H. D. Cheng. Particular solutions of Laplace's equations on polygons and new models involving mild singularities. *Eng. Anal. Bound. Elem.*, 29(1):59–75, 2005.

Z. C. Li, Y. L. Chan, G. C. Georgiou, and C. Xenophontos. Special boundary approximation methods for Laplace equation problems with boundary singularities–Applications to the Motz problem. *Comput. Math. Appl.*, 51(1):115–142, 2006.

M. T. Liang, J. T. Chen, and S. S. Yang. Error estimation for boundary element method. *Eng. Anal. Bound. Elem.*, 23(3):257–265, 1999.

M. J. Lighthill. *Introduction to Fourier analysis and generalised functions*. Cambridge Univ. Pr., 1958.

T. T. Lu, H. Y. Hu, and Z. C. Li. Highly accurate solutions of Motz's and the cracked beam problems. *Eng. Anal. Bound. Elem.*, 28(11):1387–1403, 2004.

K. Maleknejad, M. Shahrezaee, and H. Khatami. Numerical solution of integral equations system of the second kind by block–pulse functions. *Appl. Math. Comput.*, 166(1):15–24, 2005.

K. Maleknejad, N. Aghazadeh, and M. Rabbani. Numerical solution of second kind Fredholm integral equations system by using a Taylor-series expansion method. *Appl. Math. Comput.*, 175 (2):1229–1234, 2006.

M. Manzoor. *Heat flow through extended surface heat exchangers*. Springer-Verlag, NY, 1984.

J. Mason, A. Parker, R. Smith, and R. Thompson. Boundary element methods for singularity problems in fracture mechanics, singularities and constructive methods for their treatment. *Lecture notes in mathematics*, pages 181–198, 1985.

J. C. Mason and R. N. L. Smith. Boundary integral equation methods for a variety of curved crack problems. *Integral Equations and Their Numerical Treatment*, pages 239–252, 1982.

G. Mastroianni and G. Monegato. Truncated quadrature rules over $(0, \infty)$ and Nyström-type methods. *SIAM J. Numer. Anal.*, 41(5):1870–1892, 2003.

N. S. Mera, L. Elliott, D. B. Ingham, and D. Lesnic. A comparison of boundary element method formulations for steady state anisotropic heat conduction problems. *Eng. Anal. Bound. Elem.*, 25(2):115–128, 2001.

N. S. Mera, L. Elliott, D. B. Ingham, and D. Lesnic. Singularities in anisotropic steady-state heat conduction using a boundary element method. *Int. J. Numer. Methods Eng.*, 53(10):2413–2427, 2002.

M. Mohammadi, M. R. Hematiyan, and M. H. Aliabadi. Boundary element analysis of thermo-elastic problems with non-uniform heat sources. *J. Strain Anal. Eng. Des.*, 45(8):605–627, 2010.

G. Monegato and L. Scuderi. High order methods for weakly singular integral equations with nonsmooth input functions. *Math. Comp.*, 67(224):1493–1516, 1998.

H. Motz. The treatment of singularities of partial differential equations by relaxation methods. *Quart. Appl. Math*, 4:371–377, 1946.

N. I. Muskhelishvili. *Singular integral equations*. Groningen: Noordhoff, 1953.

Z. Nehari. *Conformal mapping*. McGraw-Hill, 1952.

A. Nijenhuis and H. S. Wilf. *Combinatorial algorithms*. Academic Press (New York), 1975.

E. Nyström. Über die praktische Auflösung von Integralgleichungen mit Anwendungen auf Randwertaufgaben. *Acta. Math.*, 54:185–204, 1930.

L. G. Olson, G. C. Georgiou, and W. W. Schultz. An efficient finite element method for treating singularities in Laplace's equation. *J. Comput. Phys.*, 96(2):391–410, 1991.

N. Papamichael. Numerical conformal mapping onto a rectangle with applications to the solution of Laplacian problems. *J. Comput. Appl. Math.*, 28:63–83, 1989.

N. Papamichael and A. Sideridis. The use of conformal transformations for the numerical solution of elliptic boundary value problems with boundary singularities. *IMA J. Appl. Math.*, 23(1): 73–87, 1979.

N. Papamichael and G. T. Symm. Numerical techniques for two-dimensional Laplacian problems. *Comput. Method. Appl. M.*, 6(2):175–194, 1975.

N. Papamichael and J. R. Whiteman. A numerical conformal transformation method for harmonic mixed boundary value problems in polygonal domains. *ZAMP*, 24(3):304–316, 1973.

G. Pashos, A. G. Papathanasiou, and A. G. Boudouvis. A hybrid boundary element method for elliptic problems with singularities. *arXiv:1006.3630*, 2010.

T. N. L. Patterson. The optimum addition of points to quadrature formulae. *Math. Comput*, 22 (104):847–856, 1968.

D. Porter and D. S. G. Stirling. *Integral equations: a practical treatment, from spectral theory to applications*. Cambridge Univ. Pr., 1990.

V. Postoyalko. Green's function treatment of edge singularities in the quasi-TEM analysis of microstrip. *IEEE Trans. Microwave Theory Tech.*, 34(11):1092–1096, 1986.

A. Poullikkas, A. Karageorghis, and G. Georgiou. Methods of fundamental solutions for harmonic and biharmonic boundary value problems. *Comput. Mech.*, 21(4):416–423, 1998.

H. Power and L. C. Wrobel. *Boundary integral methods in fluid mechanics*. Computational Mechanics Publications Southampton, 1995.

A. Ralston and P. Rabinowitz. *A first course in numerical analysis*. Dover, 2001.

J. Rashidinia and M. Zarebnia. Convergence of approximate solution of system of fredholm integral equations. *JMAA*, 333(2):1216–1227, 2007.

J. J. Rencis, T. J. Urekew, K. Y. Jong, R. Kirk, and P. Federico. A posteriori error estimation for the finite element and boundary element methods. *Comput. Sruct.*, 37(1):103–117, 1990.

J. B. Rosser and N. Papamichael. A power series solution of a harmonic mixed boundary value problem. MRC Technical Summary, Rept. 1405, Univeristy of Wisconsin, 1975.

R. Schinzinger and P. A. A. Laura. *Conformal mapping: methods and applications*. Dover Pubns, 2003.

R. N. L. Smith. Direct gauss quadrature formulae for logarithmic singularities on isoparametric elements. *Eng. Anal. Bound. Elem.*, 24(2):161–167, 2000.

J. Steinberg. Computation of expansion coefficients in a singular harmonic problem* 1. *J. Comput. Appl. Math.*, 18(2):213–220, 1987.

G. T. Symm. Integral equation methods in potential theory. II. *P. Roy. Soc. Lond. A Math.*, 275 (1360):33, 1963.

G. T. Symm. Treatment of singularities in the solution of Laplace's equations by an integral equation method. Technical report, NPL Report NAC (31 January 1973), 1973.

L. N. Trefethen. Is Gauss quadrature better than Clenshaw-Curtis? *SIAM review*, 50(1):67–87, 2008.

E. Trefftz. Ein gegenstuck zum ritzschen verfahren. *Proc. 2nd Int. Cong. Appl. Mech.*, pages 131–137, 1926.

F. G. Tricomi. *Integral equations*. Dover, 1985.

W. L. Wendland. *Boundary element methods and their asymptotic convergence*. Techn. Hochsch., Fachbereich Math., 1982.

W. L. Wendland. On asymptotic error estimates for the combined boundary and finite element method. *Innovative numerical methods in engineering*, pages 55–69, 1986.

J. R. Whiteman and N. Papamichael. Numerical solution of two dimensional harmonic boundary problems containing singularities by conformal transformation methods. Tr/2, Dept. of Mathematics, Brunel University, 1971.

J. R. Whiteman and N. Papamichael. Treatment of harmonic mixed boundary problems by conformal transformation methods. *ZAMP*, 23(4):655–664, 1972.

N. M. Wigley. An efficient method for subtracting off singularities at corners for Laplace's equation. *J. Comput. Phys.*, 78(2):369–377, 1988.

L. C. Woods. The relaxation treatment of singular points in Poisson's equation. *Q. J. Mech. Appl. Math.*, 6(2):163–185, 1953.

L.C. Wrobel. *Potential and viscous flow problems using the boundary element method*. PhD thesis, University of Southampton, 1981.

L. S. Xanthis, M. J. M. Bernal, and C. Atkinson. The treatment of singularities in the calculation of stress intensity factors using the boundary integral equation method. *Comput. Meth. Appl. Mech. Eng.*, 26(3):285–304, 1981.

C. Xenophontos, E. Christodoulou, and G. Georgiou. The singular function boundary integral method for Laplacian problems with boundary singularities in two and three-dimensions. *Procedia Computer Science*, 1(1):2589–2597, 2010.

R. W. Yeung. Numerical methods in free-surface flows. *Annu. Rev. Fluid Mech.*, 14(1):395–442, 1982.